DROPLET BREAKUP AND COALESCENCE IN COMPACT WELLSTREAM SEPARATION

By

Truls Chr. Vold

Department of Chemical Engineering
Faculty of Chemistry and Biology
Norwegian University of Science and Technology
N-7491 Trondheim, Norway

Thesis submitted for the Degree of Dr.ing. (Ph.D.)
December 1999

This thesis is dedicated to my wife Betty, who has given endless patience and support during my work and stay in Trondheim, and has taken all the responsibilities for the home, upbringing and education of our children during my studies.

Thanks also to Lars Christian, Eivind Andreas and Jon Amund who have given up so much time and joy that we should have shared.

Without their love and support, I could not have finished this work.

ACKNOWLEDGEMENT

I wish to express my deepest gratitude and appreciation to my supervisor, Prof. Hallvard F. Svendsen for his strongest encouragement and guidance during this study.

I am also indebted to Mr. Kai Hjarbo for fruitfull discussions and always being helpful with solutions to experimental instruments and computers.

Further, I am most thankful to to Mr. Kristian Schanke who helped me with the mechanical setup, and Mr. Hans Pettersen who helped me with the electrical work.

My office-mate, Lars J. Hagesæther, gave me invaluable friendship, strong support and interesting discussions in all topics during my stay.

Without Mr. Gjert Laading and The Research Council of Norway (NFR) it would not be possible to complete this work. Their moral and financial support is most gratefully acknowledged.

Finally, I would like to thank my family, also my mother and father, who always encouraged me to pursue what I urged for, and for giving their love, patience and support throughout the years.

ABSTRACT

In this work attention has been drawn to the processes of droplet coalescence and breakup, which are counteracting effects in the separation process where two or more liquids are present. Emphasis has been on experimental work. However, the theoretical aspects have been linked to the experimental.

In relation to petroleum production, the separation process has traditionally required large equipment volumes and weights. New technologies require lighter and more efficient equipment base on profound understanding of relevant science.

There is a documented concern from environmental authorities regarding the annual amount of oil discharges from the Norwegian petroleum activities. By the year 2000 the discharge of oil is forecasted to be nearly 3000 tons per year, based on an average oil concentration of 25 mg/l remaining in the produced water being discharged to sea. It is expected that this discharge level will stay for number of years unless drastic measures are implemented.

With this background, Ch. 1 presents a problem description and a review of technology status and comparison of processes capable of meeting the environmental demands.

Further, in Ch. 2, experimental setup and techniques are presented. The experiments were based on using a static mixer, since this unit was known for producing a fairly narrow droplet size distribution when mixing two immiscible fluids in it. It was believed that turbulence intensity, RMS velocity as well as local velocity were important parameters to study. LDA instrumentation together with Malvern instrumentation for particle size analyses facilitated such investigations in a Sulzer static mixer. Only the small droplets were of interest, being the major constituent of in-dispersion-stable dispersions. Droplets larger than 40 micron size were therefore neglected in analyses.

In Ch. 3 there is an extensive literature survey on the theoretical aspects of turbulence and droplet size distribution in static mixers. Topics that are included are:

1. Drop sizes formed in turbulent flow
2. Models for droplet breakup and coalescence
3. Turbulent mixing
4. Principles and characteristics of the static mixer
5. Calculation procedures for static mixers.

Then, in Ch. 4, characterization and measurements of the static mixer are presented. Also, results obtained from previous workers are presented, and it was found that most workers do not limit their investigations to droplets having smaller diameters than about 40 microns. The present characterization of the moving fluid volume between two mixer elements was done with water only, as well with oil/water mixtures. In these experiments it has been focused on droplets being in a stable suspension, and being smaller than about 40 microns in diameter. Characterization was done by using LDA equipment to obtain numerical values for:

1. Mean velocity
2. Root mean square velocity
3. Turbulence intensity, i.e. the standard deviation of the mean velocity.

The experimental conditions were based on variations in:

a) Single phase characterization, i.e. using tap water only
b) Beam trajectory alignment angle and vertical position within the measurement volume
c) Sealing vs non-sealing of mixer elements (to verify possible channeling effects)
d) Fluid velocities
e) Heating of fluid
f) Induced air
g) Testing of other mixer elements

It was concluded that the results obtained depend on the alignment angle, since different characterization values were obtained (velocities, turbulence intensities). Similar observations were done for variations of vertical position of beam trajectory. As expected, there was highest turbulence near the outlet from the mixer elements. Also, the recordings were different as the traverse was passed, reflecting the mixer geometry, given by the stacking of the corrugated sheets, their folding and the angle of the furrows relative to the main flow direction.

In Ch. 5 the effect of chemical additives is studied. First the theoretical aspects are presented. Then there is an explanation of the use and application of additives and emulsifying agents in the experiments. Preparatory procedure, sampling and analysis are presented and shown in figures. Results and conclusions from the attempts of droplet stabilization and destabilization are also discussed.

Finally, in Ch. 6, the experimental methods and results of conducting various practical crude oil experiments are presented. Extensive analysis instruments, such as the Malvern and Sigma Plot data treatment programs are applied and shown.

Ch. 7 presents conclusions in summary and recommendations for further work.

DROPLET BREAKUP AND COALESCENCE IN COMPACT WELLSTREAM SEPARATION

TABLE OF CONTENTS

1 INTRODUCTION 5

1.1 MOTIVATION FOR THE THESIS 5
1.2 PROBLEM DESCRIPTION 9
1.3 PRESENT TECHNOLOGY STATUS 13
1.3.1 Process Comparisons of Three Recognized Technologies 13
1.3.1.1 The Hydrocyclone 13
1.3.1.2 The Ceramic Membrane Filter 16
1.3.1.3 Granular Resin Coalescing Filter 17
1.3.2 Less Advanced or Limited Technologies 18
1.3.3 Current Produced Water Treatment Technology 20

2 EXPERIMENTAL SETUP AND TECHNIQUES 21

2.1 GENERAL 21
2.2 EXPERIMENTAL FLOW SCHEME 23
2.3 PRINCIPLES OF LASER DOPPLER ANEMOMETRY 27
2.3.1 Configuration of apparatus 27
2.3.2 Doppler burst 28
2.3.3 The fringe model 29
2.3.4 Directional ambiguity 31
2.3.5 Bragg cell 32
2.3.6 Recorded values from the LDA measurements 33
2.4 THE MALVERN PARTICLE SIZE ANALYZER 33
2.4.1 Principles 33
2.4.2 Procedure for conducting trials, sampling and analysis 36
2.4.2.1 Sample procedure when using EXXSOL D60 model oil in dispersion 38
2.4.2.2 Sampling procedure when using Statfjord crude oil in dispersion 39

3 TURBULENCE & DROPLET SIZE DISTRIBUTION IN STATIC MIXERS 41

3.1 INTRODUCTION TO TURBULENCE THEORY 41
3.1.1 General 41
3.1.1.1 Reynold's stress 41
3.1.1.2 Local velocities 42
3.1.1.3 Laminar and turbulent flow in boundary layers 43
3.2 DROP SIZES FORMED IN TURBULENT FLOW 44
3.2.1 Isotropic turbulence and droplet breakup 44
3.2.2 General approach 46
3.2.3 Dispersion and energy dissipation in static mixers 49
3.2.4 Effect of velocity and interfacial tension 52
3.2.5 Effect of dispersed-phase viscosity 53
3.2.6 Effect of pipe diameter 55

DROPLET BREAKUP AND COALESCENCE IN COMPACT WELLSTREAM SEPARATION

TABLE OF CONTENTS

3.2.7 Effect of volume fraction of dispersed phase *55*
3.2.8 Droplet size distribution in turbulent dispersion *56*
3.3 MODELS FOR DROPLET BREAKUP AND COALESCENCE 57
3.3.1 Droplet breakup *57*
3.3.2 Droplet coalescence *61*
3.3.3 Models for coalescence time *67*
3.3.3.1 Liquid phase diffusion model 67
3.3.3.2 Gas phase diffusion model 69
3.3.3.3 Dynamic surface tension model 69
3.3.4 Critical thickness for rupture *72*
3.3.5 Theoretical analysis of droplet coalescence *73*
3.4 TURBULENT MIXING 74
3.4.1 Influence of Coalescence on Drop Size in Dispersions *74*
3.4.2 Numerical simulation of mixing in static mixers *79*
3.5 PRINCIPLES AND CHARACTERISTICS OF THE STATIC MIXER 83
3.5.1 Principles *83*
3.5.2 Characteristics *84*
3.6 CALCULATION PROCEDURES FOR STATIC MIXERS 85
3.6.1 Assessing homogeneity *85*
3.6.2 In-line disperser, drop formation and droplet size prediction in static mixers *88*
3.6.3 Further aspects of turbulent energy dissipation *94*
3.6.4 Energy dissipation and solid surface effects *95*
3.6.5 Surfactants and solid surface effects *96*
3.6.6 Use of energy dissipation in static mixers *98*

4 CHARACTERIZATION AND MEASUREMENTS OF THE STATIC MIXER ..101

4.1 EXPERIMENTAL CHARACTERIZATION 101
4.1.1 Results obtained from previous workers *101*
4.1.2 Introductory explanation to the experimental characterization trials *105*
4.1.3 Single phase characterization *108*
4.1.3.1 Methodology establishment (TEST1 - TEST6) 109
4.1.3.2 Beam trajectory height variation (TEST6, TEST7, TEST8, TEST13, TEST14) . 115
4.1.3.3 Laser beam angle of incidence 90° (TEST9 - TEST12) 122
4.1.3.4 Channeling effects (TEST16 - TEST25) 127
4.1.4 Tests at different volumetric fluid velocities *132*
4.1.5 Tests with heating applied *137*
4.1.6 Trials with induced air *141*
4.1.7 Tests from 2nd mixer element elevation *145*

5 THE EFFECT OF CHEMICAL ADDITIVES 146

5.1 THEORETICAL ASPECTS 146
5.1.1 Introduction to surface active agents *146*

DROPLET BREAKUP AND COALESCENCE IN COMPACT WELLSTREAM SEPARATION

TABLE OF CONTENTS

5.1.2 Previous experience reported *149*
5.1.2.1 Gas-liquid systems 149
5.1.3 Classification and application of tensides *151*
5.2 ADDITIVES APPLIED IN THE EXPERIMENTS 152
5.2.1 Stabilizing/destabilizing agents *152*
5.3 EMULSIFYING AGENTS 154
5.3.1 Emulsions *154*
5.3.2 Electrical charge in emulsions *158*
5.3.3 Destabilization of emulsions and dispersions *159*
5.4 GIBBS' ADSORPTION EQUATION 162
5.5 EXPERIMENTAL 164
5.5.1 Preparatory procedure, sampling and analysis of emulsifier applications *164*
5.5.2 Method of stabilization of small droplets *166*
5.5.2.1 Results obtained from stabilization attempts 167
5.5.3 Method of destabilization of small droplets *168*
5.5.3.1 Results obtained from destabilization attempts 169
5.6 CHAPTER SUMMARY 173

6 PRACTICAL CRUDE OIL EXPERIMENTS 176

6.1 EXPERIMENTAL METHODS 176
6.1.1 Introduction *176*
6.1.2 Make-up of oil-in-water dispersion *177*
6.1.3 Sampling procedures *178*
6.1.4 Analysis instrumentation and principles *179*
6.1.4.1 Sigma Plot data treatment 179
6.1.5 Experimental results *182*
6.1.5.1 Establishing oil droplet size in the dispersion make-up, before entrance to the mixer 183
6.1.5.2 Establishing oil droplet concentration in the dispersion make-up, before entrance to the mixer 183
6.1.5.3 Establishing oil droplet size in the dispersion make-up, after exit from the mixer 184
6.1.5.4 Establishing oil droplet concentration in the dispersion make-up, after exit from the mixer 184
6.1.5.5 Establishing oil droplet size in a solution of oil added to the dispersion make-up, after exit from the mixer 184
6.1.5.6 Establishing oil droplet concentration in a solution of oil added to the dispersion make-up, after exit from the mixer 185
6.1.5.7 Establishing the relative concentrations of droplet size classes when oil is added 186
6.1.5.8 Establishing the coalescence/breakup contribution from the originally dispersed oil droplets to added crude oil droplets 187
6.1.6 Droplet breakup due to make-up with Ultra Turrax *187*
6.1.7 Difference between «old» and «new» batch of oil *188*

TABLE OF CONTENTS

6.1.8 Influence of elevated temperature on drop size distribution and concentration vs. dispersed phase flowrate *191*

6.2 PREVIOUS INVESTIGATIONS ON DISPERSION OF IMMISCIBLE LIQUID 193

7 CONCLUSIONS IN SUMMARY, AND RECOMMENDATIONS FOR FURTHER WORK 194

7.1 CONCLUSIONS IN SUMMARY 194

7.2 RECOMMENDATIONS FOR FURTHER WORK 197

8 LITERATURE REFERENCES 199

9 LIST OF SYMBOLS 212

CHAPTER 1 INTRODUCTION

1 INTRODUCTION

1.1 Motivation for the thesis

Norway has become one of the most important oil and gas producers in Europe. All of the Norwegian hydrocarbon production is being exploited offshore, from the Norwegian continental shelf. Harsh conditions prevail in these areas and impose serious challenges on man and equipment applied. Also, since offshore production is mostly being done on platforms, processing equipment has to be limited in weight and space.

There will always be water associated with the production of hydrocarbons. Fig. 1.2 shows the most important sources of discharges to sea from petroleum activities. The most important source of oil discharges to sea is residual oil in produced water. This water may originate from formation water from the reservoir, or a mixture of formation water and injection water (sea water).

The motivation for developing new and improved technology for separation of produced water has its background in the considerable increase in volumes which is foreseen in the coming years as seen in Fig. 1.1. The volume of offshore related produced water is also expected to increase substantially due to water increasingly penetrating the reservoirs into the production wells, and the increasing use of injection water as a means of enhanced recovery by maintaining pressure into the production wells. At the same time, the total

production of oil and gas has constantly increased and is expected to continue to do so for many years.
However, the forecast given in Fig. 1.1 must certainly be interpreted as being indicative only, since there is a high degree of uncertainty regarding the actual development of produced water volumes after year 2005. New technology as well as refined injection methods will probably make a substantially different outlook of the volumes to be expected after 2005.

MILJØSOK (1996) reports that the average oil discharge concentration was around 80 ppm in 1985, but at that time the produced water volumes were considerably smaller (approx. 5 mill. m^3/yr) and had therefore a less significant environmental impact. Oil discharges from the Norwegian petroleum activities were in 1993 estimated to be approximately 1200 tons. The discharge of oil is presently around 2000 tons per year. By the year 2000 the discharge of oil is forecasted to be nearly 3000 tons per year, based on an average oil concentration of 25 mg/l remaining in the produced water that is discharged. And it is expected that this discharge level will stay for a number of years unless some drastic measures are implemented.

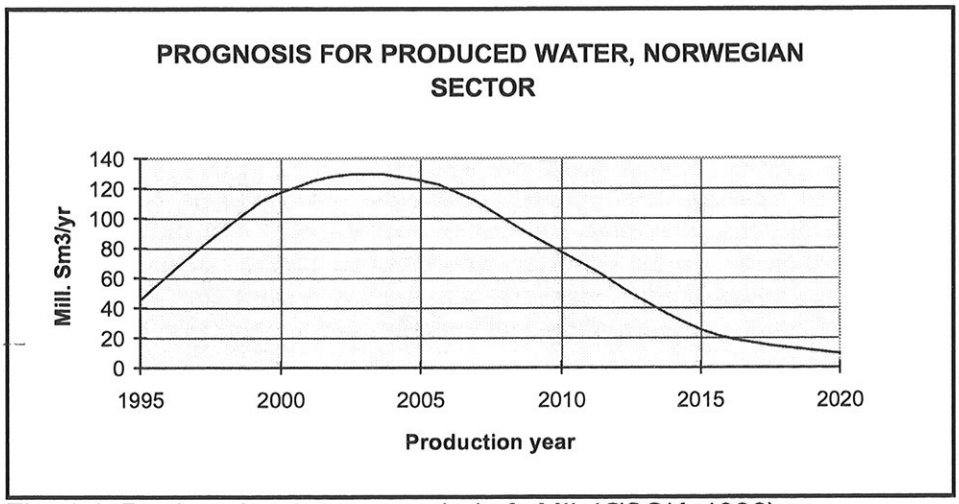

Fig. 1.1: Produced water prognosis (ref.: MILJØSOK, 1996)

Various discharges from an offshore oil and gas production platform is schematically shown in Fig. 1.2.

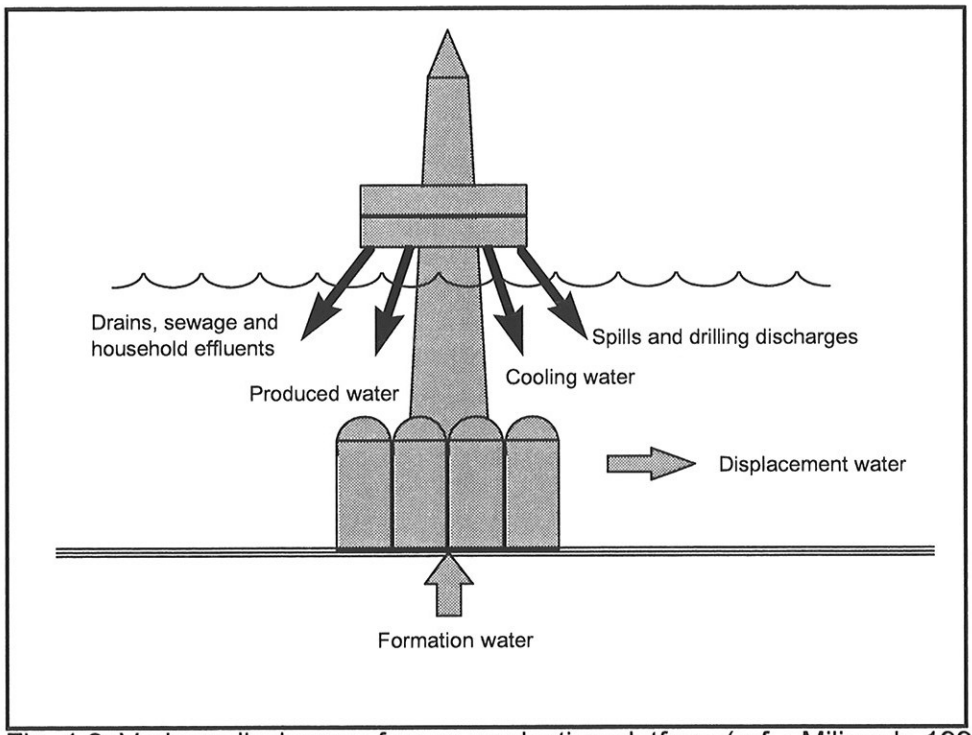

Fig. 1.2: Various discharges from a production platform (ref. : Miljøsok, 1996)

Additionally, produced water also contains various salts, dissolved gases (also hydrogen sulfide and carbon dioxide), dispersed and dissolved hydrocarbons, organic acids and heavy metals. The work presented in this dissertation is dealing with problems associated with dispersed hydrocarbons. However, produced water also contains particulate matter, mainly consisting of sand or silt.

All together this is expected to have considerable impact on the environmental aspects and on the economics of oil field development. From the environmental point of view, a major processing task in the production of oil and gas in the North Sea is therefore to achieve a best possible separation method for the water following the well stream before it is being discharged to sea. Such a separation method will also have to be simple and economic in operation.

With the increasing production of produced water, the disposal of hydrocarbons to the sea will also increase in quantity. It is therefore foreseen

that, together with the increasing demands from environmental authorities, in some near future the legislative rules for discharge concentrations will be substantially more stringent than the present allowance of 40 ppmv dispersed oil. Discharge limits of 15 ppmv dispersed oil, as well as limits for dissolved components, have been discussed in some fora (e.g. Lloyd et al, 1997).

Separation methods mostly applied until recently partially rely on large, old-fashioned coalescers. However, during the last years there has been a conversion from the traditional coalescer technology towards the technology of hydrocyclone separation, frequently with an upstream flotation cell treatment in order to increase the droplet size. Concentrations of 25 mg/l and less can be achieved today by utilizing compact centrifugal separators (centrifuges, hydrocyclones). Concentrations down to 5 mg/l can be achieved by using different filter techniques, while the last residual of dissolved oil in the water can only be removed by rather complex and expensive processes such as those based on adsorption technology (e.g. by utilization of activated carbon).

Capital costs and operating costs increase tremendously when discharge limits approach zero, and one may say that a general trend is that both the costs and the required space for process equipment increase exponentially when the effluent oil concentration limitations approach zero values.

A compact alternative to flotation cells could possibly be the application of turbulence creating equipment which, given certain conditions, may facilitate and promote coalescence and thereby contribute to larger drops for improved separation.

1.2 Problem description

The majority of the new hydrocarbon resources which have been discovered are located within a distance of 50 km from existing or planned infrastructure with process facilities. These fields are most likely to be developed as satellite fields, either by subsea systems or (unmanned) wellhead platforms.

Fig. 1.3 shows a schematic of a typical process for well stream treatment on an offshore platform. Usually there are three separator stages, and an electrostatic coalescer to meet export quality for the oil. Oil, water and gas are separated in each of the stages. The 1st stage operates with the highest pressure, frequently 70 barg or so; the 2nd stage 20 barg, and finally the 3rd stage is near atmospheric conditions. The produced water is further treated in hydrocyclone vessels to meet the discharge levels of 40 ppm oil-in-water.

Improved separation of bulk water as far upstream as possible, preferably at the wellhead or even down in the well, prior to choking and multiphase transportation to a mother platform will:

- reduce the requirement of chemical inhibitors (against hydrates, corrosion, wax, scale), and hence reduce the discharge of such chemicals to the sea.
- reduce the need for water processing capacity on a mother platform. Limitations on water processing capacity have already been foreseen on some processing platforms of today.
- reduce pipeline dimensions, and hence the costs, as transport capacity is released due to the more or less total absence of water. When most of the water is removed at the wellhead, the flow to be transferred through the pipeline will decrease throughout the field life, matching the typically decreasing wellhead pressure. If water is not removed, the pipeline capacity requirement will be high when the driving pressure is low, possibly introducing the requirement for compressors and pumps.
- improve the separation efficiency as the wellstream pressure and temperature is not reduced prior to separation. Maintaining the pressure, hence avoiding the detrimental effects of shear forces in chokes and valves, is beneficial since existing oil droplets are not broken up into smaller and more stable fragments. Also, by maintaining the high temperature there will be less foaming, and the viscosity of the continuous phase will not be increased. Hence, according to Stokes' law, separation of the two liquid phases will be easier. The total effect is larger droplets

and better separation compared to what is the case in conventional systems.

- facilitate and improve the production control of the individual wells as the individual phases can be measured separately . A test separator, or possibly a separate well test pipeline, will then not be required.

This work is motivated by the above mentioned objectives.

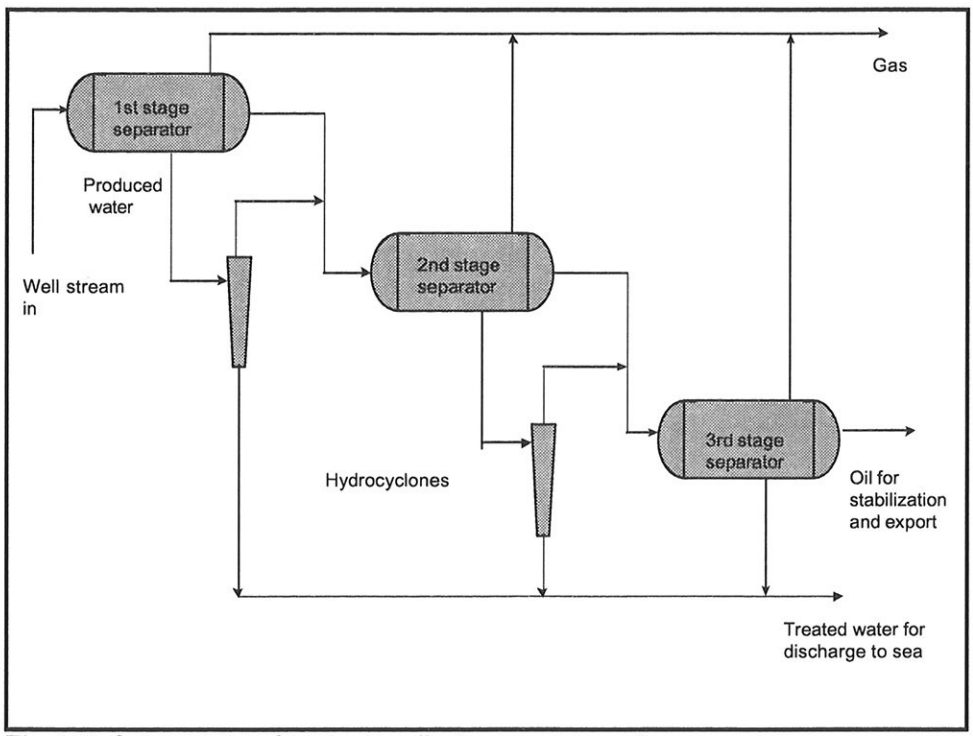

Fig.1.3: Schematic of typical well stream processing

High separation efficiency, relative to weight and size, is therefore the prime achievement in compact well stream separation systems. However, such systems are also typically characterized by conditions of high turbulence and high shear forces, which normally are considered to represent such detrimental effects on droplet breakup that it would be beneficial to minimize these. It is suspected, however, that some turbulence would be beneficial in order to achieve enhanced coalescence of droplets in a liquid/liquid system, and therefore achieve better subsequent separation.

It would be of interest to find such an optimum level of turbulence for enhanced coalescence. However, turbulent properties alone may not be sufficient, and it would also be of interest to investigate the possibility of chemical stimulation.

Often significant pressure losses in the separation system can be encountered, thus inducing gas release that may impose certain effects on the liquid/liquid separation. The pressure loss may for instance take place in a well stream choke. Here, in addition to the shear forces acting on droplets, the shift in equilibrium will dictate gas to be released. However, it has been suspected that some gas can reduce the degree of shear in the liquid dispersions, which obviously is beneficial from a separation point of view. It seems that if just some gas is released, e.g. in a valve, this will act as an "energy sink", thus possibly "protecting" the dispersed liquid phase from shearing. It would therefore be of interest to investigate such «turbulence promotion» as a method for reduced shear effects to liquid droplets.

Droplet break-up and coalescence will be counteracting effects in the separation process where two or more different liquids are present. Finding the relation between droplet shear and amount and size distribution of gas bubbles, and thus determine such a critical gas introduction to a liquid/liquid system, would be of great interest.

Interesting emerging technologies have been applied to promote/demote coalescence and should be looked further into. For example, it has been found that bubble/droplet coalescence can be promoted in sound wave or microwave based vibrational environment, in addition to the more conventional electrostatic fields.

Droplet shear, and subsequent binding mechanisms between different liquid phases, are of great importance in the understanding of phenomena such as emulsion formation and demulsification. And, when gas is introduced in turbulent environment, it is of importance to have an understanding of the foam formation mechanisms, as well as the shear inhibition effects and droplet growth. It is known that interfacial surface tension is an important parameter in this context, and it would be of interest to relate this to prevailing process conditions. However, this will not be studied in detail in this work.

Earlier work (e.g. Hinze, 1955; Coulaloglou & Tavlarides, 1977; Davies, 1985; Chesters, 1991; Kumar, Kumar & Gandhi, 1992) has shown that the main

parameters that affect movement and collision rates of drops and bubbles are, the drop/bubble collision frequency, drop/bubble diameter and size, shear rate, viscosity, density difference and water cut. There are several empirical equations describing coalescence probability with certain parameters.

Many of these empirical equations are limited in the sense that they only take into account one parameter at a time. Many academics have also been working with the desire to establish a successful relationship that could describe coalescence as a function of several parameters simultaneously.

In this work it has been desirable to look at binary liquid systems, e.g. consisting of water and oil, with the introduction of a relevant gas. Air has been used for our experiments, but it would be desirable to extend this to also include methane. It is of particular interest to study the effects of elevated pressures and temperatures, P = 10 bara; T = 20 - 90 deg. C.

The simultaneous influence of two or more of the above mentioned parameters have been studied in this work.

Scope of work and methodology

Based on the problem description outlined above, the scope of work for the dr.ing. thesis is the following:

- Effect of flow structure and chemical additives on coalescence.

- Effect of gas formation and chemical additives on droplet breakup.

The droplet coalescence and breakup rates are functions of the continuous fluid phase flow structure, possibly described by the turbulence intensity and length scale, of the physical properties of the system; viscosity, density and interfacial tension, and of the departure from equilibrium, i.e. the mass transfer taking place in the system. All these parameters will be characterized.

The main tool for flow characterization, both for the continuous and for the dispersed phase, has been Laser Doppler Anemometry (LDA). LDA does not differentiate between continuous and dispersed phases, but by means of natural (or artificially added) seeding particles, the flow pattern may be

identified in terms of local velocities and turbulence intensities. Additionally, a Malvern particle analyzer was used for determining droplet size distributions.

1.3 Present Technology Status

The purpose of this subchapter is to evaluate the performance of treatment technologies for removing oil from oilfield produced waters. A number of processes based on different technologies are commercially available, and they all have their advantages and disadvantages in some respects.

Expert discussions are frequently concerned about comparing technologies on the basis of low effluent oil concentration. However, other features, such as: (1) capital and operating costs, (2) space requirements, (3) operating complexity, and (4) maintenance, add or detract to the utility of the processes.

There are four deoiling processes that will be particularly treated since they appear to represent the most capable and advanced equipment technologies. The four processes are: (1) the static hydrocyclone, (2) the centrifuge, (3) ceramic membrane filtration, and (4) granular resin coalescing filtration. Of these, the hydrocyclone is the most developed and tested, while the granular resin filtration is the least developed and tested. The centrifuge is probably the most complicated in terms of fabrication and maintenance requirements.

1.3.1 Process Comparisons of Three Recognized Technologies

1.3.1.1 The Hydrocyclone

The Hydrocyclone has been tested and verified at hundreds of oilfield produced waters (e.g. Gullfaks, Statfjord, Snorre, etc.). It is now the leading deoiling system. It weighs less and requires less power than the same capacity of corrugated plate separator, dispersed gas flotation (DGF) or a coalescing filter separator. As for the costs, it is usually assumed that the hydrocyclone represents comparable or higher capital costs than gas flotation, whereas the operating costs are lower. Manpower requirements tend to be less than for gas flotation.

The operational principle of a hydrocyclone (see Fig. 1.4) is based on the achievement of centrifugal forces many orders of magnitude greater than in

conventional gravity based deoiling equipment. Oily water enters the unit tangentially into a cylindrical swirl chamber, where the fluid is accelerated through the reducing tapered sections of the cyclone proper.

The centripetal forces cause migration of the lighter oil droplets inwards to the lower pressure center core where an axial reversal of this flow takes place. The heavier bulk clean water moves outwards by centrifugal forces. The reject oily stream leaves the unit axially near the inlet end, while the clean water discharges as a continuous stream from the opposite downstream end.

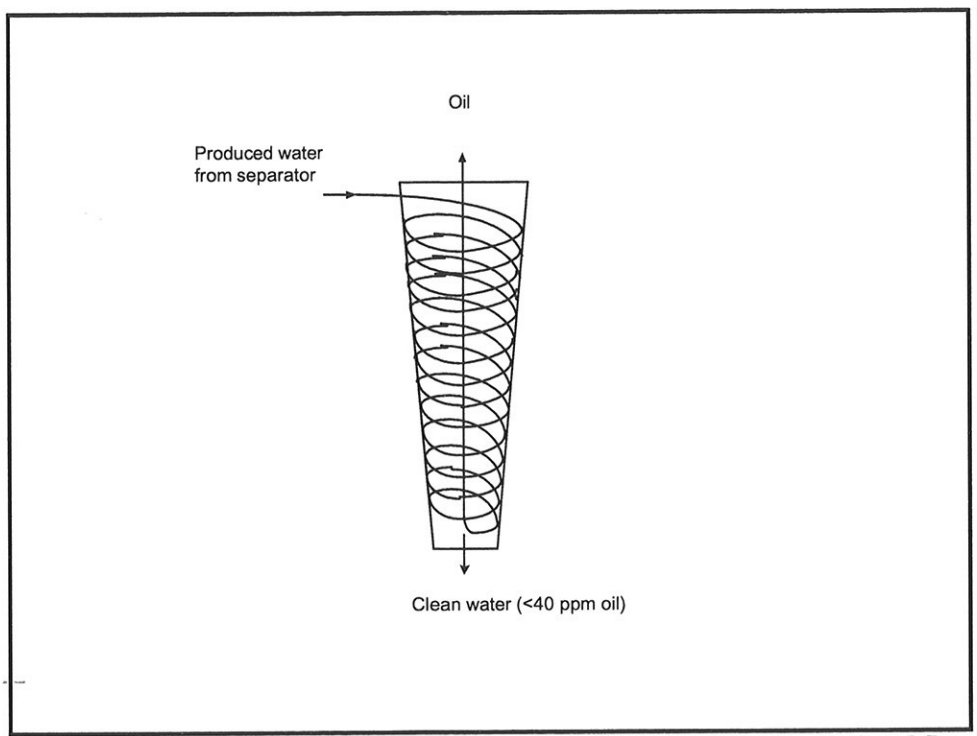

Fig. 1.4: Schematic of operational principle of a hydrocyclone (Ref.: ABB miljø).

Total residence time of the liquid in a hydrocyclone is about 2 seconds (Davies & Palmer, 1995). In contrast, the residence time in a floatation cell is about four minutes at rated capacity. Several hydrocyclones can be mounted in one pressure housing for increased capacity. Thus the number of hydrocyclones in a housing can be varied to maximize oil removal efficiency for a given flowrate. When single hydrocyclones are mounted such, they are

often termed as «liners». It is common to install 50 -100 or more liners in a pressure vessel.

The most frequently mentioned advantages of the hydrocyclone are (1) lower maintenance, and (2) often less chemical requirements. However, other attractive features include: (1) fast response time, (2) less space requirements, and (3) lighter weight. Unfortunately, they require a pumped feed when the gas/liquid separator pressure drops below 5 - 7 barg.

1.3.1.2 The Ceramic Membrane Filter

This unit consists of a number of microporous ceramic elements mounted in a housing. Being a vendor of this concept, the Canadian company ALCOA reports that each element has a number of longitudinal holes which are lined with thin ceramic layers containing very small pores. Water flows through the longitudinal holes, then perpendicular to the fine pores and the wall of the element. Most of the suspended solids and oil cannot pass through the pores and are carried out of the element by the reject stream.

To reduce plugging of the small pores a scheme known as cross flow filtration is employed. Cross flow means that a portion of the influent flows across, or parallel rather than perpendicular, to the face of the filter media, and carries a large portion of the objectionable suspended and dissolved solids out in the waste stream. Another portion of the influent passes through the filter media and becomes the very clean filtrate, called permeate.

Total flow to the membrane is much larger than the permeate volume because of the cross flow process. As a result membrane filters require larger pumps and connected power than coalescers of similar capacity.

Some manufacturers report on extremely high quality filtered water. However, the solids and oil removed by the filter gradually block the pores, thus restricting flow. To maintain a constant stream of filtered water it is necessary to increase the inlet pressure during the cycle.

To retard this plugging action the units are fitted with some special back-pulsing and fast flushing systems to remove the filter cake. Although this technique slows plugging, the pressure drop slowly increases. When it reaches some critical value, e.g. 2 - 2.5 barg, the unit must be chemically cleaned with acid to remove acid solubles, and caustic to remove the oil.

It has also been found that pretreating the raw water with unspecified chemicals retards the plugging action. Thus, the membrane filter package consists of the filtering elements, plus skid-mounted pretreatment and chemical cleaning facilities. Adding capital and operating costs the process is therefore not considered economically competitive with dispersed gas flotation.

1.3.1.3 Granular Resin Coalescing Filter

This kind of coalescing filter is also a significant development in the water deoiling field. This unit reduces the trace oil concentration in the treated water to levels lower than the current coalescing technology because of the oleophilic nature of the resin. The ability to remove water soluble organics is poorly reported (ref. Kværner).

In principle, according to Kværner, being a supplier of this type of equipment, such a unit is just a newer version of the well known oil coalescing separator, which is utilizing the oleophilic resin media. The media has usually been walnut shells, graded gravel, layers of crushed anthracite and gravel, or sand. Previous designs are either upflow or downflow, with either monobed (one grade of media) or multi-layer (different grain sizes) deep beds.

The novel coalescing medium is a synthetic ion exchange resin. Oleophilic groups are attached to a portion of the available exchange sites. These groups are strongly held, and are not removed over a pH range of 2 to 12. Furthermore, the resin is stable in strong brine solutions.

Oily water passes downward through the media bed where oil droplets coalesce on the resin beads. Coalescence is intensified by the low interfacial surface tension between the oil and the resin. An oil film develops on the resin surfaces until it reaches a critical thickness when it is removed by the flowing water. Gradually the whole resin bed becomes saturated with oil starting from the top and extending downward to the bottom. From that time until the resin is backwashed the amount of oil leaving the bed is equal to the amount of oil entering.

The enlarged drops exit the bottom of the bed and flow up through the center tube where they pass through a secondary coalescer. Here, the drops coalesce further into even larger drops. When the water carrying the larger drops exits the center tube, oil/water separation occurs according to Stokes' law.

The rising velocity of the oil droplets is enhanced because they are much larger than the oil droplets entering the coalescer. According to Stokes' law the rising velocity is proportional to the square of the droplet diameter. Therefore, according to this theory, if the average oil droplet size were

increased from 10 to 50 microns, the rising velocity would be increased 25-fold. Similarly, if the diameters were increased from 50 to 2000 microns, the rising velocity would be increased 1600-fold. However, documentation has not been found on whether it is realistic to achieve such values.

This unit will probably only have application to onshore installations because of the need for backwash facilities requiring space, which is at a premium on offshore platforms. Also, there may be problems with the formation of «mud balls», which may necessitate a complete replacement of the resin bed (ref. Kværner).

Backwashing requires: (1) at least one parallel train to carry the load during backwashing, (2) a backwash pump, (3) a backwash surge tank, (4) a backwash return pump, and (5) all the necessary piping and controls.

The backwash requirements may be the single most important disadvantage of the resin coalescer as a deoiling device for offshore platforms.

1.3.2 Less Advanced or Limited Technologies

Other oil removing technologies that are tested or reported in literature are briefly mentioned below:

Carbon Filters remove some water soluble organics, but has higher capital and operating costs than dispersed gas flotation (DGF).

Centrifugal Separators may show good performance, but may have questionable oilfield durability, and represent relatively high capital and operating costs. Requires less space and weighs less than DGF.

Biological Oxidation removes some water soluble organics, but requires excessive space, and has higher operating costs and manpower requirements than DGF.

Electrocoagulation is designed primarily for treating heavy industrial waste water high in suspended solids and biological oxygen demand. Reported to be tested in oil shale tar sand waste water. Requires post treatment settling tank and/or filter.

Rotary Hydrocyclone contains many rotating parts presenting potential offshore maintenance problem. In this unit, where the cyclone chamber comprises the rotating part, performance data is reported to be comparable to the stationary hydrocyclone, or even outperform it, but the latter leads in number of units installed and under construction. The rotary hydrocyclone requires more space than does the static hydrocyclone, and is not yet developed for high pressure applications.

Solvent Extraction is a method where raw water, containing as much as 500 ppm of dispersed and/or dissolved crude oil, commingles with a stream of clean water mixed with natural gas and a solvent (e.g. Freon), before entering a flotation unit. Extraction methods are commonly in use to separate petroleum products that have different chemical structures but about the same boiling range. In extraction the solvent must be recovered for reuse (usually by distillation), and the combined operation is more complicated and often more expensive than other similar methods, e.g. ordinary distillation without extraction. However, extraction does offer more flexibility in choice of operating conditions, since the type and amount of solvent can be varied as well as the operating temperature.

Recently there have been some successful investigations in using supercritical fluid extraction, where natural gas (LNG) fractions are used as the solvent in a supercritical state to extract dispersed and dissolved hydrocarbons from produced water to be treated by hydrocyclones. The supercritical state offers improved solvent properties, and reduces the overall density of the hydrocarbon phase in produced water, increases the density difference between water and hydrocarbons and thus improves the separation efficiency of hydrocyclones.

1.3.3 Current Produced Water Treatment Technology

Until hydrocyclones became common in produced water treatment, the best single and the most widely used technology was dispersed gas flotation. It is now assumed that the static hydrocyclone has taken over this leading role. Late model designs of DGF, which minimized moving parts and generated the highest gas/water ratios, produced very good results. The reduction of moving parts helped to reduce maintenance costs, an important factor for remote and offshore operations.

Production of clean produced water is basically considered being a three-step process. It frequently starts with the selection of an emulsion breaking chemical that will produce saleable oil and as clean water as possible from the oil/water separator, i.e. a coalescer. Basic Sediment and Water (B.S.&W.) in the oil, often set to 0.5%, rather than oil content of the produced water, is often the criteria in selecting an emulsion breaking chemical. Considering today's need for clean water for enhanced oil recovery (EOR) projects and discharge to sea, the emphasis in selecting an emulsion breaker should however rather be on water quality as well as on the lowest B. S. & W.

The three ideal steps in deoiling are as follows:

Primary separation in an oil/water separator using chemicals to enhance emulsion breaking.
A second stage separator unit for initial removal of dispersed oil down to < 2000 ppm.
A third stage separator unit for final removal of dispersed oil to meet the requirements set by environmental authorities (presently < 40 ppm oil in water, and possibly < 25 ppm later).

The two latter steps are now commonly equipped with static hydrocyclone units. In older technology, or where there is insufficient pressure available, gas flotation units are frequently applied.

Additional process units will have to handle produced sand giving erosional problems, and provisions for chemical injection , e.g. for the purpose of achieving less tear and wear on pipes and pumps as well as other process equipment. Appropriate units will also have to be installed for other particular purposes, e.g. pressure release, gas treatment, flare utilities, etc.

CHAPTER 2 EXPERIMENTAL SETUP AND TECHNIQUES

2 EXPERIMENTAL SETUP AND TECHNIQUES

2.1 General

Having in mind the main aim of obtaining improved oil/water separation in compact well stream separation systems, the particular objective of this work was to study the phenomena of droplet breakup and coalescence, and relate these processes to the effect of turbulence intensity and local velocities.

In studying the effects of turbulence intensity on various phenomena, e.g. droplet breakup and coalescence, it was required to have a measurement control volume with flow conditions being as uniform as possible. It was therefore essential to establish an apparatus that had, as far as possible, a characterizable and homogeneous turbulence level throughout its total volume.

It was believed that an appropriate unit to conduct such experiments was a static mixer, since a fairly narrow droplet size distribution is achieved when mixing two immiscible fluids in such a mixer. With reference to brochures from Sulzer Chemtec, a narrow droplet size distribution points towards a rather homogeneous turbulence level.

Contact was made with Sulzer Chemtec, and upon explaining the problem Sulzer kindly offered to send some appropriate static mixers free of charge.

CHAPTER 2 EXPERIMENTAL SETUP AND TECHNIQUES

Hence, the Sulzer static mixers were selected for the experimental trials performed in this work.

For characterization of turbulence intensity, this was done by means of laser techniques, a Laser Doppler Anemometer (LDA), model Flowlite from DANTEC, was applied.

Other required analysis instruments were made available likewise. Hence, droplet size distribution was determined by means of laser diffraction techniques, i.e. by use of the Malvern Particle Analyzer.

Analyses based on use of LDA and Malvern instrumentation are both well established techniques.

Principle of setup is depicted in Fig. 2.1.

However, the Malvern analyses were not done online, as it may appear in this schematic. Rather, samples were taken from the test rig, and given time to stabilize before analysis was performed.

CHAPTER 2 EXPERIMENTAL SETUP AND TECHNIQUES

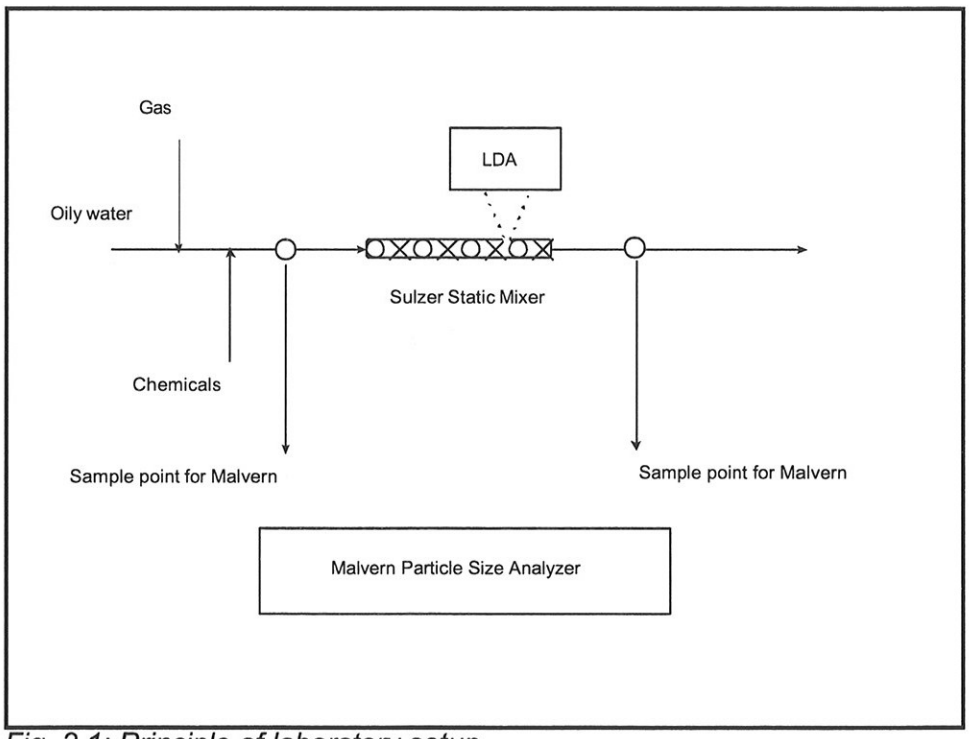

Fig. 2.1: Principle of laboratory setup

2.2 Experimental flow scheme

The flow scheme of laboratory test set-up is depicted in Fig. 2.3. Filtered tap water as the continuous phase was introduced into the 1" polyethene (PE) pipeline system at a maximum rate of 25 liters pr. minute and, if required, preheated in a plate heat exchanger (Alfa-Laval, model CB51-40H, Two-pass). In order to facilitate a variation in the water temperature, a 12 kW electric heating was provided (Norske Backer, model IU313RK). This unit, consisting of 3 x 4 kW electric coils, ensured a range in the water temperature of 10 to 90 deg. C. Alternatively, heating was affected by adding steam to the 2nd pass of the heat exchanger.

From a 60 liter mixer tank the dispersed phase, e.g. oil, was added to the heated water via the ½" polyethene pipeline system at a rate up to 5% by volume of the water. This oil was injected into the water line by means of a

membrane dosing pump (type SERA), via a buffer volume of approximately ½ liter in order to reduce the pulsations from the pump.

This mixture of oil and water was then conducted to the bottom of a vertically mounted static mixer unit (type SULZER SMV DN 15). This unit consisted of six mixing elements with diameter 15 mm. Each of the elements were 60 mm long, which again consisted of 15 mm long subelements with a 90 deg. offset to each other. Four of the 60 mm pieces were soldered together, whereas the remaining two were placed 12 mm apart. All the elements were fitted within a barium silicate glass tube. The internal diameter and the height of the glass tube were 17 mm and 550 mm, respectively.

A square transparent «cooling jacket« made of plexi glass, and filled with stagnant water, was fitted along the outer diameter of the glass tube. The purpose of this water filled jacket was to avoid undesired deflection of the measuring laser beam as it passed through the concave wall of the glass tube.

The setup of the static mixer is given in Fig. 2.2, where also the basic dimensions are stated.

CHAPTER 2 EXPERIMENTAL SETUP AND TECHNIQUES

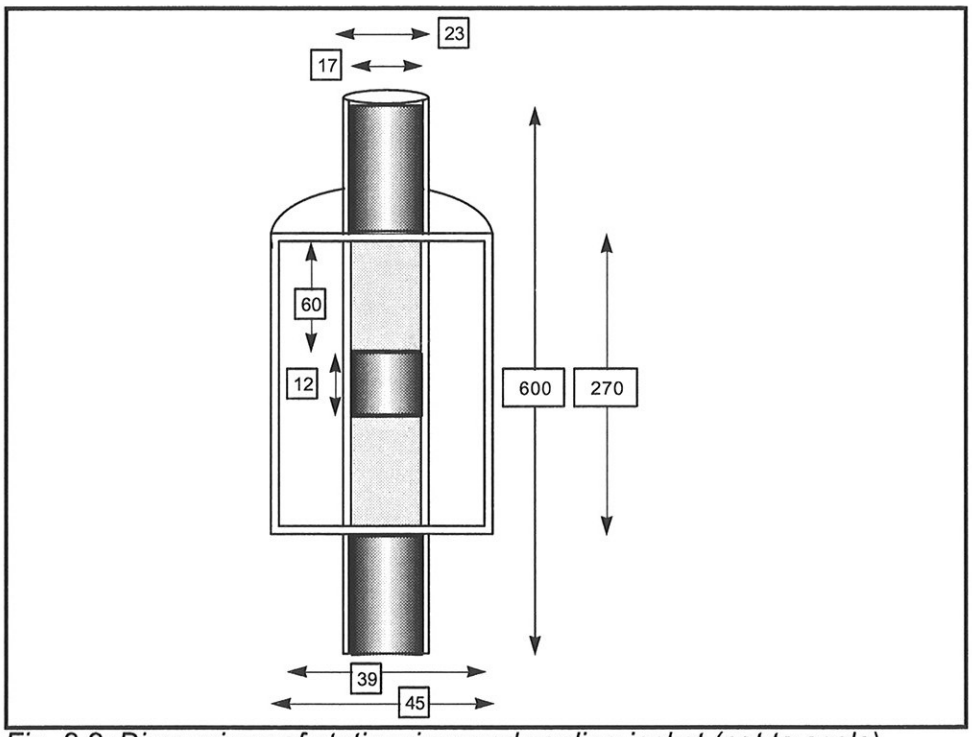

Fig. 2.2: Dimensions of static mixer and cooling jacket (not to scale)

After being conducted through the glass tube, the heat contained in the oil/water mixture was recovered in the heat exchanger before being disposed off into the 1 m^3 discharge tank. Oil was recovered from the mixture and conducted into a separate tank by means of a decanting method from the discharge tank.

The pump's dosing rate was determined and controlled by the inlet water rate to the system. This was done by imposing a frequency converter on to the pump motor. Thus, milliampere signals from the turbine flow meter on the water side controlled the pump motor via the frequency converter.

Data were logged into the PC 1 via the control panel were: Pressures and temperatures upstream and downstream of the static mixer unit; differential pressure across the static mixer unit; water and oil flowrates.

The 12 mm separation distances between mixer elements served as measurement volumes where the LDA laser beams were directed. Hence,

after the raw data had been processed in the PC 2. Local mean velocities (v_{mean}), root mean square velocities (v_{rms}) and turbulence intensities (I) were found by the DANTEC software at different points along pre-determined vertical (at points 2 mm apart) and horizontal trajectories (at points 1 mm apart) of the laser beam.

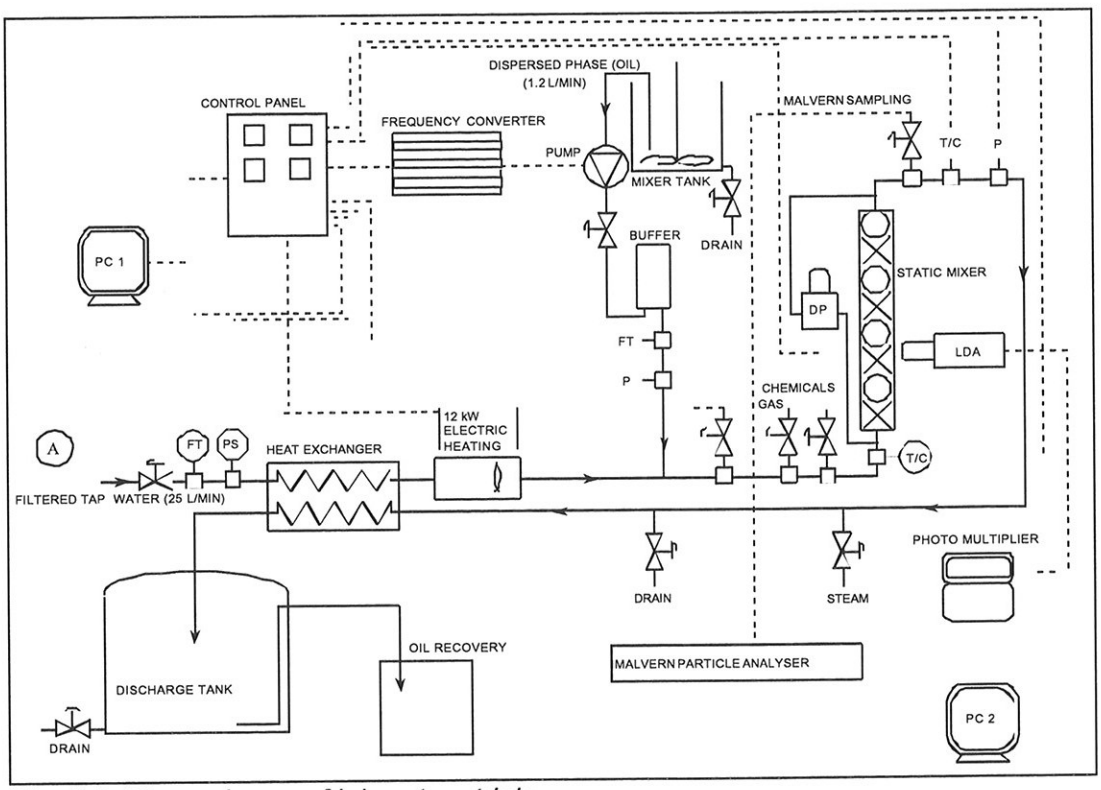

Fig. 2.3: Flow scheme of laboratory trials

For examination of drop size distribution and coalescence effects, samples are taken manually upstream and downstream of the static mixer unit for analyses in the Malvern particle analyzer.

To study the effects of gas introduction and chemical additives, the system has provisions for such also.

For the case of oily water (in terms of dispersed oil in water), the system depicted in Fig. 2.3 a) is added at the point denoted A in Fig. 2.3:

CHAPTER 2 EXPERIMENTAL SETUP AND TECHNIQUES

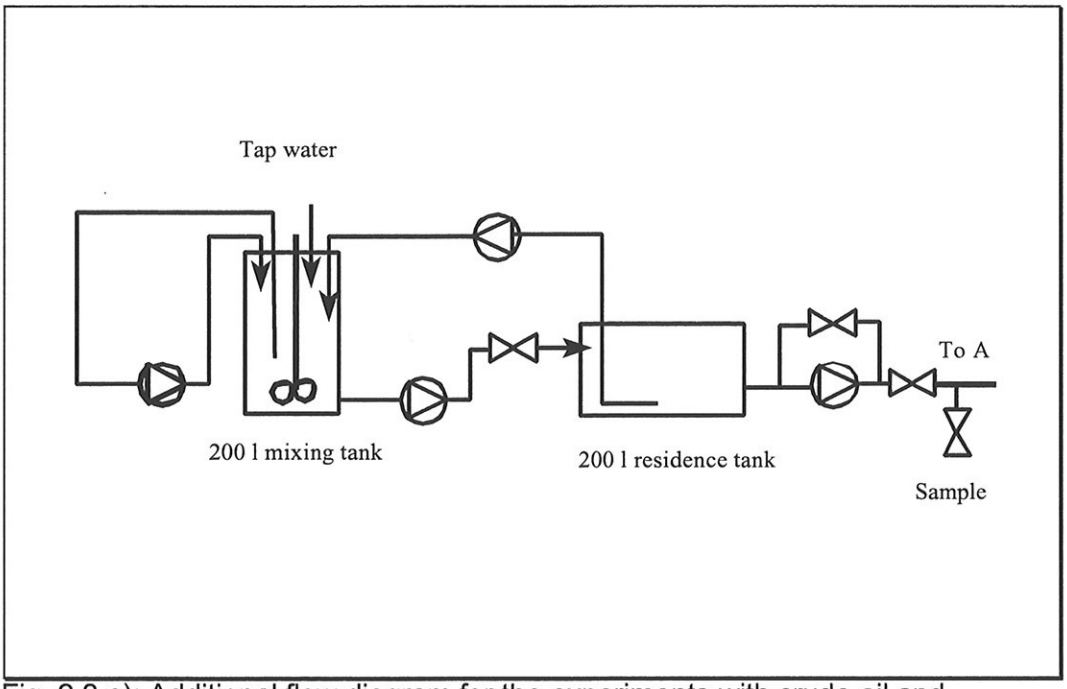

Fig. 2.3 a): Additional flow diagram for the experiments with crude oil and water

2.3 Principles of Laser Doppler Anemometry

As a measuring technique, having the advantage of not imposing any disturbances on the flowing system, Laser Doppler Anemometry (LDA) is considered to be rather appropriate for the characterization of turbulence and precise determination of local flow velocities.

This section presents some of the basic principles of LDA. Most of this material is collected from the instruction manual for the DANTEC LDA instrument.

2.3.1 Configuration of apparatus

Configuration of apparatus is shown in Fig. 2.4. The beam from the continuous HeNe laser is split into two plane parallel beams, and one of the beams is given a frequency shift by a Bragg cell. The two beams pass

through a fibreoptic cable and a spherical lens (transmitter), and they intersect within the measurement volume. The scattered light is received by a spherical lens (receiver) and is converted to an electrical signal using a high speed photodetector. The signals were processed with the software program from Dantec, using a personal computer.

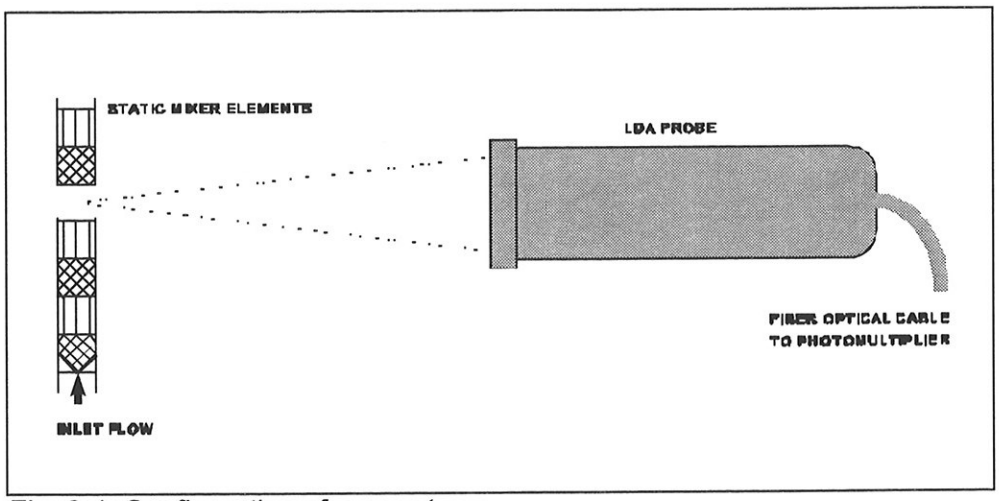

Fig. 2.4: Configuration of apparatus

Laser beams are focused by the LDA probe's front lens to cross at the intersection volume of the two laser beams.

Light scattered by particles traveling through a portion of the intersection volume were collected by the front lens and focused on the end of a fiber optical cable. This cable carried the collected light to a photomultiplier at the other end of the cable. The photomultiplier converted the light to electrical signals that are sent to the signal processor. From here they are sent to the computer for analysis and presentation.

2.3.2 Doppler burst

The two laser beams originates from a single beam that is split. The two resulting beams are focused to cross each other at a given angle so that they are coherent to each other in the volume of their intersection. If a particle traverses this volume, and a photo detector is arranged to receive light

scattered from a source in this volume, the received light will consist of two components, one corresponding to each of the beams.

Both components will have a Doppler shift due to the velocity of the particle. However, the shift is also dependent on the direction of the light beam. Since the two beams are at an angle, the two components of the scattered light have different Doppler shifts. At the surface of the photo detector, therefore, the two light components interfere, resulting in a pulsating light intensity.

This is illustrated in Fig. 2.5, where a particle is shown in two positions resulting in constructive and destructive interference, respectively. While the frequency of the electric field of the light would be too high for the photo detectors to follow, the frequency of this pulsating intensity can be well resolved.

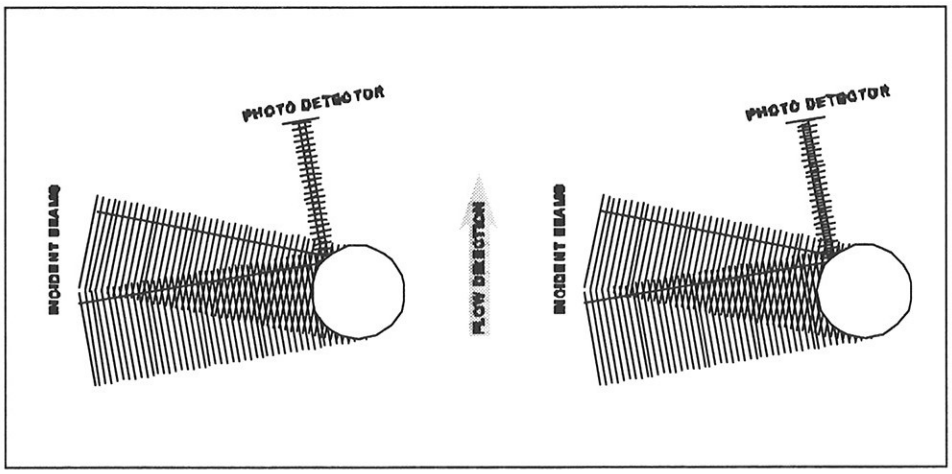

Fig. 2.5: The interference at the surface of the photo detector is dependent on the position of the particle in the intersection volume formed between the two crossing beams.(Ref.: DANTEC User Manual).

2.3.3 The fringe model

When two coherent laser beams intersect, they interfere in the volume of intersection, forming interference fringes. If, as illustrated in Fig. 2.6, the beams intersect in their respective beam waists, the wave fronts are nearly plane. Consequently, the interference fringes will be parallel, which has the

implication that a uniform velocity-frequency relationship is achieved over the entire intersection volume.

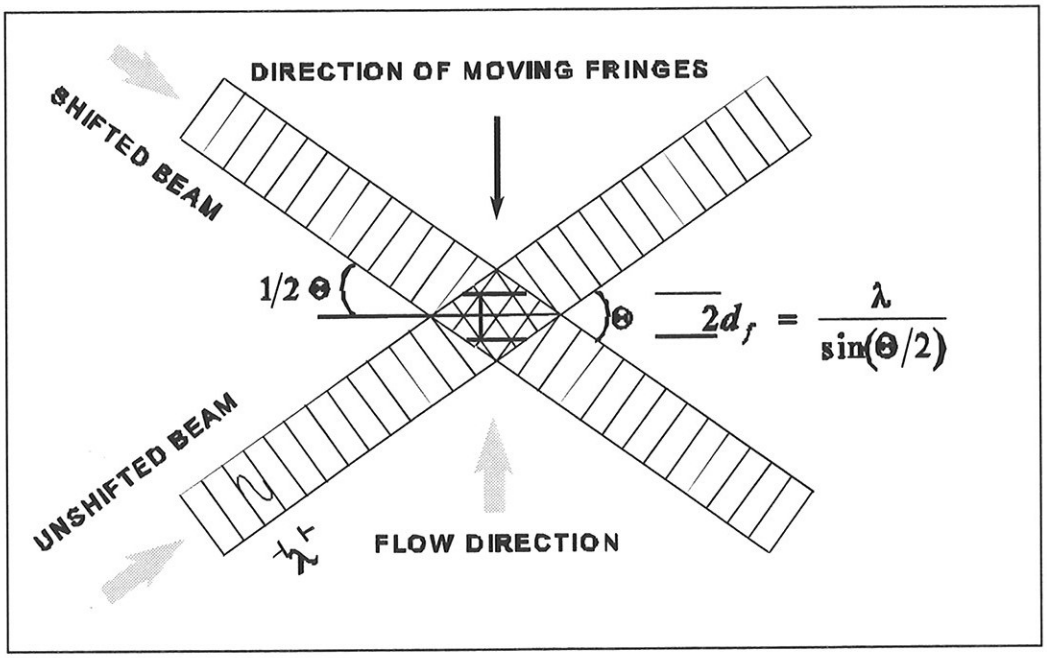

Fig. 2.6: Fringes formed where two coherent beams cross(Ref.: DANTEC User Manual).

As illustrated in Fig. 2.7, the intensity of the scattered light received by the photo detector pulsates along with the particle passing through the fringes. This pulsation has a frequency which is directly proportional to the velocity component at right angles to the fringes.

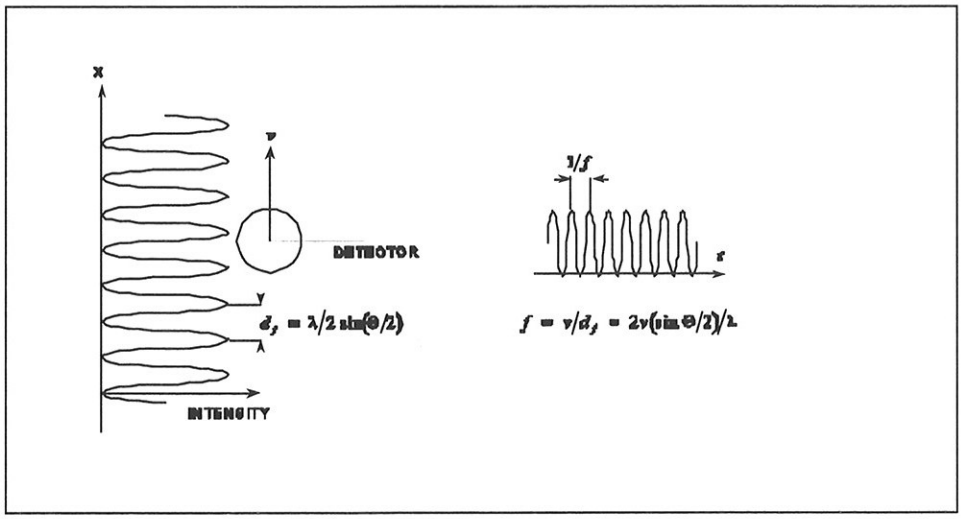

Fig. 2.7: Fringe model description of the Doppler frequency showing relationship between fringe separation, particle velocity and burst frequency. (Ref.: DANTEC User Manual).

2.3.4 Directional ambiguity

The proportionality between velocity and Doppler frequency is also shown in Fig. 2.8. Also, the frequency is not dependent on the sign of the direction of the velocity. Positive and negative velocities of the same magnitude will result in the same Doppler shift.

$$f_D = v_x\left(\left(2\sin(\Theta/2)\right)/\lambda\right) \qquad (2.1)$$

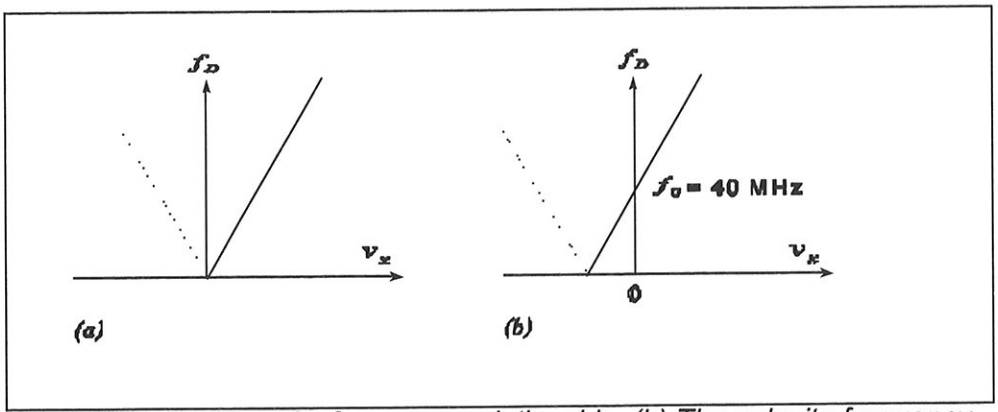

Fig. 2.8: (a) The velocity-frequency relationship, (b) The velocity-frequency relationship with frequency shift. (Ref.: DANTEC User Manual).

To overcome this problem, the frequency of one of the two crossing beams is shifted. Consequently, the fringe pattern is no longer stationary, but moves at a constant velocity. This means that the photo detector will see the scattered light from a stationary particle as pulsating at a frequency equal to the shift frequency.

Furthermore, a particle traveling against the fringes will produce Doppler bursts of a higher frequency than the shift. Similarly, a particle traveling in the same direction as the fringes will produce a lower frequency than the shift, as illustrated in Fig. 2.8 (b). In this case we have:

$$f_D = f_0 + v_x\left(\left(2\sin(\Theta/2)\right)/\lambda\right) \qquad (2.2)$$

From Fig. 2.8 (b) it is seen that, provided the bandwidth is sufficient, if the shift frequency is increased, the spread of velocity within a population of particles that can be handled also increases. This means that larger turbulence intensities can be measured.

2.3.5 Bragg cell

In the equipment used for these experiments, a shift frequency of 40 MHz is applied. This shift is achieved by letting the beam pass through a Bragg cell. The Bragg cell also functions as a beam splitter.

2.3.6 Recorded values from the LDA measurements

The following values from the data processing algorithms are recorded when doing the LDA measurements:

Mean velocity,

$$\overline{U} = \frac{\sum U_i}{N} \tag{2.3}$$

where $i = 1, 2, 3, \ldots N$ total number of samples

Variance,

$$\sigma^2 = \overline{u^2} = \frac{\sum_i \left(U_i - \overline{U}\right)^2}{N} \tag{2.4}$$

Root mean square velocity,

$$\sigma = \sqrt{\overline{u^2}} \tag{2.5}$$

Turbulence intensity,

$$T = \frac{\sigma}{U} \times 100 \tag{2.6}$$

2.4 The Malvern Particle Size Analyzer

2.4.1 Principles

In these experiments, the Malvern series 2600, as well as the Mastersizer have been used to analyze the size of oil droplets. The Malvern instruments are light scattering based particle size sensors. As explained in the Malvern instruction manuals, the analysis system comprises an optical measurement unit that forms the basic particle size sensor, and a computer that manages the measurement and performs result analysis and presentation.

CHAPTER 2 EXPERIMENTAL SETUP AND TECHNIQUES

Laser light scattering is a flexible sizing technique, which in principle is capable of measuring the size structure of any one material phase in another. It is only required that each phase must be optically distinct from the other and that the medium must be transparent to the laser wavelength. This means that the refractive index of the material must be different from the medium in which it is supported.

The instrument is based on the principle of laser ensemble light scattering, and fall into the category of non-imaging optical systems since the sizing is accomplished without forming an image of the particle onto a detector. The optical method employed by the instrument is called «conventional Fourier optics», where light from a low power Helium-Neon laser is used to form a collimated and monochromatic beam of light. This beam of light is known as the analyzer beam and any particles present within it will scatter this laser light.

The light scattered by the particles and the unscattered remainder are incident onto a receiver lens, also known as the range lens, which operates as a Fourier transform lens forming the far field diffraction pattern of the scattered light at its focal plane. Here, a detector, in the form of a series of 31 concentric annular sectors, collects the scattered light over a range of solid angles of scatter.

The unscattered light is brought to a focus on the detector and passes through a small aperture in the detector and out of the optical system. The total laser power passing out of the system is monitored, allowing the sample volume concentration to be estimated.

The range lens configuration has the useful property that wherever the particle is in the analyzer beam, its diffraction pattern is centered on the range lens optical axis. Thus, it does not matter that a particle is moving through the analyzer beam. Its diffraction pattern remains stationary and centered on the axis. Also, it does not matter where in the analyzer beam the particle passes. Its diffraction pattern is always constant at any lens distance.

In practice, there are many particles simultaneously present in the analyzer beam, and the scattered light measured on the detector is the sum of all individual patterns overlaid on the central axis. The system thus inherently measures the integral scattering from all particles present in the beam. In a typical experiment the number of particles needed in the beam simultaneously

to obtain an adequate measurement of the scattering would be somewhere between 100 and 10000, depending on their size.

Thus, an instantaneous measurement of the scattering would give a size distribution based only on the small cross section of the material. Two problems may then arise: 1) Inadequate statistical significance, and 2) possibly unrepresentative sampling of the bulk material. This is avoided by time averaged observation of the scattering as the material is continuously passed through the analyzer beam.

As material flows through the beam, the measured light scattering is continuously changing forming the instantaneous integral of the material illuminated by the analyzer beam. By making many measurements of the detector readings (sweeps), and averaging over many such sweeps of the detector, it is possible to build up an integral light scattering characteristic based on a very large number of individual particles. In this manner it will not take many seconds to build up acceptable measurements.

The detector provides an electronic output signal proportional to the light energy measured over 31 separate solid angles of collection. The computer reads these signals and performs the time averaging by successively reading the detector over a period of time set by the operator and summing this data.

When a particle scatters light, it produces a light intensity which is characteristic of the angle of observation. It scatters light so that the measured energy on the detector has a peak at a favored scattering angle which is related to its diameter and surface properties. Large particles have peak energies in small angles of scatter and vice versa.

The setup of instrumentation is as depicted in Fig. 2.9 below:

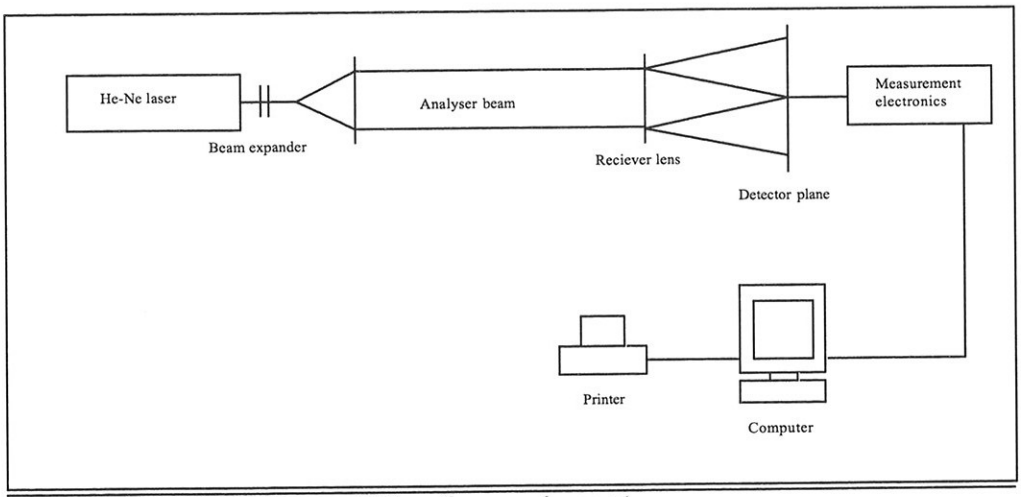

Fig. 2.9: MALVERN Laser Diffraction equipment

The optical measurement unit comprises an optical transmitter, a receiver and an optical bench. The transmitter houses the laser, its power supplies and the beam expanding optics that create the analyzer beam. The receiver houses the range lens, the detector and associated electronics and computer and computer interfaces. Each of the housings is mounted to the optical bench which purpose is to maintain the mutual alignment of the transmitter and the receiver.

The measurement area should be relatively near to the range lens (approx. 3 - 5 cm in our case) since, as the particles to be measured get further away from the range lens its scattering spreads over a larger extent until finally it cannot be collected by the lens. This distance limit, known as the vignetting distance, is different for each lens and sets the part of the analyzer beam useful for measurements.

2.4.2 Procedure for conducting trials, sampling and analysis

Bearing in mind the objective of identifying the small, in-dispersion-stable droplets only, the following procedures were applied for the model oil and Statfjord crude oil, respectively.

Both when applying the model oil and the Statfjord crude it was important to achieve an experimental method that ensured removal of most of the larger

droplets, i.e. those with diameters larger than 40 microns. Having larger particles included in the samples would significantly decrease the accuracy in determining the small droplets.

In order to maintain the small droplets that were to be analyzed, and prevent these from coalescing into larger droplets, it was considered essential to find a method to take care of this. Therefore, it was decided to pursue a method that, at the same time, kept the smallest droplets stable in suspension until analyses had been done. This method consisted of adding a stabilizing agent into the suspension, thus keeping the size of the small droplets in the samples, then carry the samples into the laboratory for droplet size analysis.

By referring to a «base case», where no stabilizing agents were added, a relative measure of the experimental results were achieved hence.

In conducting the trials, the following procedure was applied:

- Filtered tap water was entered into the system at specifically desired flowrates, maximum 25 liters/minute.
- If heating of the water was desired, this was accomplished either by adding steam into the 2nd pass of the heat exchanger, or alternatively by electric heating. (It turned out that it was easier to achieve temperature control by using steam; hence this was eventually the preferred method).
- A dispersion of oil and water, in predefined concentrations, was made in advance by using a high speed mixer (Ultra Turrax) in order to achieve small droplets. This dispersion was emptied into a 60 liter dispersion tank, where it was further diluted and mixed with water, and continuously mechanically stirred in order to maintain the droplets in suspension.
- The diluted dispersion was then injected from the tank into the water line by means of a membrane dosing pump, via buffer volume of approx. ½ liter to reduce the pulsation from the pump.
- The dispersion was further conducted to the bottom of a vertically mounted static mixer unit (type SULZER SMV DN 15), consisting of a 17 mm glass tube containing six 60 mm long mixing elements (diameter 15 mm). In the measurement area the glass tube was enveloped by a flat faced, water containing jacket, whose purpose was to ensure that undesired beam deflection did not occur due to the concave glass tube wall.

CHAPTER 2 EXPERIMENTAL SETUP AND TECHNIQUES

The sampling procedures applied to determine the droplet size were slightly different when using

- EXXSOL D60 model oil in dispersion, and
- Statfjord crude oil in dispersion.

The sampling procedures applied in the two cases are described in the following subchapters.

When using the EXXSOL D60 model oil, a number of droplet stabilizers were tried. A table of the trials performed with the different stabilizing agents is presented as follows (Table 2.1). A further description, as well as discussion, of the experiments and the applied stabilizing agents is given in Ch. 6.

Test series	Malvern Recordings No.	Surfactant:	Method of analysis - Comments	Flowrate water, Q_w (l/min)	Flowrate EXXSOL D60, Q_o (l/min)	Temp., deg. C
1	110 - 112	NaLS, 3 g/l	Peristaltic injection and magnetic stirrer	13	0.3	9
2	120 - 132	Igepal 100, 12 g/l	Peristaltic injection and magnetic stirrer	13	0.3	9
3	140 - 152	Igepal 50, 10 g/l	Peristaltic injection and magnetic stirrer	13	0.3	9
4	160 - 172	Polyvinylalcohol, 15 g/l	Peristaltic injection and magnetic stirrer	13	0.3	9
5	180 - 192	Polyvinylalcohol, 15 g/l	Peristaltic injection and magnetic stirrer	13	0.3	9
6	200 - 212	Mix.Igepal 100 (12 g/l) and DSSNa (2 g/l)	Peristaltic injection and magnetic stirrer	13	0.3	9
7		Igepal 100, 12 g/l	Reproduction trials of test series 2	13	0.3	9
8		Polyvinylalcohol, 15 g/l	Reproduction trials of test series 4	13	0.3	9
9		Mix.Igepal 100 (12 g/l) and DSSNa (2 g/l)	Reproduction trials of test series 6	13	0.3	9

Table 2.1: Trials performed with the different stabilizing agents for the EXXSOL D60 Model oil

2.4.2.1 Sample procedure when using EXXSOL D60 model oil in dispersion

The procedure described below was applied to sampling when using the EXXSOL D60 model oil in dispersion. In Ch. 6, which deals with the effect of

chemical additives, there is given a further description of the preparatory procedure, sampling and analysis.

1. Approximately 40 ml droplet stabilizing agent (see Table 2.1) was added to each of the three 500 ml (scaled) separatory funnels, which were filled with Exxsol D60 oil/water dispersion samples taken from the outlet of the static mixer. The stabilizing agent was applied to ensure that the smallest droplets remained in suspension until analyses had been done, thus preventing undesired coalescence.
2. The fine dispersion of model oil in water, made by the Ultra Turrax hig speed mixer, was then dispersed into the tap water by using a LEWA membrane dosing pump. The static mixers ensured further dispersion of the oil before sampling.
3. The separatory funnels, containing the samples, were then transported to the laboratory where the Malvern instrument was located. One separatory funnel was mounted with sufficient fluid head to allow for free flow into the Malvern measurement cell (i.e. by gravity injection through the cell.).
4. A motorized stirrer was constantly applied with a fixed low speed within the separatory funnel, to ensure a homogeneous suspension of the droplets that had not already risen to the surface.
5. The sample was allowed to rest approximately two minutes before the Malvern analysis was performed. The two other separatory funnels were mounted likewise with continuous stirring, waiting for their turn in the Malvern analysis.
6. At the instant of sampling into the separatory funnels, a stopwatch was applied, and all times were recorded hence.
7. It took approximately three minutes effectively, for analysis of each of the separatory funnels. It also took approximately three minutes from the instant of sampling at the static mixer rig, until the first Malvern analysis was done at the 500 ml indicator line (at the separatory funnel glass).
8. Malvern analyses were then further repeated for every 400, 300, 200 and 100 ml fluid levels in the separatory funnel.

2.4.2.2 Sampling procedure when using Statfjord crude oil in dispersion

Crude oil contains naturally stabilizing constituents, such as asphaltenes, waxes, etc. Hence, further addition of synthetic agents was not considered

necessary. Apart from this, the sampling procedure was similar to what is described in the previous section 2.4.2.1.

CHAPTER 3 TURBULENCE & DROPLET SIZE DISTRIBUTION IN STATIC MIXERS

3 TURBULENCE & DROPLET SIZE DISTRIBUTION IN STATIC MIXERS

3.1 Introduction to turbulence theory

3.1.1 General

Because of its importance in many branches of engineering, turbulent flow has been extensively investigated in recent years, and a large amount of literature has accumulated on this subject. Refined methods of measurement, such as the LDA-technique, have been used to follow in detail the actual velocity fluctuations of the eddies during turbulent flow, and the results of such measurements have shed much light on the nature of turbulence.

In general, turbulence can result either from contact of the flowing stream with solid boundaries (called *wall turbulence*), e.g. when flowing through channels or past solid shapes immersed in the stream; or from contact between two layers of fluid moving at different velocities (called *free turbulence*), e.g. a flow of jet trough a stagnant fluid.

3.1.1.1 Reynold's stress

CHAPTER 3 TURBULENCE & DROPLET SIZE DISTRIBUTION IN STATIC MIXERS

Turbulence alters the flow regime so much that the traditional «bulk» or Newton shear stress given by $\tau = \mu(du/dy)$ is not significant. The *apparent shear stress*, or *Reynolds stress* , which is due to local velocity differences and therefore exists wherever there is a velocity gradient across a shear plane, is being related to the fluctuating parts of the velocity by

$$\tau_{app} = -\rho\overline{u'v'} \tag{3.1}$$

where $u', v' =$ deviating velocities in the x and y directions, respectively. The bar over these denotes an average over a period of time.

This may be related to the more general form including the temporal mean velocity distribution (Roberson & Crowe, 1975):

$$\tau_{app} = \rho l^2 \left(\frac{du}{dy}\right)^2 \tag{3.2}$$

where $l =$ the mixing length, shown by the Prandtl mixing length theory to be essentially proportional to the distance from the wall $(l = \kappa y)$.

Although flow within an eddy is laminar, turbulence may be viewed as an energy transfer process where large eddies are continually formed, and break down into smaller eddies, which in turn evolve into still smaller ones. Finally, the smallest eddies, being 10 to 100 µm in diameter, disappear due to viscous shear.

3.1.1.2 Local velocities

Instantaneous local velocities, e.g. measured by LDA are defined by

$$u_i = u + u' \quad v_i = v' \quad w_i = w' \tag{3.3}$$

where $u_i, v_i, w_i =$ instantaneous total velocity components in x, y and z directions, respectively

$u =$ constant net velocity of stream in x direction

$u', v', w' =$ deviating velocities in x, y and z directions, respectively

In one-dimensional flow, the terms v and w are omitted.

The time averages vanish over a time period t_0, since for every positive value of a fluctuation there is an equal negative value:

$$\frac{1}{t_0}\int_0^{t_0} x'\,dt = 0 \qquad \text{where } x = u, v, w \tag{3.4}$$

However, the mean square is not zero, e.g.

$$\frac{1}{t_0}\int_0^{t_0} u'\,dt = \overline{(u')^2} \tag{3.5}$$

which only vanishes when turbulence does not exist.

Turbulent fields are characterized by the intensity of the field, referring to the rotational field of the eddies and the energy contained therein, and the size or scale of the eddies. A value for the turbulence intensity is obtained by measuring the root-mean-square of a velocity component, and relating this as a percentage of the mean velocity. The scale of an eddy in the y direction may be calculated by the integral

$$L_y = \int_0^{\infty} R_{u'}\,dy \tag{3.6}$$

where a function of the distance between two stations 1 and 2 is defined by the correlation coefficient

$$R_{u'} = \frac{\overline{u'_1\,u'_2}}{\sqrt{\overline{(u')^2}\,\overline{(v')^2}}} \tag{3.7}$$

3.1.1.3 Laminar and turbulent flow in boundary layers

CHAPTER 3 TURBULENCE & DROPLET SIZE DISTRIBUTION IN STATIC MIXERS

A boundary layer is defined as that part of a moving fluid in which the fluid motion is influenced by the presence of a solid boundary. Such conditions are prevailing in static mixer units. The fluid velocity at the solid-fluid interface is zero, and the velocities close to the solid surface are small. Very near the surface the flow is therefore essentially laminar, although there may occasionally be some temporary disruptions from eddies released from the main flow. Further away from the solid surface the velocity increases, and may in fact be relatively large. Flow in this part of the boundary layer may therefore become turbulent. There will also be a transition zone in between the laminar and turbulent flow conditions, which may be characterized by the Reynolds number .

3.2 Drop sizes formed in turbulent flow

It is often desirable to know something about the sizes of drops that are formed in the pipe. Knowledge of some kind of average size is often sufficient, although sometimes the distributions of sizes is required. A value for the upper limit of stable drop size is useful for several reasons, e.g.: 1) The maximum stable drop size d_{max} can itself be used in place of the average drop size for making conservative estimates of mass transfer rates; 2) Under some conditions, it may be possible to relate an average drop size to d_{max} . Failure to take into account the existence of an upper limit in estimates of a drop size distribution function may lead to considerable error; 3) Knowledge of d_{max} and the way in which drops are broken in a pipe may be valuable for comparison with results of theories of turbulence.

3.2.1 Isotropic turbulence and droplet breakup

When the root-mean-square components are equal for all directions at a given point, the turbulence situation is said to be *isotropic*, i.e. $\overline{(u')^2} = \overline{(v')^2} = \overline{(w')^2}$. Nearly isotropic turbulence exists when there is no velocity gradient, as at the centerline of a pipe or beyond the edge of a boundary layer. Turbulent flow near a boundary is anisotropic, but the anisotropy occurs mainly with the larger eddies. Small eddies, especially those near destruction from viscous action, are practically isotropic. When conditions are such that isotropic

conditions may be assumed, expressions for energy dissipation rates are convenient to use.

As stated by Keey (1967) mixing can be interpreted with the isotropic turbulence theory, when the time-smoothed velocity components are independent of direction. Homogeneous turbulence occurs when the time-smoothed variables are independent of position. The length of the region within which velocity fluctuations are significantly correlated is considered to be a characteristic eddy size, and is called the scale of turbulence.

If the length of an eddy is of order λ and its velocity is of order V_λ, then the corresponding eddy Reynolds number is

$$\mathrm{Re}_\lambda \approx V_\lambda \lambda / \nu \qquad (3.8)$$

For extensive eddies Re_λ is large and thus the viscosity does not influence the motion. In particular, there can be no appreciable viscous dissipation of energy in such eddies (Levich, 1962). The viscosity of the fluid becomes determinative only when Re_λ is in the order of unity or less. The upper limit of the corresponding eddies is then given by this dissipation scale, thus given by $\lambda_0 \approx \nu / V_\lambda$.

The energy dissipation therefore occurs within a range of frequencies, called the universal equilibrium range, which are not excited by external forces, but owe their existence to inertial interactions of large-scale motions. The energy is self-adjusting through inertial forces within this range, and is uniquely determined by the «external» parameters ε/ρ and ν. The kind of motions involved here are assumed to be isotropic.

As noted by Thomas (1981), turbulence eddies are considered in three categories, in decreasing size: 1) energy-containing range, 2) inertial subrange, 3) viscous range. In this order, energy is envisaged as cascading from small to large wave number components of the flow.

The velocity and length scales of the energy-containing eddies are identified with: 1) turbulence intensity, u (usually around 5% for pipe flow and boundary layers), and 2) the integral scale, l (usually around 10% of flow width).

CHAPTER 3 TURBULENCE & DROPLET SIZE DISTRIBUTION IN STATIC MIXERS

The Kolmogoroff energy-spectrum function may be used to describe a homogeneous turbulence. Such a function may take the form

$$E(k) = \alpha \varepsilon^{2/3} \overline{k}^{5/3} \tag{3.13}$$

and the microscale (taken as the Kolmogoroff lenght):

$$\eta = \left(\nu_c^3 / \varepsilon\right)^{1/4} \tag{3.14}$$

As reported by El-Hamouz et al. (1994), Kolmogoroff's theory (1949) on isotropic turbulence was pioneering in explaining drop-breakup. The theory was found to yield an expression (Hinze, 1955) for the maximum particle size of the dispersed phase, assuming that the smaller eddies produced by the dissipative process are statistically independent in size from the primary eddies, and assuming isotropic conditions.

In the breakup of a drop there are two principal influences to be considered: a disruptive stress tending to cause deformation and breakup of the drop and a surface force tending to resist deformation. The disruptive stress could be of viscous origin, or more usually be a dynamic pressure due to turbulent flow. The surface force resisting deformation is due to interfacial tension. In turbulent flow, drop breakup is brought about by variations in velocity and therefore stress at the surface of a drop.

The mechanism of Reynolds stresses depends on the deviating velocities in anisotropic turbulence, and may be measured by the correlation coefficients of the type given in eqn. (3.7).

3.2.2 General approach

G. Hetsroni (1983) has given an introduction to drop sizes in turbulent flow. An extract from his work will be presented here.

Most theoretically based relationships for drop sizes in turbulent flow are based on Kolmogoroff's theory of homogeneous isotropic turbulence. It is postulated that in a turbulent system there is a wide range of eddy sizes, and

energy is transferred from the larger to the smaller. The smaller eddies are responsible for the greater part of the energy dissipation in the system and, for high Reynolds number, are independent of the motion of the main stream. Under these conditions the smaller eddies, of scale Z, may be characterized by the energy dissipation per unit mass of the system, ε. For the condition that the scale of the region under consideration, D, is much smaller than L_L and much larger than Z, i.e. $L_L >> D >> Z$, then the root mean square (RMS) of the velocity difference between two points D apart, $\bar{u}$, can be written similarly to eqn. (3.11):

$$\bar{u} = (\varepsilon D)^{1/3} \quad \text{or} \quad \varepsilon = \frac{\bar{u}^3}{D} \tag{3.20}$$

where D is the drop diameter.

Eddies of the inertial subrange are largely independent both of the large-scale geometry of the flow and of the small-scale dissipative eddies, and has the function of simply conveying energy upwards through the wavenumber spectrum. Their structure is supposed to be the same for all flows with the same energy dissipation per unit mass, ε, which can be measured by pressure drops in flowing systems, or alternatively from the above relation (3.20) (Batchelor, 1953) allowing D to be representative for the integral scale previously termed as l.

From the Kolmogoroff-Hinze prediction of maximum bubble size, it is supposed that a bubble of diameter d breaks up if a critical Weber number of order unity is exceeded (i.e. a condition for pressure fluctuations to overcome capillary forces which tend to keep the bubble intact).

In an alternative approach, Hinze (1955) defined a critical droplet Weber number at which breakup occurs, i.e.:

$$We_c = \frac{\bar{u}^2 D_{max} \rho}{\sigma} \tag{3.22}$$

where $\bar{u}$ is the velocity difference across the droplet.

CHAPTER 3 TURBULENCE & DROPLET SIZE DISTRIBUTION IN STATIC MIXERS

It is usually observed that bubble sizes are such that $\left(\nu^3/\varepsilon\right)^{1/4} << D << l$, so one expects droplet breakage to be effected by eddies in the inertial subrange, which have no intrinsic velocity or length scale.

By using eqn. (3.20), a maximum drop size above which breakup would occur is determined:

$$D_{max} = C_2\left(\frac{\sigma}{\rho_c}\right)^{0.6}\varepsilon^{-0.4} \tag{3.23}$$

and has the same form as the relationship proposed by Kolmogoroff. This expression is valid provided the drop size is much greater than the Kolmogoroff scale of turbulence. Using the observation that $D_{max} = 2D_{32}$ (where D_{32} is the Sauter mean diameter) one may also obtain alternative expressions for the average drop size, e.g.

$$D_{32} = K\left(\frac{\sigma}{\rho_c}\right)^{0.6}\varepsilon^{-0.4} \quad \text{or} \quad D_{max}\left(\frac{\rho_c}{\sigma}\right)^{3/5}\varepsilon^{2/5} = C \tag{3.24}$$

which has been confirmed to be valid for low dispersed phase holdups by a number of investigators (Mersmann & Grossmann, (1980), Langner et al., (1979), Koglin et. al. (1981)). At higher volumetric ratios of the dispersed phase, this equation is usually corrected by incorporating a factor that accounts for the attenuation of turbulence intensity (Doulah, 1975), and the increasing possibility of coalescence (Delichatsios & Probstein, 1976). Little systematic investigation has been undertaken to study the kinetics of liquid dispersion and it has been generally assumed that the equilibrium, between the dispersive and the coalescive processes, is quickly reached. However, this may not be true (Langner et al., (1979), Arai et al., (1977)), and in some cases, constant dispersion characteristics are achieved only at very long mixing times (e.g. two hours in agitators).

Because of the many theoretical and experimental problems that arise in the study of drop size, discrepancies in correlating constants are not surprising. At high values of holdup, it is difficult to develop techniques that can clearly discriminate all the drops present because of the large numbers in any

sample. In addition, the mechanism of droplet breakup and coalescence is complex. Thus the question of the correlation of drop size data for turbulent flow is as yet completely solved.

However, Baird & Lane (1973) found $K=0.357$ in their reciprocating plate column, which is comparable with static mixers. Kubie & Gardner (1977) found $K=0.725$ for D_{max} in smooth pipes, which is practically identical results considering that it is frequently found that $D_{max}=2D_{32}$. This was also confirmed by Hinze (1955), using the data of Clay (1940).

3.2.3 Dispersion and energy dissipation in static mixers

As pointed out by Goldshmid, Samet & Wagner (1986), turbulent dispersion is the act of spreading out of fluid particles by random fluid motion, which, from a macroscopic point of view, is associated with eddy structure, ranging in size from very large to very small. In general, the largest eddies transfer energy to the smallest by what is believed to be a cascade process. The cascade process is also related to the scale reduction phenomenon through eddy breakdown, followed by an increase in the interfacial area and transport of momentum and mass.

Al Taweel & Walker (1983) reports that for static mixers, it has previously been found (Middleman, 1974) that the mean drop size could be expressed as a function of the Weber and Reynolds numbers:

$$\frac{D_{32}}{D}=KWe^{-0.6}\,\mathrm{Re}^{0.1} \qquad (3.27)$$

where D is the pipe diameter. This expression was deduced for a Kenics static mixer, which is geometrically different from the Sulzer mixer. Changes in the dispersed phase volume fraction, between 0.005 and 0.5, were found to exert no appreciable effect on the characteristics of the resulting dispersion. However, a similar relationship was reported (Streiff, 1977) using Sulzer static mixer elements. The exponents of the dimensionless groupings, however, are different:

$$\frac{D_{32}}{D} = 0.21 We_h^{-0.5} \mathrm{Re}_h^{0.15} \tag{3.28}$$

where the subscript h refers to the application of hydraulic diameter of mixing element channels, D_h. Matsamura et al. (1981) reported Weber number exponents varying between -0.57 and -0.67 with the numerical value of the proportionality constant, K, being dependent on the viscosity of the emulsion.

Static mixers differ from conventional mixing systems. Thus, whereas mechanically agitated dispersion equipment permits the value of ε to be varied independently from the flow rate of the fluid phases, this is not the case when static in-line mixers are used. The energy dissipated through turbulent fluctuations must be extracted from the main stream resulting in a loss of pressure. The rate of energy dissipation per unit volume is therefore a strong function of the velocity at which the fluids are pumped through the mixer.

For a fluid passing through a length L of static mixer at a volumetric flow rate Q, the residence time τ is given by:

$$\tau = \frac{\pi D^2 L}{4Q} = \frac{L}{V} \tag{3.29}$$

where V is the velocity of the fluid passing through a mixer of diameter D. The rate of energy dissipation per unit mass contained in the mixer becomes:

$$\varepsilon = \frac{4Q\Delta P}{\pi D^2 L \rho_c} = \frac{V\Delta P}{L\rho_c} \tag{3.30}$$

and

$$E = \tau\varepsilon = \frac{\Delta P}{\rho_c} \tag{3.31}$$

where E is the energy dissipation per unit mass of fluid pumped through the static mixer.

The Weber number is generally defined as:

$$We = \frac{\rho_c V^2 D}{\sigma} \tag{3.32}$$

and the friction factor as:

$$f = \frac{D\Delta P}{2\rho_c V^2 L} \tag{3.33}$$

Substituting eqns. (3.32) and (3.33) into (3.24) gives:

$$\frac{d_{32}}{D_h} = KWe^{-0.6} f^{-0.4} \tag{3.34}$$

The relationship between f and Re should depend on the type of mixer as well as the regime of flow. For pipe flow at $\mathrm{Re} \geq 3000$, $f \propto \mathrm{Re}^{-0.25}$, which may be substituted into eqn. (3.34) to yield the expression obtained by Middleman (eqn. (3.27)). At the other extreme, the data reported by Pahl & Muschelknautz (1982) indicate that for many static mixers $f \propto \mathrm{Re}^{-1}$ for $\mathrm{Re} \leq 10$. This proportionality would result in a Reynolds number exponent of 0.4 in eqn. (3.34). Since the relationship between the friction factor and the Reynolds number may also be design-dependent, its form should not be used a priori. The use of eqn. (3.34) instead of the rather limited form of eqn. (3.27) could help to reconcile some of the experimental differences between various investigators due to its more general nature.

An indicator of the efficiency of energy utilization can be obtained by comparing the free energy of the newly generated surface to the mechanical energy expended to generate it. Thus

$$\eta = \frac{6\phi\sigma}{\rho_c E}\left(\frac{1}{D_{32}} - \frac{1}{D_{32_0}}\right) \times 100\% \tag{3.35}$$

where ϕ is the volumetric fraction of the dispersed phase and D_{32_0} is the Sauter mean drop diameter upstream from the mixer (μm).

This parameter should prove beneficial in the selection of design and operating conditions which minimize the energy investment required to produce a specific degree of dispersion.

3.2.4 Effect of velocity and interfacial tension

As early as in 1962, C.A. Sleicher (1962) found a strong dependence of $D_{\max}$ on velocity, i.e. decreasing drop size with increasing velocity. He also concluded that the dispersed-phase density is not an important variable, even though in his investigations there was a slight trend toward greater stability when the dispersed phase is either lighter or heavier than the continuous phase. Hinze (1955) pointed out that when the dispersed-phase viscosity is sufficiently small, it will have no effect on drop breakup; that is viscous forces within the drop will be small compared with other forces. In the experiments of Sleicher, operating with dispersed-phase viscosities in the range 0.6 to 1.1 cP, it was shown that $D_{\max}$ was proportional to the 1.5 power of interfacial tension.

In these experiments $D_{\max}$ was nearly independent of ρ_d within the range 0.7 to 1.58 g/ml and of μ_d below about 1 cP. The velocity and interfacial tension have been shown to be important variables, and the viscosity and density of the continuous phase should be important too. Through dimensional analysis, a possible relationship among variables is

$$\frac{D_{max}\rho_c V^2}{\sigma} = B\left(\frac{\sigma}{\mu_v V}\right)^b \qquad (3.36)$$

where B and b are constants. Since it was shown that $D_{\max} \propto V^{-2.5}$, b must equal 1/2. Thus eqn. (3.36) indicates that $D_{\max}$ is proportional to $\sigma^{1.5}$, which also agrees with the data.

Since

$$\varepsilon = \frac{2fV^3}{D} \tag{3.38}$$

and throughout a wide range of Reynolds number

$$f = 0.044\left(\frac{DV\rho_c}{\mu_c}\right)^{-0.2} \tag{3.39}$$

the Hinze/Kolmogoroff relation, eqn. (3.24), can be written:

$$D_{\max}\left(\frac{\rho_c}{\sigma}\right)^{0.6}\left(\frac{V^3}{D}\right)^{0.4}\left(\frac{DV\rho_c}{\mu_c}\right)^{-0.08} = 1.9 \tag{3.40}$$

where D is the pipe diameter. According to this equation $D_{\max}$ is proportional to $V^{-1.12}$ and to $\sigma^{0.6}$. However, as Sleicher pointed out, there was disagreement between these analytical results and the experimental results due to:

- most of the variation of the dimensionless groups is caused by the variation of fluid properties
- the flow fields under investigation were different from those for which the equations were derived
- as long as marginally unstable drops always break up near the wall in the region of high shear, the Hinze-Kolmogoroff equation for drop breakup in isotropic equation cannot be applied.

3.2.5 Effect of dispersed-phase viscosity

Hinze suggested that the dispersed-phase viscosity can be taken into account by a term of the form $1 + \varphi(N_{Vi})$, where N_{Vi} is a dimensionless group that includes μ_d, and φ is a function that goes to zero as μ_d goes to zero. This form is acceptable because when μ_d is sufficiently small it will play no part in resisting deformation of the drops. Thus, eqn. (3.36) may be modified as follows:

CHAPTER 3 TURBULENCE & DROPLET SIZE DISTRIBUTION IN STATIC MIXERS

$$\frac{D_{\max}\rho_c V^2}{\sigma}\sqrt{\frac{\mu_c V}{\sigma}} = C[1 + \varphi(N_{Vi})] \tag{3.41}$$

For the viscosity group Hinze used $\mu_d/\sqrt{\rho_d \sigma d}$,where d is the drop diameter, which is a ratio of an internal viscosity force to an interfacial tension force. This dimensionless group is related to the viscosity forces that arise from the natural frequency of vibration of drops. However, since the drops become distorted to an extent far beyond the linear region of the equation for the validity for the natural frequency of vibration, the viscosity group may not be of primary importance.

The viscosity forces that are likely to be important are those that resist the stretching of a drop by the flow field. A reasonable assumption is that the rate of stretching of a drop (relative velocity of the ends of an elongated drop) is proportional to the difference of the mean fluid velocities across the drop, v. Near the wall, where the drops break up, we have:

$$v \approx 5V\sqrt{f/2} \tag{3.42}$$

where f is the friction factor for pipe flow.

For turbulent flows the variation of $\sqrt{f}$ with velocity is quite small, and the rate of stretching of the drops would be approximately proportional to the mean velocity V. Thus the force per unit area resisting the stretching is proportional to $\mu_d\,(V/d)$, which divided by σ/d is μ_d/V. This group then may be used to insert into eqn. (3.41) and to correlate the effect of μ_d.

A simple two-constant form of the function φ is $K\left(\frac{\mu_d V}{\sigma}\right)^k$. Sleicher found that $K = k = 0.7$ and $C = 38$. Thus the final correlating function becomes

$$We\sqrt{\frac{\mu_c V}{\sigma}} = 38\left[1 + 0.7\left(\frac{\mu_d V}{\sigma}\right)^{0.7}\right] \tag{3.43}$$

where

$$We = \frac{D_{\max}\rho_c V^2}{\sigma}$$

3.2.6 Effect of pipe diameter

It has been shown that gradients of the mean velocity may play an important role in the process of breakup in pipes. In addition, the eddies or fluctuating components of velocity would be expected to influence the process. However, the non-dimensionalized fluctuating components as well as the local mean velocity are approximately independent of Reynolds number, meaning that for a given bulk mean velocity the fluctuating velocities are proportional to $\sqrt{f}$, as is the relative velocity across a drop. Since, throughout a wide range of Reynolds numbers, $\sqrt{f}$ is proportional to $D^{-0.1}$ (eqn. (3.39)), the influence of pipe diameter on the breakup process is expected to be small.

3.2.7 Effect of volume fraction of dispersed phase

Volume fractions of the dispersed phase is commonly termed *holdup*. A small holdup is generally expected to have little influence on the pipe turbulence and drop breakup. As pointed out in literature (Schleicher, 1962), to avoid undesired coalescence effects one should not operate with holdups of more than 0.5%. High holdups, i.e. with values larger than 1.7%, would be expected to dampen the turbulence and thereby yield larger drops.

However, in recent experiments on vinyl chloride drops in distilled water, performed by Zerfa & Brooks (1996), it has been shown that an increase in volume fraction of the dispersed phase leads to a widening of both the volume distribution and size distribution of drops. The effect of volume fraction on the vinyl chloride drops becomes more pronounced at low turbulence intensity, where the volume distribution changes from a monomodal to a multimodal distribution. For a high turbulence intensity the distribution is mainly monomodal and the turbulence damping effect by the dispersed phase becomes less important.

CHAPTER 3 TURBULENCE & DROPLET SIZE DISTRIBUTION IN STATIC MIXERS

3.2.8 Droplet size distribution in turbulent dispersion

Unfortunately, there is not much quantitative information on mixing processes of immiscible liquids. Most of the available information is applicable only to specialized equipment or to particular liquid systems.

Due to the statistical nature of mixing, a relatively broad distribution of emulsion drop sizes is usually produced. The microscopic events occurring are extremely complex. The distribution is affected both by the breakup or dispersion process and the recombination or coalescence of drops. The demand of simultaneous treatment of these processes makes the problem almost intractable.

Sprow (1967) studied the dispersion process in the absence of coalescence by working at very small dispersed phase fractions. In this work the distribution of drop diameters produced in the vicinity of a turbine impeller was determined in a dilute iso-octane and salt water emulsion, using an electronic Coulter particle counter. A theoretical treatment based on the theory of isotropic turbulence was used to correlate the data.

Certainly, although the experimental drop size distributions are of significance themselves, if the results are to be extended to other operating conditions it is useful to fit the data to a theoretical distribution equation.

Sprow (1967) found that the best fit for his data was represented by the method of Schwarz & Bezemer (1956):

$$\ln V\% = \ln 100 + \frac{a}{d_{max}} - \frac{a}{d} \qquad (3.44)$$

where $V\%$ is the cumulative volume per cent of particles below diameter d, a is a characteristic diameter related to the maximum of the distribution function , and d_{max} the diameter of the largest drop present in the emulsion (a parameter of the equation).

CHAPTER 3 TURBULENCE & DROPLET SIZE DISTRIBUTION IN STATIC MIXERS

In considering the mechanism of droplet breakup in turbulent fields it is usually assumed that the turbulence is isotropic, at least in regions small compared to the scale of main flow, and in such cases eqn. (3.14) is a valid expression for the microscale η.

For this case, the dissipation of energy in the region of wavenumbers where shear dominates is much less than energy transfer by inertial effects.

In this region, the state of turbulence is completely described by the energy dissipation. Hinze (1955) suggested that for this situation breakup of a droplet occurs when the Weber number $We = \rho_c \overline{u^2} d_{max} / \sigma$ reaches a critical value.

3.3 Models for droplet breakup and coalescence

3.3.1 Droplet breakup

Many investigators have modeled the drop breakage process. As pointed out by Sathyagal et al. (1996), these models can be divided into two categories: (1) Models to predict d_{max}, the maximum stable drop diameter. Knowledge of d_{max} does not give any information on the dynamics of drop breakage. (2) Models for the breakage functions, $\Gamma(v)$ and $G(v,v')$. Examples of such work can be found in the works of Coulaloglou & Tavlarides (1977), Narsimhan et al. (1979), Nambiar et al. (1994) and Tsouris & Tavlarides (1994).

All of the above models make many simplifying assumptions about the flow field and the nature of breakage. The models for the breakage functions have also bee rigorously tested and their predictions compared with experimental data. Nambiar et al. have only compared their model with long time, equilibrium size distributions. In the paper by Tsouris & Tavlarides, models for the breakage functions and for the coalescence frequency have been presented and their combined predictions compared with experimental data in which both breakage and coalescence takes place. This is a much less rigorous test of the breakage model than testing the model with pure breakage experimental data.

CHAPTER 3 TURBULENCE & DROPLET SIZE DISTRIBUTION IN STATIC MIXERS

The physical and chemical phenomena taking place in a static mixer largely depend on the size of the dispersed droplets . The latter is determined by the relative contribution of breakage and coalescence mechanisms. The droplets are subject to shear stresses and to turbulent velocity and pressure variations at their interface. These processes deform the drops and may break them into smaller droplets if the dynamic forces exceed the interfacial tension forces. At the same time, these droplets are also colliding with each other and these collisions may produce coalescence if the colliding droplets remain together for a time long enough to enable the rupture of the interfacial film between the two colliding droplets. The drops will be constantly breaking up and coalescing simultaneously and after a certain time a dynamic equilibrium is reached.

A visualization of the events in a liquid-liquid dispersion is presented by Wright & Ramkrishna (1994), where, at steady state, droplet coalescence and droplet breakage are in dynamic equilibrium. There exists a maximum observed diameter, d_{max} ,and a minimum observed droplet diameter, $d_{\min}$. If a droplet significantly larger than d_{max} is formed by coalescence that droplet has a high probability of being broken in a short period of time. Likewise, if a droplet significantly smaller than $d_{\min}$ is formed it will coalesce, as further droplet breakage is unlikely. In this fashion, a steady-state drop size distribution is maintained.

As explained by Wright & Ramkrishna (1994) one may envisage that the smallest drops will be too small to break, until they have grown via coalescence for some time. It is desirable to determine the length of time of pure coalescence (i.e. coalescence in the absence of significant breakup) that dominates the evolution of the transient-size distribution.

Dispersions of one immiscible liquid in another are commonly found in chemical engineering operations. Examples of these operations include liquid-liquid extraction and dispersed phase reactions. These dispersions are commonly formed by mechanical agitation of the liquid-liquid systems. The size distribution of the drops and its dynamics in the dispersion play a very important role in the overall behavior of these systems. The processes of drop breakage and coalescence essentially determine the evolution of drop-size distributions and hence the behavior of liquid-liquid systems.

CHAPTER 3 TURBULENCE & DROPLET SIZE DISTRIBUTION IN STATIC MIXERS

A number of phenomenological models have been proposed by different investigators to describe drop breakup and coalescence in a turbulently agitated liquid-liquid dispersion. Based on these models, Coulaloglou & Tavlarides (1977) developed breakage and coalescence rate functions to solve the general population balance equation describing drop interactions in a continuous flow vessel. They found favorable agreement between experimental observations and the model, which also encouraged prediction of dispersion properties such as drop size distributions, interfacial areas and mixing frequencies.

The framework of population balances has been widely used to study the process of drop breakage. In the population balance approach, breakage events of each individual drop are taken into account, providing a mathematical equation for the evolution of the number density in drop size in a purely breaking dispersion. For a batch stirred liquid-liquid dispersion undergoing drop breakage, the balance equation can be written in terms of the cumulative volume fraction, $F(v,t)$ as (Sathyagal et al., 1996):

$$\frac{\partial F(v,t)}{\partial t} = \int_{v}^{\infty} \Gamma(v')\, G(v,v') \partial_{v} F(v',t) \qquad (3.51)$$

Successful use of this equation to quantitatively predict the transient drop-size distributions requires knowledge of two key phenomenological functions: the drop breakage rate, $\Gamma(v)$ for a drop of volume v, and the cumulative daughter drop distribution, $G(v,v')$ from the breakage of a parent drop of volume v'.

There have been numerous experimental and computational studies of drop breakage in low Reynolds number (creeping flow), well-defined flow fields in the fluid mechanical literature. Typical examples of these studies are the papers by Rumscheidt & Mason (1962), Stone & Leal (1989) and Tjahjadi et al. (1992). These papers illustrate the complexity of the drop-breakage phenomenon even in these well-defined flow fields. While such studies contribute to some insight on drop breakage, they are irrelevant for the behavior of dispersions. Studies have shown that the turbulence in a stirred vessel is inhomogeneous (Cutter, 1966). This makes it very difficult to specify

the flow field and hence, to use fluid mechanics to determine the drop-breakage functions $\Gamma(v)$ and $G(v,v')$.

Another approach to determine the drop-breakage functions has been to directly observe breakage events in a stirred dispersion. Konno et al. (1983) used high-speed photography to observe drop breakage. The major drawback of this approach is that it is almost impossible to measure a sufficient number of breakage events to get a statistically meaningful result. Konno et al. measured less than a hundred breakage events.

However, two possible mechanisms of the liquid-liquid dispersion are usually considered: 1) breakup controlled by viscous forces, first studied by Taylor (1934) where the equilibrium drop size was considered to be

$$d_p \propto \sigma/\tau \tag{3.52}$$

and 2) breakup controlled by inertial forces, first investigated by Hinze (1955). According to his dimensional analysis, the equilibrium drop size is supposed to be a function $d_p = f(\sigma,\rho,\varepsilon)$, which takes the form of a power correlation:

$$d_p \propto \sigma^{3/5}\rho^{-3/5}\varepsilon^{-2/5}$$

It is inevitable to discuss bubble/droplet breakup without giving a short introduction to the fundamental work of Hinze (1955). He claimed that in turbulence, it is the kinetic energy of the turbulent motion in the continuous phase that brings about the breakup of the other phase. The disintegration process takes place in stages. A mechanism proposed to such disintegration of liquids, to emulsification, and to atomization, is the penetration of lamellae and ligaments of one fluid into the other. These ligaments then break up into globules, which may further split up into smaller parts. He systematized the various ways in which single globules can break up, and found an expression for the average value of the maximum globule size that can withstand the forces of a known hydrodynamic flow field.

In analyzing the forces controlling the breakup he considered a globule being subject to an external shear rate with a viscous force per unit surface area, τ, as well as dynamic pressures. The surface tension σ, being in the order of

magnitude σ/D, will give rise to a surface force that will in general counteract the deformation when D is the diameter of the bubble. The dynamic pressure will be in the same order of magnitude as τ, causing flow velocities of the order of magnitude $(\tau/\rho_d)^{1/2}$. Thus the viscous stresses are of the order of magnitude

$$\frac{\mu_d}{D}\sqrt{\frac{\tau}{\rho_d}} \tag{3.53}$$

The three forces; the external τ, the surface tension σ/D, and the viscous force $(\mu_d/D)(\tau/\rho_d)^{1/2}$, control the deformation and breakup of the globule. From these, three dimensionless groups may be formed, only two of which are independent. The generalized Weber group, being the ratio of external force to surface force, $We = \tau \cdot D/\sigma$. The other dimensionless group, the ratio of viscous to surface forces, is either

$$\frac{\mu_d}{\sigma}\sqrt{\frac{\tau}{\rho_d}} \text{ or } \frac{\tau \cdot D}{\mu_d}\sqrt{\frac{\rho_d}{\tau}} = \frac{\rho_d D}{\tau}\sqrt{\frac{\tau}{\rho_d}} \tag{3.54}$$

Since the two groups contain the external force τ, the ratio between these two groups are preferred, containing only the properties of the globule:

$$Vi = \frac{\mu_d}{\sqrt{\rho_d \sigma D}} \tag{3.55}$$

The greater the value of We, i.e. the greater the external force τ compared with the counteracting interfacial-tension force σ/D, the greater the deformation. At a critical value We_c, breakup occurs.

3.3.2 Droplet coalescence

A verbal introduction to coalescence phenomena is given in the textbook of G. Whetstone. Drop coalescence plays an important role in the establishment of the steady-state drop size distribution in an agitated system, whether this is in

the form of a mechanical stirrer or a static mixer. As mentioned, this process is viewed as an equilibrium between the opposing influences of drop breakup and drop coalescence, with the nature of that equilibrium being determined by the type and degree of agitation and the physical properties of the two liquids. The physical situation is very complex, and includes the problem of predicting the number of drop-drop collisions that will occur and determine how many of these collisions will result in coalescence. Park & Blair (1975) observed that in an agitated tank only 10% of collisions lead to coalescence and, perhaps more surprisingly, that coalescence rate is proportional to turbulence level.

Coalescence studies in turbulent systems are of interest for considerations of drop size and mass transfer. For the designer, the most immediate interest is likely to be the coalescence of dispersions after e.g. mass transfer has been effected.

In coalescing dispersion bands both drop-drop and drop-interface coalescence will occur. For either case the limiting rate step will be the drainage of the continuous-phase film separating drops or drop and interface. A dispersion band will have a density intermediate between the densities of the continuous and the dispersed phases and will lie between the two.

Consequently there will be two boundaries: a passive interface between the dispersion and the continuous phase and an active interface between the dispersion and the coalesced dispersed phase. In the study of drop-interface coalescence, a sequence of steps has been identified:

1. Deformation of drop and interface as drop approaches interface.
2. Oscillation of drop and interface following deceleration of drop
3. Drainage and rupture of continuous phase film
4. Whole or partial transfer of drop contents to coalesced phase.

Of these, film drainage appears to be the controlling influence; from visual observations, steps 1 and 2 do not appear to be significant in deep dispersion bands. The principal characteristic of drop-interface coalescence times is particularly difficult experimentally (Liem & Woods 1974) in that the coalescence process is sensitive to a large number of variables, many of which are difficult to control - e.g., vibration and trace impurities. Correlations have been developed by Davies et al. (1971) for coalescence time for single drops.

However, the accuracy of such correlations is very much system-dependent. Of particular interest in the study of drop-interface coalescence is the influence of viscosity, temperature, mass transfer, and solids. Lower continuous-phase viscosities give more rapid film drainage and shorter coalescence times; increased temperature reduces viscosity and coalescence time. Mass transfer from drop to continuous phase decreases interfacial tension and increases film drainage rate. The presence of solids at an interface can result in decreases coalescence times but in some cases can result in drop stabilization.

The fundamentals of coalescence are discussed by Jeffreys & Davies (1971), including a model for coalescence in wedge-shaped dispersion bands. A later model (Doulah & Davies 1974) deals with the case of uniform dispersion band depth. However, until the relative contributions of drop-drop and drop-interface coalescence to dispersion band behavior are better understood, it will be difficult to use the models proposed to give accurate predictions of settler behavior.

Chaudari & Hofmann (1994) has also given a comprehensive review on the phenomena of coalescence, although this paper mostly focuses on the coalescence of gas bubbles in liquids. The review article attempts to identify the important physical processes and the mechanism of bubble break-up and coalescence along with critical review of available data and theories of coalescence, and may by and large also be applied to liquid droplets in liquid. Due to lack of understanding, most of the engineering design involving these phenomena has been based on empirical analysis.

Stored emulsions undergo various destabilizing processes including creaming and coalescence. Kumar et al. (1996) also points out that many experimental studies have been carried out in the past to quantify drop coalescence; however, the presence of two distinct types of coalescence mechanisms - one due to the relative motion between the drops and the other due to their permanent proximity to each other in a creamy emulsion, has not been recognized by most workers. The appearance and quality of a stored emulsion product are affected by three processes: creaming of dispersed-phase drops due o buoyancy, their flocculation, and their coalescence.

The first two processes are reversible and harmless by themselves, but they can aid coalescence of drops which is irreversible and eventually leads to complete destruction of the emulsion. A creamed or flocculated emulsion can shaken to easily restore the original homogeneous emulsion. In comparison, if drops become bigger or oil appears on the top and «oils off» due to the coalescence process, the emulsion cannot be restored to its original state unless it is homogenized again.
The two types of coalescence mechanisms are different in nature and have different implications. Kumar et al. (1996) terms the former, which is caused by relative motion due to buoyancy or Brownian motion as «coalescence in bulk» and the latter, which is caused by the permanent proximity of the drops to each other in cream as «coalescence in cream». Coalescence in bulk accelerates the creaming process by forming large drops which accumulate a large amount of dispersed phase in the cream layer in much shorter times. Furthermore, the cream undergoes accelerated coalescence because it now consists of large drops to begin with. Thus, increased coalescence in bulk has far more serious implications than the corresponding increase in coalescence in cream.

As stated by Kumar et al. (1996) emulsions being subject to a turbulent field to avoid creaming not only accelerates the coalescence, but also can actually introduce new mechanisms of coalescence. Further, large drops reach the top layer faster than the smaller ones, thus increasing the concentration of larger drops there, which can be mistakenly interpreted to be due to the coalescence process.

As for bubble coalescence, this is believed to occur in three steps (Vrij, 1966):

a. The approach of two bubbles within the liquid phase to each other and formation of a thin film (a quasi equilibrium film thickness) between them. The initial thickness of such a film can typically be 1 - 10 :m. This step is controlled by the hydrodynamics of the bulk liquid phase (Oolman & Blanch, 1986), depending on the extent of energy dissipation.

b. Thinning of the film occurs by drainage of the liquid under the influence of gravity and suction due to capillary forces at plateau borders. The process of thinning is also influenced by system properties like surface tension and viscosity. When the thickness of the film is reduced to about 100 nm, van der Waals attraction increases the draining rate, while the electrostatic

double layer repulsive force decreases it. On further thinning, some films become metastable, and others collapse between 50 - 10 nm. Metastability is reached when border suction, van der Waals attraction and double layer repulsion forces equilibrate; instability results when the attraction forces predominate (Vrij, 1966).

c. As the thickness of the film reduces below a dimension of 10 nm, it ruptures, leading to coalescence. Unstable films (often called transient films) rupture spontaneously at a characteristic «critical thickness».

In the process of bubble coalescence, the rate of film thinning is believed to be the rate controlling step, as the rupturing step is very rapid. The contact time of the bubbles is also important and when the contact time of bubbles is less than the time for thinning, coalescence will not occur. Therefore, in understanding coalescence behavior, primary attention has been focused on the analysis of the rate of thinning of the liquid film. The various factors affecting the drainage rate of thin films are (steb b) are:

1. The main force responsible for drainage of the thin film liquid is the influence of gravity an suction at the edges of the film. This process is influenced by the mobility of the bubble surfaces and the physical properties of the fluid phases like viscosity, surface viscosity, surface tension gradients and differences between density of gas and liquid phases. Increase in interfacial tension resists deformation of bubbles and leads to decrease in the area of drainage of the film and hence leads to faster coalescence (Jeffreys & Davies, 1971).

2. In electrolyte solutions, the coalescence of gas bubbles is inhibited leading to smaller bubble size, and higher interfacial area. In this case, the electrolytes lead to formation of an electrical double layer at the interfaces between the two bubbles and the draining liquid, resulting in immobility of the interfaces and retardation of the flow of the draining film through the force of attraction of the opposite charges at the interfaces. This effect is called «electroviscous effect» (Elton & Picknett, 1957), which is most pronounced when the thickness of the draining film has the same order of magnitude as the electrical double layer.

3. In the presence of surface active agents in aqueous solutions, the coalescence is inhibited similarly to that in the case of electrolytes.

Though the effect of electrolytes and surfactants is similar, the concentration levels of surfactants required to inhibit coalescence are much lower than those of electrolytes (Sagert & Quinn, 1978; Marrucci & Nicodemo, 1967). The presence of surface active agent increases the interfacial viscosity and decreases the interfacial tension. Both these effects lead to retardation of the rate of drainage of the film liquid. When interfacial tension is decreased, the probability of rupture of the film is decreased and distortion of the film is inhibited, since, with change in the area the tangential stress is taken up by the interfacial tension. The surface active agents consist of organic molecules with hydrophilic groups (-OH, >CO, -COOH, etc.) and a hydrophilic part (hydrocarbon structural group) (Keitel & Onken, 1982). The molecules of this type are surface active, which means that they will be enriched at the gas-liquid interface. On the liquid side of the interface, the surface active molecules will tend to form a monolayer, the stability of which depends on the type, concentration and size of the surface active molecule. These surface active molecules are so enriched at the surface that the hydrophilic groups point towards the liquid phase and the hydrophobic groups towards the gas phase. Due to this specific orientation, the liquid surface around the gas bubbles is electrically charged, and this surface polarization produces repulsive forces leading to inhibition of bubble coalescence.

4. The process of coalescence and drainage rate of film can also be influenced by the various diffusional processes, such as diffusion of the solute from the bulk liquid to the film, from the film to the film to the gas-liquid interface, and evaporation of the film liquid.

5. In cases where the gas bubbles react while moving through the liquid, the bubble size will change due to reaction and thus will influence the process of coalescence and the bubble distribution in general.

The above factors will contribute depending on the type of system involved. The attempts to explain quantitatively the effect of these factors have not been very successful, though several theoretical models have been proposed for the rate of thinning. Considering the practical implications and a few important observations on coalescence behavior of different systems, these systems can be classified into the following categories (Chaudari & Hoffmann, 1994):

- Liquid phase consisting of pure solvent or a mixture of non-polar solvents.
- Aqueous solutions of electrolytes.
- Aqueous solutions containing inorganic or organic surface active agents.
- Liquid phase consisting of a non-Newtonian fluid of high viscosity.

3.3.3 Models for coalescence time

First considering two gas bubbles in a liquid, the coalescence is quantitatively described through «coalescence time», which is defined as the time elapsed after the event of first contact of the two bubbles until their coalescence. The mathematical models proposed for coalescence time are categorized as

- Liquid phase diffusion model
- Gas phase diffusion model
- Dynamic surface tension model

3.3.3.1 Liquid phase diffusion model

Marrucci (1969) proposed a theory of coalescence in which the thinning of the film is assumed to occur by two mechanisms: (a) Expansion of the two surfaces and of the liquid between them (i.e. a stretching of the film as a whole), and (b) Laminar flow of the bulk liquid in the film with respect to the surfaces. The latter mechanism applies when the surfaces are considered immobile, as in the case of surfactants and electrolytic solutions. In the theory proposed by Marrucci (1969), the surfaces are assumed to be mobile and the former mechanism is considered wherein the laminar flow is neglected with respect to the stretching of the film as a whole.

The coalescence time depends mainly on a dimensionless group, $cr_b k^2/\gamma$, where c is defined as a force (N), r_b is the radius of the bubble (m), k is a parameter (1/m), and γ is the surface tension (N/m). This dimensionless group is a measure of the relative contribution of the diffusion time and the stretching time. The ratio of coalescence time t_s and diffusion time t_D $(\approx xR/D)$ is proportional to the dimensionless group, where x is the depth of the diffusion film (x), R is the radius of the disc shaped film (m), and D is the

diffusion coefficient (m^2/s). Higher values of the dimensionless group would mean $t_s > t_D$, indicating that slower diffusion step is rate controlling. On the other hand for lower values of the dimensionless group, $t_s < t_D$ and hence the rate controlling step would be the process of film thinning. Thus, $cr_b k^2/\gamma$ is an important dimensionless group that can be useful for characterization of the coalescence behavior.

Marrucci (1969) showed that below a value of $cr_b k^2/\gamma \approx 2$, the process of coalescence is extremely rapid, and this case applied for pure liquids and some dilute solutions. Here, the quasi-equilibrium film thickness does not exist. It was also shown that for $cr_b k^2/\gamma > 2$, which means that the quasi-equilibrium thickness may exist, the time required to thin the film down to it from initial thickness is negligible with respect to the coalescence time. Therefore, the coalescence time is determined by further thinning of the quasi-equilibrium thickness of the film down to critical thickness of the film at which rupture occurs. This model was found to be satisfactory for predicting the coalescence time of gas bubbles in electrolyte solutions (Marrucci et al., 1969; Nicodemo et al. 1972). However, it was not found to be satisfactory to represent the data on solutions containing surfactants (Nicodemo et al. 1972; Sagert et al., 1976).

Sagert & Quinn (1978) extended Marrucci's model to incorporate the influence of electrostatic double layer repulsion force in addition to the capillary and Hamaker-London forces. They observed, however, that the electrostatic interactions are not important at distances typical of quasi-equilibrium thickness, h_0, and that there is a minimum value of $cr_b k^2/\gamma$ of 28.5, below which the equilibrium film thickness h_e does not exist. For intermediate values of $cr_b k^2/\gamma$, it would lie between h_0 and the final thickness of the film, h_f. The analysis of Marrucci (1969) as well as Sagert & Quinn (1978) indicate that $cr_b k^2/\gamma$ is an important parameter characterizing the process of coalescence. For $cr_b k^2/\gamma < 2$, the coalescence is very rapid and for $cr_b k^2/\gamma > 28$, the coalescence is suppressed due to very strong electrostatic double layer force. However, these models do not incorporate important features like surface diffusion, diffusion of the film liquid to the gas bubbles (which is likely to occur for the volatile liquid phase) and changes in the shape

of the film and the bubble. Use of these models requires a prior knowledge of r_b, the average bubble radius, which has to be determined experimentally.

3.3.3.2 Gas phase diffusion model

Nicodemo et al. (1972) proposed that for the case of volatile solutes, an additional factor involving diffusion of the solute from the liquid bulk to the gas bubble will also contribute to the concentration gradient. Sagert et al. (1976) have analyzed such a model following the procedure used by Marrucci (1969). They reported that for ethanol-water and n-amyl alcohol systems the diffusion distances, estimated by this model, were considerably higher than the quasi-equilibrium film thickness, which is unrealistic, and hence they concluded that the model is not adequate to represent the data for solutions containing volatile solutes.

3.3.3.3 Dynamic surface tension model

Andrew (1960) considered a model wherein it is assumed that a relatively thick film is being stretched and the surface tension increases as a result of slow diffusion of the solute from the bulk film liquid to the surface.

Sagert et al. (1976) further extended this model to incorporate the contribution of electrostatic double layer repulsion force.

Further, Radoev et al. (1974) and Manev et al. (1976) proposed a new model in which the surface motion is assumed to be induced by diffusion of the solute (e.g. surfactant) along the entire surface.

Ivanov et al. have reported a theoretical analysis for the rate of thinning of films with deformable surfaces. The role of soluble surfactant with diffusion controlled surfactant transfer onto the surface has been analyzed , and also it is assumed that the two bubbles involved have different radii and surface properties. Analytical solutions for thickness of the film have been obtained for limiting cases of small and large deformations. This analysis is applicable mainly to small bubbles.

CHAPTER 3 TURBULENCE & DROPLET SIZE DISTRIBUTION IN STATIC MIXERS

The above presented models can be used to predict the time required for stretching of the liquid film to the final thickness, h_f, in the derivation of which the inertial influence on the film was neglected. Sagert et al. (1976) proposed that the coalescence time, t_c, can be considered to consist of three parts:

$$t_c = t_s + t_i + t_b \tag{3.68}$$

where t_s is the stretching time. The term t_i is a correction for the inertial force on the liquid film. The breaking time t_b represents the lifetime of the film at the final thickness h_f and can be estimated. The critical thickness of rupture is typically in the order of about 10 nm and the breaking time (time of rupture) is around 5 - 10 :s. For most practical purposes, therefore, t_b is negligible.

Chesters & Hofmann (1982) and Chesters (1991) have reported models for coalescence in pure gas-liquid dispersions, and proposed an approximate equation for coalescence time. Their model also predicts if the bubbles will bounce rather than coalesce, if their relative velocities are very large. They have also predicted deviation from a plane parallel geometry and formation of a dimple around the edge of the film. The film thinning time for pure liquids is estimated to be of the order of 1 - 10 ms.

Chesters (1991) splits the flow into an internal and external field, rather as is done when employing the concept of a boundary layer:

CHAPTER 3 TURBULENCE & DROPLET SIZE DISTRIBUTION IN STATIC MIXERS

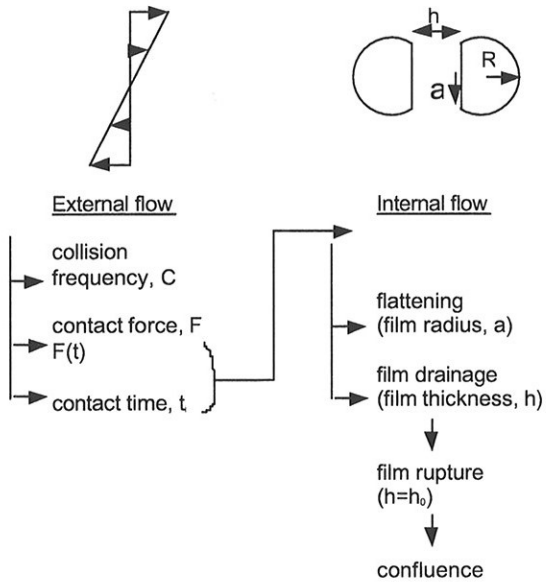

The external flow (the continuous-phase flow, in which the particles are embedded) governs the frequency, force and duration of collisions, the latter two providing the boundary conditions for the internal flow. The internal flow (in the draining film between the particles) is characterized by deformation of the approaching interfaces and, if sufficient time is available, by rupture and confluence. The role of gravity is implicitly assumed negligible in the above picture, which may not be true for large bubbles where buoyancy-induced velocities can be the principal source of collisions.

3.3.4 Critical thickness for rupture

In the process of coalescence of bubbles, the thinning of the liquid film reaches a stage at which spontaneous rupture occurs. The thickness of the film, h_c, at this stage is defined as the critical thickness of the film for rupture.

Scheludko (1962, 1967) was the first to relate the rupture of thin films to their instability to small surface deformations via a thermodynamic treatment. Vrij (1966) described mechanisms of rupture of metastable and unstable films. Metastable films exist when suction at the edge of the film, van der Waals attraction and double layer repulsion forces equilibrate. Instability results when the attraction forces predominate. Rupturing of metastable films, if it takes place, is likely to occur in a irregular manner because of the lack of control over the external disturbances like thermal shock, vibration and dust, etc. For films larger than 10 nm thickness, a high activation energy is required for spontaneous rupture of the film through the formation of nucleus (hole). The unstable films, often called transient films always rupture spontaneously at a characteristic «critical thickness».

Scheludko (1962) proposed that at critical thickness of the film, total free energy decreases because of the van der Waals forces in spite of an increase of free energy through the increase of surface area.

Vrij (1966) proposed that, when the film thins, the draining rate slows down, whereas the stable fluctuations grow faster and faster until a critical thickness h_c is reached at which one of the fluctuations grows so fast that the film breaks.

Vrij & Overbeek (1968) proposed that the surfaces of thin liquid films are slightly corrugated due to thermal fluctuations. The corrugations having wavelengths larger than a critical wavelength grow spontaneously due to the van der Waals forces and cause the film to thin rapidly and break.

Ivanov & Dimitrov (1974) developed an expression for h_c, the critical thickness at the moment of rupture. This model incorporates the effect of surface viscosity on the rupture of the film; however, these authors pointed out that the theory suffers from a defect, in that surface viscosity is assumed to be constant with respect to surfactant concentration and the flow velocity.

CHAPTER 3 TURBULENCE & DROPLET SIZE DISTRIBUTION IN STATIC MIXERS

Ruckenstein & Jain (1974) reported an approximate solution for the critical wavelengths and the time of rupture of thin films. Their model predicts critical thickness of about 10 nm and the time of rupture of about 10 μs.

3.3.5 Theoretical analysis of droplet coalescence

As explained in the review of Chaudari & Hofmann (1994), the aspects of modelling of coalescence and flow simulation codes in fluid-fluid dispersions for pure liquids have been reviewed by Chesters (1991). A few attempts have also been made to analyze the drop size distribution for liquid-liquid dispersions (Curl, 1963; Valentas et al., 1966; Valentas & Amundson, 1966; Zeitlin & Tavlarides, 1972, and Coulaloglou & Tavlarides, 1977), but even in these models the coalescence mechanism has not been considered adequately.

Curl (1963) was the first to propose the population balance approach for analysis of drop size distribution in dispersed liquid phase mixing. He assumed that the drop size was uniform with binary coalescence, the probability of which being the same for all drops. It was further assumed that the droplets coalesce at the same rate and after coalescence, the redispersion occurs immediately to form two new drops of equal size.

Valentas et al. (1966) and Valentas & Amundson (1966) proposed a more comprehensive model incorporating the fundamental concepts of coalescence and breakage of droplets in a turbulent flow field. They used a population balance model to predict the drop size distribution. An attempt was also made to include the effect of operating parameters and physical properties of the system; however, the results were not compared with available data on drop size distribution.

Zeitlin & Tavlarides (1972) and Coulaloglou & Tavlarides (1977) proposed a two-zone model for fluid-liquid interactions in an agitated dispersed phase. The first zone characterizes high turbulence where the break-up of drops predominates and in the second zone, essentially the coalescence takes place. Using this simulation model, they attempted estimation of coalescence and breakage parameters.

CHAPTER 3 TURBULENCE & DROPLET SIZE DISTRIBUTION IN STATIC MIXERS

Following a similar approach, Lee et al. (1987a) developed theoretical models for efficiency of coalescence and breakage of gas bubbles in a gas-liquid dispersion. This model is based on probability theory, and an attempt was made to account for the fundamental mechanism of bubble coalescence. However, the well known contribution of the electrostatic double layer repulsion force (Sagert & Quinn, 1976) was not considered in the coalescence model.

One may therefore say that, from review of previous workers, that the various mechanisms of coalescence and the effect of different parameters on these are qualitatively understood and summarized. the trends observed on the effect of electrolytes, surfactants and properties like surface tension and viscosity on coalescence behavior are consistent, but quantitative prediction of these has so far not been very precise. It is known that mere incorporation of physical properties in correlations does not explain the wide differences in the hydrodynamic parameters observed for systems of different properties.

The parameter $cr_b k^2/\gamma$ proposed in the theory of Marucci (1969) appears to be very important, as also demonstrated by Sagert & Quinn (1976) in understanding the mobility of thin films. For example, for $cr_b k^2/\gamma < 2$, the coalescence is very rapid, while for $cr_b k^2/\gamma > 28$, the coalescence is suppressed due to the significance of the electrostatic double layer forces. Nevertheless, the application of this group parameter needs to be tested for a further variety of systems, which has not yet been done. To explain the variation of coalescing frequency in the intermediate range of $cr_b k^2/\gamma$, from 2 to 28, a satisfactory theoretical model is not yet available. Beyond this range, the approximations would be reasonable. Previous comparisons of available experimental data with theory indicates that the dynamic surface tension models incorporating electrostatic double layer repulsion force can be used to obtain reasonable predictions of coalescence times for surfactant solutions.

3.4 Turbulent mixing

3.4.1 Influence of Coalescence on Drop Size in Dispersions

It has previously been shown (Delichatsios & Probstein, 1976) that an increase of drop sizes with the holdup in agitated liquid-liquid dispersions

cannot be attributed entirely to turbulence damping caused by the dispersed phase. In fact, these workers have shown that increased drop size with higher fractional holdup can only be accounted for by allowing for coalescence, turbulence damping playing a secondary role.

An alternative mechanism proposed by e.g. Mlynek & Resnick (1972) is that holdup behavior represents an effect of coalescence.

Average drop sizes in agitated liquid-liquid dispersions can be correlated by the relation (see e.g. Mlynek & Resnick, 1972):

$$d = C_1 \varepsilon^{-2/5} \left(\frac{\sigma}{\rho} \right)^{3/5} f(\phi) \tag{3.78}$$

where C_1 is a constant of order 1; ε is the rate of turbulent energy dissipation per unit mass; σ is the density of the continuous phase, assumed not much different from that of the dispersed phase; ϕ is the volume fraction of the dispersed phase, i.e. holdup; and $f(\phi)$ is the holdup function, expressed empirically by the linear relation $f(\phi) = 1 + C_2 \phi$, C_2 being reported to adopt values between 2.5 and 9 (Mlynek & Resnick, 1972).

Damping of turbulent intensities can be approximated by (Laats & Frishman, 1974):

$$\frac{u'}{u_0'} = \frac{1 + 0.2\phi}{1 + \phi} \tag{3.79}$$

where u' is the root-mean-square turbulent fluctuating velocity in a dispersion of particles and u_0' is the respective value in a free particle fluid. Using this equation and the relation (Batchelor, 1960):

$$\varepsilon \sim \frac{u'^3}{L} \tag{3.80}$$

where the macroscale of turbulence L is essentially determined by the physical dimensions of the apparatus, it follows that the available turbulent energy is damped by the factor $\left(u'/u_0'\right)^3$.

From the functional dependence of drop size on the rate of turbulent energy dissipation per unit mass, eqn. (3.41), it follows that we can expect a drop size with a finite holdup which is at most $\left(1+\phi/1+0.2\phi\right)^{6/5}$ greater than for the case where ϕ is negligibly small. Provided ϕ is not too large, say less than 0.25, this would imply a holdup function $f\left(\phi\right) \approx 1+C_2\phi$ with $C_2 = 0.96$. Comparison with the empirically determined values of $2.5 < C_2 < 9$ makes it clear that the turbulence damping effect would, by itself, be insufficient to account for the experimental results, at least for small holdup.

The holdup function is defined by (Delichatsios & Probstein, 1976):

$$\frac{d_0}{d_{\min}} = 1+f\left(\phi\right) \tag{3.81}$$

where d_0 is the mean diameter and

$$f\left(\phi\right) = \left[\frac{\ln\left(C_3+C_4\phi\right)}{\ln C_3}\right]^{-3/5} \tag{3.82}$$

where

$$C_3 = \exp(-4.5) = 0.011 \tag{3.83-a}$$

$$C_4 = 3\left(\frac{A}{B}\right) \tag{3.83-b}$$

The constant C_4, which depends only on the ratio of the coalescence to breakup coefficients, must be determined empirically. However, in the assumptions made by Delichatsios & Probstein (1976) it is expected C_4 to be

a constant of order 1, with its exact value being dependent on the stability of the dispersion.

With the help of the Kolmogoroff theory of universal equilibrium, Doulah (1975) derived an expression to account for the increase in mean drop size with volume fraction (holdup) of dispersed phases in the absence of coalescence. And he found that the relative increase in the mean drop size between dilute and concentrated dispersions agrees well with the data from literature when the dispersion viscosity is expressed by the Einstein equation.

Doulah's starting point was that, at high holdup values of the dispersed phase the mean drop size formed under a breakup mechanism can be correlated empirically by the equation

$$d_{32} = d_{32}^{0}\left(1 + C_2\phi\right) \tag{3.84}$$

C_2 in this equation is a dimensionless coefficient for which the following values have been reported by several authors: 2.5 (Vermeulen et al.,1955), 5.4 (Mlynek & Resnick, 1972), 3.14 (Brown & Pitt, 1970) and 9.0 (Calderbank, 1958). In the absence of coalescence, the drop sizes should be independent of holdup values. The functional dependence of the mean drop size on holdup in eqn. (3.58), even in the absence of coalescence, has led some authors (Van Heuvan & Beek, 1971; Brown & Pitt, 1972) to believe that the observed holdup function is due to a reduction of turbulence intensity in the presence of the dispersed phase.

Doulah (1975) showed that, using Kolmogoroff's theory of universal equilibrium, because the dispersion viscosity depends on holdup and because turbulent scales are affected, drop sizes in concentrated dispersions depend on dispersion viscosity. Assuming homogeneous turbulence described by the Kolmogoroff energy spectrum function, $E(k)$, previously stated in eqn. (3.13):

$$E(k) = \alpha\,\varepsilon^{2/3}\overline{k}^{5/3} \tag{3.85}$$

and the microscale, previously stated in eqn. (3.14):

$$\eta = \left(\nu^3/\varepsilon\right)^{1/4} \tag{3.86}$$

CHAPTER 3 TURBULENCE & DROPLET SIZE DISTRIBUTION IN STATIC MIXERS

Since the drop size is greater than the microscale where viscous action is negligible, the effect of the dispersion viscosity on drop sizes is not easily discernible. However, the viscosity effect on the average lengths of the energetic eddies responsible for drop breakup can be found, and hence the effect of drop sizes can be obtained as in the following discussion:

Consider a dispersion formed in the universal equilibrium range of turbulence with viscosity ν_1 and at two levels of energy input rates, ε_1 and ε_2. For equal fluctuation intensities the average length scales of energetic eddies can be related by

$$l_{k_2}/l_{k_1} = \varepsilon_1/\varepsilon_2 \tag{3.87}$$

For the same dispersion at ε_1 let the viscosity be changed from ν_1 to ν_2 so that the microscale η_2 corresponding to ε_1 and ν_2 equals that at ε_2 and ν_1. Thus from eqn. (3.85) it follows that

$$\eta_2 = \left(\nu_2^3/\varepsilon_1\right)^{1/4} \tag{3.88}$$

or

$$\varepsilon_1/\varepsilon_2 = \left(\nu_2/\nu_1\right)^3 \tag{3.89}$$

Eqs. (3.87) and (3.89) yield

$$l_{k_2}/l_{k_1} = \left(\nu_2/\nu_1\right)^3 \tag{3.90}$$

Eqn. (3.90) shows that the change in the viscosity of a turbulent medium causes a corresponding change in the average length scales of energetic eddies even at a constant level of external power input to the system. As viscosities of dilute and concentrated dispersions differ due to differences in dispersed-phase volumes, the turbulence structures originally present in concentrated dispersions at ε_1 rearrange in a way such that drop sizes

formed there correspond to an energy level ε_2 if viscosity is changed from ν_1 to ν_2.

The maximum drop size in distribution can be represented by the expression developed by Shinnar & Church (1960). For dilute dispersions at an energy input ε_1

$$d^0_{max} = C_3\left(\gamma/\rho_c\right)^{3/5}\varepsilon_1^{-2/5} \tag{3.91}$$

Doulah (1975) shows that in concentrated solutions, in absence of coalescence, we have that

$$d_{32} = d^0_{32}\left(\nu_2/\nu_1\right)^{6/5} \tag{3.92}$$

The viscosity of concentrated dispersions of oil and water up to $\phi = 0.2$ can be represented by the Einstein equation (Ward & Knudsen, 1967):

$$\mu_e/\mu_c = 1 + 2.5\phi \tag{3.93}$$

As $\nu_c = \nu_1$ and $\nu_e = \nu_2$, and assuming $\rho_c = \rho_e$, we eventually obtain the following expression:

$$d_{32} = d^0_{32}\left(1 + 3\phi\right) \tag{3.94}$$

The holdup coefficient C_2 derived in eqn. (3.92) is 3.0, nearly equal to the value obtained by Brown & Pitt (1970) for a non-coalescing system of kerosene and water. This value may represent the maximum possible contribution of the dispersion viscosity.

3.4.2 Numerical simulation of mixing in static mixers

Until recently static mixers have only been developed and tested by experimental techniques. Due to the availability in CFD (**C**omputational **F**luid **D**ynamics) programs and powerful computers it has become easier to

approach the calculation of the fluid flow and the mixing process in a static mixer. This will most certainly have an impact on the the development technique for static mixers. Numerical simulation provides more insight into the flow and mixing processes due to the data being available in the whole flow field. The fundamental equations for conservation of mass, momentum and energy must be solved to calculate the mixing process in a static mixer. In the last few years there have been an increasing number of attempts in using simulation techniques for the study of mixing applications.

Lang et al. (1995) analyzed the fluid flow and mixing process in a Sulzer SMV static mixer to gain insight into the character of the mixing process and to check the numerical simulation as a tool for the design of single mixers and entire facilities with mixers incorporated. In a first step the mixing process in a straight pipe was analyzed by the numerical simulation, and good agreement was found with experimental data. The investigation was extended to an infinite, ideal mixer element. The vortices generated by the structure of the mixer was observed to be the main driving force of the mixing of the fluid. According to Lang et al. (1995) mixing is not mainly due to increased turbulent diffusion generated by the mixer structure. In fact, the main mixing therefore occurs in the wake of the mixer.

Lang et al. (1995) found by comparing with experimental LDA data that the computed results agreed relatively well with respect to the velocity components, being from 0 to 0 1.5 m/s for the v-component and -0.5 to 2.5 m/s for the u-component.

The investigation showed that numerical simulations can be used to compute the fluid flow and the mixing process in static mixers. A numerical simulation can give much more insight into the flow and the mixing of such a facility because the simulation gives data at every gridpoint, whereas an experiment only gives data at locations where measurements have been carried out. Hence, this can lead to a better design and a faster design process, which in turn leads to facilities with higher efficiencies and reduced operating costs.

Mixing in the Kenics static mixer has been studied by a number of workers. Most of these workers have calculated a pressure drop and simulated the mixing processes. However, the agreement between simulation and experiments have partly been poor, partly due to errors in the governing equations. Ling & Zhang (1995) performed new investigations, where these

equations were corrected, and satisfactory agreement with experimental results was achieved.

Most recently, Avalosse & Crochet (1997), applying finite-element method, pursued the development of numerical tools with a view to the analysis of complex three-dimensional mixing devices. They applied this method to the analysis of a Kenics mixer, assuming stationary flows of generalized Newtonian fluids through an open domain (having an entry and exit section) and that the geometry is periodic in the axial direction.

However, high computational cost of simulating complex 3-D flows imposes serious restrictions on the type of problems that can be handled with computational resources of today.

As stated by Avalosse & Crochet (1997), the central problem of mixing calculations is the accuracy; a relatively coarse finite-element mesh may generate acceptable velocity fields, but the computation of pathlines, essential for any mixing calculation, is then severely impaired. The usual symptom of inaccuracy is the loss of material particles through solid walls. While high accuracy can be reached for 2-D viscous-flow problems with appropriate grid refinement, the situation is quite different for complex 3-D shapes.

In addition to the accuracy problem, a 3-D mesh generation in moving domains is presently considered to be a major obstacle, thus justifying the self-imposed restriction of Avalosse & Crochet (1997) to only investigate the static-mixer.

It is also assumed that one possible refinement method for achieving better agreement with numerical techniques consists of using a higher grid resolution. Lang et al. (1995) reports that fairly good agreement between numerical computations and experimental results were achieved. In their study on the Sulzer SMV mixer, the grid consisted of 89 375 nodes, where the inlet part was modeled by 4 200 and the channel section by 12 000 grid points. This is a rather coarse grid, and it was stated that a higher grid resolution should therefore lead to a better agreement for these workers too.

In the work of Fradette et al. (1998), investigations on the Sulzer SMX Static Mixers concluded that CFD can generate reliable information to understand and eventually predict mixer's performance. From simulation results, one can

extract local information about energy levels, shear, stress, etc. The flexibility of such a software also allows thye non-Newtonian behaviour to be taken into account and even predicted. It was concluded that possible future work should investigate power and elongation along flow paths. Information taken on a plane location, although it can reveal very interesting characteristics of the geometry, do not provide any information on the history of the flow at a given position.

Hobbs et al. (1998) modeled for low Reynolds number flow in a six element Kenics static mixer, using commercially available CFD software, producing a discretized approximation to the velocity field. It was claimed that the simulation solution represented an improvement over approximated analytical solutions for the velocity field used in previous studies which did not take into account transitions between mixer segments or finite-thickness mixer elements. The spatial periodicity of the mixer geometry produced a periodic velocity field, with each pair of adjacent mixer elements forming a periodic unit. Analysis of the velocity field within a single mixer element indicated that for $\mathrm{Re} \leq 10$, the flow is well-developed with respect to the axial coordinate over the central 75% of each element. In the remaing 25% of the flow at the entrance and the exit of the element, the velocity field is strongly affected by the element-to-element transition. Comparison of the velocity fields obtained from simulation over a range of Reynolds numbers from 0.15 to 100 indicated that identical velocity profiles are obtained for $\mathrm{Re} < 10$ within a maximum deviation of 3% at $\mathrm{Re} = 10$. Above $\mathrm{Re} = 10$, the velocity field begins to deviate more strongly from the profiles obtained for creeping flow conditions.

The ability to develop accurate numerical representations of the flow field makes it possible to seek answers for many questions of both fundamental and applied interest. For example, since element-to-element transitions contribute to mixing more than other regions of the flow, one might investigate whether a mixer with short elements (and therefore more frequent transitions) would achieve faster mixing for comparable pressure drops. Methods described could be used to obtain similar solutions for other static mixers in order to compare mixing performance. It is also possible to obtain Lagrangian simulations and investigate dispersion of various types of tracers in the flow (although such calculations represent a significant computational burden, much greater than the computational time required to obtain the initial velocity field from CFD computations). One could also investigate the evolution of aggregates, drops, and chemical reactions in this flow.

CHAPTER 3 TURBULENCE & DROPLET SIZE DISTRIBUTION IN STATIC MIXERS

3.5 Principles and Characteristics of The Static Mixer

3.5.1 Principles

A schematic of the SMV mixer is shown in Fig. 3.4.

The mixer consists of a number of similar mixer elements, consecutively oriented 90° relative to each other, thus forcing a homogenizing of the flowing stream inside. The intersecting channels within the mixer ensure a lateral displacement of the fluid, such that a portion of the bulk stream shears off into the adjacent channel at each intersection. Hence, homogenization is attained by means of the motionless elements by using the flow energy of the fluid. The state of mixing is frequently stated by means of statistic terms such as the variation coefficient, or the relative standard deviation.

The mixing effect depends on the continuous separation, distribution, and reuniting of the streams. Using a model with two triangular channels crossing at 90° (height 15 mm), and injecting with tracer streams, Pahl & Muschelknautz (1982) described the flow patterns in the SMV mixer. Denoting the channels as I and II, it was found that about 2/3 of the product from channel I flows into channel II by displacement of the crossing point.

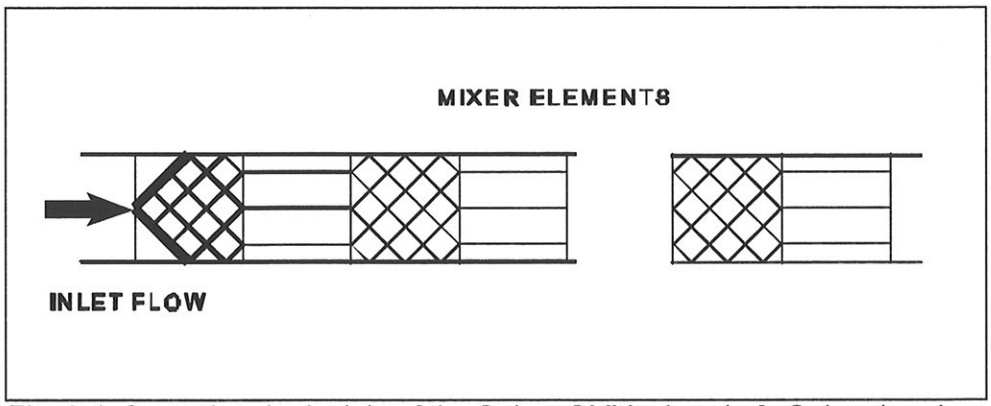

Fig. 3.4: Operational principle of the Sulzer SMV mixer (ref.: Sulzer brochure: «Sulzer Technical Review, 3/1977»)

3.5.2 Characteristics

Motionless mixers, or static mixers as they are called in popular terms, are well established for different purposes in process engineering. Their particular advantages are in-line mixing, no moving parts, low power consumption and simultaneous homogenization of fluids flowing within. As shown by several workers (e.g. G. Gaiser, 1994), different geometrical patterns of static mixers lead to different flow phenomena. Some patterns lead to no mixing at all, while other patterns lead to a homogeneous mixing within a small length.

Fundamentally, as in most flow situations, the equations for conservation of mass, momentum and energy must be solved to calculate the mixing process in a static mixer. For liquids, the system may be assumed to be incompressible and steady.

The Sulzer SMV 15 mixers applied in these experiments are of the corrugated type. Flow and mixing behavior within such a unit is affected by the wavelength of the corrugation, as well as by the intersecting angle of the corrugated plates. Some workers have performed detailed modeling of the flow structures. G. Gaiser, (1994) showed that at high intersection angles, the main part of the flow follows the furrows of the structure, while only a minor part of the flow follows the longitudinal direction, leading to an inefficient mixing behavior. Better mixing was achieved when decreasing the intersection angle, which increased part of the flow following the longitudinal direction and decreased the part of the flow following the furrows.

Also, short relative corrugation wavelengths lead to a flow behavior where the flow predominantly follows the furrows of the structure, is reflected at the side wall and flows back in the furrows of the opposite plate, such that only a minor part of the flow follows the longitudinal direction. With an increasing wavelength, the part of the longitudinal flow component increases, leading to better mixing at intermediate wavelengths. At higher wavelengths the longitudinal flow component becomes dominant, thereby worsening the mixing behavior since the lateral displacement of the fluid becomes insufficient.

Static mixing means homogenization without the use of moving parts. In the absence of large recirculation flows, all pipeline type mixers are basically continuous mixers predominantly with the driving mixing force in the radial

direction. In contrast to tank agitation devices they do not backmix. Stationary guiding elements within the fluid conducting pipe split the stream into partial streams, which in turn are redirected in such a manner that a homogeneous mixture eventually is achieved. Thus, only radial inhomogeneities are reduced. Such pipeline devices cannot correct axial or time variations.

In the description that follows in the next subchapter, regarding calculation procedures, material about the Sulzer SMV mixers has been collected from the vendor's information brochures .

The basic criteria for the selection of motionless mixers are the relative mixer length L/D required for a given homogeneity, and the corresponding pressure drop for that relative mixer length. Other criteria, such as overall length, holdup, and residence time spectrum may also influence a preliminary selection.

However, the Sulzer SMV 15 mixers applied in these experiments are of standard commercial type. Each mixing element is made from corrugated plates and designed in such a manner that they provide open, intersecting flow channels. The mixing follows a geometric pattern, and homogenization is attained by the fluid being forced to follow this pattern. The shear forces set up in static mixers are generally small. The SMV type mixer is principally used in the turbulent flow regime.

3.6 Calculation procedures for static mixers

3.6.1 Assessing homogeneity

Literature provides numerous criteria of mixing quality for the analysis of mixing processes. In most cases the standard deviation σ is used:

$$\sigma = \sqrt{\frac{\sum_{i=1}^{n}\left(x_i - \bar{x}\right)^2}{n-1}} = \sqrt{\frac{\sum_{i=1}^{n}\left(x_i^2 - 2x_i\bar{x} + \bar{x}^2\right)}{n-1}}$$
$$= \sqrt{\frac{\sum_{i=1}^{n}x_i^2 - 2\bar{x}\sum_{i=1}^{n}x_i + \sum_{i=1}^{n}\bar{x}^2}{n-1}} = \sqrt{\frac{\sum_{i=1}^{n}x_i^2 - n\bar{x}^2}{n-1}} \qquad (3.95)$$

with

$$\bar{x} = \frac{\sum_{i=1}^{n}x_i}{n} \text{ and } \sum_{i=1}^{n}\bar{x}^2 = n\bar{x}^2 \qquad (3.96)$$

where x_i is the locally measured variable (e.g. concentration) and n is the number of samples.

The standard deviation σ_0 for the initially unmixed state of two fluids with the volume flows $\overset{*}{V}_1, \overset{*}{V}_2$ $\left(\overset{*}{V}_1 << \overset{*}{V}_2\right)$ and concentrations $x_1 = 1$ and $x_2 = 0$ is:

$$\sigma_0 = \frac{\sum \overset{*}{V}_1 \overset{*}{V}_2}{\overset{*}{V}_1 + \overset{*}{V}_2} = \sqrt{\bar{x}(1-\bar{x})} \qquad (3.97)$$

with

$$\bar{x} = \frac{\overset{*}{V}_1}{\overset{*}{V}_1 + \overset{*}{V}_2} \qquad (3.98)$$

Usually the results of measurements are represented by the relative standard deviation σ/σ_0, which indicates the change in the mixture as compared with its initial state. The relative deviation σ/σ_0 depends on the ratio of bulk rates

of the components, and can therefore be adopted as a quantitative comparative characteristic of the mixers. However, it is impossible from this ratio to judge the final state of the mixture or the deviation from the average value $\bar{x}$.

According to the experimental results achieved by Grosz-Röll (1980), the relative standard deviation is not a function of the volumetric flow ratio. Therefore, measurements with different volumetric flow ratios fall on the same line. In the initial state the relative standard deviation is unity. However, the characteristic quantity of a mixture is the mean value $\bar{x}$, which therefore is the value required in a mixing task

Thus, the degree of homogeneity of a mixture, expressed as standard deviation from the mean, is quantifiable by means of the variation coefficient defined as:

$$V = \frac{\sigma}{\bar{x}} \tag{3.99}$$

The smaller the value of $\sigma/\bar{x}$ is, the more homogeneous the mixture will be. Adequate values for mixing duties in industry are around 0.05, i.e. 5% standard deviation from the mean. At the start of mixing the relative standard deviation is unity.

For the variation coefficient to remain the same, even for small ratios of bulk flow rates, the relative dispersion should inevitably be reduced. This means that the relative length of the mixer should be increased for lower ratios of bulk flow rates. Only for a mixture with equal component flow rates

$$\overset{*}{V}_1 : \overset{*}{V}_2 = 1:1 \tag{3.100}$$

i.e. $\bar{x} = 0.5$, are the quantities $\sigma/\bar{x}$ and σ/σ_0 equal.

Basically, according to Grosz-Röll (1980), for viscosity ratios less than 100:1, the only parameters that influence homogeneity are the volumetric flow ratio and the relative mixer length L/D.

CHAPTER 3 TURBULENCE & DROPLET SIZE DISTRIBUTION IN STATIC MIXERS

The SMV mixer is used primarily in turbulent flow, requiring a pipe Reynolds number larger than 2300. This implies a smaller mixer Reynolds number (based on a d_h being smaller). As described by Etchells & Short (1988), the mechanisms of mixing in the laminar and turbulent modes are completely different. In the turbulent mode, the mechanism is that of radial eddy diffusion due to turbulence, while in laminar mode it is a shearing, shuffling and striation forming mechanism. Davies (1972) has shown that the eddy diffusivity is proportional to the square root of the friction factor. Turbulent radial eddy diffusion is enhanced by increased energy dissipation and by reduced effective diameter due to the internal structures, both of which result in an apparent increase in the friction factor. This enhancement lasts the length of the mixer and downstream until the high turbulence decays to the appropriate mainstream turbulence. In the SMV mixer, the homogeneity increases exponentially with increasing mixer length. This is in contrast the situation in an empty pipe, where it is typically required a length of 100 diameters to produce a practical homogeneity (Gross-Röll, 1980).

3.6.2 In-line disperser, drop formation and droplet size prediction in static mixers

Correctly, however, mixing of two immiscible liquids is not termed «mixing». Rather, for such temporary mixing, the term «dispersion» is more appropriate when working with an immiscible system, such as oil and water. However, using the term «static mixer» represents a well defined unit, and for this reason the term is also adopted in this work even though the unit has an application as a disperser.

Not all the energy needed to overcome the pressure drop is converted to heat; a part of it is used to produce the interfacial surface area. This is appropriately illustrated in the work of F. Streiff (1977). As shown in Fig. 3.5, the thin plates of the mixing elements first provide coarse subdivision. When a drop enters the interfacial area of the intersecting channels, it is subjected to dynamic pressure fluctuations due to the velocity components being displaced 90° and, as a result of this, becomes deformed. In agreement with the basic theory of Levich (1962), if the drop's diameter exceeds a critical size, and $D > D_{\max}$, it will finally break up due to turbulence.

CHAPTER 3 TURBULENCE & DROPLET SIZE DISTRIBUTION IN STATIC MIXERS

As long as viscous shear forces can be neglected, the criterion for stability can be expressed as a force balance between the surface force and the force due to pressure fluctuations (F. Streiff, 1977):

$$dF_\gamma = dF_p = \Delta p dA \tag{3.101}$$

By applying the well known Young-Laplace equation, the surface force may be expressed as

$$dF_\gamma = \left(1/R_1 + 1/R_2\right)\gamma \, dA \tag{3.102}$$

where R_1 and R_2 are the mean curvature radii (being typical of a droplet exposed to pressure fluctuations) of the surface element dA. For a sphere with diameter D, or rather D_{max}, it follows that

$$dF_\gamma = \left(4\gamma/D_{max}\right)dA \tag{3.103}$$

CHAPTER 3 TURBULENCE & DROPLET SIZE DISTRIBUTION IN STATIC MIXERS

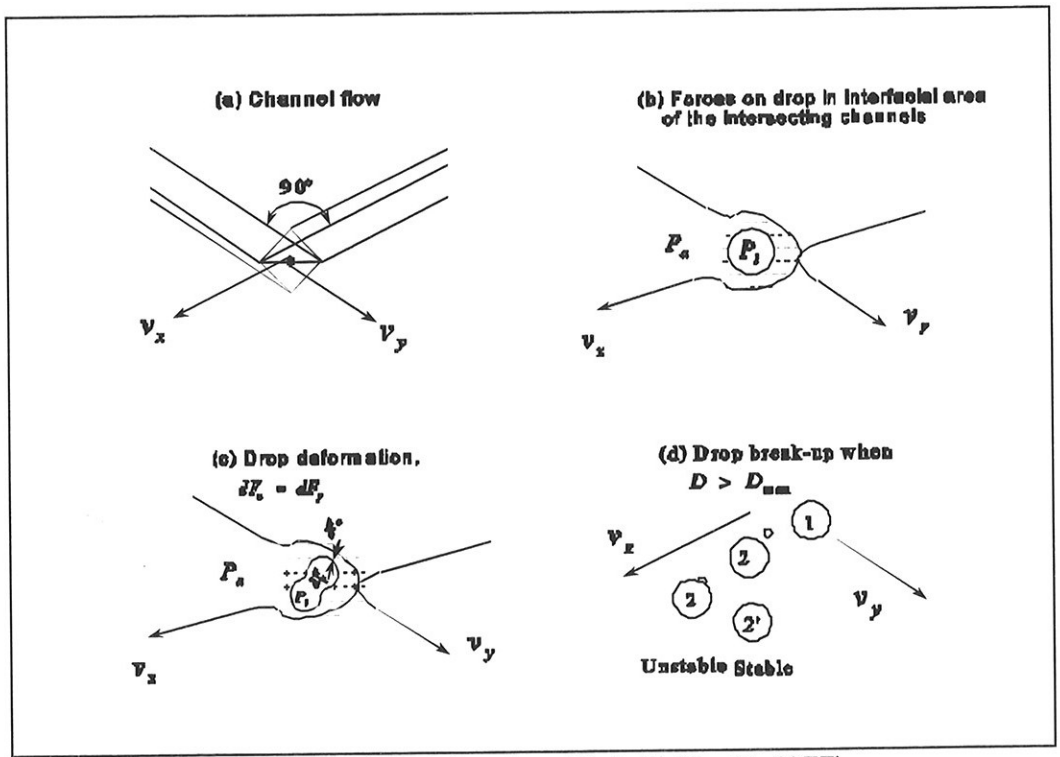

Fig. 3.5: Drop formation in the static mixer (Ref.: F. Streiff, 1977)

The forces due to pressure fluctuations are not distributed evenly on the surface, so in reality the drop cannot be spherical. Nevertheless, the assumption of a spherical form will be made in this work.

From the drag force law for the sphere:

$$\Delta p \approx c_D \frac{\rho_c v^2}{2} \tag{3.104}$$

Since we are considering drops which on the average are only a fraction of the size of the channel dimensions, the drag is greater than that of free drops. Many small droplets represent a larger drag resistance than a single larger

droplet having the same total volume. An approximation may be made with the following function:

$$c_D \approx \frac{K}{\mathrm{Re}^{\alpha}\left(d_h D_{max}\right)^{\beta}} \tag{3.105}$$

where K is a constant, Re is Reynolds number $\left(\rho_c v d_h/\eta_c\right)$, d_h is the hydraulic diameter of mixing element channels. It is desirable to find a relationship between d_h and D_{max} (or D_{32}). Substitution of eqns. (3.103), (3.104) and (3.105) into eqn. (3.101) yield a relation for $D_{\max}/d_h$:

$$D_{\max}/d_h \approx \left(\frac{8\gamma\ \mathrm{Re}^{\alpha}}{\rho_c v^2 d_h}\right)^{1/(1+\beta)} \approx We^{-n}\ \mathrm{Re}^{m} \tag{3.106}$$

where the Weber number is defined as $We = \dfrac{\rho_c v^2 d_h}{\gamma}$, and

$n = 1/(1+\beta)$

$m = \alpha/(1+\beta)$

When drops break up, however, not only drops of roughly the same size result, but also a number of small satellite drops are created which may combine with larger drops in the mixing cells following. These new drops do not break up again as long as their diameter is less than $D_{\max}$. Accordingly a whole range of drop sizes is formed.

To characterize such a collection of drops, the Sauter drop diameter D_{32} is introduced:

$$D_{32} = \frac{6V_d}{A} = \frac{\sum n_j D_j^3}{\sum n_j D_j^2} \tag{3.107}$$

where V_d is the volume of dispersed phase, and n_j is the number of drops of size class j. The related interfacial area per unit volume of the mixture is linked with the diameter D_{32} according to:

$$a = 6\varepsilon / D_{32} \tag{3.108}$$

where ε is the dispersed phase volume fraction.

As reported by El-Hamouz et al. (1994), under isotropic conditions Kolmogoroff's (1949) theory gives a relation for D_{max} as follows, which is valid for low dispersion hold-up:

$$D_{max} = k \frac{\sigma^{0.6}}{\rho^{0.6} \varepsilon^{0.4}} \tag{3.109}$$

A homogeneous field of velocity differences is set up by the mixing elements, and opportunities for drop combination are offered by the continuous reunion of partial streams. Consequently, a narrow range of drop sizes may be expected, and it is therefore reasonable to substitute D_{32} for D_{max} in eqn. (3.108).

In experiments performed by Streiff (1977), the values of the constant and the exponents n and m in eqn. (3.106) were found to be such that the following empirical equation was obtained:

$$D_{32}/d_h = 0.21 We^{-0.5} \, \mathrm{Re}^{0.15} \tag{3.110}$$

In the experiments of Streiff (1977), no influence of the dispersed phase volume fraction could be found in the range investigated $(\varepsilon \leq 0.25)$. Eqn. (3.110) was examined in the range $200 \leq \mathrm{Re} \leq 20000$. With mixing elements having a hydraulic diameter $d_h < 0.15d$, d = pipe diameter, Streiff concluded that coarser mixing elements should be arranged upstream in order to avoid coalescence.

CHAPTER 3 TURBULENCE & DROPLET SIZE DISTRIBUTION IN STATIC MIXERS

As the drop sizes in liquid-liquid dispersions are not uniform, many investigators (e.g. Levich, 1962; Middleman, 1974) usually assume that there is a maximum drop diameter, D_{max}, above which stable drops do not exist (i.e. a drop breakage control) and a minimum drop diameter, $D_{\min}$, below which there are no stable drops (i.e. a coalescence control). This assumption is important for the work presented in this dissertation, since it has been the basis for our method.

It is commonly assumed by scientists, and recently verified by workers such as Zerfa & Brooks (1996), that there is a linear relationship between the Sauter mean drop diameter D_{32} and D_{max}. Berkman & Calabrese (1988) found the proportionality constant to be 1.5, i.e. $D_{max} = 1.5\,D_{32}$. The validity of the proportionality between D_{32} and D_{max} is important, as it gives credibility to the use of an equation such as

$$\frac{D_{32}}{D} = Cf(\phi)We^{-0.6} \qquad (3.111)$$

initially derived by Middleman (1974), and which in similar forms is now commonly used by a number of investigators (e.g. Chen & Libby, 1978; Berkman & Calabrese, 1988) This equation assumes that the disruptive energy acting on a drop is due to inertial subrange eddies and that drop stability is due only to interfacial tension.

In the inviscid limit (i.e. where the viscosity group $Vi = (\mu_d \overline{V}/\sigma)(\rho_c/\rho_d)^{1/2}$ approaches zero), Berkman & Calabrese (1988) did systematic experiments combined with photos of dilute suspensions of viscous oils in a Kenics mixer, and they found that $Cf(\phi) = 0.49$.

While Middleman (1974) considered the Reynolds number range of this study, most of his data were acquired at lower Re where the friction factor depends weakly on Re. Therefore $Cf(\phi) = 0.49$ is not strictly valid. However, it shows that the dispersed phase should be considered when evaluating mixer performance.

El-Hamouz et al. (1994) reports that Chen & Libby (1978) found the following relation for an oil-water system in a Sulzer static mixer:

$$\frac{D_{32}}{D} = 1.14\,We^{-0.75}\left(\frac{\mu_d}{\mu_c}\right)^{0.18} \tag{3.112}$$

3.6.3 Further aspects of turbulent energy dissipation

Knowledge of the rate of turbulent energy dissipation, frequently termed ε, in static mixers is needed to make predictions about dispersion, e.g. bubble and drop sizes. The procedures for gaining such information from experiments are appropriately described in the work of Bourne and Maire (1991).

The average rate of total energy dissipation, Φ, in a static mixer is related to the volumetric flow rate Q, the pressure drop Δp, the fluid density ρ, and the working volume V_M by

$$\Phi = Q\Delta p/\left(V_M \rho\right) \tag{3.113}$$

Φ is expressed per unit mass of fluid in the mixer, so that V_M is the total internal volume minus that of the metal internals. The pressure drop is related to the Newton number Ne, which is a dimensionless drag coefficient, the mixer length L, the internal pipe diameter d and the superficial liquid velocity $\bar{u}$ by

$$\Delta p = Ne\rho\,\bar{u}^2 L/d \tag{3.114}$$

The working volume is the total internal volume multiplied by the fractional liquid holdup e, so that from the two previous equations

$$\Phi = Ne\bar{u}^3/(ed) \tag{3.115}$$

CHAPTER 3 TURBULENCE & DROPLET SIZE DISTRIBUTION IN STATIC MIXERS

The dissipation rate Φ can be divided into turbulent dissipation ε , caused by the gradients of the turbulent velocity fluctuations, and direct dissipation E_D, due to gradients of the mean velocity. Thus,

$$\Phi = \varepsilon + E_D \tag{3.116}$$

3.6.4 Energy dissipation and solid surface effects

The metal internals of static mixers direct the flow through relatively narrow channels, so that wall drag influences the velocity field much more than in an empty pipe, and direct dissipation is likely to be a significant part of the total dissipation. Whereas Φ is an average over the volume V_M, ε and E_D generally vary widely with position, although the turbulence in a static mixer will be more uniform than in e.g. a stirred tank, because the flow is constrained and directed by the mixer elements.

Bourne and Maire (1991) found by experiments that a mixer with small hydraulic diameter (narrowest channels) causes a greater pressure drop from the larger wall surface per unit volume and more frequent changes in the flow direction in the SMV element with narrow channels than those with wider channels. A further effect of increasing channels size is the increasing Reynolds number, whereby flow irregularities and turbulence can grow and spread more than in narrow channels. The extreme case is the empty tube where direct energy dissipation near the wall is relatively small. The static mixer having the largest hydraulic diameter produced the lowest absolute, but the highest relative, turbulent energy dissipation rate. This emphasizes the importance of channel width in the design of static mixers: as it increases, the turbulent energy dissipation decreases somewhat at constant flowrate, while the fraction of the turbulent energy loss increases.

For a given fluid (density and viscosity) and a given element design (hydraulic diameter of channels, void fraction, shape of elements) the energy dissipation rate is determined by the fluid velocity ($\varepsilon \propto \bar{u}^3$ in the fully turbulent regime).

It is worth noting that other workers have found (Sembira, Merchuk & Wolf (1988)) a remarkable difference in behavior between mixers of different material (i.e. SMV mixers with SS316 steel with and without Teflon coating), suggesting that the dispersed phase (kerosene) interacts with the surface of

the mixer and that this interaction has a strong influence on the processes of a drop breakup and coalescence.

This difference is related to the relative wettability of the surface by the two liquids. The contact angle of kerosene/Teflon/water is 157° while that of kerosene/SS316/water is 59°.

As described by these workers, kerosene therefore preferentially wets the Teflon surface, and waters the metallic surface, thus anticipating a larger amount of kerosene being retained and even trapped in corners when the mixer is Teflon coated and therefore that more time would be needed to reach the new dynamic equilibrium state.

3.6.5 Surfactants and solid surface effects

Similar considerations as those given in the previous subchapter may be applied in the system used in this work. As described in the textbook of P. Mørk (1994), contact angles may be modified by means of wetting chemicals (surfactants). Such surfactants, often termed tensides, may have strong influence on surface tension and interfacial tension. Different tensides are capable of making a system either wetting or non-wetting (i.e. water resistant when the liquid is immersed in water), depending on the chemical compositions of the surface and the tenside molecule. Irregular molecules are often particularly effective for wetting since the formation of micelles is unfavorable due to steric effects. Generally, non-ionic tensides do also have good wetting properties.

Wetting chemicals have a broad range of applications and are generally applied where it is desirable with a good contact between a liquid - usually water - and a hydrophobic, e.g. a fatty, oily or waxed surface.

For qualitative judgment of how a surfactant will influence the wetting in a given system it is necessary to consider the interfacial tensions that will be influenced. By using

- Young's equation: $\gamma_{sg} - \gamma_{sl} = \gamma_{lg}\cos\theta$
- Young-Dupre equation: $W_a = \gamma_{lg}(1+\cos\theta)$

one may achieve an idea of how the contact angle will be changed. In these equations, γ_{sg}, γ_{sl}, γ_{lg} denote the interfacial tensions for solid-gas, solid-liquid and liquid-gas, respectively. W_a denotes the adhesion work, while θ is the contact angle.

Water has a relatively high surface tension, approximately 72 mN/m (reflecting the strong intermolecular attractive forces), and will not spontaneously spread out on covalent materials having surface free energies smaller than 72 mJ/m^2. However, high-energy surfaces (e.g. containing Si, or being metallic) will normally be wetted. Thus, by using tensides capable of modifying the interfacial tensions in a system, these «naturally» given wetting properties may be altered.

The same considerations are valid for the experimental systems presently applied, i.e. Exxsol/water and Statfjord crude/water. Crude oils are mixtures of numerous aliphatic and aromatic hydrocarbons, and oxygen, nitrogen and sulphuric compounds. Some of these compounds are surface-active in nature, and can adsorb to water-crude oil interfaces (Sjöblom et al., 1997). Two such classes of compounds are asphaltenes and resins. They are both polymeric in nature and have structural similarities, as observed from infrared spectroscopy. There are different definitions of asphaltenes as they are not one compound, but a solubility-class of compounds. Part of the heterocyclic molecules in a crude oil is dissolved in a molecular state and the rest is in an undissolved colloidal state. The asphaltenes are stabilized in the crude oil by the lighter resins. The asphaltenes precipitate when the crude oil is treated with a light aliphatic hydrocarbon.

Surfactants thus have a stabilizing effect and demote coalescence of oil droplets. Similar explanations may be given in considering the aging effects of crude oils, where asphaltenes and waxes diffuse from the bulk to the surface where they form a surface film. The light paraffin components will also diffuse likewise to the surface, and in doing so disappear by evaporation.

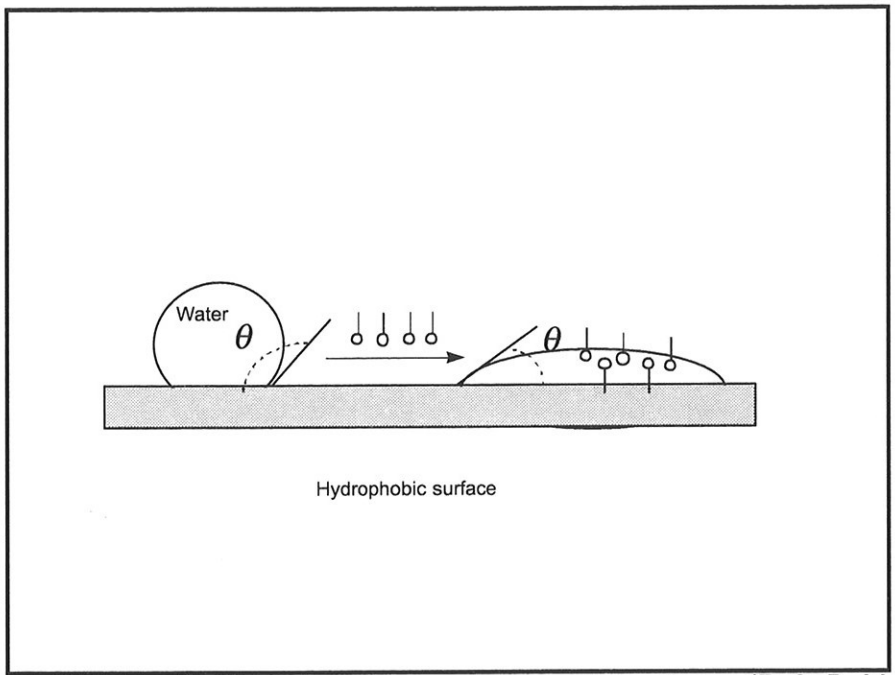

Fig. 3.6: Modification of contact angles on solid surfaces (Ref.: P. Mørk, 1994)

A hydrophobic surface, e.g. Teflon or wax $(\theta \approx 110^\circ)$, will not be wetted by water. However, the situation can be altered as indicated schematically above by adding a tenside that adsorbs on the surface, thereby leading to a reduction in γ_{sl}. Further, the tenside will be adsorbed on the water-air surface, thus reducing the γ_{lg}. The result is that $\theta < 90^\circ$, and at least a partial wetting is obtained.

3.6.6 Use of energy dissipation in static mixers

Berkman & Calabrese (1988) reports on the application of measurements concerning static mixers; e.g. pressure drop measurements in their trials were converted to Fanning friction factors (Bird et al. (1960)) by:

$$\Delta p = \frac{4L}{D_0}\frac{1}{2}\rho_c \overline{V}^2 f \tag{3.117}$$

which is similar to eqn. (3.113).

Middleman (1974) assumed that f showed a dependency on *Re* similar to that for a smooth pipe. Mean energy dissipation rates may be estimated from the previously stated eqn. (3.30)

$$\overline{\varepsilon} = \frac{\overline{V}\Delta P}{\rho_c L} \tag{3.118}$$

where $\overline{V}$ is the mean velocity of the continuous phase in empty pipe. Combined with eqn. (3.117) this yields:

$$\overline{\varepsilon} = \frac{2\overline{V}^3 f}{D_0} \tag{3.119}$$

As stated previously, an estimate of the Kolmogoroff microscale is given by eqn. (3.14):

$$\overline{\eta} = \left(\nu_c^3/\overline{\varepsilon}\right)^{1/4} \tag{3.120}$$

In static mixers, the largest eddies are of order $0.5\,D_0$, where D_0 is the pipe diameter, while the smallest eddies are of order $\overline{\eta}$.

As stated in the textbook of Tennekes & Lumley (1992), it is known that eddies of different sizes exchange energy with each other. And turbulence commonly receives its energy at large scales, while the viscous dissipation of energy occurs at very small scales. It is further stated that there often exists a range of eddy sizes which are not directly affected by the energy maintenance and dissipation mechanisms; this range is called the inertial subrange.

The strain rate of the large, «energy-containing» eddies is comparable to the strain rate of the mean flow. Thus, due to the strain rate of the mean flow maintaining a steady orientation, the large eddies are steady anisotropic. On

the other hand, the strain rate of small eddies is large compared to that of the mean flow and of the large eddies, so that no permanent anisotropy can be induced at small scales. The inertial subrange expresses an equilibrium range of eddy wave numbers exhibiting local isotropy, i.e. where turbulence have been «scrambled» at small scales and any permanent sense of direction is lost.

To meet Kolmogoroff's theory for the inertial subrange, it is required that the maximum stable drop sizes are much larger than the microscale but much smaller than the macroscale, such that the turbulent disruptive force per unit area acting on the drop is given by (Shinnar (1961)) for $D = D_{max}$.

$$\tau_c = 1.5\alpha\rho_c\varepsilon^{2/3}D^{2/3} \qquad (3.121)$$

CHAPTER 4 CHARACTERIZATION AND MEASUREMENTS OF THE STATIC MIXER

4 CHARACTERIZATION AND MEASUREMENTS OF THE STATIC MIXER

4.1 Experimental characterization

4.1.1 Results obtained from previous workers

It has to be emphasized that, in the present experimental trials, it has been focused on droplets being in a stable suspension, and being smaller than about 40 μm in diameter. The larger droplets have been neglected in this work.

The reason for adopting this approach is that these experimental trials emphasize on investigating the small concentrations of the smaller droplets. Hence, to achieve a reasonable degree of accuracy, it was found desirable to minimize the influence of the larger droplets, defined to be larger than about 40 μm in diameter.

Additionally, the larger droplets have a tendency of creating problems for the oil separation apparatus, since the presently applied techniques are unable to separate the smallest droplets being suspended in the bulk oil/water mixture..

Investigators involved in the study of droplet diameters do not normally limit their investigations to droplets having diameters smaller than about 40 μm. In the literature it has not been found any documentation on investigators

working with this kind of constraint in the study of droplet diameters. It is therefore worth noting what other workers for the larger droplet size classes have achieved.

El-Hamouz et al. (1994) reported on experiments performed with static mixers of Lightnin «in-line» type.

At constant velocity they found that the Sauter mean diameter D_{32} decreased as the number of mixing elements increased. Further, they found that for a fixed number of elements, D_{32} decreased from 460 μm to 46 μm with increasing fluid velocity from 0.5 m/s to 2.8 m/s. These results were as expected, showing that the mean drop size decreases as the amount of shear in the system is increased.

It was also found that the rate of change of D_{32}, in a situation with increasing number of elements, gradually decreased until a constant value was reached. This was taken as the point of dynamic equilibrium where the rate of coalescence was equal to the rate of dispersion.

Further, El-Hamouz et al. (1994) found that the best energy utilization was obtained when the number of mixing elements was small and the velocity high where D_{32} is greater than the equilibrium value. As noted, this can be attributed to the rapid rate of droplet break-up which dominates the mixing process when the average drop size is much larger than the equilibrium drop size.

It was also noted that the dispersed phase concentration had a significant influence on the dispersion process. As the concentration of the dispersed phase was increased, the collision frequency became higher and the resulting mean droplet diameter would be expected to be become higher.

The residence time did also have an impact on the degree of coalescence, thus indicating that the pipes and fittings in a flow network can have a profound effect on the nature of the dispersion at the exit to the liquid system.

With the primary goal of characterizing the drop-size distributions formed when a liquid-liquid dispersion was exposed to turbulent pipe flow, Collins & Knudsen (1970) designed an apparatus to produce through turbulent pipe

flow an unstable dispersion of immiscible liquids and to allow the dispersion to be photographed at intervals along the length of the pipe as well as at varying distances from the pipe wall. Separate pumping of the water and organic phases was provided to eliminate dispersion caused by the high shear rates in a pump.

In their investigation tap water was used as the continuous phase. The dispersed phase was mostly Shellsolv, a kerosene-like solvent, which had a viscosity of 1 cP and an interfacial tension 40 dynes/cm ($40*10^{-3}$ N/m).

The experimental results were analyzed to determine the effect of turbulence alone, and the log-normal distribution was found to be inadequate: As the mixture flowed through
the pipe, the distribution was increasingly divergent from the log-normal type. In the nearly 1300 photographic prints obtained by Collins & Knudsen, they claimed that no indications of coalescence were indicated; thus either the coalescence happened very fast or it occurred very infrequently.

From these observations they concluded in their report that no adequate distribution law with a theoretical basis could be found which correlated experimental distributions with theoretical models.

At 0.6% by volume dispersed phase, only 5% of the drops measured had diameters above 230 μm, the maximum stable drop size as predicted by the Kolmogoroff/Hinze relation, and further refined by Sleicher (1962), e.g. eqn. (3.36). It appeared that little breakup occurred at this concentration, which is not surprising in view of the small number of unstable drops present. For concentrations of 1.3 and 5%, the percentages of drops with diameters greater than 230 μm were 19 and 22%, respectively. Considerable breakup was found.

The distributions did all have the same shape for varying velocities, i.e. initially linear on the log-normal graph, but increasingly diverging into a parabolic type as the mixture flows through the pipe.

In discussing this, because of the low dispersed phase concentrations (less than 10%) used in the experiments and the short residence time (less than 3 secs, coalescence effects were considered negligible compared to breakup.

CHAPTER 4 CHARACTERIZATION AND MEASUREMENTS OF THE STATIC MIXER

The proposed three-parameter model, stochastically based, should allow the parameters to be determined (D_{max} , $D_{1,0}$ and R_v), and predict not only the correct individual distributions, but also the proper sequence of distributions or kinetics as the dispersion flows through the pipe. Central to the proposed model was the postulate that the entire process may be considered to take place in independent discrete steps. Previous workers (Paul & Sleicher, 1962; Sleicher, 1962) have shown experimentally and theoretically the existence of a maximum stable drop size for liquid-liquid dispersions in turbulent pipe flow (230 μm). Thus any model would be expected to include the maximum stable drop size as a parameter.

Judging by the ability to simulate the experimental distributions observed downstream it was shown that the model predicted a sequence of distributions very similar in form to those observed experimentally, and it was concluded that this model gave an adequate qualitative representation of the events occurring in the pipe.

The model states that: «Probability of breakup is zero below a diameter equal to $D_{\max}$ (the maximum stable drop diameter) and increases linearly to a 1.0 probability at a diameter equal to $D_{1.0}$ (the droplet diameter at which probability of breakup becomes one). Two uniformly distributed daughter drops (i.e. having uniformly distributed volume ratios) and a small satellite drop are produced.«.

The reason no simple size-distribution law could be found to describe the experimentally observed distribution may appear obvious from the form of the model. The existence of a maximum stable drop size $D_{\max}$ means that the portion of the initial distribution with diameters less than $D_{\max}$ remains unchanged by the action of the turbulence. Thus, what was actually measured was a superposition of two distributions, one initially present and the other produced by the turbulence.

The model is a three-parameter model, including: 1) $D_{\max}$, 2) $D_{1,0}$, the drop diameter at which probability of breakup becomes one, 3) R_v , the range of volume ratio of satellite to daughter drops.

The first two parameters define the probability of breakup of an individual drop. If $D < D_{\max}$, the probability of breakup is zero. If $D > D_{1.0}$, the probability of breakup is unity. If $D_{max} < D < D_{1.0}$, the probability of breakup is a linear function of diameter.

The model should predict not only the correct individual distributions, but also the proper sequence of distributions or kinetics as the dispersion flows through the pipe. Agreement between theory and experiment provides evidence that the proposed mechanism may be a reasonable one for breakup in the turbulent field of a pipe.

In conclusion, according to the model, when drops break up in the turbulent core of a pipe, two daughter drops are produced which have uniformly distributed volume ratios. On the average, one very small satellite drop was also produced by each breakage event.

Further, the existence of a maximum stable drop size was clearly indicated by experimental data.

Finally, highly distorted drops and breakup appear to be restricted to the neighborhood of the pipe wall.

4.1.2 Introductory explanation to the experimental characterization trials

In the set of experiments presented in this subchapter the objective was to characterize the system of static mixer elements by obtaining numerical values for:

Mean velocity
Root mean square velocity
Turbulence intensity, i.e. the standard deviation of the mean velocity.

All results with the LDA equipment were obtained made optical measurements from within a cylindrical body of moving liquid. The moving liquid body to be measured had boundaries represented by a 16 mm ID cylindrical glass column, and the distance between two mixer elements which

was 12 mm. Each mixer element was soldered onto a thin steel wire and inserted inside the glass column. The mixer elements were mounted such that the mixer geometry at the outlet from one element had an angular position 90 degrees off the inlet geometry of the next mixer element.

Using a standard 60 mm LDA probe, with a focal length of 160 mm, the measuring volume size was 75 μm times 630 μm. With a maximum measuring length of 630 μm it was therefore considered appropriate to do the measurements at approximately every 1 mm along the diameter of the column of 16 mm ID. Thus, data for flow conditions were collected and mapped at a number of system combinations of radial and axial positions.

At each measuring position the time averaged velocity was calculated from 3000 accepted Doppler signals or maximum 10 minutes of sampling time, depending on the transparency of the fluid (i.e. the amount of bubbles/droplets following the main stream). Thus, in the figures representing the experimental results, each point represents 3000 Doppler sigals.

A schematic of the performed trials, the variations within these trials, as well as comments and results obtained from these, are presented in the following table:

CHAPTER 4 CHARACTERIZATION AND MEASUREMENTS OF THE STATIC MIXER

TEST NO.	OBJECTIVE	VARIABLES	COMMENTS	RESULTS
TEST1 to TEST4	Methodology establishment; functional testing.	No variation; full flow of tap water at approx. 23 l/min and 4 - 5° C. Beam trajectory positioned to midway between elements, i.e. H=6mm.	Arbitrary alignment of beam trajectory vs. mixer element geometry; approx. 15° deviation.	Pressure at inlet: barg Pressure at outlet: 0.78 barg. Characteristic shape of mean velocity and turb. intensity curves was identified.
TEST4B	Confirm results obtained in previous experiments.		Effect of wall channeling identified.	Shape of the curves was similar to curves in TEST1 - TEST4.
TEST5 to TEST6	Test the effect of beam trajectory alignment.	Angle of beam trajectory set to 0° relative to mixer element geometry.	Similar curve behavior identified at traverse lengths 7 mm.	Shape of the curves was significantly different. Steady RMS velocities achieved (0.70 m/s) in all tests, independent on traverse lengths.
TEST6, 7, 8, 13, 14	Test the effect of beam trajectory heights.	H set to 2, 4, 6, 8, 10 mm.		As H decreases from 10 to 2 mm, RMS increases from approx. 0.5 to 1.0 m/s.
TEST9 to TEST12	Test the effect of perpendicular beam trajectory.	Laser beam angle of incidence set to 90 °. Variation in H as above.		Similar RMS curve shapes as found in previous experiments.
TEST16 to TEST20	Test the effect of channeling along the wall.	Laser beam angle of incidence set to 0°. Variation in H as above.	Sealing tape wound around the 1st mixer element only.	No significant channelling effects were identified. RMS velocity increased from 0.4-1.6 m/s as H decreased from 10 to 2 mm.
TEST21 to TEST25	Further testing of wall channeling effects. Identify possible variations in data logged.	Variation as in previous set of experiments. However, in this set of experiments, both mixer elements were taped.	Sealing tape wound around both the 1st and 2nd mixer elements.	No significant channelling effects were identified. RMS vel. increased from 0.4-1.6 m/s as H decreased from 10 to 2 mm.
TEST21 to TEST35	Testing for different volumetric fluid velocities.	Variation in bulk volumetric velocities, Q, set to 7.5, 15, and 23 l/min. Variation in H as above.		RMS increased with increased bulk flowrate. Also, RMS increased as H decreased from 2 to 10 mm.
TEST29, 34,37,40, 41,42,43, 44	Testing the effect of heating applied to the system.	H was constantly set at 8 mm for all tests. Q values were 7.5, 15 and 23 l/min. Set values for temperature T: 5, 50 and 75 ° C.		Heat was not found to have any influence on mean velocities or RMS velocities.
TEST49 to TEST51	Testing the influence of induced air.	Variation in volumetric flowrates of air introduced.		Values for RMS increased as volumetric flowrates of air increased.
TEST52, 53	Testing turbulence conditions from mixer elements further downstream of 1st mixer element.	TEST52: 180° angle of incidence. TEST53: 0° angle of incidence. No air introduced.		Shape of mean velocities' curve is similar. However, the 2nd element gave higher recorded values .

Table 4.1: Schematic descriptions of performed trials

Within each of those denoted as TESTXX, XX being the test number, as specified in Table 4.1, there was also a number of repetitive experiments performed in order to achieve maximum consistency of the data as given in Table 4.2:

TEST NO.	NO. OF REPETITIVE EXPERIMENTS	REPLICA OF ...	COMMENTS
TEST1 to TEST4	5		Measurements were repeated 5 times within each traverse length.
TESTT5	2		Measurements were repeated 2 times within each traverse length.
TEST6 to 25	1		Measurements were only performed once within each traverse length.
TEST19		TEST15	Setup of experiment was repeated.
TEST26	2		Measurements were repeated 2 times within each traverse length.
TEST27 to 40	1		Measurements were only performed once within each traverse length.
TEST36		TEST22	Setup of experiment was repeated.
TEST37		TEST29	Setup of experiment was repeated.
TEST38		TEST34	Setup of experiment was repeated.
TEST39		TEST29	Setup of experiment was repeated.
TEST40		TEST34	Setup of experiment was repeated.
TEST41 to TEST44	2		Measurements were repeated 2 times within each traverse length.
TEST45 to 47	5	TEST34	Measurements were repeated 5 times within each traverse length for verification of previous tests.
TEST48 to 53	5		Measurements were repeated 5 times within each traverse length .

Table 4.2: Schematic of repetitive sequence of experiments

Hence, the total number of experiments performed was 111, from which numerical values were obtained. Also, each of the numerical values obtained, actually represented as the mean of 3000 doppler measurements.

4.1.3 Single phase characterization

Single phase characterization was performed by using water only. No second phase, in terms of solid particles, oil, gas or even chemicals were added.

Only tap water was used in this set of experiments. It was not considered necessary to add any particle seeding into the tap water with the purpose of aiding the LDA equipment, as a sufficient amount of naturally occurring particles was already present in the water.

It would be of interest to compare the presently obtained results with the experimental data results from other workers. However, in the available literature no information was found on similar experimental data achieved by

other investigators working on the same kind and same size of Sulzer SMV mixers.

4.1.3.1 Methodology establishment (TEST1 - TEST6)

These trials were purely introductory, in order to establish methodology for the measurements and become acquainted with the equipment.

In TEST1 - TEST4 no attempt was made to ensure the same alignment for each of the four trials; i.e. the angle of incidence for the trajectory of the beam was arbitrarily aligned with the orientation of the mixer element geometry.

In retrospect it was noted that there was approximately 15 degrees deviation of the beam trajectory from the orientation of the geometrical pattern in the mixer elements (i.e. the pattern of the corrugated plates of which the mixer elements are made). However, in TEST5 - TEST6 the beam was in alignment (i.e. 0 degrees deviation) with the orientation of the corrugated plates at the outlet of the 1st mixer element. This may be visualized by considering Fig. 4.1 below.

CHAPTER 4 CHARACTERIZATION AND MEASUREMENTS OF THE STATIC MIXER

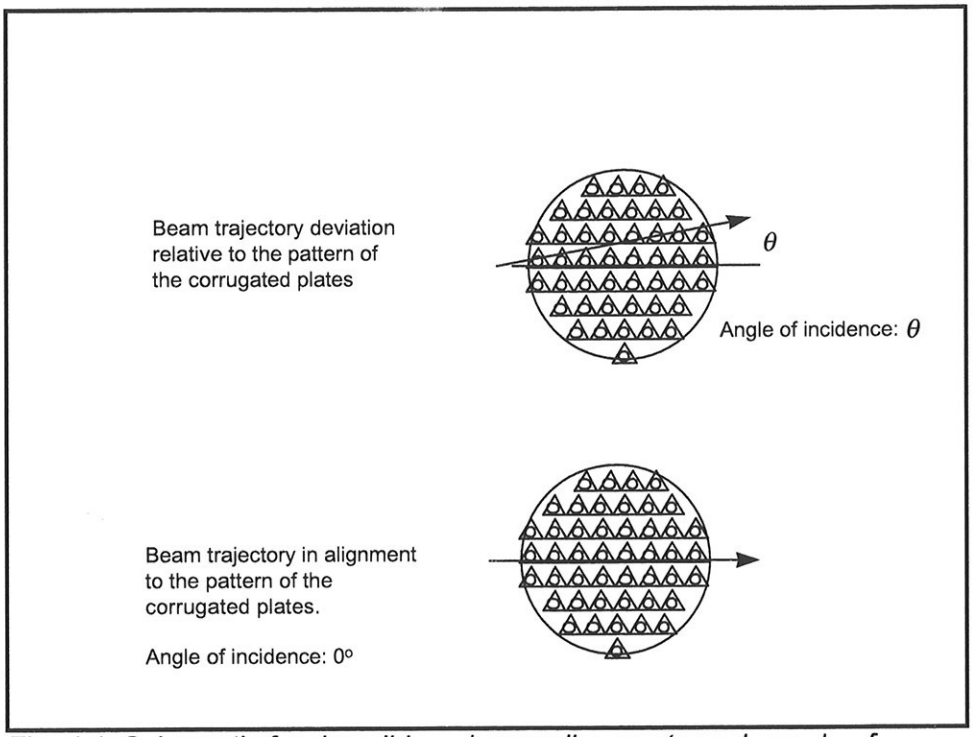

Fig. 4.1: Schematic for describing «beam alignment» and «angle of incidence»

All of these measurements were taken at conditions where no heating was applied and with a maximum available bulk flow from the tap water system. Thus, the water temperature was approximately 4 - 5 °C and the flowrate was approximately 23 l/min. This flow rate resulted in a fluid pressure of 2.3 barg at the inlet of the mixer element, and 0.78 barg at the outlet.

The traversing line of measurement points was set at a height H = 6mm from the outlet of the 1st mixer element. This height represents the middle position between the two mixer elements. Measurements were taken along the traverse of the column diameter, representing a total trajectory length of 16 mm.

CHAPTER 4 CHARACTERIZATION AND MEASUREMENTS OF THE STATIC MIXER

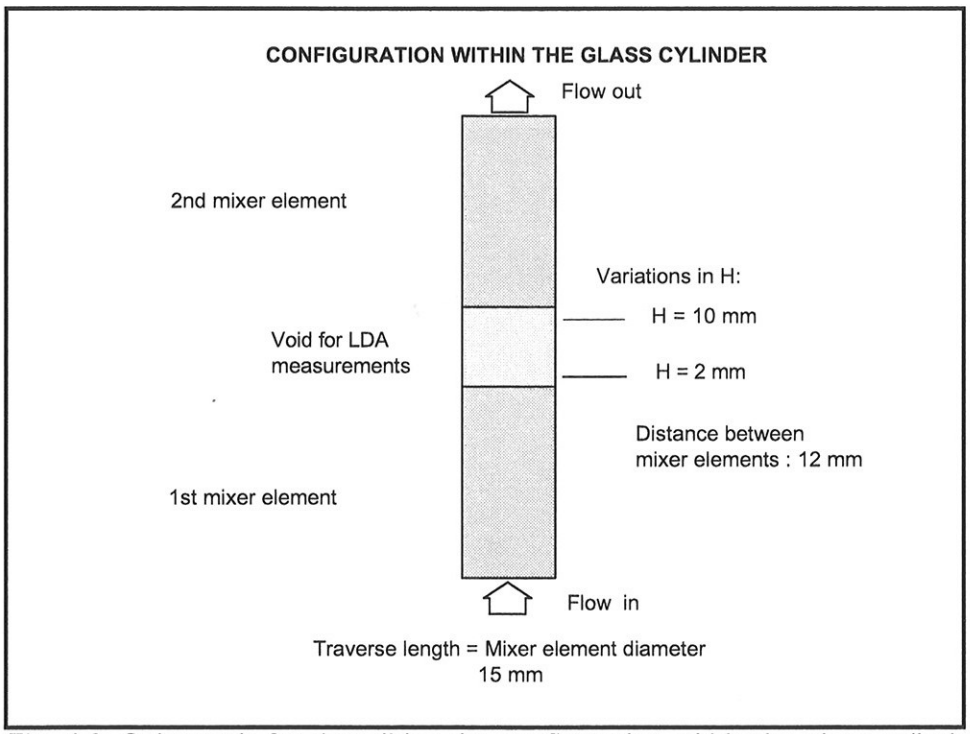

Fig. 4.2: Schematic for describing the configuration within the glass cylinder

Typical results from these trials are seen in Fig. 4.3 for TEST 4B and in Fig. 4.4 for TEST6. The difference between these two trials is the beam trajectory alignment. The beam trajectory alignment angle was approximately 15° relative to the mixer element geometry in the first case, whereas the angle was 0° in the latter case. It is stressed that only the mean values are presented as points on the curves. However, the variation of the obtained values are also indicated as +/- levels around the plotted mean values, as shown in Fig. 4.3.

CHAPTER 4 CHARACTERIZATION AND MEASUREMENTS OF THE STATIC MIXER

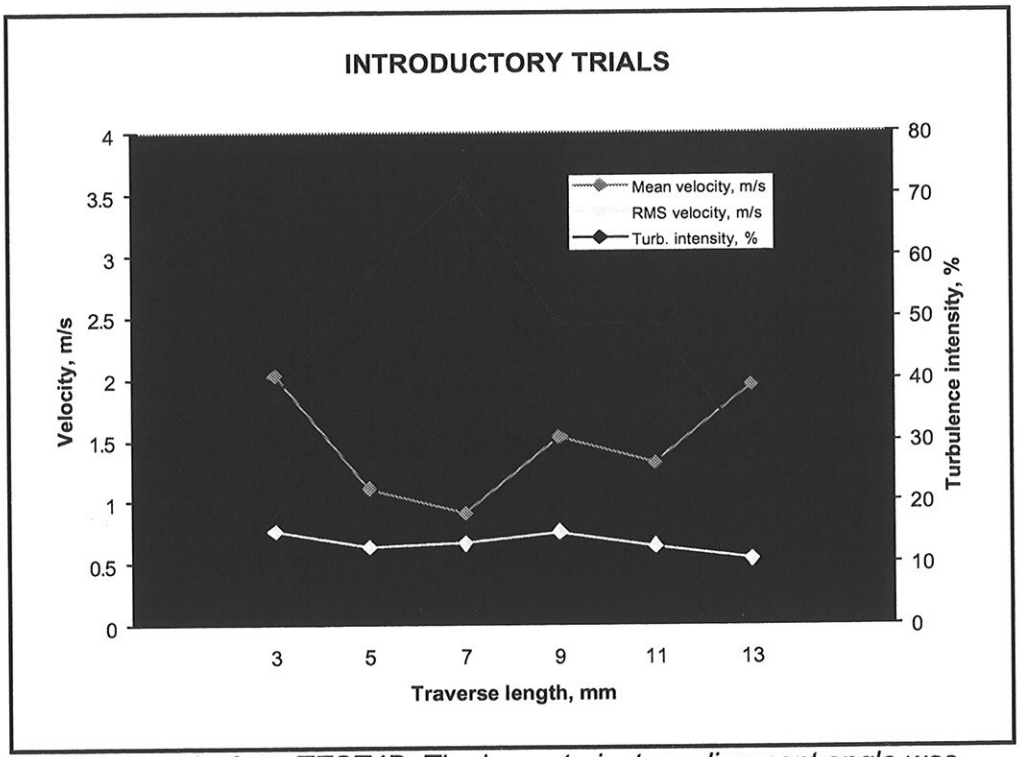

Fig. 4.3: Results from TEST4B: The beam trajectory alignment angle was approximately 15° relative to the mixer element geometry.

CHAPTER 4 CHARACTERIZATION AND MEASUREMENTS OF THE STATIC MIXER

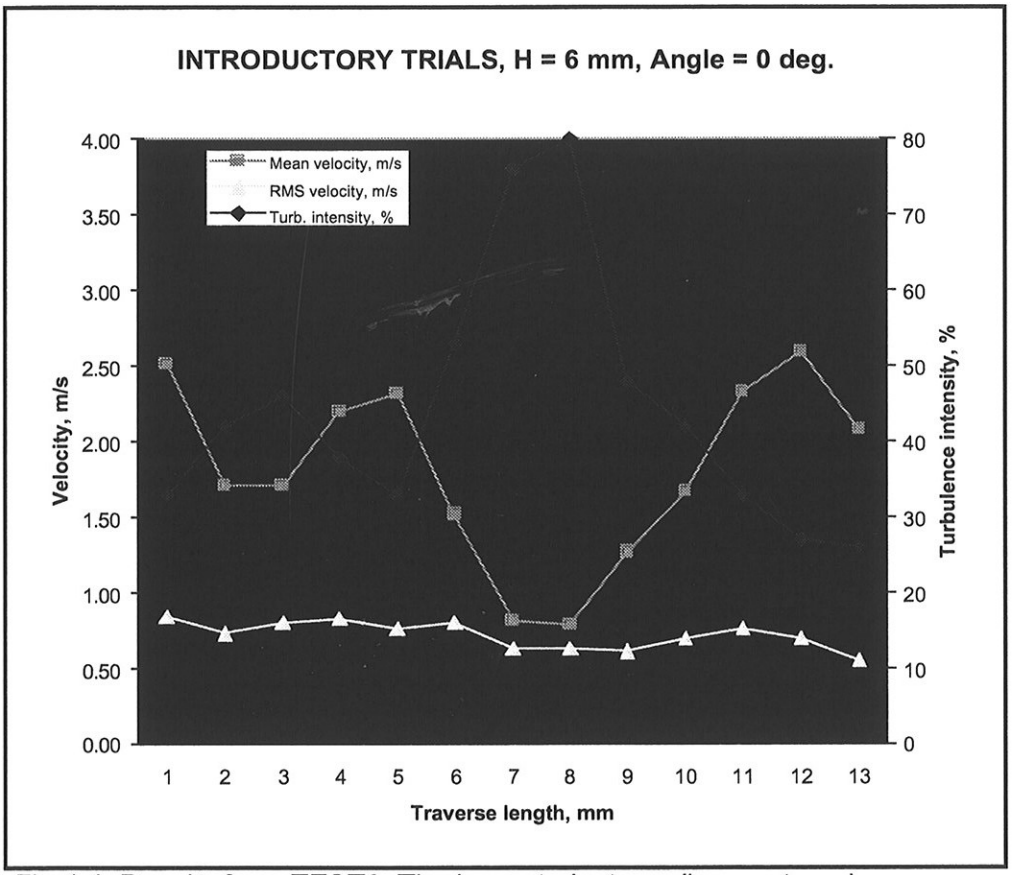

Fig.4.4: Results from TEST6: The beam trajectory alignment angle was approximately 0^{o} relative to the mixer element geometry.

Finally, there is also a schematic presentation of a velocity and turbulence intensity comparison between the two tests (TEST4B and TEST6), given in Fig. 4.5:

CHAPTER 4 CHARACTERIZATION AND MEASUREMENTS OF THE STATIC MIXER

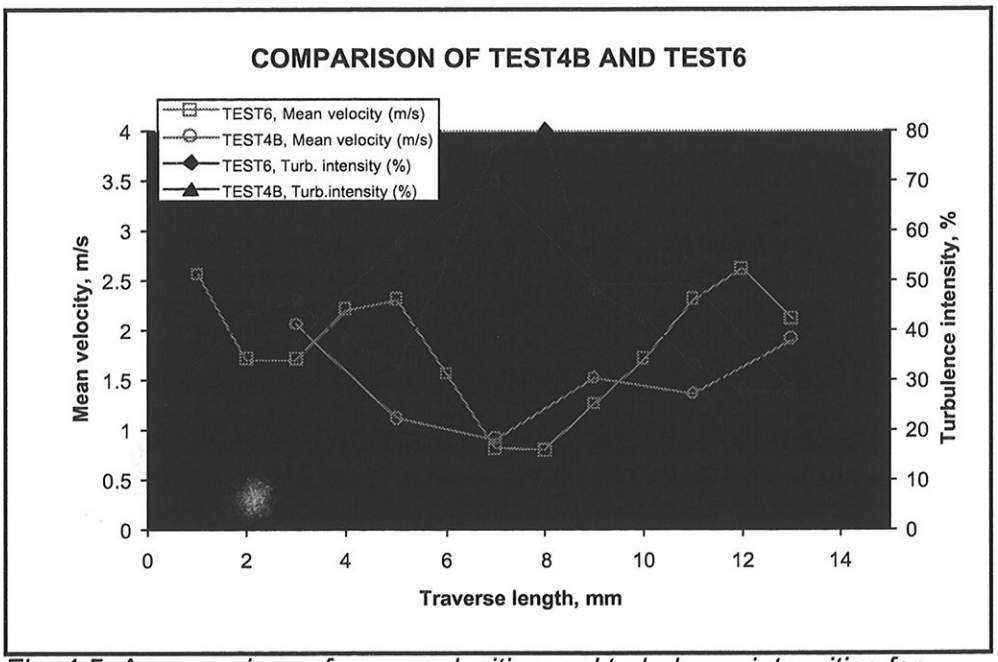

Fig. 4.5: A comparison of mean velocities and turbulence intensities for TEST4B and TEST6. In TEST4B the beam alignment angle was approx. 15°, whereas in TEST6 it was 0°.

It may be concluded from Figs. 4.3, 4.4 and 4.5 that results obtained depend on the alignment angle. The shape of the curves is different for the two cases. This becomes clear when considering the comparison given in Fig. 4.5.

In Fig. 4.5, it is seen that a turbulence intensity peak value of approximately 70 - 80% is identified in both tests, the peaks being positioned approximately halfway along the traverse of the beam (i.e. at traverse length 7mm). At the same position, low values for mean velocities are identified at approximately 0.8 m/s for the two cases. This identification of coherent low and high values at the center position is not surprising, since the beam alignment angle should have no influence on the turbulence values at the center point of the mixer element.

However, two mean velocity peaks are identified at traverse lengths 5 and 12 mm for TEST6. These peaks may probably be attributed to «open areas»

being available for the fluid flow at alignment angle of 0°, an «open area» not being available for flow in TEST4 having an alignment angle of approx. 15°. At other traversal positions, however, the flow behavior is significantly different for the two cases. Hence, it is clear that the curves for mean velocity and turbulence intensity in Fig. 4.4 follow the orientation of the corrugated plate pattern differently from those obtained in Fig. 4.3. However, as pointed out in the previous paragraph, the similarity of recorded values is good at traverse length 7 mm, which represents the center position of the cylindrical mixer element.

The RMS velocity, as shown in Figs. 4.3 and 4.4, is practically identical for the two cases, and is found to be constant across the pipe traverse. This is an important feature of the Sulzer static mixer as it provides a homogeneous turbulence field and thereby has a potential for creating narrow drop size distributions.

The feature of achieving coherent values at the center position was also seen in other recorded experiments, represented by e.g. the mean velocities presented for TEST9 - TEST12 in Fig. 4.9.

Values obtained for mean velocities close to the wall have a tendency to be higher than elsewhere along the beam traverse. When installing the mixer elements it was noted that these did not fit tightly within the glass pipe. There was obviously some clearance between the glass wall and the mixer elements.

Higher recorded mean velocities close to the wall gave some suspicions of channelling effects along the wall. It was therefore decided to conduct some tests to check the presence of such effects. These tests are presented in Ch. 4.1.3.4.

4.1.3.2 Beam trajectory height variation (TEST6, TEST7, TEST8, TEST13, TEST14)

These tests have the following parameters in common:

Water flow rate: 23 l/min
Water temperature: 5 °C

Angle of incidence: 0° (see Fig. 4.1)
Inlet pressure mixer element: 2.3 barg
Outlet pressure mixer elements: 0.78 barg

The variable in this set of experiments was the beam trajectory height H relative to the outlet from the 1st mixer element, as shown in the configuration within the glass cylinder given schematically in Fig. 4.2.

This variation in height H was set to 2, 4, 6, 8 and 10 mm, resulting in a development of the RMS as shown in Fig. 4.6.

From this it is seen that RMS decreased from approximately 1.0 m/s to 0.5 m/s as H increased from 2 mm to 10 mm. This was as expected, since there is most turbulence near the outlet from the mixer element. The RMS profiles for this test series were basically quite flat, with small variations within each value for H. Most of the recorded RMS values were within 0.5 - 0.8 m/s, regardless of H.

However, there was one pronounced exception at H = 2 mm: Two peaks were identified at traverse lengths 3 and 10 mm, where the RMS achieved values around 1.0 m/s. These peaks may probably be attributed to the proximity of the measurement volumes to the channel outlets of the mixer elements.

As a whole the RMS data at H = 2 mm vary more than at other heights, indicating that the turbulence levels may vary more inside the mixer element.

Lang et al. (1995) report that they performed numerical investigations on the Sulzer SMV mixers, and compared the results with other experimental values. They concluded from these trials that there was a fairly good agreement between CFD data and experimental data.

It is to be noted, however, that data from the their work was based on a gas mixer (as a part of a DeNOx facility, i.e. removal of nitrogen compounds) with dimensions of length 3.4 m, height 3.0 m and depth 15.0 m. The main flow velocity at the inlet was 26.9 m/s, turbulence intensity was chosen to be 5% and the turbulence length scale was 0.5 m.

Lang & Drtina (1995) did numerical simulations on Sulzer SMV static mixers to gain insight into the character of the mixing process and to check the

numerical simulation as a tool for design of single mixers. Their computed results agreed well with their measured results. Similar work with SMV mixers being in the size of those applied in the work presented here has not been found documented in literature.

However, in the work of Lang & Drtina (1995), the vortices generated by the structure of the mixer were observed to be the main driving force of the mixing of the fluid; this being the reason why the main mixing occurs in the wake of the mixer. The static SMV mixer consists of several corrugated sheets being stacked on each other. The folded edges of the sheets have a certain angle to the main flow direction, and the sheet layers are aligned in opposing directions. Lang & Drtina (1995) demonstrated that the points where the two mixer sheets touch were the starting points for vortices. The vortices which are generated by the first row of touching points in the main flow direction travel downstream till they disappear due to diffusion or are merged with the new vortices which are produced by the second and last rows of touching points. These vortices could be found for a long distance downstream in the wake of the SMV mixer under ideal conditions (i.e. at infinite size of the mixer and no channel walls present).

From this point of view, the two RMS peaks at 1.0 m/s for H = 2 mm, attributed to the proximity of measurement volumes to the channel outlets of the mixer elements, may be explained by means of the vortices generated by the touching points of the sheets. Further downstream (for H > 2 mm) , where such peaks are not found, the vortices disappear due to diffusion.

The mean velocity, shown in Fig.4.7, varied between the values 0.34 and 2.74 m/s but did not have such a straightforward relationship with respect to H as the RMS had with H in Fig.4.6. It was noted that the absolute minimum mean velocity value in these experiments was obtained for H = 2 mm, while the maximum value was obtained for H = 4 mm, at a traverse length of 9 and 10 mm, respectively. The minimum mean velocity obtained for the other heights was not less than 0.82 m/s. A value of 0.34 m/s as the absolute minimum for the mean velocity, at traverse length 9 mm, introduces a significant peak for the turbulence intensity (not shown here).

When comparing the individual curve patterns for mean velocities obtained in this set of experiments some similarities are recognized. Firstly, when considering the curve shapes, it is seen that the mean velocity variation

basically had the same progression along the traversing length of the beam. Basically, for all values of H, a U-shape was identified for the mean velocity progression, the minimum value being in the vicinity of the middle position of the traversing length.

However, a gradual shift in the position of the curves has been identified: in the beginning of the traversing length the recorded curves were close to each other. After the middle position along the traversing length had been passed, an increasing difference in the recorded values was recorded. The difference was largest at traverse length 10 mm, where at H = 2 mm the mean velocity was recorded to be approx. 0.4 m/s, whereas it was approx. 2.9 m/s at H = 4 mm.

The shape and progression of the curves follow the mixer geometry, given by the stacking of the corrugated sheets, their folding and the angle of the furrows relative to the main flow direction.

Inevitably, when positioning the laser beam manually there are certainly some inaccuracies occurring, possibly giving a contribution to the curve shift observed. However, the results appear to be reproducible, and therefore it is suspected that other factors have stronger influence on the results. For example, it is suspected that the curve shifts originate from the formation of stable circulating flows, i.e. that the flow circumstances are such that some eddies tend to stay fixed, in terms of energy and size, at certain points in the void between the mixer elements.

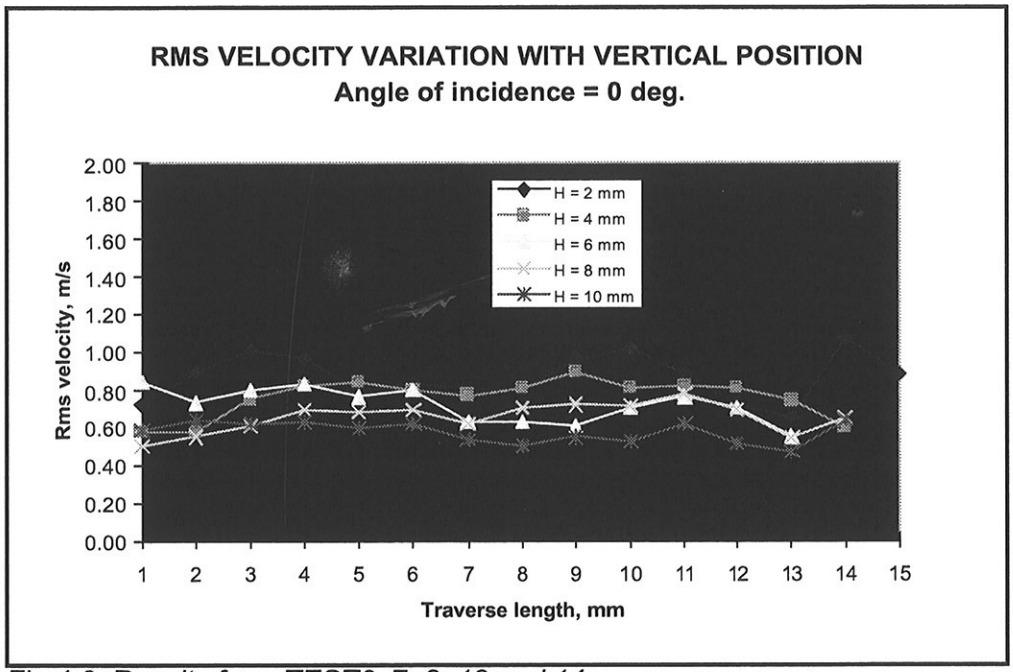

Fig.4.6: Results from TEST6, 7, 8, 13 and 14

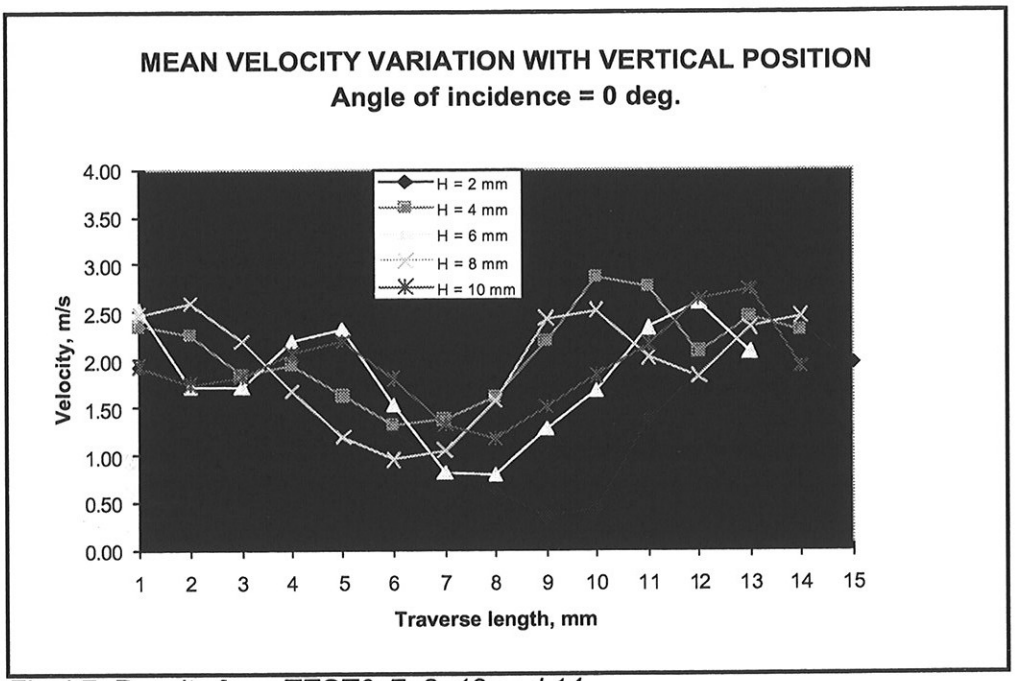

Fig.4.7: Results from TEST6, 7, 8, 13 and 14

No obvious channeling effects are revealed when observing the curves in Figs. 4.6 and 4.7. Such effects should be identifiable near traverse lengths 1 - 2 mm and 14 - 15 mm. However, there are no such indications in the behavior of the curves.

It is common practice within the mixer pipe to introduce a short void space, where there are no mixer elements inserted. This practice may be explained by the gradual shifts in the RMS levels that occurs. The length of such a void space is often in the order of one mixer length.

As indicated in Fig.4.8, which gives the mean velocities at different levels and traversing lengths within the void between two mixer elements, different stable eddies may be identified.

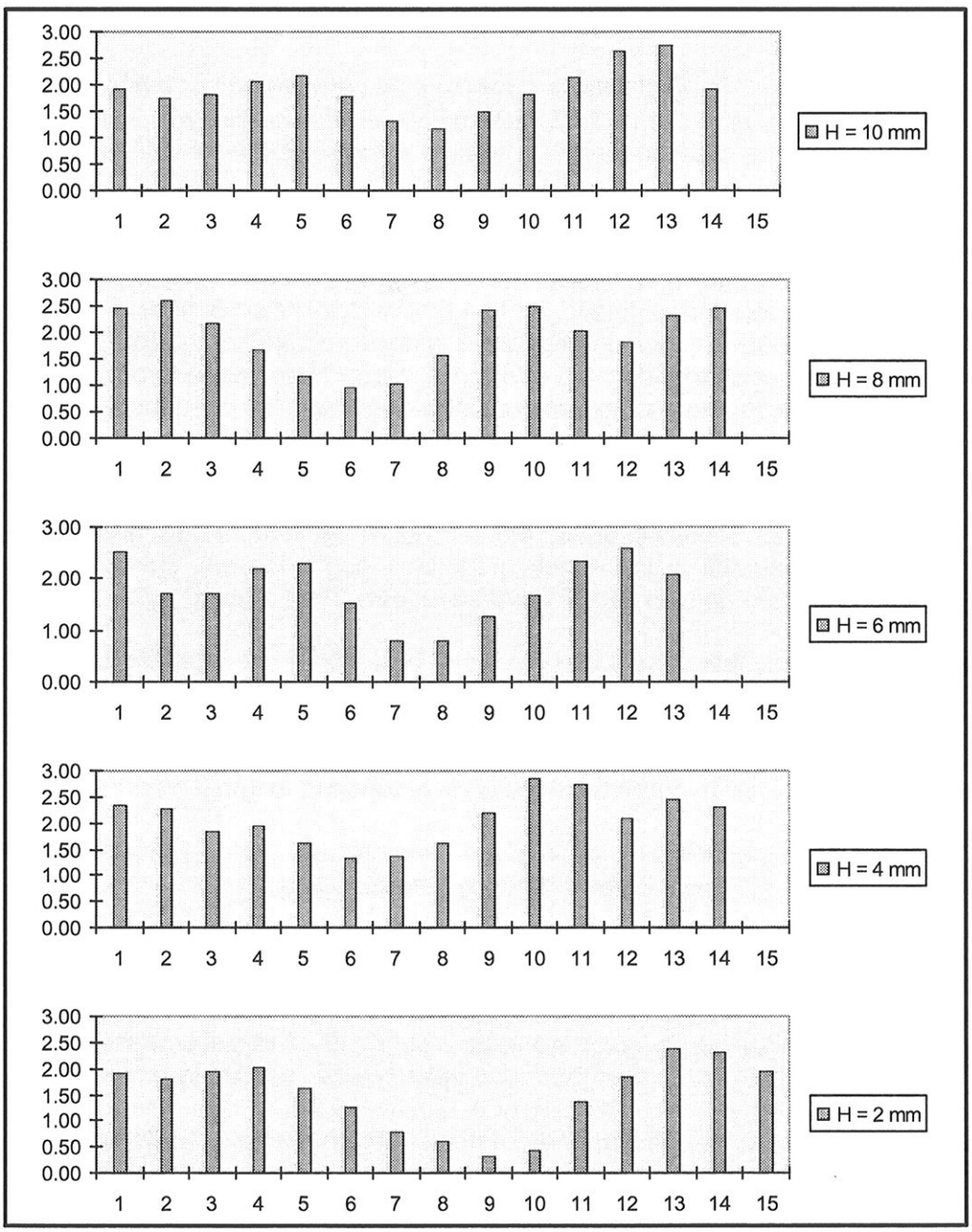

Fig.4.8: Mean vel. (m/s) vs. traverse (mm) at levels between two mixer elements

4.1.3.3 Laser beam angle of incidence 90° (TEST9 - TEST12)

This series of tests is practically identical to those presented in section 4.1.3.2. The only exception is that these tests were performed with a 90° angle of incidence of the laser beam relative to the mixer element plates (see Fig. 4.1).

The resulting development of RMS when changing the angle of incidence of the laser beam is shown in Fig.4.9. When studying the curve progression, and comparing this with that obtained in Fig.4.6, a number of similarities is identified. For instance, also in this case it is documented that the RMS increased from approximately 0.5 m/s to 1.0 m/s as H decreased from 10 mm to 2 mm. Again, this was as expected, since it obvious that there must be most turbulence close to the outlet from the mixer element.

However, there is a major difference, since for H = 2 mm two pronounced velocity peaks are identified in Fig. 4.6. (Or, there are in fact three, taking into account the peak due to wall effects at traverse length 14 mm). The two pronounced peaks are located at traverse lengths 3 mm and 10 mm.

In Fig.4.10 it may first appear that the same basic pattern is repeated for this series of tests as that shown in Fig. 4.7. It is also seen, as in the case described in the previous section, that there is a similar minimum for the mean velocity at H = 2 mm, now valued to 0.23 m/s which also introduces a very significant peak for the turbulence intensity at traverse length 7 mm.

However, upon closer examination of the mean velocity curves presented in Figs. 4.7 and 4.10, major detail differences are revealed.

First of all, at an incident angle of 90° (Fig. 4.10), a considerably higher mean velocity was recorded at the beginning of the beam traverse. This was an observation for all values of H. For instance, at traverse length 1 mm, the mean velocity was mostly recorded to be around 3.5 - 4 m/s. For higher values of the traverse lengths, the mean velocity was reduced in proportional manner, obtaining a minimum value of 0.23 m/s at length 7 mm, before again increasing in a proportional manner for most of the remaining traversing length, and finally obtaining mean velocity values close to those obtained initially along the traverse. The curve terminates by regaining stable and high

mean velocity values of nearly 3.5 m/s at traverse lengths 12 - 14 mm. Thus, a V-shape of the curve is clearly identified for most of traverse.

At incident angle 0° (Fig. 4.7) the obtained velocity values behave differently. Values obtained at first along the traverse are considerably reduced compared to those obtained at an incident angle of 90°. For example, for all values of H, the mean velocities are found to be within 2 -2.5 m/s at traverse length 1 mm. Further, there is no such pronounced V-shape of the mean velocity profile in this case, even though the minimum value obtained is of the same magnitude and appears to be located near the same point of traverse (i.e. at traverse length 7 mm). The curve cannot be defined to be within a certain shape; the obtained values were fluctuating too much in relation to the traverse length in order to establish a specific trend.

It is difficult to find a plausible explanation of the V-shape of the mean velocity traversing profile when applying the 90° beam incident angle, with an obvious minimum value at the center, while there was no clearly defined shape for the 0° beam incident angle.

Both cases will obviously be influenced by wall effects. For example, upon geometrical measurements of the mixer dimensions, it is clear there must be fluid flow streamlines that exit next to the corrugated wall, and which will cross the traverse of the beam at four points when applying 0° beam incident angle. These points are measured to be located at traverse lengths of 2, 6 and 12 and 16 mm. Upon investigation of the results shown in Fig. 4.7, these data appear to be in fairly good agreement with the physical geometry, since there are clearly two peaks identified at approx. 5 mm and 10 - 11 mm traverse. A possible peak at 2 mm is more concealed, and the 16 mm traverse is not included in our data logging due to inaccuracies of the instrument setup.

Similar crossing of such fluid flow streamlines must also be present in the case where 90° beam incident angle has been applied. Physical measurements reveal that there must be three such points, located at 1, 6 and 12 mm. However, no particular behavior in the curve shape (Fig. 4.10) can be identified to have any relation to these points along the traverse.

It should be noted, however, that the difference between Figs. 4.7 and 4.10 also may be attributed to circulating flows being somehow different for the two cases.

As in the previous set of experiments regarding the RMS profiles, these were relatively flat, with only small variations in the obtained RMS values within each value for H. Most of the recorded values for H were within 0.5 - 0.9 m/s. These results agree well with the results obtained in the previous set of experiments (shown in Fig.4.6). It is of less significance that the general upper limit is 0.9 m/s in Fig. 4.9 instead of 0.8 m/s as in Fig. 4.6. Thus, in this respect, it appears that the angle of incidence for the laser beam had no influence on the results obtained.

Further, still comparing Figs.4.6 and 4.9, there was no pronounced exception observed regarding the RMS values obtained for H = 2 mm in Fig.4.9. No peaks are identified to be similar to those in Fig.4.6, i.e. at traverse lengths 3 and 10 mm for H = 2 mm. However, for this H, the curve in Fig.4.9 shows a maximum RMS of approximately 0.95 m/s at traverse length 2 mm. It is difficult to interpret the significance of this peak in relation to the other results obtained in this test series, but a higher RMS value agrees well with what would be expected from the mixer geometry. At the other end of the traversing length (13 mm) an opposite effect is observed: An RMS dip observed to be approximately 0.4 m/s for several values of H. The location of the dip itself agrees well with a similar dip in Fig.4.6, although the values making up for the minimum in the curve dip are slightly different.

Recalling that a 90° angle of incidence implies a beam traverse being perpendicular to the orientation of the corrugated plates, and also recalling that these plates are not symmetrically oriented around the center line of the cross sectional area of the mixer element, such an opposite effect of obtained RMS values along the traversing line is quite reasonable. As confirmed by measurements, due to the non-symmetry, the corrugated plate will be closer to the cylindrical glass wall at one end of the traversing line than the corrugated plate will be at the opposite end of the traversing line. This will inevitably imply different turbulent conditions at each end, i.e. a higher turbulence and higher RMS values where there is a short distance to the glass cylinder wall and lower turbulence and smaller RMS values where there is a longer distance to the glass cylinder wall. This agrees reasonably well with what is obtained in Fig. 4.9.

As for the mean velocity, shown in Fig.4.10, this varied between 0.2 and 4.0 m/s for these experimental series. Again, as was the case in the previous experimental series, the absolute minimum mean velocity value logged

(approx. 0.2 m/s) was obtained for H = 2 mm at traverse length 7 mm, while a maximum value of approximately 3.5 m/s was obtained for H = 4 mm. Obtaining the minimum value at a traverse length 7 mm instead of at 9 mm as was the case in the previous set of experiments gives an indication that the geometrical orientation of the mixer element is different in the two cases. Also, it is observed that the U-shape of the curves in Fig.4.10 is very similar to that in Fig.4.7. However, it is clear the U-shape is more accentuated in Fig.4.10 than in Fig.4.7, in which there also is a larger gap between the extreme min and max values (of approximately 0.2 and 4.0 m/s). Also, the minimum point (saddle) is located further to the left, which again is an indication of the influence of the geometrical position of the mixer element.

However, in Fig.4.10, a shift of the curve positions as the data are logged for different values of H in the traversing direction was not as readily observed as in Fig.4.7. And at no points along the traversing length there were observed any substantial differences between the recorded velocity values for the various values of H, as was the case for e.g. H = 2 mm at the traverse length 10 mm shown in the previous experimental set, plotted in Fig.4.7.

The shape and progression of the mean velocity curves follow the mixer geometry and its orientation relative to the traversing line of the laser beam. The U-shape pattern of the plotted data is recognized to be identifiable with the similar pattern of mean velocities achieved in Fig.4.7.

Again, of course, when positioning the laser beam manually there will inevitably be some inaccuracies occurring. Obviously, one should also be aware of natural variations around the mean values, and that peaks would easily be identified next to the glass cylinder walls since there is an annular void existing between the mixer elements and the inner face of the cylinder wall. Such an annular void inevitably makes it possible for the bulk fluid to pass more or less unhindered, which in turn leads to velocity recordings being different from other recordings obtained along the traversing length. Nevertheless however, the results appear to be reproducible, and the identified U-shape is clear for all values of H.

No obvious channeling effects are revealed when observing the curves in Figs. 4.9 and 4.10. Such effects should be identifiable near traverse lengths 1 - 2 mm and 14 - 15 mm. However, there are no such indications in the behavior of the curves.

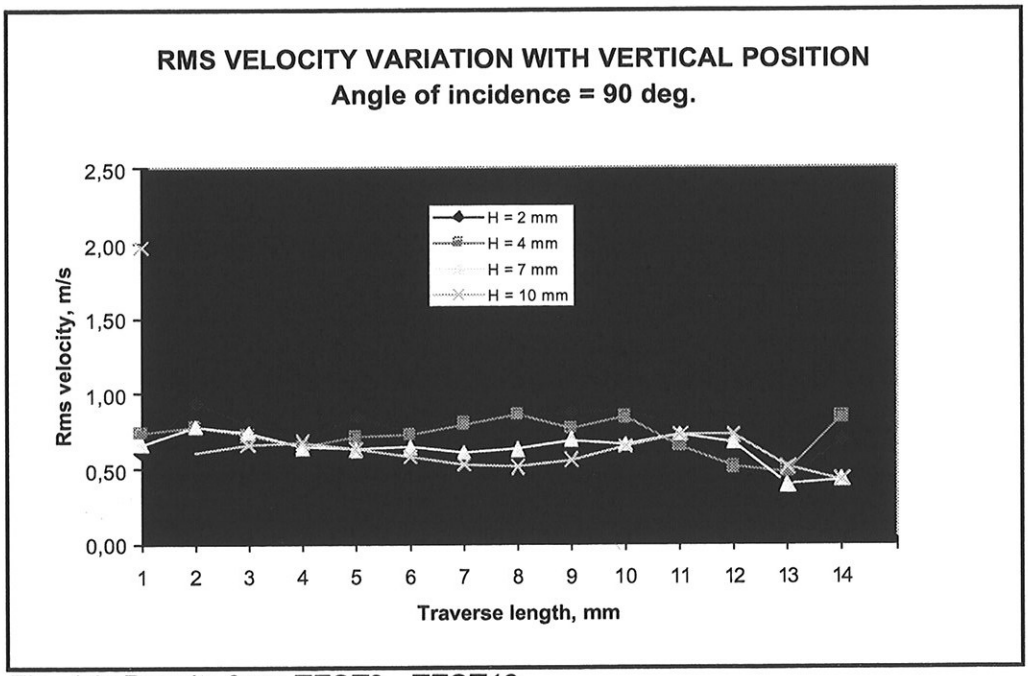

Fig. 4.9: Results from TEST9 - TEST12

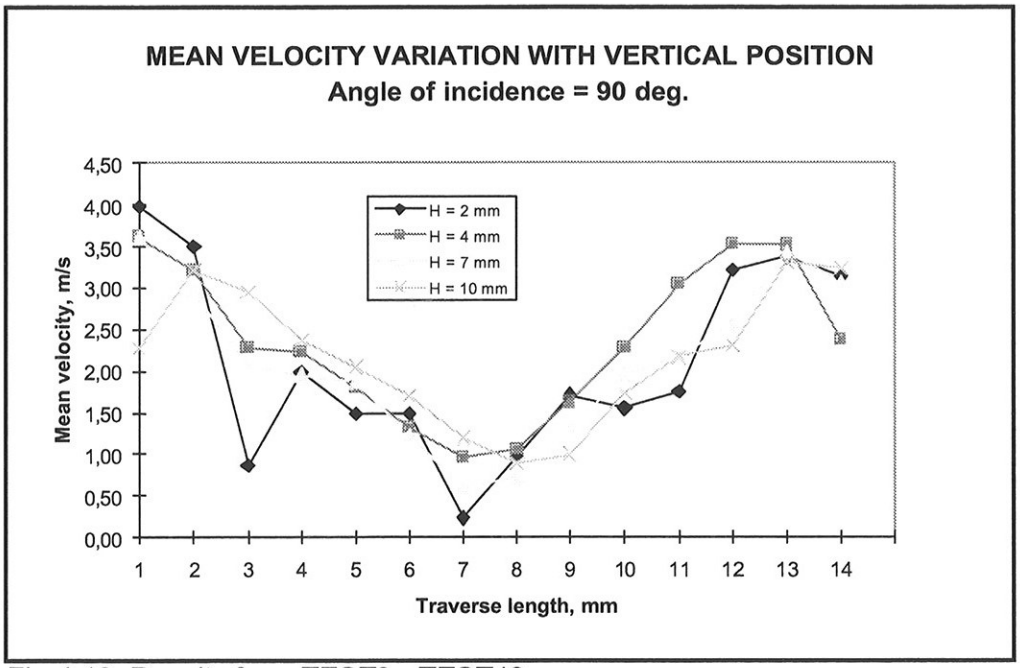

Fig.4.10: Results from TEST9 - TEST12

4.1.3.4 Channeling effects (TEST16 - TEST25)

In the previous tests, described in sections 4.1.2.2 and 4.1.2.3, it was suspected that channelling effects were influencing the results since it was known that the diameter of the mixer elements was not precisely the same as the internal diameter of the glass column.

To check this suspicion it was therefore decided to perform repeated trials, but now including a taping around the 1st and the 2nd mixer elements. The intention of this was to seal the mixer elements, and thereby minimize fluid flow between the glass wall and mixer elements. By comparisons this should identify previous channelling effects, and hopefully prevent any future problems.

TEST16 - 25 may be divided into two groups, in which the angle of incidence for the laser beam was 0°:

a. TEST16 - 20, where taping was done around the 1st mixer element only (also denoted «little taped»). The resulting RMS velocity variation with the vertical position H is shown in Fig. 4.11.

b. TEST21 - 25, where taping was done around the 1st and the 2nd mixer elements (also denoted «fully taped»). The resulting RMS velocity variation with the vertical position H is shown in Fig. 4.12.

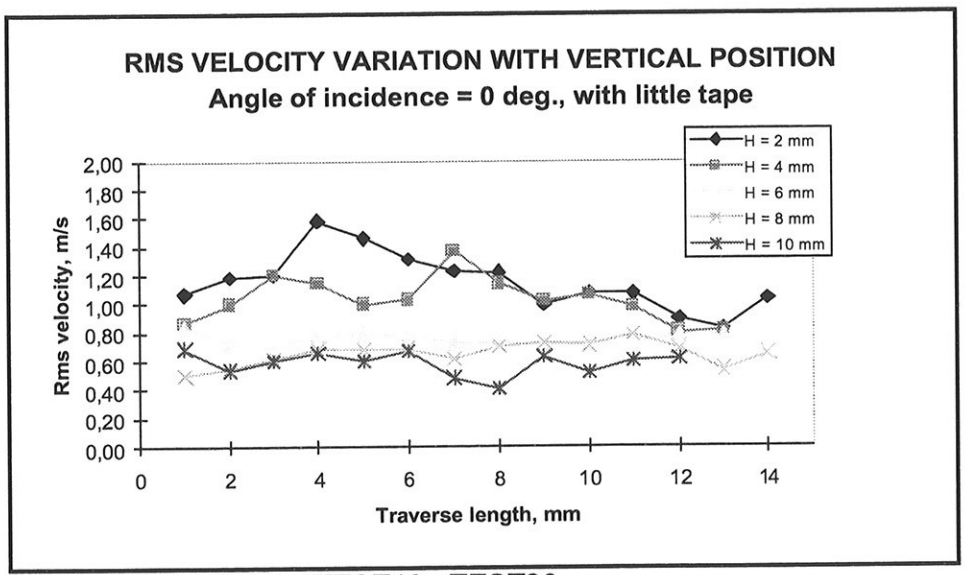

Fig. 4.11: Results from TEST16 - TEST20

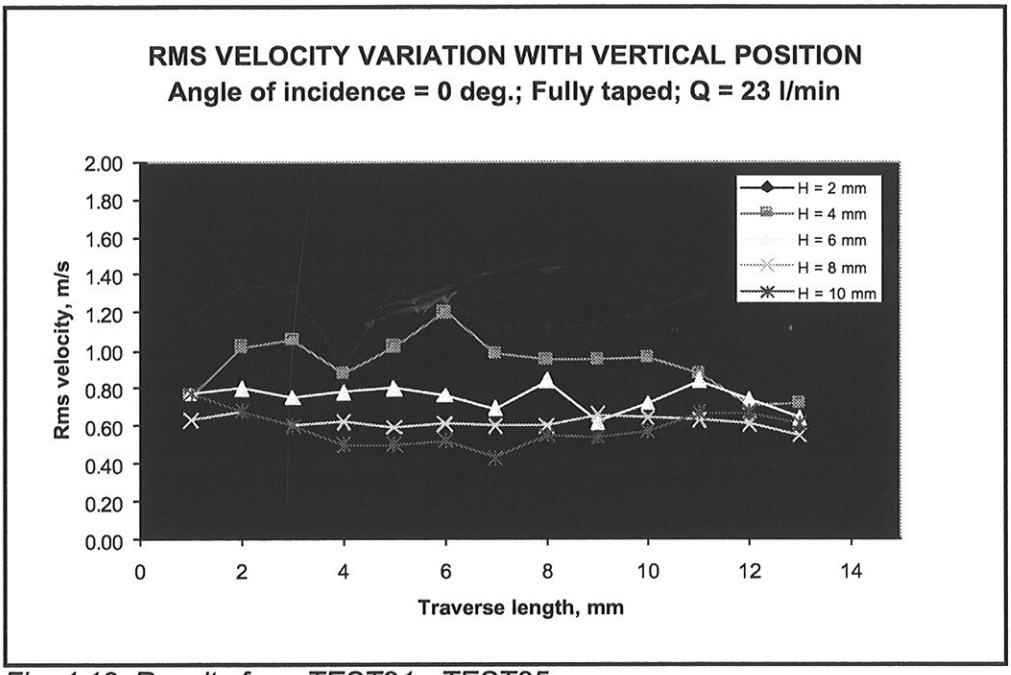

Fig. 4.12: Results from TEST21 - TEST25

Comparing Figs. 4.11 and 4.12 show only small differences between the two forms of sealing. The RMS velocities lie within 0.4 - 1.6 m/s for both cases; smallest values for large values of H and vice versa.

In a detailed evaluation of the figures the following observations were made: Starting with H = 10 mm it was seen that the RMS velocity profiles in the figures were fairly comparable, both starting with RMS values within the 0.7 - 0.8 m/s range at traverse length 1 mm, and then maintaining a relatively stable profile around 0.60 m/s during the rest of the traversing length. For H = 8mm the two profiles resemble each other even more; both being more stable, and the plotted values being nearly identical in both cases. In evaluating the curve plots for H = 6 mm, relatively stable profiles were once again observed, now holding values around 0.70 m/s.

Velocity profiles resembling each other were also observed for H = 4 mm in Figs. 4.11 and 4.12. For H = 4 mm the recorded RMS velocities in both cases were in the vicinity of 0.8 - 0.9 m/s at traverse length 1 mm. Then, in both cases, the RMS increases at traverse lengths 2 and 3 mm before it decreases

again into a «dip». In following the profiles further, they both reveal RMS peaks at traverse lengths 6 - 7 mm, before again decreasing steadily down to values within 0.7 - 0.8 m/s.

The largest difference in the data plots observed between the two figures was found at H = 2 mm. The curve patterns partly reveal opposite effects for H = 2 mm. For example, at traverse lengths 3 mm, Fig. 4.11 shows a peak value for the RMS while the corresponding curve in Fig. 4.12 shows a dip at this location of the traverse length. Further, in Fig. 4.11 for traverse lengths beyond 3 mm, the RMS values are steadily decreasing while from a maximum of approximately 1.60 m/s down to nearly 0.80 m/s, while such a curve progression is not observed at all in Fig. 4.12 for H = 2 mm. Instead, in Fig. 4.12, there was an indication of quite the opposite effect when traversing beyond the dip at approximately 3mm traverse length.

To come to an overall conclusion regarding channeling effects a similar comparison had to be made for the untaped tests. The results obtained for the different values of H were basically comparable, and resembling each other for all traversing lengths of H. It was therefore chosen to let the tests for H = 10 mm, with (little) and without tape, be representative for such a conclusive comparison, as shown in Fig. 4.13.

Since the results were fairly similar, whether the mixer elements were little or fully taped, it was considered appropriate to select one or the other. It was therefore just decided to select the results obtained from experiments which had little taping at H = 10 mm.

In Fig. 4.13, where the experiments are shown both with 0° and 90° angle of incidence, plots of mean velocities have also been included since channeling effects are easier to discover by considering these.

As mentioned previously in Ch. 4.1.3.2, basically, for all values of H, a U-shape was identified for the mean velocity progression, the minimum value being in the vicinity of the middle position of the traversing length. This was seen for H = 10 mm in experiments performed without taping. Comparing this with the values obtained when taping was applied to the mixer element, it is seen that a U-shape may be identified also in this case.

However, it was also seen that the starting value for the mean velocity, i.e. at traverse length 1 mm, was higher for the case with taping: Approximately 2.4 m/s (taped) versus 1.9 m/s (not taped). The minimum point of the U is approximately at the same point along the traverse for both cases, i.e. in the vicinity of 7 - 8 mm traverse length. At the far end of the traverse, i.e. at 12 - 13 mm traverse length, it was once again noted that the mean velocities took different values in the two cases: Approximately 2.7 m/s mean velocity peak (not taped, 0° angle of incidence) versus 1.7 m/s (taped).

Also, in addition to the 2.7 m/s peak, an additional mean velocity peak was found at traverse length 5 mm, valued to approximately 2.2 m/s. This observation was not made when tape was applied to the mixer element. However, beyond the 2.7 m/s peak, which was observed to reach its maximum at traverse length 13 mm, it was noted that mean velocity decreased to approximately 1.9 m/s at traverse length 14 mm.

Discussions regarding the differences between the curves for 0° and 90° angle of incidence have been done previously (see Ch. 4.1.3.3), and will not be repeated here.

As for the curves plotted from the RMS data obtained, it can be noted that the obtained RMS velocities were constant at around 0.6 m/s along the traverse length, for the taped as well as for the untaped mixer elements, thus justifying the conclusion that these results have a high degree of reproducibility regardless of applied taping.

The RMS curve achieved for the 90° angle of incidence had a misbehavior at traverse length 1 mm. The RMS value at this point was obviously erroneous and has therefore been neglected.

Taking into account both the mean velocity and the RMS values it can be concluded that significant channeling effects could not be identified for the mixer elements, these being either taped or not taped.

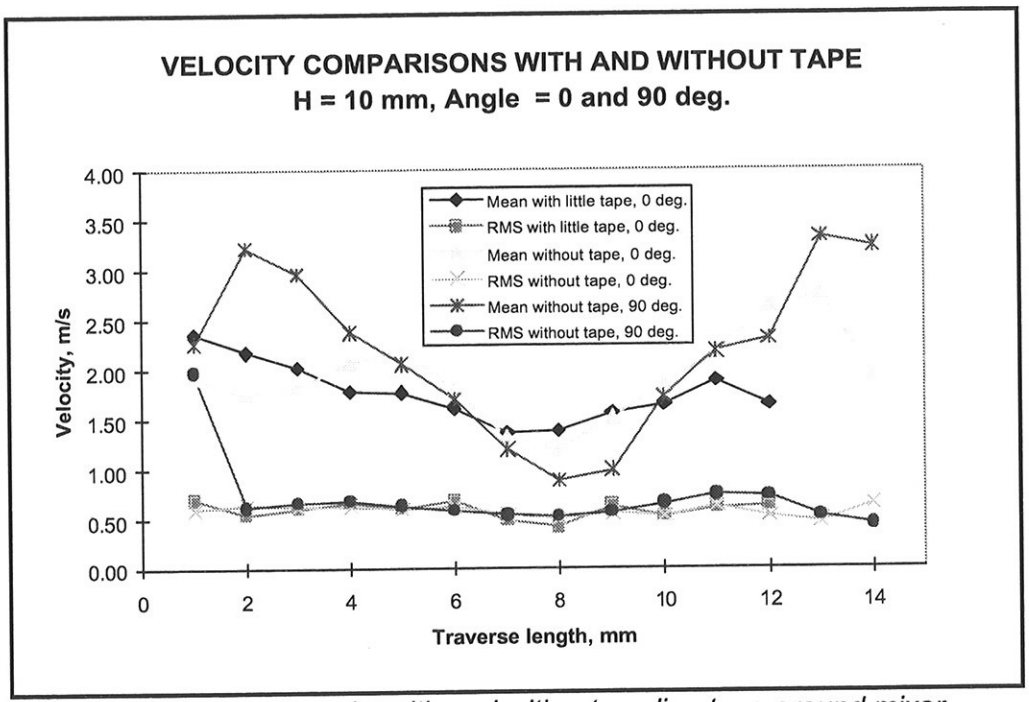

Fig. 4.13: Comparing results with and without sealing tape around mixer elements

4.1.4 Tests at different volumetric fluid velocities

The aim of these experiments, denoted TEST21 - TEST35, was to identify possible variations in mean and RMS velocities, as well as turbulence intensities, and correlate these with the volumetric bulk flow rates. Two representative sets of curves were made from the results, as shown for H = 8mm in Figs. 4.14 and 4.15.

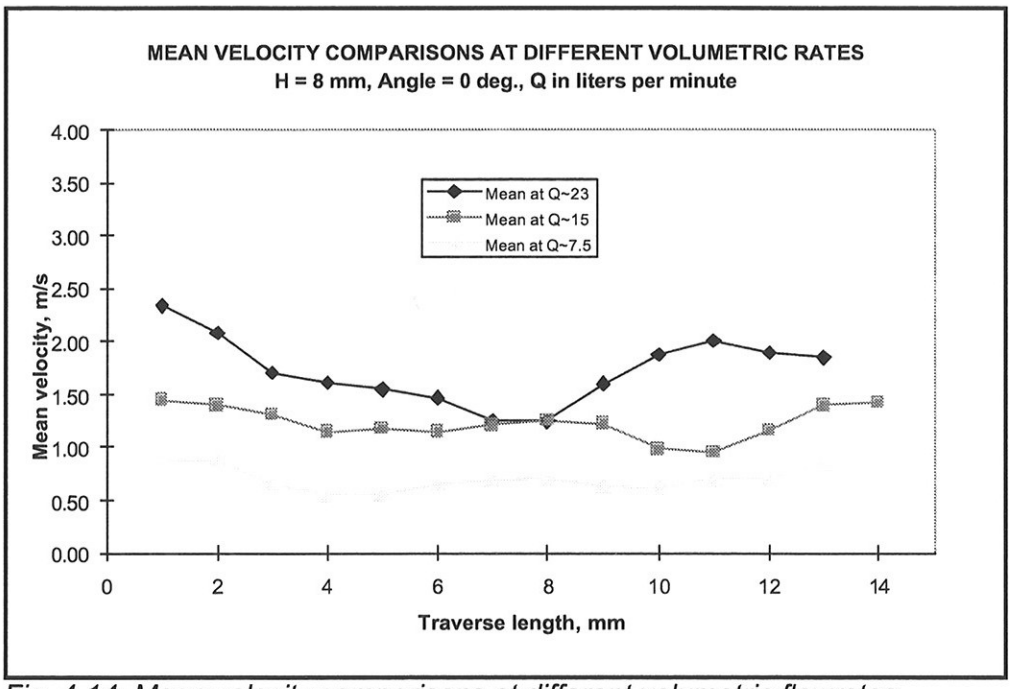

Fig. 4.14: Mean velocity comparisons at different volumetric flowrates

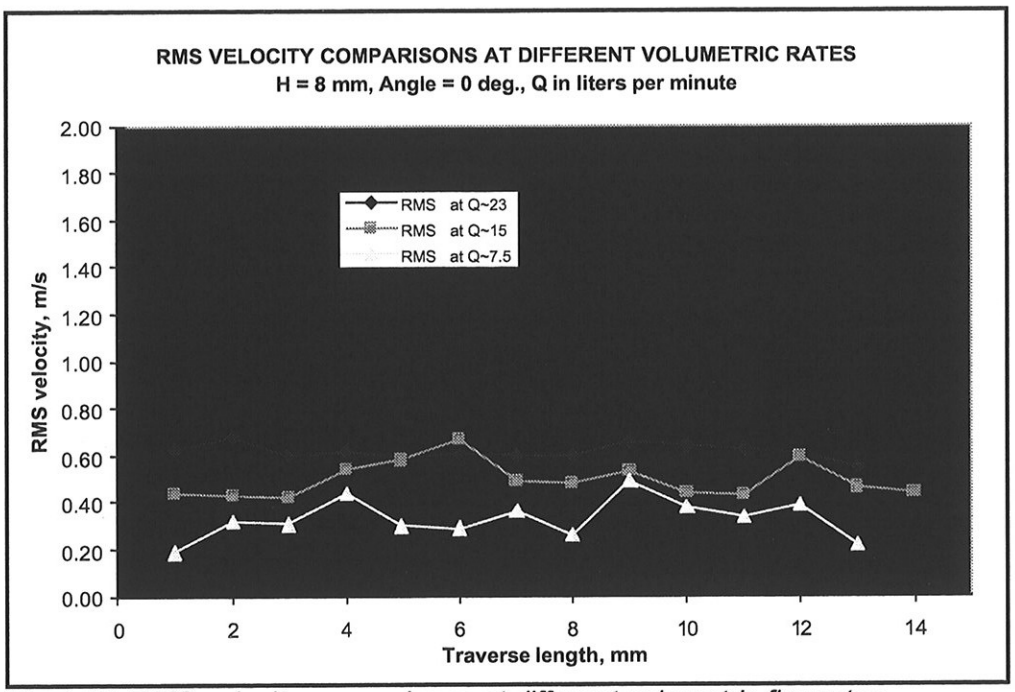

Fig.4.15: RMS velocity comparisons at different volumetric flowrates

From Fig.4.15 it is seen that the RMS velocities are reasonably constant across the traverse for all liquid flowrates. The stability seems to increase with increasing velocity. This increase is expected and is the main reason for the decrease in stable droplet diameter with increasing flowrate. For H = 8 mm the RMS velocity for Q = 7.5 l/min. flowrate is stable in a range of 0.19 - 0.49 m/s. Similar RMS velocity ranges for flow rates of 15 and 23 l/min are 0.42 - 0.67 and 0.55 - 0.68 m/s, respectively.

The mean velocity, as shown in Fig.4.14, increases as the flowrate Q increases. For the lower flowrate of approximately 7.5 liters/min the mean velocity is quite steady at around 0.6 m/s. For Q = 15 l/min the shape of the curve is very similar, but is located at a higher velocity level, approximately around 1.0 - 1.2 m/s. A slight increase close to the walls can be seen, however. Finally, for the higher flowrate at Q = 23 l/min, there is a U-shape of the velocity curve as the laser beam traverses. In this curve, there is a high velocity of approx. 2.3 m/s recorded at traverse length 1 mm. The velocity

decreases steadily down to approx. 1.25 m/s at the middle position of the traversing length (7 mm), and then increases steadily again up to a max of approx. 2 m/s at 11 mm traverse length and basically stays steady at that level for the rest of the traverse length. The U-shape of the curve is therefore not symmetrical, which probably may be attributed to the asymmetry of the mixer elements installed. It thus seems that the effect of the geometry becomes more accentuated at higher flowrates.

In Fig. 4.16 are shown the averaged RMS and mean velocities obtained for the different volumetric bulk flowrates Q.

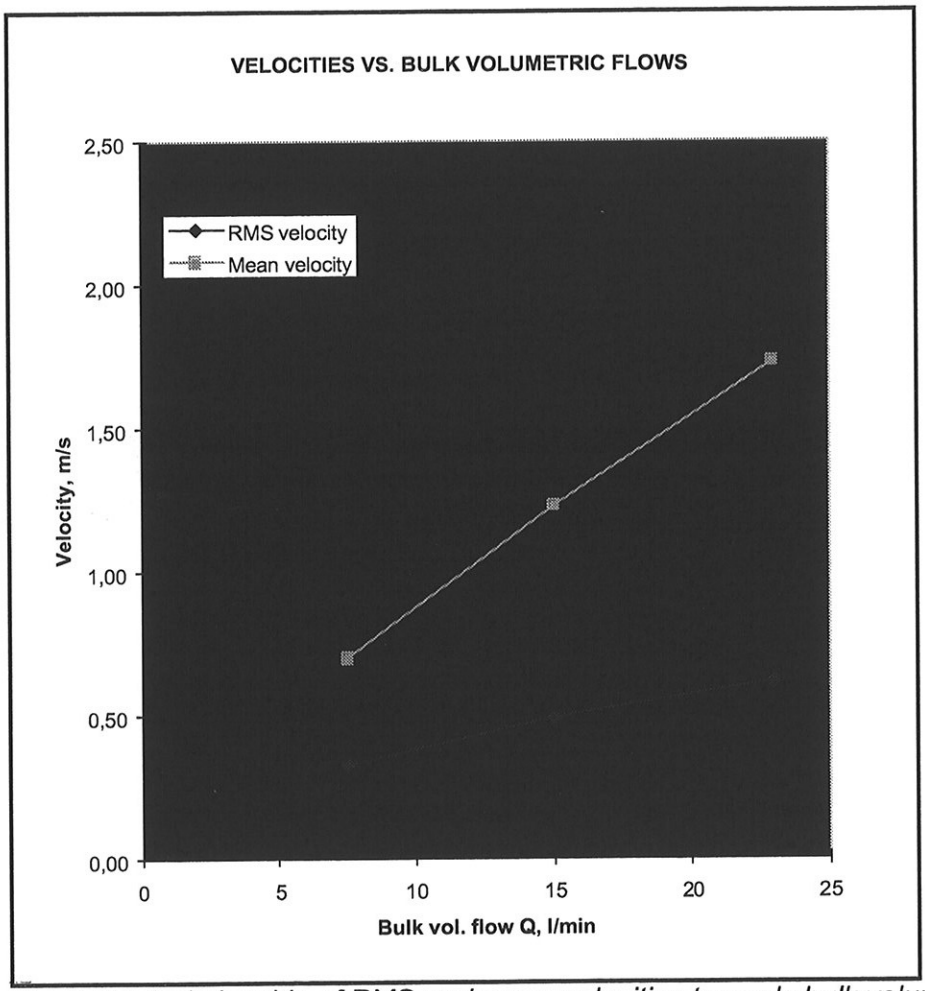

Fig. 4.16: Relationship of RMS and mean velocities towards bulk volumetric flowrates. Typical deviations from the mean values are indicated.

From Fig.4.16 it is seen that, within the experimental data range (i.e. approximately superficial velocities 0.7 - 2.12 m/s) the RMS velocity is close to being proportional to the mean bulk flowrate Q.

In addition to these observations however, the RMS values obtained may be termed as reproducible, since the resulting curves are very similar to previously obtained results.

4.1.5 Tests with heating applied

The aim of these experiments, denoted TEST29, 34, 37, 40, 41, 42, 43 and 44 (all for H = 8mm), was to identify possible variations in mean and RMS velocities, as well as turbulence intensities, and correlate these with the application of heat to the bulk flow rates as shown in Fig.4.17 a) and b). TEST29, 37, 41, and 43 had a flow rate of 15 l/min (Fig. 4.17 a)), while TEST34, 40, 42 and 44 had a flow rate of 7.5 l/min (Fig. 4.17 b). TEST37 is a reproduction trial for TEST29, and TEST40 is a reproduction trial for TEST34. The maximum temperature applied was 75 °C.

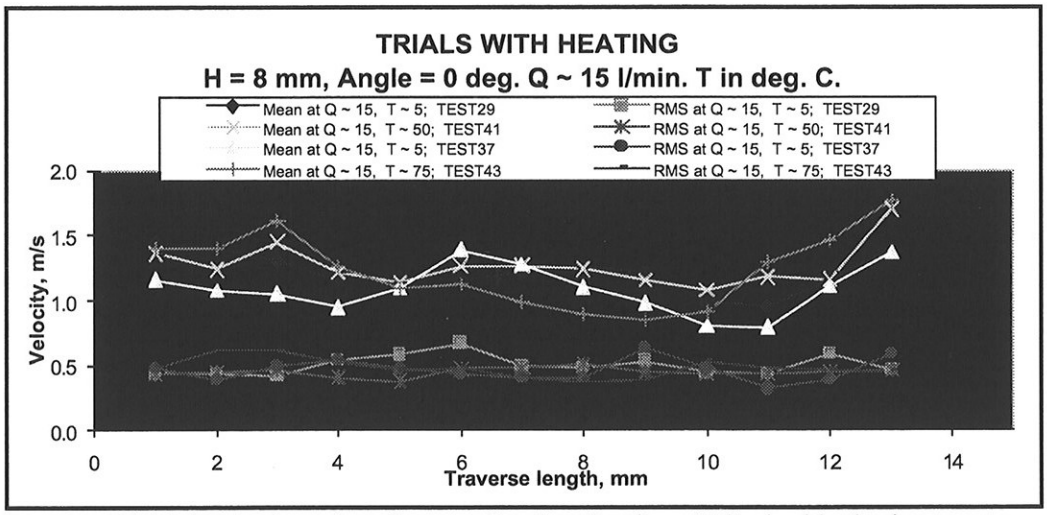

Fig.4.17 a): Results from heating application for Q = 15 l/min. Typical deviations from recorded values are indicated for TEST41 and TEST43. Note that TEST37 is a reproduction trial forTEST29.

CHAPTER 4 CHARACTERIZATION AND MEASUREMENTS OF THE STATIC MIXER

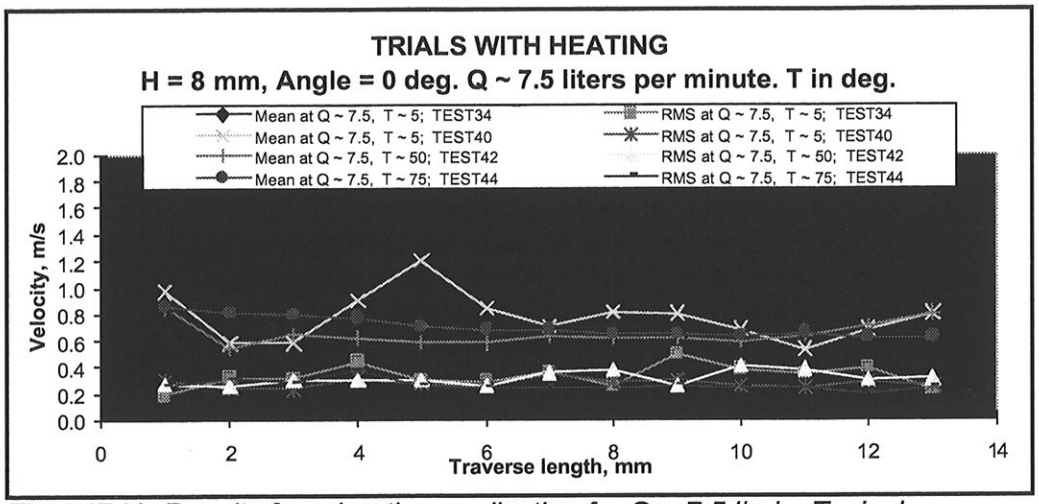

Fig.4.17 b): Results from heating application for Q = 7.5 l/min. Typical deviations from recorded values are indicated for TEST44. Note that TEST40 is a reproduction trial forTEST34.

It is well known that for water, the viscosity decreases with temperature. The curve is often described as being in the form of an exponential curve, e.g. by means of the Guzman-Andrade equation, $\mu = Ae^{B/T}$, where A and B are constants to be found. Equivalent to the use of this equation is a linear plot of $\log\mu$ vs. $1/T$. From Perry (1973) it was found that the viscosity of water increases with decreasing temperature. Typical values are: approx. 0.39 cP at 75°C, 1.12 cP at 15°C and 1.72 cP at 5°C. Hence there is less resistance to fluid motion as temperature increases. It would therefore be expected that the RMS and mean velocities recorded when performing these experiments would show substantially increased values when applying elevated temperatures.

However, it is seen that from the data plots shown in Fig. 4.17 a) and b), which are plotted as mean values assumed to be representative for the experiments performed, that the application of heat has no influence on the mean velocity or the RMS velocity in the measurement volume. This is a strong indication of turbulent viscosity being the most dominant, while molecular viscosity has little or no influence.

In Fig. 4.17 two similar tests with water temperature at 5 °C (i.e. no heating applied) are included in order to show that there is some randomness with respect to the mean velocity recordings at the beginning and the end of the traversing length of the laser beam. The first of the 5°C recordings shows a starting mean velocity of approx. 1.44 m/s, while the second 5°C recordings shows a starting mean velocity of approx. 1.16 m/s.

Both of the remaining recordings, for 15°C and 75°C, start with mean velocities between these values, i.e. at 1.36 m/s and 1.40 m/s, respectively, and end up at near 1.70 m/s and 1.78 m/s at the end of the traverse. Both of the 5°C recordings end up with a velocity very near 1.40 m/s at the end of the traverse. As such, the terminal results obtained at the end of the traverse agree well with what was expected according to the viscosity considerations. However, this behavior is not representative for velocity values obtained at the traverse positions in between. It is to be noted, however, that these results also must obey the Law of Continuity, i.e. that variations in the cross-sectional area of fluid flow will have impact on the fluid velocity.

As for the case without heating, the RMS velocity attains relatively steady values within the range of approximately 0.35 - 0.70 m/s. As noted, the similar mean velocities attain values in the range of approximately 0.80 - 1.75 m/s. Hence, it is to be concluded that the temperature has no influence on the achieved velocity values, which is probably due to RMS being dependent on the energy dissipation (since RMS $=\sigma=\sqrt{\overline{u^2}}=f(\varepsilon)$). Hence, this situation may be better described in terms of pressure drop dependencies.

Pressure drop vs. temperature is shown in the following diagram, Fig.4.18. As expected, the pressure drop decreases with increasing temperature since the viscosity decreases. However, only three values were plotted for this volumetric flow (15 l/min). It appears that the pressure drop does not decrease further when the temperature exceeds 50°C, which by intuition appears to be an incorrect observation.

However, observing that the pressure drop becomes constant is quite in agreement with theory. When considering friction factor diagrams for pressure drop calculations in pipes (e.g. Moody, 1944), it is seen that the friction factor is expressed as a function of Reynolds number. Therefore, at higher temperatures the viscosity decreases, and hence the Reynolds number

becomes larger, which in turn gives smaller numeric values for the friction factor according to e.g. the Moody diagram.

However, at higher Reynolds number (starting in the vicinity of Re = 20000), the friction factor becomes relatively independent of the bulk liquid viscosity (as expressed by Re). In the case presented in Fig.4.18 , with a bulk volumetric flow of 15 l/min within static mixer elements with a hydraulic diameter of 15mm we have Re > 21000.

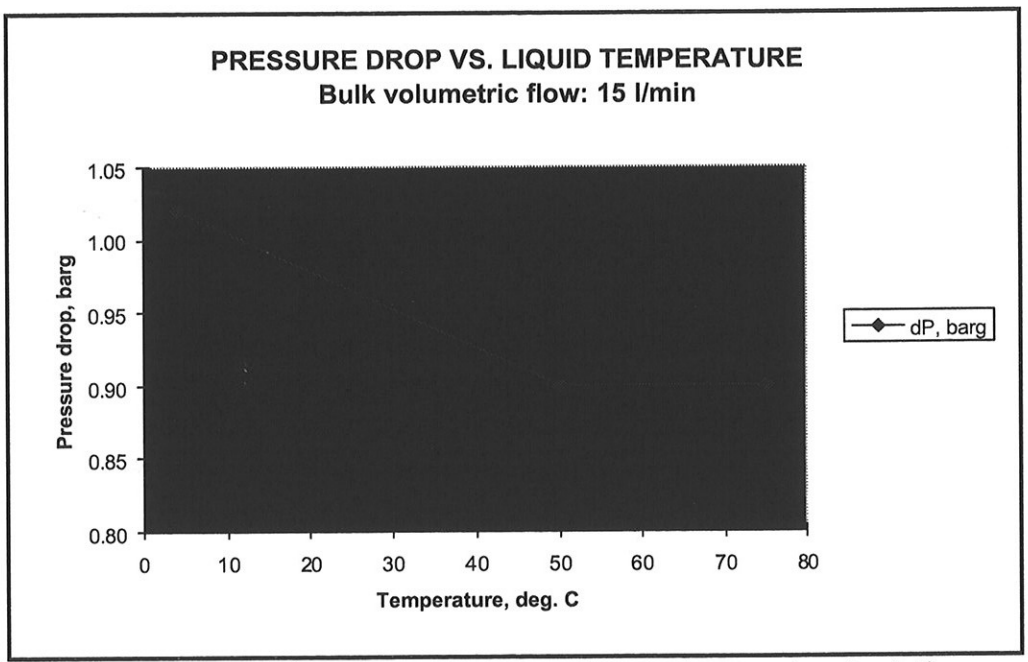

Fig.4.18: Experimental values for Pressure drop vs. temperature in static mixers. Calculation according to the «Sulzer method» (from brochure) gave 0.96 barg pressure drop.

The above observation is in agreement with the work performed by Li et al. (1997), where it was shown that the pressure drop across static mixers increases with the number of mixer elements as well as the level of the fluid viscosity. Li and his co-workers also showed in the same presentation that, on the other hand, the pressure drop decreases with the fluid temperature when the wall of static mixer is heated. Logically, a reduction of the fluid viscosity due to thermal effects induces a lower pressure drop. However, from their

experiments that were performed in the temperature range of 30 - 90° C, it is also seen that the pressure drop difference between a cold and a hot fluid is more pronounced at lower flowrates than at the higher flowrates. Thus, at some point of flowrate loading it will be irrelevant to consider the thermal effects of pressure drop.

For the sake of comparison it is interesting to note that a calculation according to the «Sulzer method» (from brochure) gave 0.96 barg pressure drop.

4.1.6 Trials with induced air

The objective of this set of trials, denoted TEST49 - TEST51, was to investigate the possible influence of inducing air into the system. Elsewhere in this dissertation results from oil/water mixtures are presented. It has been suspected that the release of small amounts of gas will have an effect on the local turbulence intensities.

Air was introduced and measured by means of a rotameter.

In Figs. 4.19 and 4.20 a comparison is given between trials done with and without air introduction, and it appears that air has the effect that values for the RMS velocities increase. As expected, this is particularly apparent for high volumes of air introduction, e.g. as seen in Fig. 4.19 when 2.15 l/min air was introduced to 7.5 l/min liquid mixture as in TEST50 (pressure: approx. 0.4 barg). 2.15 l/min of air implies a superficial velocity of approx. 0.20 m/s within the 15 mm pipe.

The amount of air introduced in TEST51 was only approx. 0.25 l/min, which was otherwise performed at the same conditions of pressure (i.e. approx. 0.5 barg) as in the previous test. The superficial velocity was then approx. 0.024 m/s.

However, in TEST49 as seen in Fig.4.20, where the air was kept at 1.5 barg when introduced to the bulk liquid, the actual air flow rate was approx. 1.7 l/min, being equivalent to a superficial velocity of 0.16 m/s.

TEST34, 40, 45 and 46, which were all done without air, were otherwise set up to be identical. Ideally, therefore these tests should also give almost identical results.

When applying the maximum capacity of air introduction given by the rotameter it was clearly seen that the RMS velocity level was substantially higher than for those with little or no air introduced. The elevated level is also seen when lesser amounts of air were introduced; particularly at the end of the traversing length (commencing at a traverse length around 9 - 10 mm).

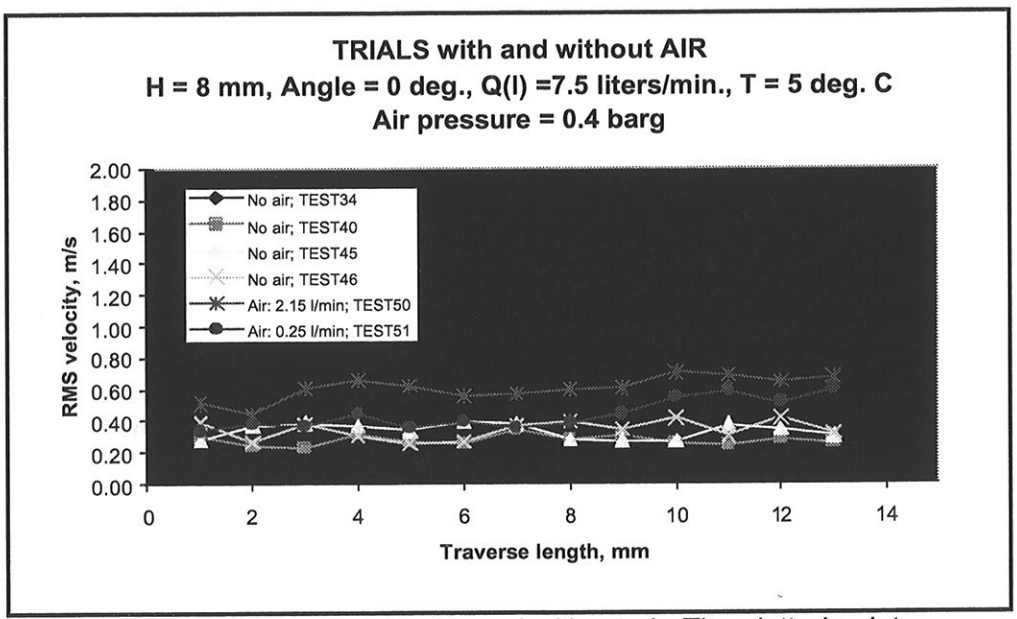

Fig. 4.19: Comparison of trials with and without air. The plotted points represent the mean of 5 samples. Measurement deviations from means are indicated. Ideally, results from TEST34, 40, 45, and 46 should be identical since there is no difference in the setup of these trials.

CHAPTER 4 CHARACTERIZATION AND MEASUREMENTS OF THE STATIC MIXER

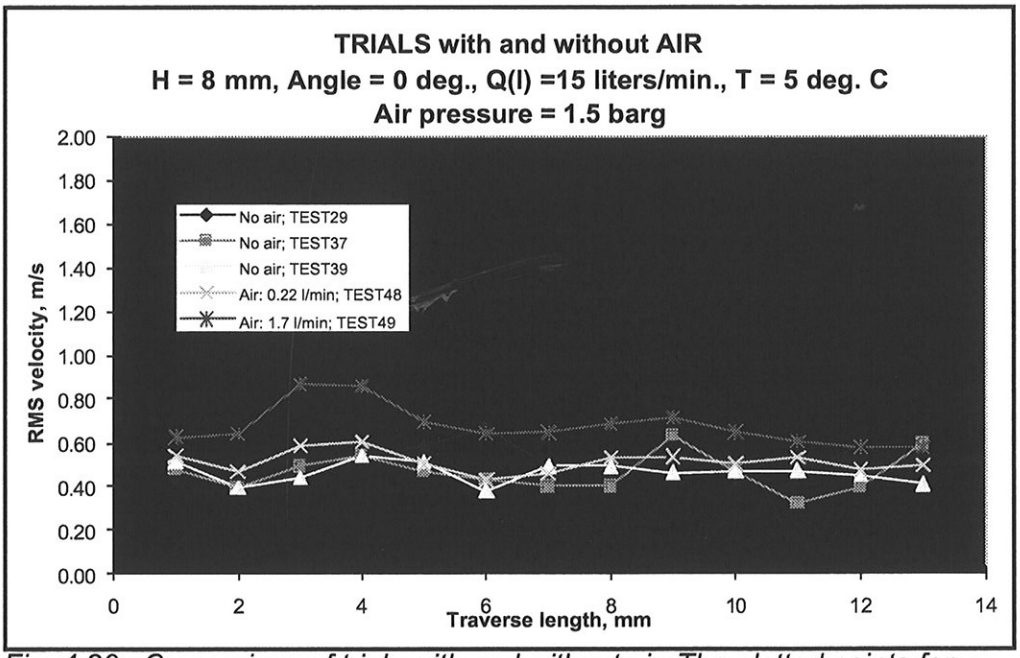

Fig. 4.20: Comparison of trials with and without air. The plotted points for TEST48 and TEST49 represent the mean of 5 samples. Measurement deviations from means are indicated. Ideally, results from TEST29, 37 and 39 should be identical since there is no difference in the setup of these trials.

Experimental studies of the influence of induced air has recently been performed for a linear turbulent shear flow (without static mixers), and presented by Lance et. al. (1996). This work was performed with emphasis on the longitudinal (i.e. along the main direction of flow) evolution of the Reynolds stress tensor. The Reynolds stress tensor may, at least for low void fractions, be crudely approximated as the sum of bubble induced and shear-induced turbulence.

Without bubbles in a linear shear flow, the mean velocity gradient results in an increase of the streamwise turbulent energy $u'^2_L = \overline{u_L^2}$,where the bar stands for the local phase average, and the subscript L for the liquid phase. Since the effect of strain in the direction perpendicular to the mean flow is to increase the transverse components of the Reynolds tensor, it is expected a

more rapid decrease in the turbulent fluctuations in the streamwise direction than in the transverse one.

However, when injecting gas bubbles, it was observed a considerable reduction in the effective production of turbulence, and hence in the non-isotropy between the longitudinal and transverse velocity components. An explanation for this trend is the inherent competition between distortion of turbulence by the mean shear and the random straining of turbulent conditions by the flow around the bubbles (which give rise to the so-called pseudo-turbulence).

In a turbulent air-water bubbly flow, taking place in a plane vertical mixing layer, it is expected that the relative motion of the bubbles should strongly modify the turbulent field of the continuous phase when the mean bubble diameter is greater than the Kolmogoroff length scale. In further experiments of Lance et. al. it was observed a self-preservation of the fluctuating velocities, being the same as in single phase flow, but with a higher level of global turbulence. Thus, to clarify the nature of shear-induced turbulence in bubbly flows, it was necessary to separate the liquid velocity fluctuations produced by shear stress and the bubble-induced velocity fluctuations.

There was a variation in the observations done by Lance et. al. In spite of this, it was concluded that the presence of gas bubbles did not affect the qualitative behavior of the liquid phase, regardless of the forces induced by the bubbles. Also, the entrapment of gas bubbles by the largest turbulent structures proved to be one of the most important mechanisms responsible for the void migration near the wall in an experiment on the vertical, co-current boundary layer flow.

Further, in his work there was a remark concerning the modification of the turbulence in the liquid phase. Due to the non-negligible bubble slip velocity, a significant amount of the fluctuating energy in the liquid is due to the added mass effect. This can reasonably be estimated from inviscid fluid theory. However, there are more difficulties in assessing the energy produced into the wakes of the bubbles, and to understand how this pseudo-turbulence is connected to the shear induced turbulence.

4.1.7 Tests from 2nd mixer element elevation

Reference is made to Fig.4.2 for clarification of the term «2nd mixer element elevation».

In order to check the flow conditions in the outlet from the mixer elements further downstream of the 1st element, where all of the previous measurements were taken, two sets of trials for H = 8mm were performed above the 2nd mixer element (denoted TEST52, with 180° angle of incidence, and TEST53, with 0° angle of incidence). Results of these trials are shown in Fig. 4.21, and it is shown that the major difference identified from the mean velocity curves appears to be due to the angle of incidence of the laser beam.

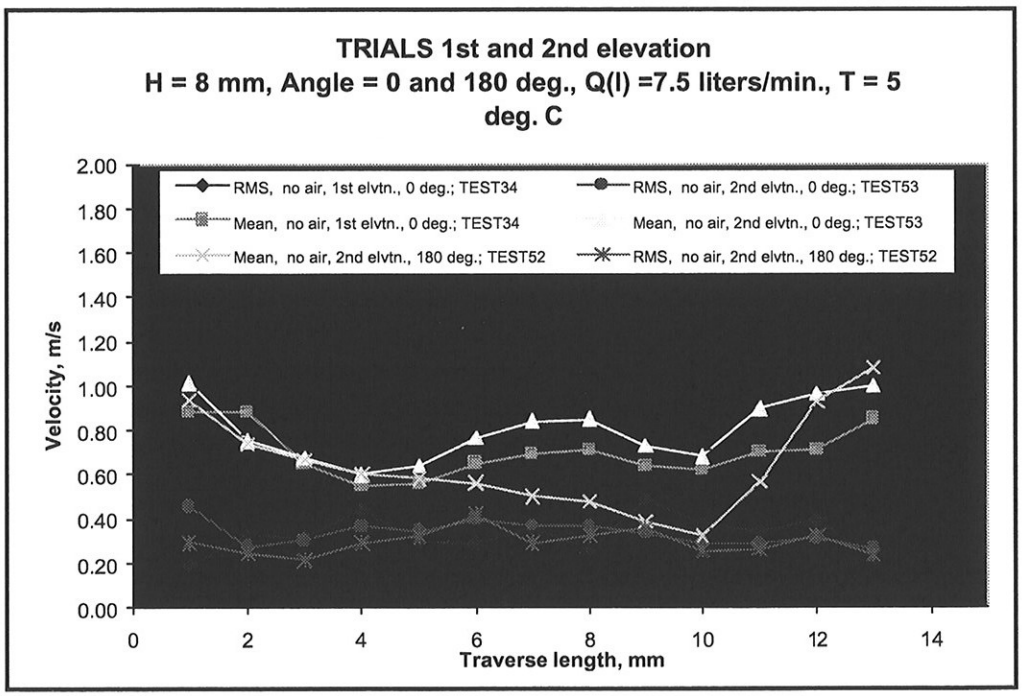

Fig. 4.21: Comparison of trials taken at 1st and 2nd elevation. Plotted values for TEST52 and TEST53 represent mean of 5 recordings. Deviations from the mean are indicated.

CHAPTER 5 THE EFFECT OF CHEMICAL ADDITIVES

5 THE EFFECT OF CHEMICAL ADDITIVES

5.1 Theoretical aspects

5.1.1 Introduction to surface active agents

As noted in the review paper on coalescence by Chaudari & Hofmann (1994), coalescence is strongly influenced by the presence of electrolytes and surfactants. Droplet size and hold-up are therefore strongly dependent on system properties, where an understanding of surface and colloid chemistry is essential. For instance, it is known that in most pure solvents, bubbles tend to coalesce faster, while addition of electrolytes or surfactants lead to suppression of bubble coalescence and a lower average bubble size, higher gas-holdup and interfacial area. Similarly, temperature and pressure have a significant influence on flow regimes, gas hold-up and bubble size (Grover et al., 1986). Correlations developed by different investigators show large deviations, and mere incorporation of physical properties does not explain the observed variation in the design parameters.

In electrolyte solutions, the coalescence of gas bubbles is inhibited leading to smaller bubble size, and higher interfacial area. In this case, the electrolytes lead to formation of an electrical double layer at the interfaces between the two bubbles and the draining liquid. This results in immobility of the interfaces and retardation of the flow of the draining film through the force of attraction of the opposite charges at the interfaces. This effect is called «electroviscous effect» (Elton & Picknett, 1957), which is most pronounced when the

thickness of the draining film has the same order of magnitude as the electrical double layer.

In the presence of surface active agents in aqueous solutions, the coalescence is inhibited similarly to that in the case of electrolytes. Though the effect of electrolytes and surfactants is similar, the concentration levels of surfactants required to inhibit coalescence are much lower than those of electrolytes (Sagert & Quinn, 1978; Marucci & Nicodemo, 1967).

The presence of a surface-active agent increases the interfacial viscosity and decreases the interfacial tension. Both these effects lead to retardation of the rate of drainage of the film liquid. When interfacial tension is decreased, the probability of rupture of the film is decreased and distortion of the film is inhibited, since, with change in the area the tangential stress is taken up by the interfacial tension.

The surface-active agents consist of organic molecules with hydrophilic groups (-OH, >CO, -COOH, etc.) and a hydrophilic part (hydrocarbon structural group) (Keitel & Onken, 1982). The molecules of this type are surface active, which means that they will be enriched at the gas-liquid interface. On the liquid side of the interface, the surface-active molecules will tend to form a monolayer, the stability of which depends on the type, concentration and size of the surface-active molecule.

These surface-active molecules are so enriched at the surface that the hydrophilic groups point towards the liquid phase and the hydrophobic groups towards the gas phase. Due to this specific orientation, the liquid surface around the gas bubbles is electrically charged, and this surface polarization produces repulsive forces leading to inhibition of bubble coalescence.

As explained by Mørk (1994), surface-active agents, i.e. compounds that have the tendency to adsorb on an interface, and thereby change its properties, have been used since prehistoric times. An example is soaps, produced by boiling fats and ash. Modern surface active agents, however, are predominantly highly synthetic.

Surface-active agents are frequently also termed surfactants or tensides. They are characterized by being amphiphilic in nature, meaning that the molecules contain hydrophilic as well as hydrophobic groups.

CHAPTER 5 THE EFFECT OF CHEMICAL ADDITIVES

The fundamental phenomenon that causes the surfactants' efficiency is that they have the property of adsorbing onto the interface, and that this adsorption may lead to one or both of the following two, completely different effects:

a. Reduction of the involved surface tensions or interfacial tensions.
b. Formation of mechanically strong adsorbed monomolecular layers.

If a typical tenside, such as sodium dodecyl sulphate ($C_{12}H_{25}OSO_3^-Na^+$), is dissolved in water, the hydrophobic part (the alkyl group chain) will disturb the structure of the water and thereby increase the free energy of the system. The water will, however, try to minimize this effect by pushing the alkyl group chain into the gas phase.

The tenside molecules will therefore have a tendency to concentrate (adsorb) onto the surface, with the alkyl group chains becoming oriented towards the air phase. This adsorption implies a reduction in the imbalance of the intermolecular forces that normally occur at the surface. Accordingly, less energy is required to make the water molecule rise to the surface, i.e. increase the surface area of the water. Thus, there is a reduction of the surface free energy of the system, i.e. the surface tension or the interfacial tension. An analogy to this is the condition obtained at the interface between water and a hydrophobic liquid, such as oil in Fig. 5.1 (b).

A number of compounds are surface active without actually being classified as tensides. These compounds are either too inefficient, or they are too limited in their areas of application. Examples of such compounds are short-chained fatty acids and alcohols. The longer the hydrocarbon chain is, the more the interfacial tension is reduced, i.e. there is a larger tendency for the molecules to adsorb onto the interface.

The fundamental process facilitating the application of surface-active agents is the adsorption of these onto the interface between a solution of the surface-active compound and another phase, whether this is a gas, liquid or solid. This adsorption will usually make a contribution to a particularly desired effect, by reducing the interfacial tension, or in some cases by the formation of an interfacial film causing a mechanical stabilizing of the interface.

Thus, in the presence of a surface-active agent, the interfacial tension of the system will be reduced.

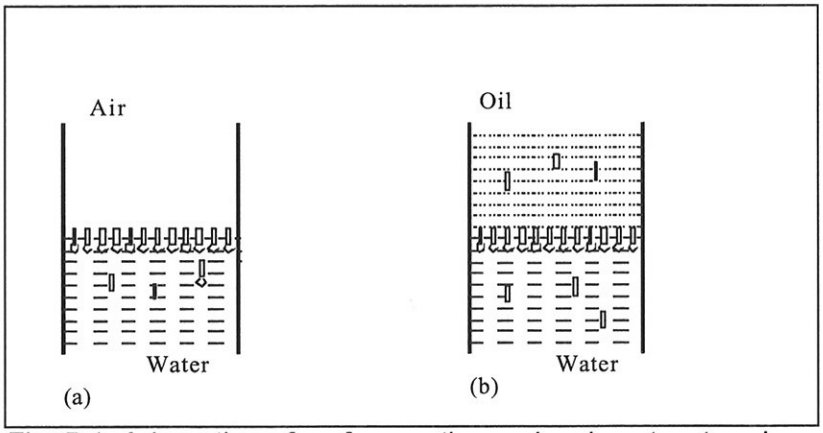

Fig. 5.1: Adsorption of surface-active molecules at water-air and water-oil interfaces. The hydrophilic group is directed towards the water phase.

5.1.2 Previous experience reported

5.1.2.1 Gas-liquid systems

In the review of Chaudari & Hofmann (1994) it was reported that Marrucci & Nicodemo (1967) discussed the retarding effect of electrolytes on coalescence, and it was shown that the effect of electrolyte concentration on bubble diameter could be correlated through a parameter G_1 defined as

$$G_1 = \frac{1}{2} Z c_1 \left[\frac{d\gamma}{dc_1} \right] \frac{1}{1 + \dfrac{d \ln a_1}{d \ln c_1}} \qquad (5.1)$$

where Z is the ion valency, c_1 is the concentration of the species (kmol/m^3), γ is the surface tension (N/m), and a_1 is the activity coefficient of the species (kmol/m^3). The parameter G_1 represents the contributions of surface potential, ionic strength and the nature of the ions. Marrucci & Nicodemo (1967) also observed a lower asymptotic bubble size (0.4mm) at higher electrolytes and surfactants (alcohols) concentrations. It is interesting to note that the asymptotic d_B is the same for electrolytes and surfactants. The reason for this can be explained by the hypothesis of film-thinning to the stage of equilibrium

thickness h_e at which ΔP tends to be zero. This means that at higher concentrations of both electrolytes and alcohols (surfactant), the electrostatic double layer force balances with van der Waals and other attracting forces leading to a metastable equilibrium thickness and hence suppression of the process of coalescence.

The work of Sagert et al. (1976) and Sagert & Quinn (1978) is one of the few cases where a systematic comparison of the experimental coalescence times with model predictions have been attempted. It also appears that the dynamic surface tension model is more realistic to represent data on solutions of surfactants and electrolytes, while the liquid phase diffusion model of Marrucci (1969) is suitable mainly for $cr_b k^2/\gamma$ values in the range of 2 - 10.

It has been reported that the frequency of coalescence decreases drastically with increase in the surfactant concentration. And it has been observed that the coalescing frequency is not only dependent on liquid properties, but is also affected by bubble size and the bubbling frequency. The typical results showing coalescence time and surface tension as a function of the concentration indicates that a correlation between coalescence time and surface tension exists. The coalescence time increases with increase in chain lengths of the solute, and is much greater for fatty acids then for n-alcohols having the same number of C-atoms. The polarity differences in the carboxylic acid and hydroxyl group may be the possible reason for such observations.

Yang & Maa (1984) determined coalescence times for N2-aqueous surfactant (sodium lauryl sulfate, n-octanol) solutions to understand the behavior of stretching of gas-liquid interface. They observed a sharp increase in coalescence time with increase in surfactant concentration and the t_s values ranged between 1 - 500 ms, depending on the concentration of the surfactant. They observed that the surface active solutes which gave large $d\gamma/dc$ have a retarding effect on coalescence, caused by local depletion of surfactants and increase of surface tension at the position where gas-liquid interface is stretched.

Investigations on the temperature effects in the work of Grover et al. (1986), where it was found a significant observation of increased bubble size and decreased hold-up in air-water systems, indicates that at higher temperatures coalescence is accelerated because of the significant vapor pressure of the liquid phase. These authors have not explained the mechanism of

coalescence, but correlated the gas hold-up data in terms of vapor pressure of the solvent. This observation can be explained on the basis of additional force through vaporization of the film liquid (and mass transfer to the bubble phase), leading to faster drainage of the liquid film. A theoretical model considering this important practical aspect is not known to exist. For benzene-water systems, Valentas & Amundson (1966) have observed that increase in temperature aids coalescence by promoting film drainage and reducing interfacial tension.

Li & Slattery (1988) measured coalescence times as a function of NaCl concentration in a solution of dodecyl sodium sulfate and compared the experimental results with those predicted by the theory of Hahn et al. (1985) and Hahn & Slattery (1985). The addition of NaCl to surfactant solution causes decrease in the electrostatic forces and the surface tension. Initially, the coalescence time decreases dramatically with increase in NaCl concentration due to diminished electrostatic repulsive forces. Predictions from the theory have been shown to agree with the experiments.

Venkatesan (1991) studied the effect of electrolytes and surfactants on the bubble size distribution, and found that the addition of such chemicals leads to a significant increase in the fraction of the bubble size in a range less than 0.1 mm.

5.1.3 Classification and application of tensides

As mentioned, the condition for a compound to be surface active is that it contains lyophilic as well as lyophobic groups. However, this condition is not always sufficient. Since temperature and conditions of use (e.g. in the presence of electrolytes or organic additives) vary, it may be necessary to modify or change the structure of the lyophilic and/or lyophobic groups to maintain the surface activity at an acceptable level. A more general formulation for the condition of a compound to be surface active is therefore that the molecule has a chemical structure making it amphiphilic in the solvent at the experimental conditions.

In aqueous solutions the hydrophobic part of the tenside molecule will usually be a long chained hydrocarbon residual (C_8 - C_{20}). The hydrophilic part is either ionic or a strongly polar group.

CHAPTER 5 THE EFFECT OF CHEMICAL ADDITIVES

The tensides are classified according to the nature of the hydrophilic group, resulting in four major groups:

1. Anionic tensides, where the hydrophilic group is negatively charged, e.g. a soap ($RCOO^-Na^+$).

2. Cationic tensides, where the hydrophilic group is positively charged, e.g. in salts of long chained amines ($RNH_3^+Cl^-$).

3. Amphoteric tensides, where both positive and negative charges can be present, e.g. long chained amino acids.

4. Non-ionic tensides, where the hydrophilic part has no formal charge, e.g. monoglycerides and derivatives of polyethylene glycol ($-(CH_2CH_2O)_n$).

5.2 Additives applied in the experiments

5.2.1 Stabilizing/destabilizing agents

A number of chemicals were tested in these experiments; partly to stabilize the oil droplets in the oil/water dispersion. The objective of stabilizing oil droplets was to avoid the process of coalescence for the smallest droplets while doing droplet size analyses with the Malvern instrument. Chemicals tested out were:

1. Dodecyl sodium sulfate, $CH_3(CH_2)_{11}OSO_2ONa$

This alkylsulphate is also termed «NaLS» as an abbreviation for sodium lauryl sulfate. It is classified as an anionic tenside, and is a sulphonated linear alcohol with chain length C_{12}. It is also considered as a good foaming agent. As noted by Wright & Ramkrishna (1994), where a disperse-phase system of neutrally buoyant droplets of benzene/carbon tetrachloride in water was investigated, this is a surfactant that stabilizes the sample against coalescence and drop breakup even at vigorous stirring conditions

Assuming that each of these molecules provides a surface coverage of 50 $Å^2$ at the interface, and that the oil/water ratio is 3% (v/v), it was roughly estimated that a solution consisting of 3 g NaLS pr. litre should be sufficient for a dilution ratio 1:500.

2. Polyvinylalcohol 72000

This polymer is a very large and long molecule (MW = 72000), supposedly being able to wrap in the small oil droplets, thus preventing the coalescence process to proceed. Polyvinylalcohol 72000 has a high degree of hydrolysis, approx. 98%.

Assuming that each of these molecules provides a surface coverage of 5000 $Å^2$ at the interface, and that the oil/water ratio is 3% (v/v), it was roughly estimated that a solution consisting of 15 g NaLS pr. litre should be sufficient for a dilution ratio 1:500.

3. Igepal CO-970 and Igepal CO-990

These compounds are classified as non-ionic tensides, being long-chained polyethylene oxide derivatives. The number of ethylene oxide (EO) groups in such molecules is indicative for the area of application. Low number of EO (n = 1 - 6) are typical for oil-in-water emulsifiers, medium number of EO (n = 6 - 15) are frequently applied in detergents and emulsifiers, while tensides with high contents of EO (n > 15) are often used in special emulsification applications.

Igepal CO-970 has EO = 50, while Igepal CO-990 has EO = 100.

An Igepal CO-970 molecule is assumed (MW = 2423) to provide a surface coverage of 120 $Å^2$ at the interface, while the Igepal CO- molecule is assumed (MW = 4625) to provide a surface coverage of 173 $Å^2$. Appropriate concentrations for these tensides were therefore estimated to be 10 and 12 g/l for Igepal CO-970 and Igepal CO-990, respectively.

4. Dioctyl sulphosuccinate, $C_{20}H_{37}O_7SNa$

This surfactant is mostly known for its wetting properties.

Assuming that each of these molecules provides a surface coverage of 90 $Å^2$ at the interface, and that the oil/water ratio is 3% (v/v), it was roughly estimated that a solution consisting of 2 g NaLS pr. litre should be sufficient for a dilution ratio 1:500.

5.3 Emulsifying agents

Two different chemical additives, which were added to the pure crude oil phase only, were tested on the 0.01% oil-in-water dispersion. This was done in order to investigate whether these chemicals could influence the capability of the added crude oil to absorb the smaller droplets originally contained in the oil-in-water dispersion, i.e. promote or inhibit coalescence.

The chemicals applied for these purposes were:

1) Decanol
2) Benzyl alcohol.

In similar experiments performed by Sjöblom et al. (1990), it was found that, by measuring the separation of water from the emulsion after 30 mins, 0 and 90 % of water (v/v) were separated when applying decanol and benzyl alcohol, respectively. With the results of Sjöblom et al. (1990) in mind, a rapid separation of oil and water would be expected in the present experiments when using benzyl alcohol, while no separation would be expected when using decanol.

5.3.1 Emulsions

Alther (1998) explained that, whenever two immiscible liquids, such as oil and water, contact each other, one liquid tends to disperse, but do not dissolve into the other. Such a dispersion of liquid, typically in an aqueous medium, is frequently termed as an emulsion. Few emulsion droplets are smaller than 0.25 microns in diameter, but larger ones can be 100 times larger in size.

The two main categories of emulsions are oil in water (OW) and water in oil (WO), with water including the most highly polar, hydrophilic liquids. Hydrophobic nonpolar liquids are considered «oils». Most often the OW phase is of concern, and this is divided into three subgroups: 1) less than 30% oil, 2) 30 - 74% oil, and 3) 74% or more oil.

CHAPTER 5 THE EFFECT OF CHEMICAL ADDITIVES

Emulsions consist of three phases: The internal, or discontinuous, phase consists of finely divided droplets. The external, or continuous phase is the matrix that keeps droplets in suspension. The interphase consists of an emulsifier, or stabilizer, that keeps the emulsion stable, binding the internal and external phases together, and preventing droplets from approaching each other and coalescing (Lissant, 1974).

Usually emulsifiers are surfactants and soaps, present either by themselves or as part of the makeup of a detergent formulation. An emulsifier consists of a molecule with hydrophilic and hydrophobic ends. In the presence of immiscible liquids, the emulsifier migrates to the interface of the internal and external phases, forming a protective sheath around droplets of the dispersed phase as shown in Fig. 5.2. While the hydrophobic end of the molecule migrates, or partitions, into droplets, the hydrophilic end stays in the water.

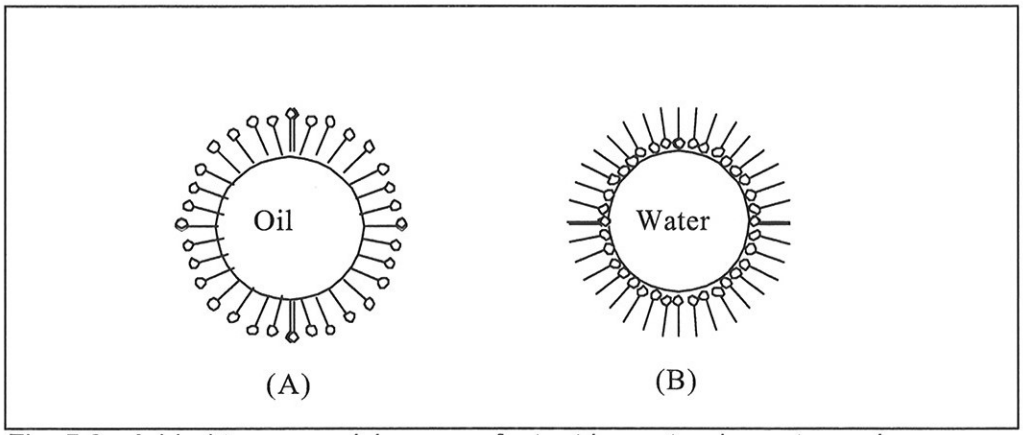

Fig. 5.2 : Added to an emulsion, a surfactant has a tendency toward orientation. The hydrophilic end is attracted to the water, while its hydrophobic end is oriented toward the oil. (A) Oil in water, (B) Water in oil.

In effect, the emulsifier acts as a coupling agent, lowering the interfacial tension of the internal and external phases. When the interfacial tension is reduced to zero, an emulsion forms spontaneously. This means that the surface area of the internal phase has reached its maximum. The dispersion of fine droplets, generally less than 1 micron in diameter, gives the emulsion a milky appearance. This effect can be achieved mechanically with colloid mills (e.g. Ultra Turrax) and centrifugal pumps.

CHAPTER 5 THE EFFECT OF CHEMICAL ADDITIVES

At equilibrium, the particle size of an emulsion's internal phase depends on the amount of emulsifier available to maintain that equilibrium. Hence, the concentration of an emulsifier must be balanced by its droplet size to keep particles from coalescing. The smaller the droplets, the more emulsifier required to cover the larger surface area. In other words, the concentration of emulsifier determines the amount of stabilizer absorbed at the interface (Lissant, 1974).

An important factor in emulsion stability is the diameter of the dispersed droplets, which correlates to the volume of the dispersed phase and the interfacial area available. For example, if oil is added to a container partially filled with water, the oil, upon impact, will coalesce and float as sheen on the water's surface. The water forms a second layer or phase because its specific gravity is lower than that of water.

If water is then blasted into the container, the physical impact of the water on the oil will cause some droplets to emulsify, or disperse, in the water. When the blast ceases, oil droplets will coalesce rapidly.

A surfactant or emulsifier added to the container will disperse the oil into the water. The system can be imagined as a collection of small spheres dispersed in the continuous water phase. Unless the droplets are small enough to be kept in suspension by thermal forces, they will eventually settle out or rise to the surface and form a layer of droplets in a process called creaming. Left idle, oil droplets will collide and coalesce, unless enough emulsifier is added to cover the entire interfacial area. Over a period of time, larger particles will rise to the surface and coalesce into a single layer (Becher, 1965).

As described by Stokes' Law, large droplets rise, or fall, faster than small ones, and drops move faster in a low-viscosity liquid. And, since the oil's density is usually less than that of the water, upward sedimentation, or creaming, will occur (Becher, 1965).

Flocculation, or aggregation, is a second process that takes place in emulsions with low-internal-phase ratios. Particles slide together without coalescing to form clumps, or chains of clumps, of larger effective size. The settling rate then increases, even though the particles do not behave as spheres, as Stokes' Law demands (Lissant, 1974).

CHAPTER 5 THE EFFECT OF CHEMICAL ADDITIVES

Emulsifier solubility can be enhanced, if necessary, by adding a co-solvent or co-emulsifier, such as propylene glycol, that will act as coupler to assure stability at all temperatures. A blend of several surfactants can be added to form a tightly packed film around the droplets. The presence of finely divided solids, such as clays, can also act as emulsifiers. The oil droplets then coat these solids, resulting in an emulsion or settling.

As explained in the textbook of Laidler & Meiser (1982), an emulsion consists of droplets of one liquid dispersed in another liquid. The droplets are usually from 0.1 to 1 microns in diameter. Emulsions are generally unstable unless a third substance, known as an emulsifying agent or a stabilizing agent is present. Soaps and detergents are effective emulsifying agents, particularly for oil-water emulsions. They consist of long-chain hydrocarbon molecules, each having at one end a polar group such as a carboxylic acid or sulphonic acid group. These molecules are readily adsorbed at oil-water interfaces; the hydrocarbon chains become attached to the oil and the polar groups to the water.

The term *micelle* is used to refer to aggregates of tenside molecules that are stabilized by emulsifying agents in this manner. The hydrophobic hydrocarbon chains are thus located in the internal of the micelle, while the hydrophilic groups are oriented towards the water phase. Usually, when the tenside concentration is lower than a certain value, the micelle formation is quite modest. At values higher than the critical micelle concentration (CMC), the micelle formation increases rapidly, since all the tenside that is added in excess of this concentration will contribute to the formation of micelles. Such a micelle formation is a spontaneous process, leading to a reduction in the free energy of the system.

The action of emulsifying agents is to reduce the interfacial tension between the two phases. The effect of surface tension is to cause the surface to be as small as possible. A high surface tension between the dispersed phase and the dispersion medium will therefore cause an emulsion to separate into two bulk phases, i.e. to *coagulate*. The adsorption of an emulsifying agent on an interface reduces this tension and therefore decreases the tendency of the emulsion to coagulate.

An emulsion with no stabilizing agent has properties similar to those of lyophobic sols, e.g. they are easily coagulated by electrolytes. Stabilized

emulsions, on the other hand, behave more like lyophilic sols and are only affected by electrolytes at high concentrations.

As noted by Sjöblom et al. (1992), to stabilize an emulsified system is to control four fundamental processes, i.e. sedimentation (creaming), flocculation, coalescence and Ostwald ripening. The first process is a formation of a droplet concentration gradient within the emulsion. Flocculation is the process where the interparticular distance between the droplets is strongly diminished due to a net attraction between the droplets. In this process the individual droplets maintain their identity. Coalescence means the formation of large droplets with a concomitant phase separation. Ostwald ripening is a phenomenon in polydisperse emulsions where larger droplets will form at the expense of smaller.

5.3.2 Electrical charge in emulsions

As explained by Alther (1998), there is an electrokinetic gradient across the interface of all solids and liquids. This is termed the Zeta potential, and is largely responsible for colloidal stability. Discharge of the Zeta potential, accompanied by precipitation of colloid, occurs by addition of polyvalent ions of a sign opposite that of colloidal particles. Adding an ionized emulsifier that is attracted to the oil-water interface will impart a positive or negative charge to each droplet. The coalescence rate will slow down as electrically repulsive forces build up between droplets.

Oil droplets in an oil-in-water emulsion are likely to have a negative charge, as described by the Helmholtz theory of the electrical double layer. This states that if the negative charges are aligned or closely bound to the interlayer, charges of the opposite type will line up parallel to them, forming an electrical double layer that causes oil droplets to repel each other.

The molecular structure of surfactants consists of two distinct sections. One is polar and water soluble, while the other is non-polar and insoluble in water.

When a surfactant, or emulsifier, is added to an oil-in-water emulsion, it has a tendency toward orientation, whereby the emulsifier's hydrophilic end is dissolved into the water and its non-polar hydrocarbon end is oriented toward the oil. When the molecules become crowded around an oil droplet, and space becomes limited, the film of the surfactant around the droplet

compresses and the surfactant molecules are packed in an oriented position, as shown in Fig. 5.2.

If sufficient emulsifier is added to coat the entire surface area of the droplets, a stable emulsion will form that can last for years, such as those found in cosmetics and shampoos. The emulsifier thus forms a skin around each droplet, preventing it from colliding with other droplets.

Emulsion breaking, or demulsification is the separation of a dispersed liquid from the liquid in which it is suspended. All chemical and mechanical methods of emulsion breaking conform to Stokes' Law.

The objective of demulsification is to destroy the interface and drive the surfactant to either the oil side or the water side, allowing the oil particles and sediments to coalesce and rise to the surface, as in creaming. Decreasing water-phase viscosity or increasing oil viscosity can enhance demulsification. Increasing the diameter of oil droplets and lowering the density of oil to water also works.

Demulsification is divided into several processes:

- Gravity separation of free, nonemulsified oil
- Chemical treatment and separation of emulsified oil
- Electrolytic methods

Anionic and nonionic surfactants, and solids present on the interfacial film maintain the stability of emulsified droplets. An emulsion achieved with solids is most stable when the contact angle of the solids with the interface is close to 90 degrees. While the Zeta potential of the solids may increase the strength and stability of the emulsion, surfactants are largely responsible for the film's high Zeta potential, high interfacial-shear viscosity, high interfacial elasticity, and relatively low interfacial tension (Lissant, 1974).

5.3.3 Destabilization of emulsions and dispersions

As explained by Alther (1998), there are several strategies for counteracting emulsions:

- Decompose the emulsion, using dissolved air flotation, ozonation or other oxidation process. This method, however, is expensive.
- Chemically react the emulsion, modifying the surfactant's charge so that it no longer acts as an emulsifier. For an ionic surfactant, neutralization is often the simplest method, using an acid, base or ionizer. If a calcium or magnesium salt, such as CaCl or $MgSO_4$ is added to an emulsion stabilized by a sodium soap, the soap will convert into a calcium or magnesium soap, which is less soluble in water because the interfacial film has changed. The emulsion may break.
- Increase the solubility of the surfactant in either bulk phase. Alcohol or other polar solvents, such as acetone, can be used to increase solubility in the water phase and pull the emulsifier out of the oil phase. If the aqueous phase is brine, dilution with water may be all that is needed to achieve separation.
- Disrupt the oriented structure of the emulsifier's interfacial phase with demulsifiers. Because these materials are not very soluble in either phase, they concentrate at the interface. Separation occurs when the agents insert themselves between the surfactant molecules, increasing the intermolecular distance and weakening the binding forces constructed by the emulsifier.

Chemical demulsifiers provide the opposite charge to the emulsion, allowing the accumulated electrical charge on the interface of the emulsified oil droplets to be neutralized. Normally, cationic demulsifiers, which exhibit a positive charge when dissociated in water, are used to destabilize oil-water emulsions. Coalescence occurs when the Zeta potential of the surfactant approaches zero, at which point coalescence is in progress (Kemmer et. al, 1979).

The meaning of a "*stable*" dispersion or suspensions is that the smaller dispersed droplets are prevented from combining into larger droplets by coalescence. Hence, when using the term "destabilizing" a dispersion system it means that the system is more susceptible to undergo coalescence. As noted by Woods & Diamadopoulos (1988), there are three considerations taken into account for keeping dispersions stable:

1) At *equilibrium* conditions, repulsive forces between the two surfaces counteract the attractive forces (surface charge effects due to electrochemical double layer, or adsorbed polymers due to steric stabilization),

2) At *rate* conditions, insufficient time is allowed for the intervening fluid to thin down to distances where attractive forces become significant,
3) The fluid dynamics may create *shear* fields that break the surfaces or tear the drops apart.

One of the three above-mentioned considerations for stabilization of dispersions should be kept in mind, also when considering the destabilization processes.

Surfactants are usually present in all industrial oil/water systems, either naturally or artificially, and these tend to stabilize the dispersions. Only in the confines of a research laboratory one is able to prepare oil/water systems that are free from surfactants. Normal «pure» tap water, for example, contains about 0.01 mg/l of anionic surfactant as typified by sodium dodecyl sulfate (Woods & Diamadopoulos, 1988). Naturally, some oil/water systems contain more of the important naturally occurring surfactants than do others, e.g. asphaltenes that may form two-dimensional or lamella structures that stabilize emulsions.

Hence, most oil/water dispersions produced from unrefined oils tend to abound with naturally occurring surfactants that often thwart attempts to destabilize the suspensions. For example, Luthy et al. (1977), working with model systems of crude oil/distilled water, altered the conditions so that there was no charge on the surface; the oil drops should coagulate and coalesce, yet no coalescence occurred. Churchill & Kaufman (1973) report similar findings.

However, with the addition of an appropriate surfactant the stability of the dispersion may be broken. Such a destabilizing surfactant may chemically dissolve or displace the initial stabilizing surfactant, or simply neutralize the charge.

One of the mechanisms used to control stability is the addition of ions. Ionic surfactants are popular choices because relatively small additions can make drastic changes. In principle, this approach works for many solid-liquid systems. However, for oil/water systems the effectiveness of this as a method of treatment has been mixed.

CHAPTER 5 THE EFFECT OF CHEMICAL ADDITIVES

The term «coagulation» usually applies to processes where chemical species are added. Alternatively, the use of «chemical destabilizers» usually results in coagulation, flocculation or coalescence.

(No agreement has been reached on a definition of the terms coagulation or flocculation. It has been suggested that coagulation relate to the «change in the charge « on the drops, while flocculation relates to the transport of drops toward each other. Some workers use «flocculation» when the chemicals added are polymers, and «coagulation» when inorganic chemicals are added. Both terms are used loosely, and sometimes even refer to chemical additions that compress the double layer without adsorbing. However, as noted by Mørk (1994), coagulation implies the formation of compact aggregates with a significant reduction of the total surface area, while flocculation implies the formation of loose or open networks with a relatively small reduction in the total surface area.)

In the context as described by Woods & Diamadopoulos (1988), *coagulant* refers to any chemical added other than to alter the pH, usually being inorganic or organic. Inorganic coagulants are usually salts of such metals as aluminum or iron. They are called hydrolyzing coagulants, since they tend to hydrolyze in water. Inorganic, nonhydrolyzing coagulants are the salts or bases of such metals as calcium and magnesium.

Polymeric flocculants (often called emulsion breakers) are classified according to their charge rather than their structural unit: anionic, cationic, or nonionic if they carry negative, positive, or no charge, respectively. Often they are used in conjunction with inorganic coagulants to produce flocs that dewater and separate easily. When used in this context, polymeric flocculants are often referred to as coagulant aids, although they are called destabilizing agents or emulsion breakers.

5.4 Gibbs' adsorption equation

From a thermodynamic viewpoint, Gibbs' adsorption equation provides the relationship between the concentration in the solution, the amount adsorbed on the interface and the resulting change in the interfacial tension.

Gibbs introduces the concept of «surface excess concentration», denoted Γ (mol/m^2). The reason for this is that, even though it can be convenient to

consider the interface between two liquids as a mathematical plane, this is unrealistic, particularly if an adsorbed film is present. Such a film will inevitably have a certain thickness, and will thus have some influence on its environment, e.g. by dipole-dipole interactions. This will result in an interface consisting of a of transitional volume, with variable concentrations and considerable thickness (from a molecular point of view). This transitional volume may be considered as a separate phase («surface phase»), σ, and has a separate contribution to the total energy of the system.

Gibbs introduced a hypothetical plane situated somewhere in the σ-phase, where there is a continuous change in the concentration of a given component. The location of this plane determines how much of the surface phase is shared between the two involved phases, typically termed as α - and β - phases, respectively.

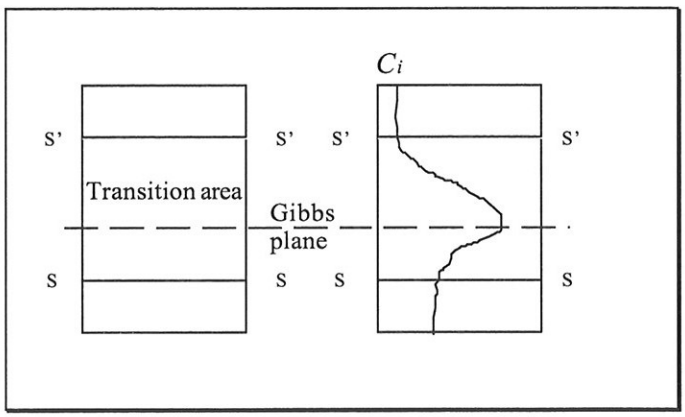

Fig. 5.3: (a) Illustration of the transition area between two bulk phases, (b) Changes in concentration for component i in this area

Defining the «excess quantity», n_i^{σ}, as the difference between the number of moles of a component i in the σ-phase and the concentration one would have if α and β had reached the Gibbs plane with unchanged concentrations. With a surface area A, the surface excess concentration of component i is given by

$$\Gamma_i = n_i^{\sigma} / A \qquad (5.1)$$

By giving further labor on this expression (Ref: Mørk, 1994), an equation for diluted solutions ($C_B < 10^{-2}$ mol/dm^3) is achieved:

$$\Gamma_B = -\left(C_B/RT\right) d\gamma/dC_B \qquad (5.2)$$

This equation is particularly applicable at low concentrations where Γ_B can be approximated to be the amount of component B at the surface. Using Γ_B, the area per molecule at the interface can be calculated. This area gives information about the packing density and orientation of the adsorbed tenside molecules.
Eqn. (5.2) can be directly applied to the adsorption of non-ionic tensides. For dissolvable or ionic compounds this evaluation is slightly more complex, since one has to take into account the dissociation equilibria and adsorption of counter ions.

5.5 Experimental

5.5.1 Preparatory procedure, sampling and analysis of emulsifier applications

The following procedure for preparation, sampling and analysis was applied when using the agents decanol or benzyl alcohol:

1) Make-up of system dispersion: 40 ml of crude oil was added to 8 l of distilled water in a bucket.
2) Ultra-Turrax was applied to this mixture for approximately 30 mins. Hence small oil droplets is achieved in the oil/water dispersion. Malvern analyses of this showed that two size classes of droplets are formed thus; one basically around 1.5 - 2.5 μm and another around 10 - 25 μm.
3) The bucket contents were then poured into the test rig tanks. Here, tap water was added until 400 liters was contained in the system, this now being a solution of 0.01% crude oil-in-water dispersion. To ensure a homogeneous dispersion before sampling, the dispersion was mixed thoroughly between the two mixers and residence tanks (each containing 200 liters).

4) This mixing of the dispersion, lasting approximately 20 minutes before any sampling was allowed and continuing throughout the experimental period, was achieved by using the following setup for the two tanks:

i) The first tank, basically having the function of being a mixer unit, was equipped with a mechanical stirrer and a recirculation pump (centrifugal type, capacity 100 l/min) which takes the dispersion from the bottom of the tank and delivers back to the top.

ii) The second tank, basically having the function of being a residence tank receiving (via a centrifugal pump) the dispersion from the first tank, was equipped with a centrifugal pump. The purpose of the pump was to transport the dispersion back to the first tank. The second residence tank also had an outlet for pumping (via a lobe pump, capacity 30 l/min) the dispersion to the static mixer test rig.

5) The chemical additive, this being either decanol or benzyl alcohol, was added to the pure crude oil and mixed. Additive concentration in the crude oil was selected to be 1.5% by volume. The crude oil mixture, contained in a separatory funnel of 3 liters volume, was then pumped into the dispersion, via a LEWA membrane dosing pump, at a constant rate of 0.3 l/min regardless of the dispersion flowrate.

6) Sampling was done by collecting the dispersion from appropriate sample points in the rig into three 500 ml separatory funnels, each containing:

i) Sample from the dispersion immediately after the lobe pump, before entry into the static mixer (not containing added oil).

ii) Sample from the dispersion immediately after the static mixer (not containing added oil).

iii) Sample from the dispersion immediately after the static mixer when oil is added.

7) Before doing analyses in the Malvern instrument each of the above samples were allowed to rest for at least 30 mins, in order to ensure that analyses are representative for the smallest and stable oil droplets only. When performing the Malvern analyses, the contents of each of the separatory funnels were transferred to the Malvern instrument in three separate batches such that three independent measurements were obtained from each 500-ml sample.

8) A printout was taken for each of the three analysis results obtained from analyzing the contents in each separatory funnel. All results, however, were also stored in the hard disk of the personal computer belonging to the Malvern instrument.

9) After inspection of the printout results obtained, in order to reduce the workload involved in the analyses, only one of the three results was

selected as being «representative» for further use in the statistical Sigma Plot analysis.

10) The software package Sigma Plot makes it possible to analyze data further and hence identify the two classes of droplet size distribution.

5.5.2 Method of stabilization of small droplets

For the purpose of stabilization of the small droplets, a number of chemicals were tested out. The chemicals tested out are listed in Ch. 5.2. They all gave different results.

The methodology for the experiments was as follows:

Four 250 ml separatory funnels were applied in the simultaneous sampling from the rig, where 0.3 l /min of oil (Exxsol D60) had been mixed with 13 l/min of water in the Sulzer static mixer unit. Prior to sampling injection, approximately 40 ml of surfactant solution (as described in Ch. 5.2) was added to each of the separatory funnels. These funnels were then carried to the Malvern laboratory.

The variation in trials, as well as the procedure for conducting trials, sampling and analysis have been described previously (see Ch. 2.4.2).

A mechanical stirrer was applied to each of the separatory funnels, and analyzed by injection into the Malvern cell consecutively, with 15 minutes between each measurement; thus 1st separatory funnel was analyzed after 15 minutes, 2nd after 30 minutes, 3rd after 45 minutes and finally the 4th separatory funnel after 60 minutes. For each of the 15 minutes analyses there was only time for three measurements in the Malvern, thus numbering the droplet size data to a total of 12 for each simultaneous sampling taken from the rig.

Two methods for the injection procedure into the Malvern were used:

A) Peristaltic injection using a recirculation pump and magnetic stirrer in a beaker (acting as a fluid reservoir).
B) Gravimetric injection by simply utilizing the potential energy of the fluid being located in an elevated separatory funnel The dispersion then flowed through the Malvern cell without any aid from external mechanical forces.

It turned out that method B) was the most reliable one, giving the more stable values for droplet diameters. By using method A), the peristaltic movement, implying «squeezing « of the fluid and its droplets when the pump wheel turns, is suspected to have an impact on the results in terms of undesired breakup and coalescence.

5.5.2.1 Results obtained from stabilization attempts

Results from using «NaLS» (recs 100 - 112)
Large variations in obscuration (concentration) and droplet diameter D[4,3] led to the conclusion that «NaLS» was inappropriate for stabilizing the oil/water emulsion.

Results from using «Igepal 50» (recs 140 - 152)
Large variations in obscuration (concentration) and droplet diameter D[4,3] led to the conclusion that «*Igepal 50*» was also inappropriate for stabilizing the oil/water emulsion. The immediate formation of a creamy emulsion on top of the fluid sample strengthens this conclusion.

Results from using «Igepal 100» (recs 120 - 132)
As for the previous «*Igepal 50*», large variations in obscuration (concentration) and droplet diameter D[4,3] led to the conclusion that «*Igepal 100*» was also inappropriate for stabilizing the oil/water emulsion. However, it was found that the results were slightly more stable than the previous *Igepal*. Also in this case it was found an immediate formation of a creamy emulsion on top of the fluid sample, which again strengthens conclusion of the inappropriateness of this chemical additive.

Results from using «DSSNa» (or Dioctylsulfosuccinate) (recs 180 - 192)
In this case the solution became more obscure than in the previous cases, and it was noted that emulsion was rapidly formed, consisting of spherical droplets. However, it did not take long before these droplets returned to be individual droplets in dispersion. As for the Malvern results, however, these droplets were relatively stable when considering and comparing the behavior for each of the four separatory funnels.

Results from using «PVA» (or Polyvinylalcohol) (recs 160 - 172)

Also in this case it was noted that a droplet-like emulsion was rapidly formed. Also, a negative obscuration was observed. Besides, it was impossible to identify any particular trend in the fluid behavior when using this chemical additive. Therefore, this chemical was also found to be inappropriate for the purpose.

Results from using a mixture of Igepal 100 and DSSNa (recs 200 - 212)
Finally, using this mixture of chemicals, satisfactory results were achieved with respect to obtaining a reasonable stability of droplet size development.

5.5.3 Method of destabilization of small droplets

With the intention of destabilization of the smallest droplets, thus enhancing the property of the larger oil droplets to absorb the smaller ones, trials were carried out using decanol and benzyl alcohol as added chemicals to the crude oil.

Crude oil applied in the experiments had been collected from the Statfjord field, at the Norwegian continental shelf. Two batches of the Statfjord crude oil were available for the experiments: 1) an «old» batch, probably dating from 1994, 2) a «new» batch of more recent origin, dating from March 1997.

It is well known that crude oil batches collected at dates representing such a long time interval from «old» to «new», and which is expected to have been through different histories with respect to transportation, storage etc., most likely will have different chemical compositions.

Hence, samples from two such different batches are also expected to behave quite differently. This was easily seen when making the oil droplet dispersions from each of these. It then appeared that oil from the new batch was somewhat harder to disperse into small droplets than oil from the old batch.

That is, more energy was required in terms of approximately 10 minutes longer Ultra Turrax application on the oil/water dispersion. Besides, it was readily seen that a thin oil film was more easily formed on top of the bulk liquid a little while after the Ultra Turrax was switched off for the last batch of Statfjord oil.

Such an observation may be explained by the fact that in the «old» batch, the most volatile components have had a long time to become released from the bulk liquid, while the opposite is the case for the «new» batch. Diffusion, as well as exposure to air and chemical reactions may also be contributing factors to the transformation taking place in the aging process for oil. The lighter constituents of the crude oil are more easily transported within the bulk and upwards to the surface.

It was therefore decided to do trials on both batches of crude oil.

5.5.3.1 Results obtained from destabilization attempts

Figs. 5.3 and 5.4 represent samples from the «old» batch using decanol and benzyl alcohol, respectively, whereas Fig. 5.5 represent a similar sample from the «new» batch using benzyl alcohol.

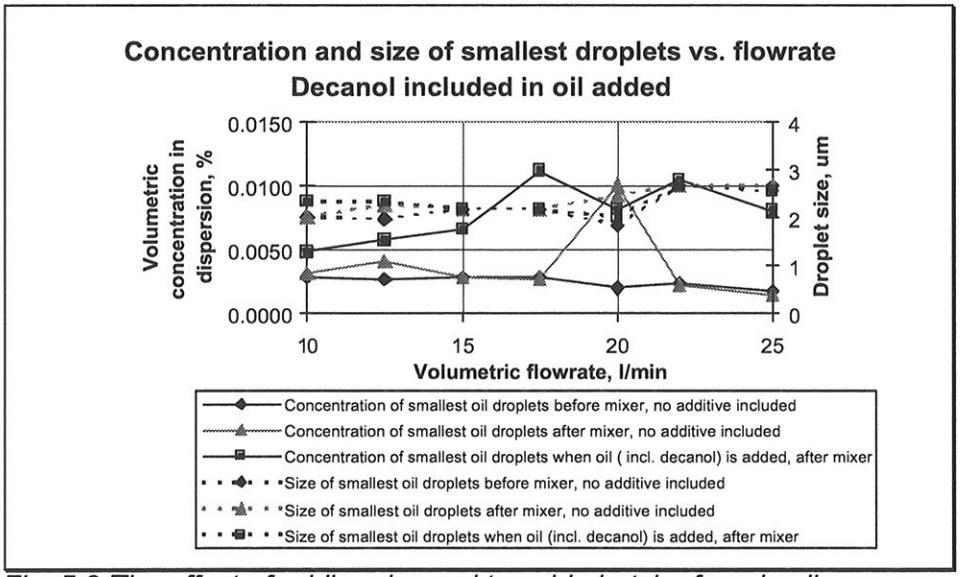

Fig. 5.3 The effect of adding decanol to «old» batch of crude oil

Decanol was mixed into the added oil with a concentration of 1.5 % v/v. This decanol/oil mixture was then dosed into the oil/water dispersion at a rate of 0.3 l/min. Temperature of the dispersion was 13°C.

CHAPTER 5 THE EFFECT OF CHEMICAL ADDITIVES

In the preparatory procedure of sampling and analysis, when using decanol or benzyl alcohol as emulsifying agents, it was noted that there were two droplet size classes being formed. After Ultra-Turrax was applied, the Malvern analyses showed concentrations of droplets with sizes around 1.5 – 2.5 μm and 10 – 25 μm. This distinction in droplet sizes is the basis for defining "smallest oil droplets" as those being around 2 μm in diameter.

Fig. 5.3 shows the experimental results of adding decanol to the pure crude oil phase. The concentration and size of the smallest droplets were recorded according to the Malvern analyses. Recordings were done for samples taken before and after mixer, with and without decanol additive.

The curves in Fig. 5.3 show significantly higher oil concentrations when decanol is applied, particularly at the higher volumetric flowrates. However, the droplet size appears to be unaffected by decanol as well as the flowrate.

Since higher oil concentrations were observed when applying decanol, it may be concluded that this agent acts as an emulsifier for the smallest oil droplets. It may also be concluded that decanol has little or no influence on the droplet size.

Further, as noted from Fig. 5.3, there also appears to be a steeper gradient in concentration curve when the decanol is applied. For a continuously higher dispersion flowrate from 10 l/min to 25 l/min, the oil concentration level of 2 μm size class also becomes continuously higher from approx. 0.0040 %v/v to 0.0100 % v/v, respectively.

This effect is identified even though the total added oil is reduced from 3 % v/v at 10 l/min dispersion flowrate to 1.2 % v/v at 25 l/min dispersion flowrate, since the flowrate of added oil is constantly held on 0.3 l/min, regardless of the dispersion flowrate.

It is interesting to see this effect in light of the experimental results obtained by Sjöblom et al. (1990), where there was no separation of water from the emulsion when decanol was used. When there is no separation of water, there should not be any separation of oil either; hence the chemical additive decanol should contribute to maintain or even enforce the emulsification property of oil and water when these are combined. This observation is indicative of coalescence inhibition in the experiments of Sjöblom et al.

CHAPTER 5 THE EFFECT OF CHEMICAL ADDITIVES

Keeping in mind that the process of emulsification also involves the process of gathering smaller droplets and form larger oil droplets from these (i.e. coalescence), where the larger droplets subsequently rise to the surface rapidly, there should rapidly be observed a reduction in the concentration of the smallest oil droplets suspended in the dispersion. It is therefore somewhat surprising when comparing the obtained results with the results of Sjöblom et al. (1990). In fact, comparing the obtained results with the results of Sjöblom, quite the opposite effect would in fact have been expected in Fig. 5.3.

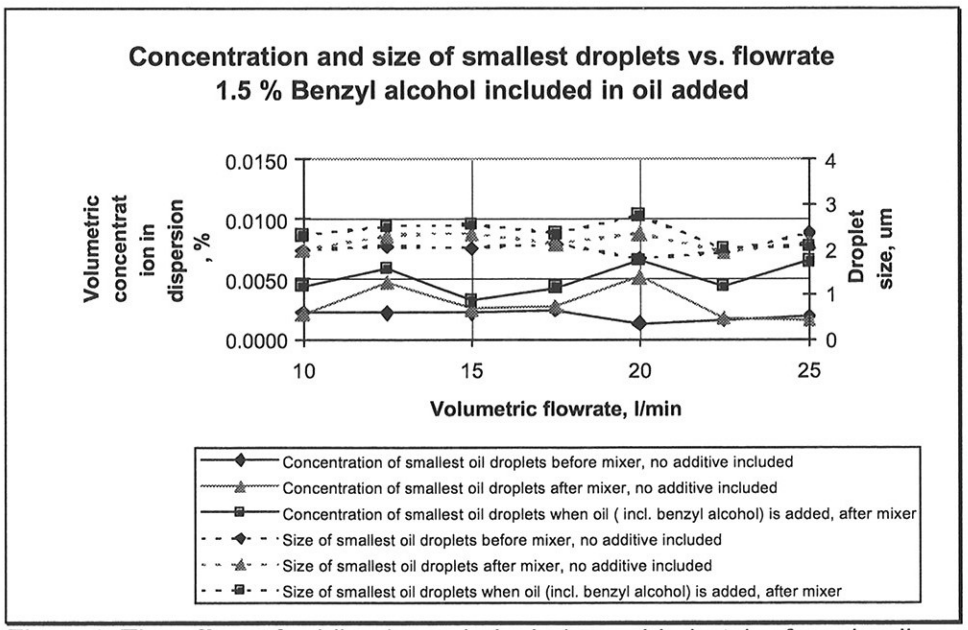

Fig. 5.4: The effect of adding benzyl alcohol to «old» batch of crude oil

Fig. 5.4 shows the experimental results of adding benzyl alcohol to the pure crude oil phase. As in the previous case, the concentration and size of the smallest droplets were recorded according to the Malvern analyses. Recordings were done for samples taken before and after mixer, with and without benzyl alcohol additive.

In comparison to what was observed when decanol was applied, the curves in Fig. 5.4 show that only slightly higher oil concentrations were obtained when benzyl alcohol was applied. This is also seen at the higher volumetric

flowrates. Also in this case, the droplet size appears to be unaffected by benzyl alcohol as well as the flowrate.

It may therefore be concluded that the benzyl alcohol acts as a significantly weaker emulsifying agent than decanol was for the smallest oil droplets. Further, it may be concluded that the diameter size shifted to a level representing only a slightly larger diameter when using benzyl alcohol as an additive.

As for the concentration of these droplets, this appears to be consistently shifted to higher concentration level than those of before and after the static mixer when no chemical was added. However, this level appears to be at a steady level, with no increase of the concentration with increase in the dispersion flowrate, as was the case when using decanol as the added chemical.

Hence, also in this case, the objective of achieving a lower concentration of the smaller class size of droplets remaining suspended in the dispersion has not been successful, when this particular chemical was added to the pure crude oil phase. If a lower concentration had been a reality, the concentration curve for this case would have been at a lower level than the concentration curves for before and after the static mixer when no chemical was added.

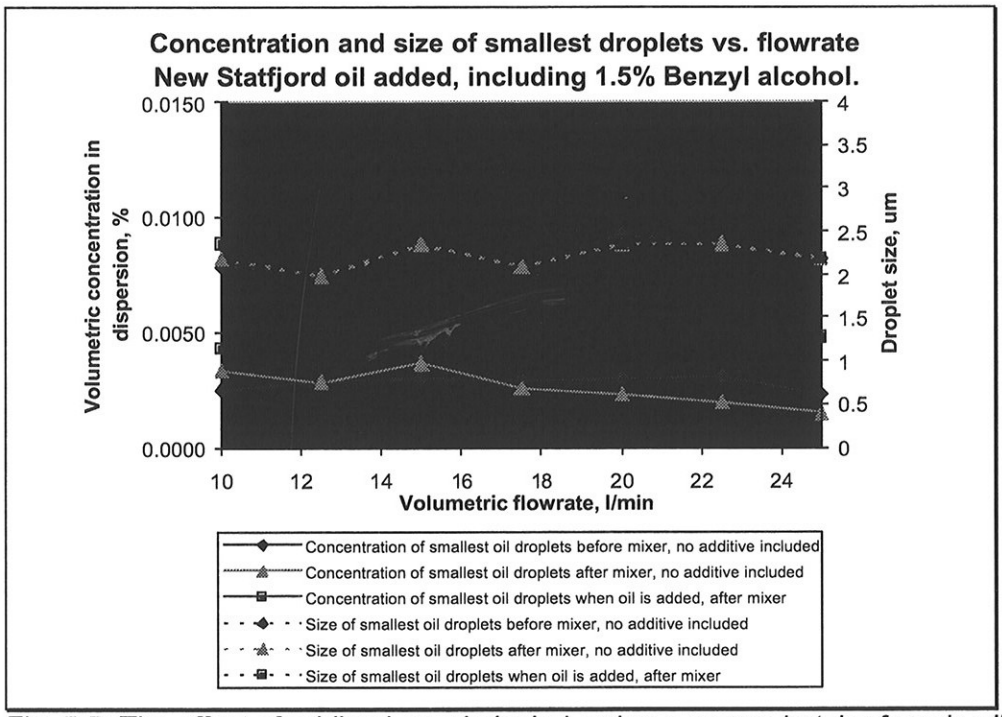

Fig. 5.5: The effect of adding benzyl alcohol, using a «new» batch of crude oil

However, as shown in Fig. 5.5 and by comparing this with Fig. 5.4, the effect of adding benzyl alcohol to crude oil appears to be unaffected with respect to the ability of larger droplets to absorb smaller droplets originally suspended in the dispersion, whether this crude oil originates from the «old» or the «new» batch.

5.6 Chapter summary

In summary, when studying the effect of chemical additives, there have been a number of findings.

For example, it is noted that more work is probably required to explain the mechanism of coalescence when temperature variations are imposed to the system. Following in the wake of this, is the desire to achieve fundamental understanding of vapor pressure effects of the solvent.

Hence, it would be of utmost value to pursue further work in order to develop a theoretical model taking care of such practical aspects of temperature and vapor pressure effects.

Further, from the practical work presented, the following conclusive points have been achieved regarding the stabilization attempts of oil/water emulsions:

Chemical applied	Stabilizer	Destabilizer
NaLS	No	
Igepal 50	No	
Igepal 100	No	
DSSNa	Doubtful	
PVA	No	
Igepal 100 + DSSNa	Yes	

As for the destabilization attempts:

Chemical applied	Stabilizer	Destabilizer
Decanol		Emulsifier properties shown, particularly for small droplets (approx. 2 μm)
Benzyl alcohol		Emulsifier properties shown, particularly for small droplets (approx. 2 μm).

Neither decanol nor benzyl alcohol were suitable to improve the ability of larger droplets to absorb smaller droplets in dispersion.

CHAPTER 6 PRACTICAL CRUDE OIL EXPERIMENTS

6 PRACTICAL CRUDE OIL EXPERIMENTS

6.1 Experimental methods

6.1.1 Introduction

The objectives of the experiments performed, for a dispersion system with crude oil-in-water, were as follows:

- measure the oil droplet size in the dispersion make-up, before entrance to the mixer
- establish oil droplet concentration in the dispersion make-up, before entrance to the mixer
- establish oil droplet size in the dispersion make-up, after exit from the mixer
- establish oil droplet concentration in the dispersion make-up, after exit from the mixer
- establish oil droplet size in a solution of oil added to the dispersion make-up, after exit from the mixer
- establish oil droplet concentration in a solution of oil added to the dispersion make-up, after exit from the mixer
- establish the relative concentrations of droplet size classes when oil is added
- establish the coalescence/breakup contribution from the originally dispersed oil droplets to added crude oil droplets.

CHAPTER 6 PRACTICAL CRUDE OIL EXPERIMENTS

Crude oil applied in the experiments had been collected from the Statfjord field, at the Norwegian continental shelf. Two batches of the Statfjord crude oil were available for the experiments:

1) an «old» batch, probably dating from 1994,
2) a «new» batch of more recent origin, dating from March 1997.

It is well known that crude oil batches collected at dates representing such a long time interval from «old» to «new», and which is expected to have been through different histories with respect to transportation, storage etc., most likely will have different chemical compositions.

Hence, samples from two, such different batches, are also expected to behave quite differently. This was easily seen when making the oil droplet dispersions from each of these. It then appeared that oil from the new batch was somewhat harder to disperse into smaller droplets than oil from the old batch. Thus more energy was required in terms of approximately 10 minutes longer Ultra Turrax application on the oil/water dispersion. Besides, it was readily seen that a thin oil film was more easily formed on top of the bulk liquid a little while after the Ultra Turrax was switched off.

Such an observation may be explained by the fact that in the «old» batch, the most volatile components have had a long time opportunity to become released from the bulk liquid, while the opposite is the case for the «new» batch. Thus the lighter constituents of the crude oil are more easily transported upwards to the surface.

It was therefore decided to do trials on both batches of crude oil.

6.1.2 Make-up of oil-in-water dispersion

It was desirable to have a well-defined dispersion for use in the rig experiments, thus demanding the following prerequisites:

A stable and well-defined oil-in-water dispersion concentration, 0.01 vol%.
Oil droplet sizes capable of being in a stable suspension, preferably with a diameter smaller than 40 :m.

In order to make such a well-defined dispersion of oil droplets in the rig water, the following procedure was applied:

1) 40 ml of crude oil was mixed into 8 liters of distilled water by means of an Ultra Turrax. The shear forces created by sufficient us of an Ultra Turrax are so powerful that the added oil droplets are broken down to very small fragments, with diameters predominantly smaller than 40 :m.

2) An Ultra Turrax is an electrically driven dispersal unit, suitable for laboratory trials where finely dispersed droplets have to be made. It is based on the stator-motor principle, schematically consisting of a motor and a tube. The end of the «tube« is equipped with slits in the stator, through which the fluid is forced at high velocities. This forms large shear forces, giving very small droplet sizes.

3) This oil/water mixture was agitated with the Ultra Turrax for approximately 30 minutes, before being entered into the static mixer rig system.

4) Tap water was added to the dispersion, thus making a system of total 400 liters of 0.01 vol% dispersion.

5) A mixing system within the rig, consisting of a mechanical stirrer and two centrifugal pumps for recirculation, ensures a homogeneous dispersion after approximately 20 minutes (See Fig. 2.3 a) for schematic drawing of setup).

6) The desired dispersion flowrate through the static mixer was facilitated by means of a lobe pump and bypass valve.

6.1.3 Sampling procedures

There were two sampling points in the static mixer rig, one immediately after the residence tank (i.e. before the static mixer), and one immediately after the static mixer

Samples taken from the rig were collected into appropriately sized 500 ml (scaled) separatory funnels.

The samples were allowed to rest for approximately 30 minutes before being analyzed by the Malvern instrument.

Such a procedure of including the resting period was chosen, since it was considered to be particularly important that the larger drops in the added oil were allowed to separate. Further, in the Malvern analyses it was of particular interest to identify the stable droplets suspended in the dispersion.

Such droplet fractions do include only those of small sizes, i.e. smaller than 40 :m. The larger droplets are neglected, since they are irrelevant when considering the droplets of a stable dispersion.

6.1.4 Analysis instrumentation and principles

6.1.4.1 Sigma Plot data treatment

To facilitate the achievement of the listed aims in section 6.1.1, a particle size analyzer was used. MALVERN Instrumentation Ltd., UK, manufactured this instrument, model «Mastersizer». A description of this instrumentation principle was given in the Users manual of the instrument (see Chapter 2.4).

The Malvern measures the diffraction pattern. Having measured the diffraction pattern, the computer uses the method of non-linear least square analysis to find the size distribution which gives the closest fitting diffraction pattern.

The analysis results, a size distribution of the sample, may be displayed graphically on the PC screen or printed out. These size distributions may, in turn be applied by the computer program to obtain useful derived diameters such as Sauter Mean Diameter, Weight Median Diameter, concentrations, etc.

However, the data achieved from the Malvern analyses are not sufficient for a complete analysis of the particle size classes, and their relative contributions with respect to size and concentration. Thus, the resulting data from the Malvern analyses are exported to the «Sigma Plot», a scientific graphing software program from Jandel Scientific Corp.

By tailoring the mathematical curve fitting and the mathematical transform routines, this program facilitates further resolution of the sampling data achieved via the Malvern tools.

This Sigma Plot procedure proved to be quite useful when resolving the individual droplet size classes, and their respective concentrations in the oil/water dispersion. It was assumed that a Gaussian distribution could describe each droplet size class:

$$f(x) = \left(\frac{k}{s}\right) e^{\frac{-\left(\frac{x-m}{s}\right)^2}{2}} \qquad (6.1)$$

If the experimental data results indicate e.g. two droplet size classes, resembling the Gaussian distribution, the curve fitting equation will be (ref: Sigma Plot User's Manual):

$$f(x) = \left(\frac{k_1}{s_1}\right) \exp\left[\frac{\left(\frac{x_1 - m_1}{s_1}\right)^2}{2}\right] + \left(\frac{k_2}{s_2}\right) \exp\left[\frac{\left(\frac{x_2 - m_2}{s_2}\right)^2}{2}\right] \qquad (6.2)$$

The curve fitting is done by iteratively varying the values of the parameters k_i, m_i and s_i $(i = 1,2)$.

An example of this curve fitting obtained in the experiments is presented at the next page.

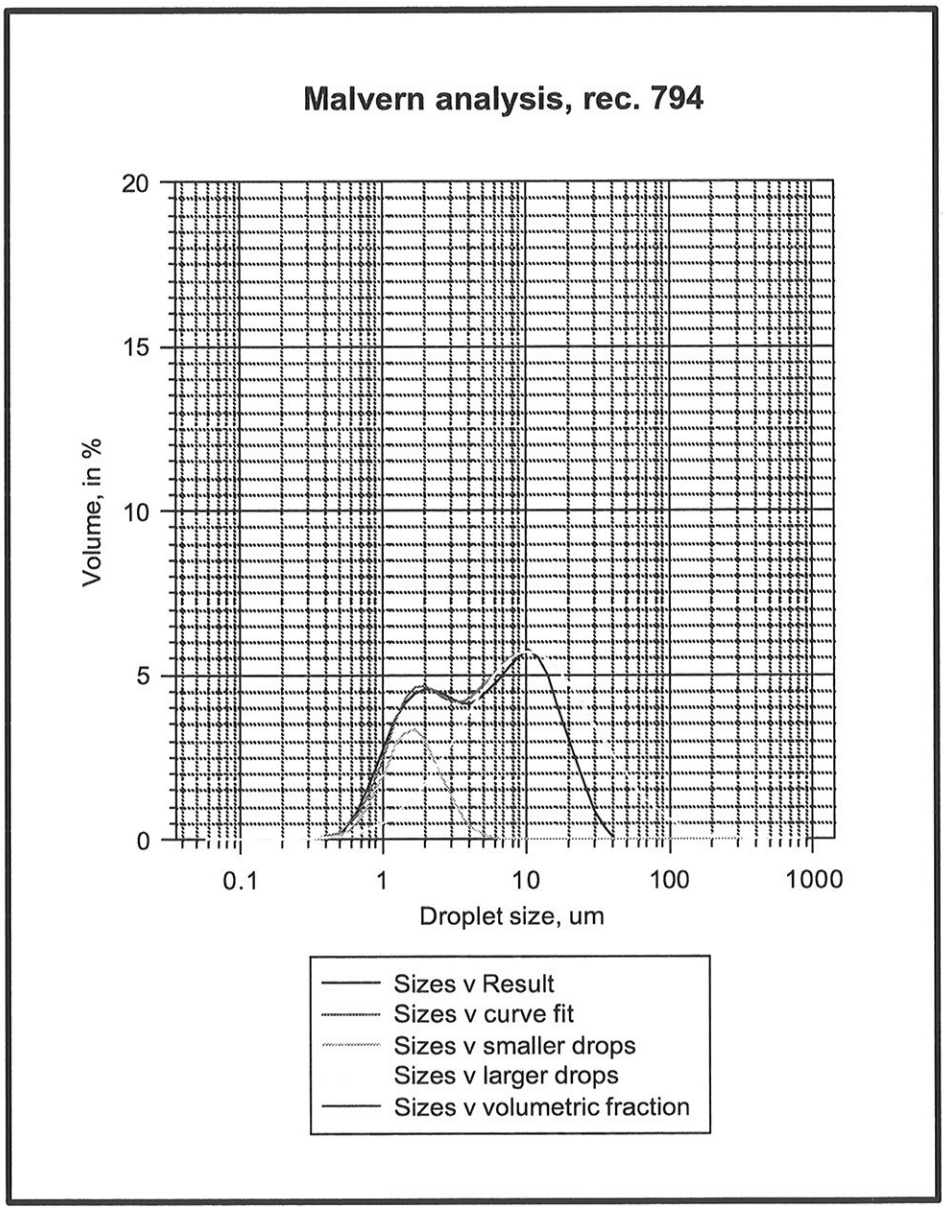

Fig. 6.1: An example of Sigma Plot curve fitting obtained in the experiments with Malvern analyses

The Sigma Plot software allows constraints to be used to set limits and conditions for parameter values, thus restricting the curve fit search range and improving curve fitting speed and accuracy. Such use of constraints in problems, which have a relatively large number of parameters (in our case 6 parameters), is a convenient way to guide the curve fitter and avoid searching in unrealistic regions of parameter space.

6.1.5 Experimental results

In the trials that follow the make-up dispersion had a constant value of 0.01 vol% of oil-in-water. For the different experimental aims, the results achieved are summarized in the graph as follows:

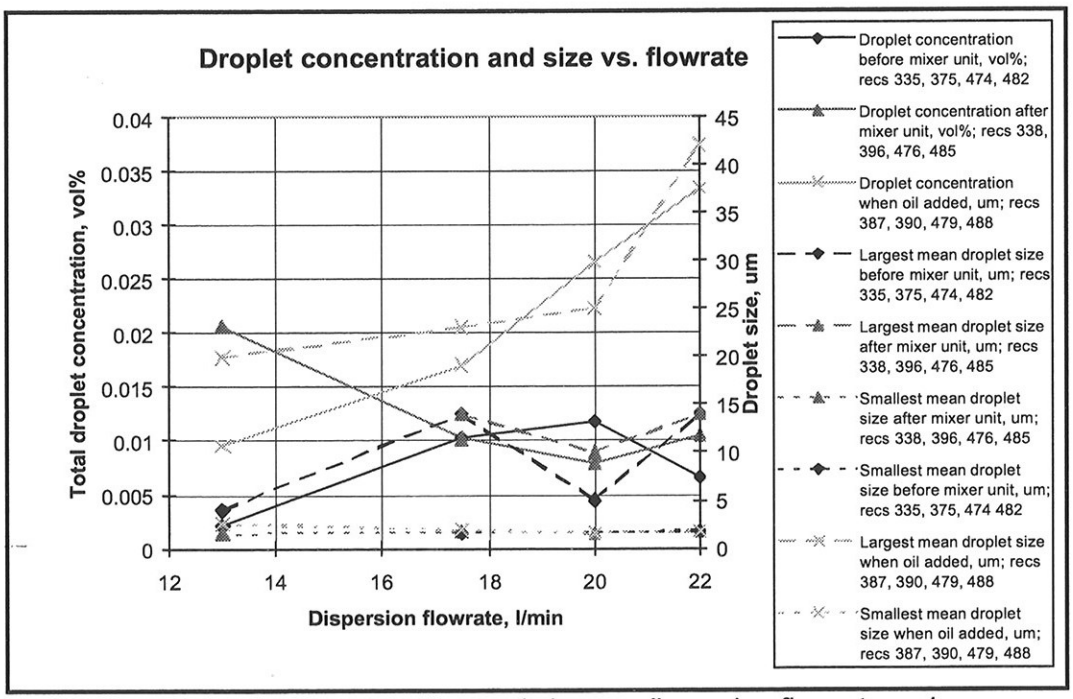

Fig. 6.2: Total droplet concentration and size vs. dispersion flowrate, using «old» batch of crude oil

The graphical presentation given in Fig. 6.2 has been made by applying the «Sigma Plot» analyses on a sample of the experimental droplet size

distribution investigations. In these investigations, pure Statfjord crude oil was added at a constant rate 0.3 l/min to a dispersed oil-in-water solution, containing 0.01% of oil by volume. The constant rate of 0.3 l/min added crude oil to this dispersion was maintained regardless of dispersion flow rate applied. From Fig. 6.2, further attention may be drawn to the following points:

6.1.5.1 Establishing oil droplet size in the dispersion make-up, before entrance to the mixer

In general, two classes of droplet sizes were identified; one very stable around 1.5 - 2 :m being quite independent on dispersion flow rates, and one basically around 5 - 15 :m, somewhat varying in an irregular fashion.

However, since it is observed that the small droplets are extremely stable in size, regardless of the dispersion flowrate, it may be concluded that these droplets were unaffected. The larger droplets were to a larger extent subject to changes under the prevailing conditions applied.

6.1.5.2 Establishing oil droplet concentration in the dispersion make-up, before entrance to the mixer

Make-up of an oil-in-water dispersion was done with the purpose of obtaining dispersion with a total droplet concentration close to 0.01 % by volume.

However, it turned out to be difficult to achieve stable values for these concentrations, regardless of the dispersion flowrate. These observations in oil droplet concentrations may be due to inaccuracies in analyzing these media by the use of Malvern instrumentation.

It appears that the first point of the curve in Fig. 6.2, representing the value achieved for dispersion flowrate 13 l/min, is pinpointed at 0.0021 vol%. This concentration then rises to 0.0102 vol% at dispersion flowrate 17.5 l/min, and stabilizes around this value for increasing flowrates.

Hence, as a conclusion from these observations, the importance of taking samples of the dispersion, and analyze these before pure oil is added cannot be sufficiently emphasized.

6.1.5.3 Establishing oil droplet size in the dispersion make-up, after exit from the mixer

Generally, two classes of droplet sizes were identified; one very stable around 1.5 - 2 :m being quite independent on dispersion flow rates, and one basically around 10 - 14 :m.

These observations revealed a very similar pattern to that observed in the case for dispersion measurements before entrance to the static mixer unit.

Again, the small droplets were observed to be extremely stable in size, regardless of the dispersion flowrate. It may therefore also in this case be concluded that the droplets in this size class were unaffected by the dispersion flowrate.

The droplets belonging to the larger size class were subject to changes under the prevailing conditions applied. This observation is similar to what was observed for the data obtained from samples taken before entrance to the mixer.

6.1.5.4 Establishing oil droplet concentration in the dispersion make-up, after exit from the mixer

Total droplet concentration appears to be reduced from 0.0206 vol% to 0.0102 vol%, when increasing the dispersion flowrate from 13 l/min to 17.5 l/min.

For the rest of the flowrate range investigated, i.e. in the dispersion flowrate range from 17.5 l/min to 22 l/min, the total droplet concentration was remaining relatively stable around 0.01 vol%.

This is the oil droplet concentration value that was desirable to obtain in the dispersion.

6.1.5.5 Establishing oil droplet size in a solution of oil added to the dispersion make-up, after exit from the mixer

When oil was added to the dispersion, the small size class of around 1.5 - 2 was still very stable regardless of dispersion flowrate. However, quite differently from the cases where no oil was added to the dispersion, a completely new large-size class, consisting of even larger droplets, was identified.

The largest mean droplet size in this mode of experiments started at 20 :m for a dispersion flowrate of 13 l/min, which steadily increased to 25 :m at 20 l/min, and then increased further in a very steep fashion to 42 :m at 22 l/min.

It thus appears that the medium-size class of droplets originally in the dispersion system, being in the range 10 - 15 :m, has some influence when pure oil is added. The medium-size class of droplets is no longer easily identifiable, and may thus have undergone a coalescence process due to the addition of pure oil.

6.1.5.6 Establishing oil droplet concentration in a solution of oil added to the dispersion make-up, after exit from the mixer

As expected, the total oil droplet concentration increased steadily with increasing dispersion flowrate, beginning with 0.0095 vol% at 13 l/min and ending with 0.0334 vol % at 22 l/min. This increase was mainly due to the injected pure oil being finely dispersed as the agitation in the static mixer increases with increasing flowrates.

The addition of pure oil was constantly set at 0.13 l/min, regardless of the dispersion rate. This implied that the added oil concentration was steadily decreasing with increasing dispersion flowrate, from 1 vol% at 13 l/min dispersion flowrate to 0.6 vol% at 22 l/min.

Thus, even as the added oil concentration was reduced with a factor of 1.7, when increasing from the lowest to the highest dispersion flowrate, the total oil-in-water dispersion concentration was increased with a factor 3.5 within the same range of dispersion flowrates.

6.1.5.7 Establishing the relative concentrations of droplet size classes when oil is added

Reconfiguring and recalculating the data used as a basis for Fig. 6.2 we achieve the following diagram in Fig. 6.3, which more conveniently describes the relative concentrations of droplet size classes when oil is added:

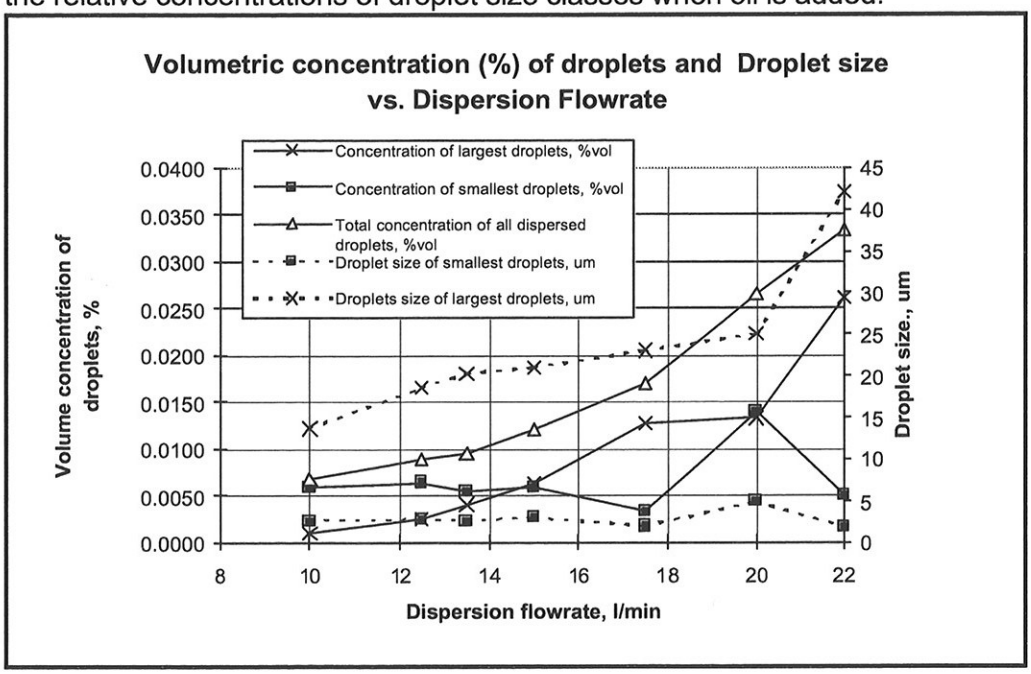

Fig. 6.3: Volumetric concentration of Droplets and Droplet size vs. Dispersion flowrate, using «old» batch of oil

From this graph it is confirmed that the total oil droplet concentration in the dispersion increased steadily with increasing dispersion flowrate, as described in section 7.1.5.6.

However, in Fig. 6.3 it may also be observed that the concentration of the largest droplets followed the trend of the total droplet concentration, whereas the concentration of the smallest droplets in the dispersion was relatively stable around 0.006 vol%.

6.1.5.8 Establishing the coalescence/breakup contribution from the originally dispersed oil droplets to added crude oil droplets

At an early stage of the experimental trials with crude oil added to tap water or 0.01% v/v oily water, it was observed that the use of dispersed oil-in-water (as the «water phase») resulted in somewhat larger oil droplet sizes than when using only pure tap water. It was also observed that the volumetric oil concentration in the resulting dispersion was higher when using dispersed oil-in-water (as the «water phase») instead of pure tap water. This is illustrated in the following figure:

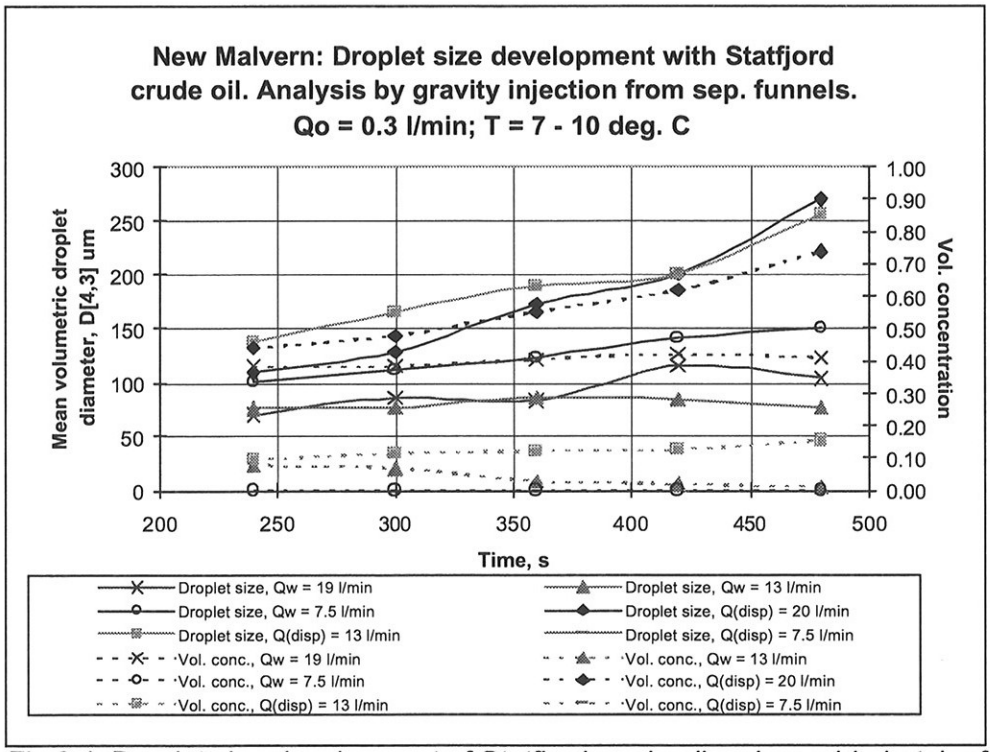

Fig.6.4: Droplet size development of Statfjord crude oil, using «old» batch of oil.

6.1.6 Droplet breakup due to make-up with Ultra Turrax

As noted from the experimental results, there are typically two classes of droplet sizes created by the Ultra Turrax; one class containing smaller droplets with diameters of around 1.5 :m and one class containing larger droplets with diameters of around 10 - 15 :m.

This phenomena of not obtaining a uniform droplet size, i.e. droplets within the same size class, when the original mother droplets have undergone deformation and breakup in a shear field, agrees well with observations made by other workers, e.g. Karam & Bellinger (1968).

As noted by Karam & Bellinger (1968), the best dispersion of a component A in matrix B occurs when operating in the vicinity of the crossover point, which is defined as that point where the viscosities of the two phases are equal or nearly equal. Further, for a given shear field, there exists a maximum viscosity ratio beyond which a liquid droplet cannot be broken up.

Only in rare instances does the deformed liquid droplet break up into two equal droplets. In most cases, the liquid droplets break up into a series of small droplets.

6.1.7 Difference between «old» and «new» batch of oil

Fig. 6.5 and Fig. 6.6 show the concentration and size of smallest droplets vs. flowrate, using «old» and «new» oil batch, respectively.

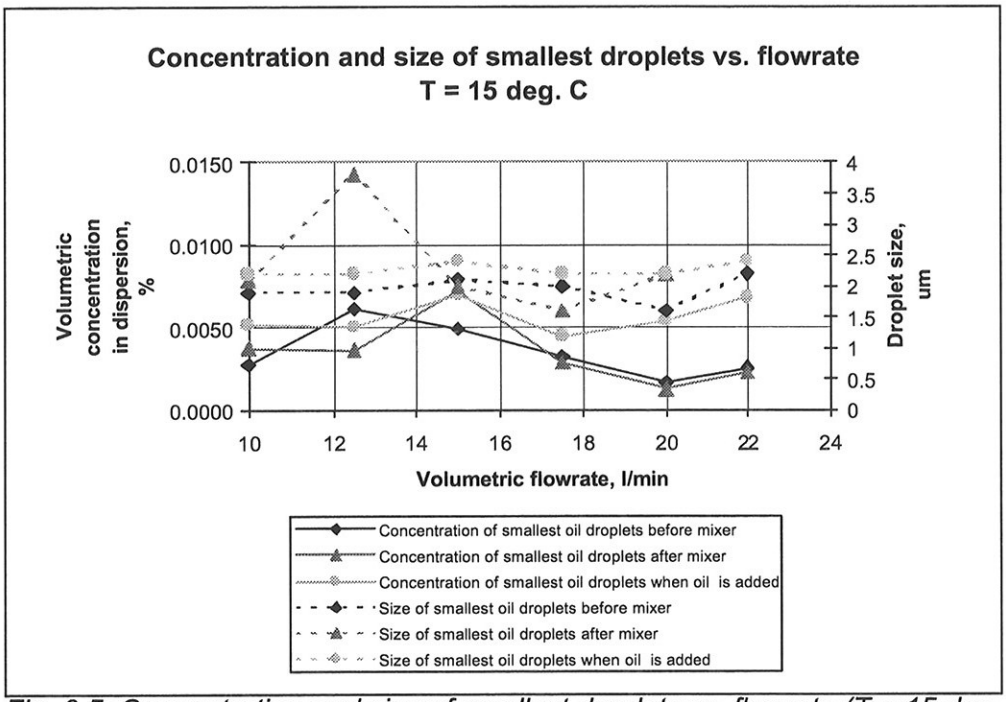

Fig. 6.5: Concentration and size of smallest droplets vs. flowrate (T = 15 deg. C), using «old» oil batch

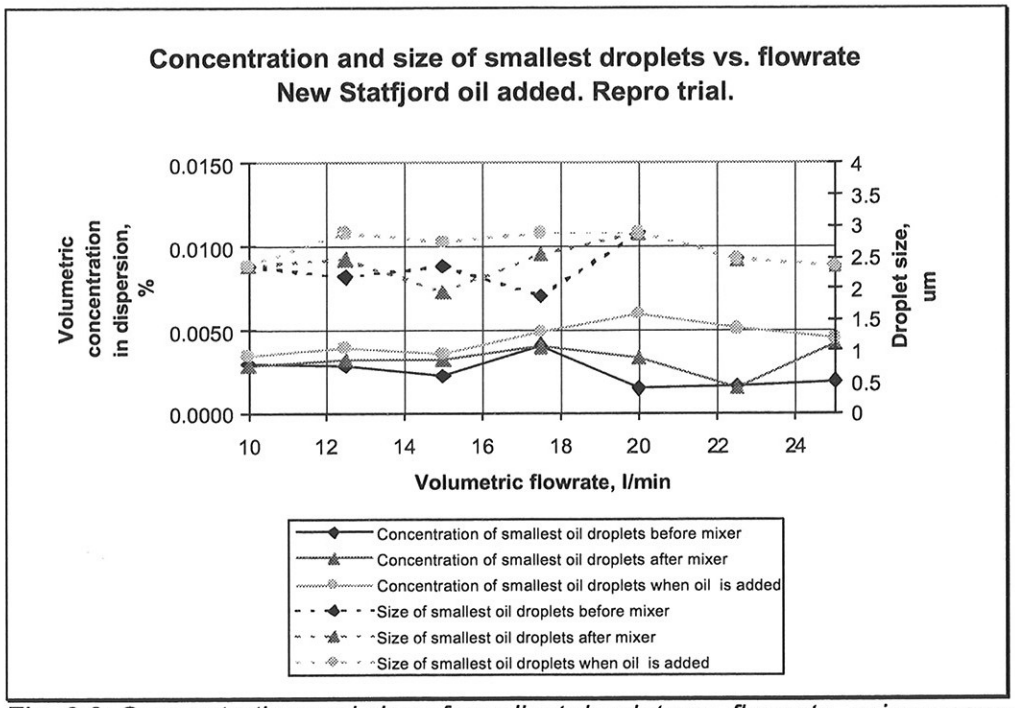

Fig. 6.6: Concentration and size of smallest droplets vs. flowrate, using «new» oil batch

By comparison of Figs. 6.5 and 6.6 it is seen that there is little difference between «old»» and «new» crude oil batches, when discussing their ability of larger drops to absorb the smallest oil droplets originally dispersed in suspension.

In the «old», as well as the «new» case, the concentration of smallest droplets (of around 2 μm) when oil is added is relatively constant. This level, which varies slightly between 0.0040 to 0.0060 % v/v, appears to be common for both cases.

Thus, in this respect, a differentiation in the behavior of the two oils is difficult to identify uniquely.

Also, in both cases, the concentration level is higher than that for before and after the static mixer unit, when no pure oil was added to the dispersion.

This confirms that the added oil has no influence on the smallest droplets originally contained in the dispersion.

6.1.8 Influence of elevated temperature on drop size distribution and concentration vs. dispersed phase flowrate

Further experimental investigations were performed using elevated temperatures, with focus on the smallest droplets with diameters up to 40 :m in order to establish any possible relationship to an increase in the temperature applied in the static mixer liquid system. As a first approach to this kind of investigation, a temperature of 60 deg. C was applied. Droplets larger than 40 :m in diameter were neglected, since these are assumed to be relatively unstable in the oil-water dispersion; they separate easily, coalesce with other droplets, and hence rise to the surface shortly after the sample is taken from the rig.

Two classes of small droplets (smaller than 40 :m) were identified in this case when applying elevated temperature on the dispersion. One class of droplets was represented by diameters basically around stable values in the range 2 - 2.5 :m, the other class was represented by droplets of larger diameters, basically around 15 - 25 :m. Only the curve for the smaller size class is shown in Fig. 6.5. The droplets in the larger diameter class were considerably more variable in size than those in the smaller diameter class.

As for the concentration profiles, from a separation viewpoint, it would be desirable to achieve an effect where the larger droplets in the dispersion due to the turbulence effects within the static mixer would be capable of absorbing the smaller droplets. This would have resulted in a reduction in the concentration of smaller droplets in the final dispersion that eventually leaves the static mixer unit.

If there had been such a case, i.e. that the larger droplets in the dispersion were able to absorb the smaller droplets originally contained in the dispersion, the concentration curve for the smallest droplets in Fig. 6.7, when oil was added, would have indicated lower values. A curve with such lower values would have been located below the level of the two curves indicating the concentration levels of the smallest droplets originally contained in the dispersion before and after the mixer.

However, such an effect, where the larger droplets absorb the smaller droplets, is not clearly identified in Fig. 6.7. The concentration curve for the smallest droplets when oil was added is relatively stable for the dispersion flowrate range10 - 22 l/min, with values around 0.004 % by volume in this set of reproduction trials. Values for the first set of these trials were around 0.005 % by volume (not shown in this figure). The values for the two curves indicating the concentration levels of the smallest droplets originally contained in the dispersion before and after the mixer vary somewhat more, but they are certainly located at a level representing the same order of magnitude.

Since temperature elevation reduces the interfacial tension, and thereby enhances the coalescence capabilities, it was anticipated a reduction in the contents of smallest oil droplets in the outlet dispersion from the static mixer, when pure oil was added to this dispersion. However, a temperature elevation, according to these experimental results, has no significant effect on the capability of the added larger droplets to absorb the smaller droplets originally dispersed in the oily water.

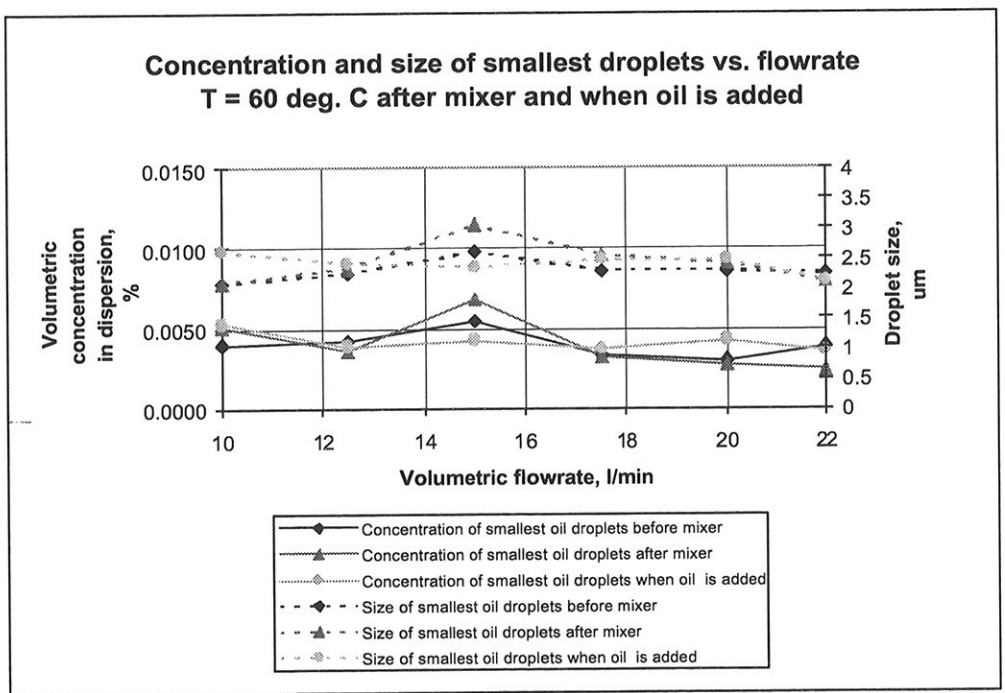

Fig. 6.7: Concentration and size of smallest droplets vs. flowrate when oil is added; T = 60 deg. C

CHAPTER 6 PRACTICAL CRUDE OIL EXPERIMENTS

6.2 Previous investigations on dispersion of immiscible liquid

It is somewhat surprising that limited information is found available in literature, concerning the ability of static mixers to disperse one liquid phase into another, especially when drops become smaller than 100 μm diameter. Middleman (1974), Streiff (1977), Chen & Libby (1978) and Berkman & Calabrese (1988) have reported phase dispersive performance of various static mixers.

The results obtained by Berkman & Calabrese (1988), using dilute dispersions of various oils in water, indicates that as d_{32_∞} increases, and the size distribution broadens, with increasing dispersed phase viscosity. The equilibrium drop sizes were found to be almost normally distributed, and were correlatable when normalized using d_{32_∞}.

However, Al Taweel & Chen (1996) recently performed some experiments with a novel static mixer, where the elements were made of woven screen. With the objective to determine the effectiveness of the novel static mixing elements in producing oil-in-water dispersions, it was found that drop diameters decreased as the two-phase system was passed through successive screens. Ultimately the droplet diameter reached an equilibrium size which could be as small as 100 μm. The rate at which equilibrium was approached was found to increase with increasing fluid velocity, decreasing dispersed-phase volume fraction, and reduced screen open area.

In the work of Al Taweel & Chen (1996) it was also found that the spatial equilibrium drop diameter decreases with increasing energy dissipation rate according to

$$d_{32_\infty} = \varepsilon^{-0.6} \qquad (6.3)$$

This equation describes the effect of average dissipation rate on drop diameter. The exponent value of 0.6 is higher than the 0.4 value predicted by the homogeneous isotropic breakup theory given by Hinze (1955). This discrepancy can most probably be attributed to deviations, in the high-energy dissipation region, from the ideal flow conditions assumed in the theoretical behavior.

CHAPTER 7 CONCLUSIONS IN SUMMARY, AND RECOMMENDATIONS FOR FURTHER WORK

7 CONCLUSIONS IN SUMMARY, AND RECOMMENDATIONS FOR FURTHER WORK

7.1 Conclusions in summary

In this work attention has been drawn to the processes of droplet coalescence and breakup, which are counteracting effects in the separation process where two or more liquids are present. Emphasis has been on experimental work. However, the theoretical aspects have been linked to the experimental.

In Ch. 1 there was a review of technology status and process comparisons. It is concluded that the separation process has traditionally required large equipment volumes and weights. New technologies require lighter and more efficient equipment base on profound understanding of relevant science.

Further, in Ch. 2, experimental setup and techniques were presented. It was believed that turbulence intensity, RMS velocity as well as local velocity were important parameter to study. LDA instrumentation together with Malvern instrumentation for particle size analyses facilitated such investigations in a static mixer from Sulzer. Only the small droplets were of interest, being the major constituent of in-dispersion-stable dispersions. Droplets larger than 40 micron size were therefore neglected in analyses.

CHAPTER 7 CONCLUSIONS IN SUMMARY, AND RECOMMENDATIONS FOR FURTHER WORK

In Ch. 3 there was an extensive literature survey on the theoretical aspects of turbulence and droplet size distribution in static mixers. Topics that were included: Drop sizes formed in turbulent flow; Models for droplet breakup and coalescence; Turbulent mixing; Principles and characteristics of the static mixer; Calculation procedures for static mixers.

Then, in Ch. 4, characterization and measurements of the static mixer were presented. Results obtained from previous workers were presented, and it was found that most workers do not limit their investigations to droplets having smaller diameters than about 40 microns. The present characterization of the moving fluid volume between two mixer elements was done with water only, as well with oil/water mixtures. In these experiments it has been focused on droplets being in a stable suspension, and being smaller than about 40 microns in diameter. Characterization was done by using LDA equipment to obtain numerical values for:

4. Mean velocity
5. Root mean square velocity
6. Turbulence intensity, i.e. the standard deviation of the mean velocity.

The experimental conditions varied as follows:

h) Single phase characterization, i.e. using tap water only
i) Beam trajectory alignment angle and vertical position within the measurement volume
j) Sealing vs non-sealing of mixer elements (to verify possible channeling effects)
k) Fluid velocities
l) Heating of fluid
m) Induced air
n) Testing of other mixer elements

It was concluded that the results obtained depend on the alignment angle, since different characterization values were obtained (velocities, turbulence intensities). Similar observations were done for variations of vertical position of beam trajectory. As expected, there was highest turbulence near the outlet from the mixer elements. Also, the recordings were different as the traverse was passed, reflecting the mixer geometry, given by the stacking of the

corrugated sheets, their folding and the angle of the furrows relative to the main flow direction.

However, when positioning the laser beam manually, there were certainly some inaccuracies occurring, possibly giving a contribution to the curve shift observed. An improvement in the method adopted here would possibly be to make an arrangement of positioning the beam by mechanical/automatical means.

Suspicions of channeling effects were withdrawn, since it could not be documented that such were documented for the mixer elements, these being either taped or not taped.

Further, it may be concluded that the mean velocity across the traverse increased with increasing volumetric flowrates.

When applying heat to the system it was also documented that this had no influence on the recordings of mean velocity or RMS in the measurement volume. This is an indication of turbulent viscosity being the most dominant, while the molecular viscosity has little or no influence.

When introducing air to the system it was documented that this led to higher RMS values. This effect was substantial, even when there was only small amounts of air introduced.

In Ch. 5 the effect of chemical additives is studied. First the theoretical aspects are presented. Then there is an explanation of the use and application of additives and emulsifying agents in the experiments. Preparatory procedure, sampling and analysis are presented and shown in figures. Results and conclusions from the attempts of droplet stabilization and destabilization are also discussed.

Finally, in Ch. 6, the experimental methods and results of conducting various practical crude oil experiments are presented. Extensive analysis instruments, such as the Malvern and Sigma Plot data treatment programs are applied and shown.

CHAPTER 7 CONCLUSIONS IN SUMMARY, AND RECOMMENDATIONS FOR FURTHER WORK

7.2 Recommendations for further work

In the course of this work it has been suspected that there have been a number of error sources. The manual means of positioning the laser beam when using the LDA is one such source. It turned out to be difficult to obtain exactly the same position within the measurement volume for all the experiments when traversing the beam.

For future experiments of the same kind it would certainly be advisable to achieve better positioning by mechanical or automatic means.

Also, in doing the sampling for Malvern analyses, it is quite possible that more reliable results could have been obtained if the Malvern instrument had been online connected. However, it is also seen that such an online method also could have imposed more errors instead, since the Malvern relies on extremely clean lenses in order to be accurate. Keeping the lenses clean, particularly when dealing with oil droplets in the suspension, was a cumbersome and time consuming process in conducting these experiments.

In this work binary liquid systems have been investigated, consisting of water and oil, with the introduction of air. However, it would be desirable to extend these investigations to also include natural produced water, representing better agreement in terms of salt and mineral contents.

Also, as for the introduction of gases, it is recommended that future investigations should be based on more natural gases, e.g. starting with methane.

Further, it is always of particular interest to study the effects of elevated pressures and temperatures, thus approaching real conditions. It is therefore recommended that laboratory based experimental conditions could start with e.g. P = 10 bara.

It is uncertain what should be recommended regarding the temperature, since no particular effects were revealed when this was increased in the experiments. However, in literature there are indications that at higher temperatures coalescence is accelerated because of the significant vapor pressure of the liquid phase. It would certainly be of great interest to do

laboratory experiments and develop models considering such important practical aspects.

Limited information has been found available in literature, concerning the ability of static mixers to disperse one liquid phase into another, especially when droplets become smaller than 100 microns. It is recommended to do further investigations on such information, and possibly implement experimental work on this.

As for the use of chemical additives, it is clearly shown that the selection of such additives is not always a straight-forward matter even though the theory may seem to be quite clear. Whether the intention is to stabilize or destabilize oil droplets being in a suspension, a careful selection has to be taken, and one has to be prepared to mix different additives to obtain the desired effect.

The capability of the added crude oil to absorb the smaller droplets originally contained was confirmed in terms of conxcentration of the smallest droplets (2microns), when using decanol as an emulsifier. However, it was also concluded that the decanol had little or no influence on the droplet size.

In comparison it was concluded that benzyl alcohol is significantly weaker as an emulsifying agent than decanol was for the smallest oil droplets (2 microns). The effect of adding benzyl alcohol to crude appeared to be unaffected with respect to the ability of larger droplets to absorb smaller droplets originally suspended in the dispersion, whether this crude originated from the "old" or the "new" batch.

It was noted that more work is probably required to explain the mechanism of coalescence when temperature variations are imposed to the system. Following in the wake of this, is the desire to achieve fundamental understanding of vapor pressure effects of the solvent.

Hence, it would be of utmost value to pursue further work in order to develop a theoretical model taking care of such practical aspects of temperature and vapor pressure effects.

CHAPTER 8 LITERATURE REFERENCES

8 LITERATURE REFERENCES

AL TAWEEL, A.M. & CHEN, C.: A Novel Static Mixer for the Effective Dispersion of Immiscible Liquids, *Trans I ChemE*, **74**, Part A, May 1996.

AL TAWEEL, A.M. & WALKER, L.D.: Liquid Dispersion in Static In-Line Mixers, *Can. J. of Chem. Eng.,* **Vol. 61**, 1983.

ALTHER, G. R.: Put the Breaks on Wastewater Emulsions, *Chem. Eng.*, March 1998.

ANDREW, S.P.S.: Frothing in Two-Component Liquid Mixtures, *Int. Symp. On Distillation*, Rottenburg, P.A. (ed.), pp. 73 - 78, Inst. of Chem. Engrs., London, 1960.

ARAI, K., KONNO, M., MATUNAGA, Y. & SAITO, S.: Effect of Dispersed Phase Viscosity on the Maximum Stable Drop Size for Breakup in Turbulent Flow, *J. Chem. Eng. Jpn.*, **10**, 325, 1977.

AVALOSSE, TH. & CROCHET, M.J.: Finite-Element Simulation of Mixing: 2. Three-Dimensional Flow Through a Kenics Mixer, *AIChE Journal*, **43**, No. 3, 588 - 597, 1997.

BAIRD, M.H.I. & LANE, S.J.: Drop Size and Hold-Up in a Reciprocating Plate Extraction Column, *Chem. Eng. Sci.*, **28**, pp. 947-957, 1973.

CHAPTER 8 LITERATURE REFERENCES

BATCHELOR, G.K.: Homogeneous Turbulence, p. 103, *Cambridge University Press*, Cambridge, 1960.

BECHER, P.: Emulsions: Theory and Practice, *Reinhold Publishing Co.,* N.Y., 1965.

BERKMAN, P.D. & CALABRESE, R.V.: Dispersion of Viscous Liquids by Turbulent Flow in a Static Mixer, *AIChE Journal*, **34**, No. 4, pp. 602 - 609, 1988.

BIRD, R.B., STEWART, W.E., & LIGHTFOOT, E.N.: Transport Phenomena, *Wiley*, New York, 1960.

BLASS, E.: Formation and Coalescence of Bubbles and Droplets, *Intn. Chem. Eng,* **30**, No. 2, pp. 206 - 221, 1990.

BOURNE, J.R. & MAIRE, H.: Micromixing and Fast Chemical Reactions in Static Mixers, *Chem. Eng. Process*, **30**, pp. 23 - 30, 1991.

BRODKEY, R.S.: Mixing Theory and Practice, Uhl, V.W. & Gray, J.B. (Eds.), *Academic Press*, **Vol. 1**, Ch. 2, N.Y., 1966.

BROWN, D.E., PITT, K.: Paper presented at CHEMCA, Australia, 1970.

BROWN, D.E., PITT, K.: *Chem. Eng. Sci.,* **27**, 577, 1972.

CALDERBANK, P.H.: *Trans. Inst. Chem. Eng.,* **36**, 443, 1958.

CHAUDARI, R.V. & HOFMANN, H.: Coalescence of Gas Bubbles in Liquids, *Reviews in Chemical Engineering*, **Vol. 10**, No. 2, 1994.

CHEN, S.J., DEVELION, P.D. & BOR, T.P.: *DECHEMA Monogr,* **74**, 77, 1974.

CHEN, S.J., & LIBBY, D.R.: Gas-Liquid and Liquid-Liquid Dispersions in a Kenics Mixer, paper presented at *the 71st Annual AIChE Meeting*, 1978.

CHESTERS, A.K.: The Modeling of Coalescence Processes in Fluid-Liquid Dispersions, *Trans I Chem., Part A,* **69**, 259 - 281, 1991.

CHAPTER 8 LITERATURE REFERENCES

CHESTERS, A.K. & HOFMANN, G.: Bubble Coalescence in Pure Liquids, *Appl. Sci. Res.*, **38**, 353, 1982.

CHURCHILL, R.J. & KAUFMAN, W.J.: Water Processing Related Surface Chemistry of Oil Refinery Wastewater, *SERL Report 73-3*, Univ. of California, Berkeley, Calif., 1973.

CLAY. P.H.: The Mechanism of Emulsion Formation in Turbulent Flow, *Proc. Roy. Acad. Sci. (Amsterdam)*, **43**, pp. 852, 979, 1940.

COLLINS, S.B. & KNUDSEN, J.G.: Drop-Size Distributions Produced by Turbulent Pipe Flow of Immiscible Liquids, *AIChE Journal*, pp. 1072 - 1080, 1970.

COULALOGLOU, C.A. & TAVLARIDES, L.L.: Description of Interaction Processes in Agitated Liquid-Liquid Dispersions, *Chem. Eng. Sci*, **32**, 1289 - 1297, 1977.

CURL, R.L.: Dispersed Phase Mixing: I. Theory and effects in simple reactors, *AIChEJ.*, **9**, 175, 1963.

CUTTER, L.A.: Flow and Turbulence in a Stirred Tank, *A.I.Ch.E.J.*, **12**, 34, 1966.

DANTEC MEASUREMENT TECHNOLOGY: Instruction manuals for the LDA instrument, 1993.

DAVIES, G.A., JEFFREYS, G.V. & SMITH, D.V.: Coalescence of Liquid Droplets - Correlation of Coalescence Times, *Proc. Int. Solvent Extr. Conf., The Hague*, pp. 385 - 399, Society of Chemical Industry, London, 1971.

DAVIES, J.T.: Turbulence Phenomena, *Academic Press*, 1972.

DAVIES, J.T.: Drop Sizes of Emulsions Related to Turbulent Energy Dissipation Rates, *Chem. Eng. Sci.*, **40**, No. 5, pp. 839 - 842, 1985.

DAVIES, S.R.H. & PALMER, A.J.: Use of Hydrocyclones for Solids Separation and Cleaning Applications in Topsides Processing Systems, *4th International Conference in Water Management Offshore, IBC*, Aberdeen, 1995.

CHAPTER 8 LITERATURE REFERENCES

DELICHATSIOS, M.A. & PROBSTEIN, R.F.: The Effect of Coalescence on the Average Drop Size in Liquid-Liquid Dispersions, *Ind. Eng. Chem. Fundam.* **15**, pp. 134-8, 1976.

DOULAH, M.S.: An effect of Hold-Up on Drop Size in Liquid-Liquid Dispersions, *Ind. Eng. Chem. Fundam.* **14**, pp. 137-8, 1975.

DOULAH, M.S. & DAVIES, G.A.: A Queue Model to Describe Separation of Liquid Dispersion in Vertical Settlers, *Proc. Int. Solvent Extr. Conf., Lyon,* pp. 1651 - 70, Society of Chemical Industry, London, 1974.

EL-HAMOUZ, A.M., STEWART, A.C. & DAVIES, G.A.: Kerosene/water Dispersions Produced by a Lighnin «In-Line» Static Mixer, *IChemE Symposium Series*, No, 136, 1994.

ELTON, G.A.H. & PICKNETT, R.G.: Coalescence of Aqueous Droplets with an Oil-Water Interface, *Proc. Int. Congress on Surface Activity*, Butterworths, London, **1**, 288- 294, 1957.

ETCHELLS, A.W. & SHORT, D.G.R.: Pipeline Mixing - A User's View. Part 1 - Turbulent Blending, *6th European Conference on Mixing*, Pavia, Italy, pp. 539 - 544, BHRA, 1988.

FRADETTE, L., LI, H. Z. & CHOPLIN, L.: 3D Finite Element Simulation of Fluid Flow Through a SMX Static Mixer, *Computers Chem. Engng.*, **22**, Suppl., pp. S759 - S761, 1998.

GAISER, G.: Fluid Mixing Characteristics in Motionless Mixers: Structure Optimization by Simulation, *ICHEME Symposium Series No. 136*, pp. 431 - 440, 1994.

GOLDSHMID, J., SAMET, M. & WAGNER, M.: Turbulent Mixing at High Dilution Ratio in a Sulzer-Koch Static Mixer, *Ind. Eng. Chem. Process Development,* **Vol. 25**, No. 1, 1986.

GROSZ-RÖLL, F.: Assessing Homogeneity in Motionless Mixers, *Int. Chem. Eng.*, **Vol. 20**, No. 4, pp. 542 - 549, 1980.

GROVER, G.S., RODE, C.V. & CHAUDARI, R.V.: Effect of Temperature on Flow Regimes and Gas holdup in a Bubble Column, *Can. J. Chem. Eng.*, **64**, 501 - 504, 1986.

CHAPTER 8 LITERATURE REFERENCES

HAAS, P.A.: The Dispersion of Aqueous Drops in Organic Liquids, *AIChEJ.*, **33**, 987 - 992, 1987.

HAHN, P.S., CHEN, J.D. & SLATTERY, J.C.: Effects of London-van der Waals Forces on the Thinning and Rupture of a Dimpled Liquid Film as a Small Drop or Bubble Approaches a Fluid-Fluid Interface, *AIChEJ.*, **31**, 2026 - 2038, 1985.

HAHN, P.S. & SLATTERY, J.C.: Effect of the Surface Viscosities on the Stability of a Draining Plane Parallel Liquid Film as a Small Bubble Approaches a Liquid-Gas Interface, *AIChEJ.*, **31**, 950 - 956, 1985.

HETSRONI, G.: Handbook of Multiphase Systems, Chap. 4, *McGraw-Hill*, 1983.

HESKETH, R.P., ETCHELLS, A.W. & RUSSELL, T.W.F.: Bubble Size in Horizontal Pipelines, 1987.

HESKETH, R.P., ETCHELLS, A.W. & RUSSELL, T.W.F.: Experimental Observations of Bubble Breakage in Turbulent Flow, *Ind. Eng. Chem. Res.*, **30**, 845, 1991a.

HESKETH, R.P., ETCHELLS, A.W. & RUSSELL, T.W.F.: Bubble Breakage in Pipeline Flow, *Chem. Eng. Sci.*, **46**, 1, 1991b.

HINZE, J.O.: Fundamentals of the Hydrodynamic Mechanism of Splitting in Dispersion Processes, *A.I.Ch.E. Journal* , **1**, pp. 289 - 295, 1955.

HOBBS, D.M., SWANSON, P.D. & MUZZIO, F.J.: Numerical Characterization of Low Reynolds Number Flow in the Kenics Static Mixer, *Chem. Eng. Sci.*, **53**, No. 8, pp. 1565 - 1584, 1998.

IVANOV, I.B. & DIMITROV, D.S.: Hydrodynamics of Thin Liquid Films: Effect of Surface Viscosity on Thinning and Rupture of Foam Films, *Colloid & Polymer Sci.*, **252**, 982 - 990, 1974.

IVANOV, I.B., DIMITROV, D.S., SOMASUNDARAM, S. & JAIN, R.K.: Thinning of Films with Deformable Surfaces: Diffusion Controlled Surfactant Transfer, *Chem. Eng. Sci.*, **40**, 137 - 50, 1985.

CHAPTER 8 LITERATURE REFERENCES

JEFFREYS, G.V. & DAVIES, G.A.: Coalescence of Liquid Droplets and Liquid Dispersion, Recent Advances in Liquid-Liquid Extraction, ed. C. Hanson, Chap. 14, pp. 495 - 584, *Pergamon*, Oxford, 1971.

KARAM, H.J. & BELLINGER, J.C.: Deformation and Breakup of Liquid Droplets in a Simple Shear Field, *I & EC Fundamentals*, **7**, No. 4, 576 - 581, 1968.

KEEY, R.B.: Interpreting Mixing with Isotropic Turbulence Theory, *British Chem. Eng.*, **12**, No. 7, pp. 1081 - 1085, 1967.

KEITEL, G. & ONKEN, U.: Inhibition of Bubble Coalescence by Solutes in Air/Water Dispersions, *Chem. Eng. Sci.*, **37**, 1635 - 1638, 1982.

KEMMER, F.N. & McCALLION, J.: The Nalco Water Handbook, *McGraw-Hill Co.*, N.Y., 1979.

KOGLIN, B., PAWLOWSKI, J. & SCHNORING, H.: Kontinuierliches Emulgieren mit Rotor/Stator - Maschinen: Einfluss der Volumenbezogenen Dispergier leistung und der Verweilzeit auf die Emulsions feinheit, *Chem. Ing. Tech.* **53**, pp. 641 - 7, 1981.

KOLMOGOROFF, A.N., The Breakup of Droplets in a Turbulent Stream, *Doklady Akad. Nauk SSSR (NS)*, **66**, No. 5, pp. 825 - 828, 1949.

KONNO, M., AOKI, M. & SAITO, S.: Scale Effect on Breakup Process in Liquid-Liquid Agitated Tanks, *J. Chem. Eng. Japan*, **16**, 312 - 319, 1983.

KUBIE, J. & GARDNER, G.C.: Drop Sizes and Drop Dispersion in Straight Horizontal Tubes and in Helical Coils, *Chem. Eng. Sci.*, **32**, pp. 195 - 202, 1977.

KUMAR, S., NARSIMHAN, G. & RAMKRISHNA, D.: Coalescence in Creaming Emulsions. Existence of Pure Coalescence Zone, *Ind. Eng. Chem. Res.*, **35**, No. 9, pp. 3155 - 3162, 1996.

LAATS, M.K. & FRISHMAN, F.A.: Fluid Dynamics, **8**, 304, (1974).

LAMB, H.: Hydrodynamics, 6th ed., *Cambridge University Press*, Cambridge, U.K., 1932.

CHAPTER 8 LITERATURE REFERENCES

LANCE, M., MARIE, J.L., MOURSALI, E., BATAILLE, J., SUZANNE, C., ROIG, V., BLE FDHILA, R. & MASBERNAT, L.: Experimental Study of Turbulent Bubbly Shear Flows, *Chem. Eng. Comm.,* **Vols. 141 - 142**, pp. 51 - 70, 1996.

LANG, E., DRTINA, P.: Numerical Simulation of the Fluid Flow and the Mixing Process in a Static Mixer, *Int. J. Heat Mass Transfer,* **Vol. 38,** No.12, pp. 2239 - 2250, 1995.

LANG, E., DRTINA, P., BORTH, J. & STREIFF, F.: Analysis of Mixing in the Sulzer SMV Mixer by Numerical Simulation, *Industrial Mixing Fundamentals with Applications*, AIChE Symposium Series, **Vol. 91**, No. 305, 1995.

LANG, E., DRTINA, P., STREIFF, F. & FLEISCHLI, M.: Numerical Simulation of the Fluid Flow and the Mixing Process in a Static Mixer, *Int. J. Mass Transfer*, **38**, No. 12, pp. 2239 - 2250, 1995.

LANGNER, F., MORITZ, H.-U. & REICHERT, K.-H., *Chem. Ing. Tech.* **51**, pp. 746 - 747, 1979.

LAIDLER, K.J. & MEISER, J.H.: Physical Chemistry, Benjamin & Cummings Publishing Co., 1982.

LEE, C.H., ERICKSON, L.E. & GLASGOW, L.A.: Bubble Breakup and Coalescence in Turbulent Gas-Liquid Dispersions, *Chem. Eng. Commun.*, **61**, 181 - 195, 1987.

LEVICH, V.G.: Physiochemical Hydrodynamics, *Prentice Hall*, p. 20, 1962.

LI, D. & SLATTERY, J.C.: Experimental Support for Analysis of Coalescence, *AIChEJ.*, **34**, 862 - 864,1988.

LI, H.Z., FASOL, C. & CHOPLIN, L.: Pressure Drop of Newtonian and Non-Newtonian Fluids across a Sulzer SMX Static Mixer, *Trans IChemE,* **75**, Part A, Nov. 1997.

LIEM, A.J.S. & WOODS, P.R.: Review of Coalescence Phenomena, Water-1974: Industrial Waste Treatment No. 144, *AIChE Symp.Ser.*, 29, pp. 8 - 23, 1974.

CHAPTER 8 LITERATURE REFERENCES

LING, F.H. & ZHANG, X.: A Numerical Study on Mixing in the Kenics Static Mixer, *Chem. Eng. Comm.*, **136**, pp. 119 - 141, 1995.

LISSANT, K.J.: Emulsions and Emulsion Technology, **Vol. I, II, III**, Marcel Dekker Inc., N.Y. 1974.

LLOYD, D., MUBARAK, A. & EVANS, W.: Produced Water Tightening Legislation - The issues and options, presented at *Production Separation Systems Forum*, 1997.

LUMLEY, J.L. & PANOVSKY, M.A.: The Structure of Atmospheric Turbulence, *Interscience*, N.Y., 1964.

LUTHY, R.G., SELLECK, R.E. & GALLOWAY, T.R., *Environmental Sci Technol.*, 11(13):1211, 1977.

MANEV, E.D., VASSILIEF, C.S. & IVANOV, I.B.: Hydrodynamics of Films, *Colloid & Polymer Sci.*, **254**, 99, 1976.

MARUCCI, G.: A Theory of Coalescence, *Chem. Eng. Sci.*, **24**, 975 - 985, 1969.

MARUCCI, G. & NICODEMO, L.: Coalescence of Gas Bubbles in Aqueous Solutions of Inorganic Electrolytes, *Chem. Eng. Sci.*, **22**, 1257 - 1265, 1967.

MARUCCI, G., NICODEMO, L. & ACIERNO, D.: In «Co-current Gas-Liquid Flow», Rhodes, E. and Scott, D.S. (eds.), p. 95 - 108, *Plenum Press*, N.Y., 1969.

MATSAMURA, K., MORISHIMA, Y., MASUDA, K. & IKENAGO, H.: Some Performance Data of the Hi-Mixer - an IN-Line Mixer, *Chem. Ing. Tech.*, **53**, pp. 51-52, 1981.

MERSMANN, A. & GROSSMAN, H.: Dispergieren im Flussigen Zweiphasensystem, *Chem. Ing. Tech.*, **52**, pp. 621 - 8 , 1980.

McCABE, W.L., SMITH, J. & HARRIOT, P.: Unit Operations of Chemical Engineering, 5th edn., *McGraw-Hill*, 1993.

CHAPTER 8 LITERATURE REFERENCES

MIDDLEMAN, S.: Drop Size Distributions Produced by Turbulent Pipe Flow of Immiscible Fluids through a Static Mixer, *Ind. Eng. Chem., Process Des. Develop.,* **Vol. 13**, No. 1, pp. 78 - 83, 1974.

MILJØSOK: Oljeindustrien tar ansvar, Report from the Steering Committee of MILJØSOK, 1996.

MONIN, A.S. & YAGLOM, A.M.: Statistical Fluid Mechanics, *The MIT Press,* **Vol. 1**, Boston, 1971.

MOODY, L.W.: Friction Factor for Pipe Flow, *Trans. Am. Soc. Mech. Engrs., 1944.*

MORUD. K.E. & HJERTAGER. B.H.: LDA Measurements and CFD Modeling of Gas-Liquid Flow in a Stirred Vessel, *Chem. Eng. Sci.*, **51**, No. 2, pp. 233 - 249, 1996.

MLYNEK, Y. & RESNICK, W.: *A. I. Ch. E .J.,* **18**, 122, 1972.

MØRK, P.C.: Overflate- og kolloidkjemi, Inst. for industriell kjemi, *Norges Tekniske Høgskole*, 1994.

NAMBIAR, D.K.R., KUMAR, R., DAS, T.R. & GANDHI, K.S.: A Two-Zone Model of Breake Frequency of Drops in Stirred Dispersions, *Chem. Eng. Sci.*, **49**, pp. 2194 - 2198, 1994.

NARSIMHAN, G., GUPTA, J.P. & RAMKRISHNA, D.: A Model for Transitional Breakage Probability of Droplets in Agitated Liquid-Liquid Dispersions, *Chem. Eng. Sci.*, **34**, 257 - 265, 1979.

NARSIMHAN, G., NEJFELT,G. & RAMKRISHNA, D.: Breakage Functions for Droplets in Agitated Liquid-Liquid Dispersions, *A. I. Ch. E .J.,* **30**, 457 - 467, 1984.

NARSIMHAN, G., RAMKRISHNA, D. & GUPTA, J.P.: Analysis of Drop-Size Distributions in Lean Liquid-Liquid Dispersions, *A. I. Ch. E .J.,* **26**, 991 - 1000, 1980.

NICODEMO, L., MARRUCCI, G. & ACIERNO, D.: *Quad. Ing. Chim. Ital.*, **8**, 1, 1972.

CHAPTER 8 LITERATURE REFERENCES

OOLMAN, T.O. & BLANCH, H.W.: Bubble Coalescence in Stagnant Liquid, *Chem. Eng. Commun.*, **43**, 237 - 261, 1986.

PAHL, M.H. & MUSCHELKNAUTZ, E.: Static Mixers and their Applications, *Int. Chem. Eng.*, 1982.

PARK, J.Y. & BLAIR, L.M.: The Effect of Coalescence on Drop-Size Distribution in an Agitated Liquid-Liquid Dispersion, *Chem. Eng. Sci.*, **30**, pp. 1057 - 64, 1975.

PERRY, R.H. & CHILTON, C.H.: Chemical Engineer's Handbook, 5th ed., McGraw-Hill, 1973.

RADOEV, B.P., DIMITROV, D.S. & IVANOV, I.B.: Hydrodynamics of Thin Liquid Films: Effect of the Surfactant on the Rate of Thinning, *Colloid & Polymer Sci.*, **252**, 50 - 55, 1974.

RAMKRISHNA, D.: Drop Breakage in Agitated Liquid-Liquid Dispersions, *Chem. Eng. Sci.*, **29**, pp. 987 - 992, 1974.

ROBERSON, J.A. & CROWE, C.T.: Engineering Fluid Mechanics, *Houghton Mifflin Co.*, 1975.

RUCKENSTEIN, E. & JAIN, R.K.: Spontaneous Rupture of Thin Liquid Films, *J. Chem. Soc. Faraday Trans.*, **70**, 132 - 147, 1974.

RUMSCHEIDT, F.D. & MASON, S.G.: Break-up of Stationary Liquid Threads, *J.Colloid Sci.*, **17**, 260 - 269, 1962.

SAGERT, N.H., QUINN, M.J., CRIBBS, S.C. & ROSINGER, E.L.J.: Bubble Coalescence in Aqueous Solutions of n-Alcohols, in «Foams», Akers, R.J. (ed.), p. 147 - 162, *Academic Press*, London, 1976,

SAGERT, N.H. & QUINN, M.J.: The Coalescence of H_2S and CO_2 in Water, *Can.J.Chem. Eng.*, **54**, 392 - 398, 1976.

SAGERT, N.H. & QUINN, M.J.: The Coalescence of Gas Bubbles in Dilute Aqueous Solutions, *Chem. Eng. Sci.*, **33**, 1087 - 1095, 1978.

CHAPTER 8 LITERATURE REFERENCES

SATHYAGAL, A.N., RAMKRISHNA, D. & NARSIMHAN, G.: Solution of Inverse Problems in Population Balances II: Particle Breakup, *Comp.Chem. Eng.*, **19**, 437 - 451, 1994.

SATHYAGAL, A.N., RAMKRISHNA, D. & NARSIMHAN, G.: Droplet Breakage in Stirred Dispersions. Breakage Functions from Experimental Drop-Size Distributions. *Chem. Eng. Sci*, **51**, No. 9, pp. 1377 - 1391, 1996.

SCHELUDKO, A.: *Proc. K. Ned. Akad. Wet.*, **B65**, 76, 1962.

SCHELUDKO, A.: Thin Liquid Films, *Adv. Colloid Int. Sci.*, **1**, 391, 1967.

SCHWARZ, N. & BEZEMER, C.: *Kolloidzeitshrift*, **146**, 139, 145, 1956.

SEMBIRA, A.N., MERCHUK, J.C. & WOLF, D.: Characteristics of a Motionless Mixer for Dispersion of Immiscible Fluids - III. Dynamic Behaviour of the Average Drop Size and Dispersed Phase Holdup, *Chem. Eng. Sci*, **43**, No. 2, pp. 373 - 377, 1988.

SHINNAR, R.: On the Behavior of Liquid Dispersions in Mixing Vessels, *J. Fluid Mech.*, **10**, 259, 1961.

SHINNAR, R. & CHURCH, J.M.: Ind. Eng. Chem., **52**, 253, 1960.

SJöBLOM, J., SÆTHER, Ø., MIDDTUN, Ø., URDAHL, O. & FØRDEDAHL, H.: Asphaltene and Resin Stabilized Crude Oil Emulsions - Experimental Characterization and Destabilization, 1997.

SJöBLOM, J., URDAHL, O., HØILAND, H., CHRISTY, A. A. & JOHANSEN, E.J.: Water-in-crude Emulsions. Formation, characterization, and destabilization. *Progr. In Colloid & Polymer Science,* **82**: 131 - 139, 1990.

SJöBLOM, J., URDAHL, O., NORDLI BØRVE, K.G., MINGYUAN, L., SAETEN, J., CHRISTY, A. A. & GU, T.: Stabilization and Destabilization of Water-in-Crude oil Emulsions from the Norwegian Continental Shelf. Correlation with Model Systems., *Advances in Colloid and Interface Science*, **41**, p. 241 - 271, Elsevier Science Publisher, 1992.

SLEICHER, JR., C.A.: Maximum Stable Drop Size in Turbulent Flow, *A.I.Ch.E. Journal,* **Vol. 8**, No. 4, pp. 471 - 477, 1962.

CHAPTER 8 LITERATURE REFERENCES

SPALDING, D.B.: Computer Simulation of Two-Phase Flows, with special reference to nuclear reactor systems, in *Computational Techniques in Heat Transfer*, (Edited by Lewis, R.W., Morgan, K., Johnson, J.A., Smith, R.), pp. 1 - 44, Pineridge Press, Swansea, 1985.

SPROW, F.B.: Distribution of Drop Sizes in Turbulent Liquid-Liquid Dispersions, *Chem. Eng. Sci.*, **Vol. 22**, 435 - 442, 1967a.

STONE, H.A. & LEAL, L.G.: Relaxation and Breakup of Initially Extended Drop in an otherwise Quiescent Fluid, *J. Fluid Mech*, **198**, 399 - 427, 1989.

STREIFF, F.: In-line Dispersion and Mass Transfer using Static Mixing Equipment, *Sulzer Technical Review (3)*, pp.108 - 13, 1977.

TAYLOR, G.I.: The Formation of Emulsions in Definable Fields of Flow, *Proc. R. Soc. Lond.*, **A146**, 501, 1934.

TENNEKES, H. & LUMLEY, J.L.: A First Course in Turbulence, The Massachusetts Institute of Technology, 1992.

THOMAS, R.M.: Bubble Coalescence in Turbulent Flows, *Int. J. Multiphase Flow*, **7**, No. 6, pp. 709 - 717, 1981.

TJAHJADI, M., STONE, H.A. & OTTINO, J.M.: Satellite and Sub-satellite Formation in Capillary Breakup, *J. Fluid Mech*, **243**, 297 - 317, 1992.

TSOURIS. C. & TAVLARIDES, L.L.: Breakage and Coalescence Models for Drops in Turbulent Dispersions, *A.I.Ch.E.J.*, **40**, 395 - 406, 1994.

VALENTAS, K.J., BILOUS, O. & AMUNDSON, N.R.: Analysis of Breakage in Dispersed Phase Systems, *Ind. Eng. Chem. Fund.*, **5**, 271, 1966.

VALENTAS, K.J. & AMUNDSON, N.R.: Breakage and Coalescence in Dispersed Phase Systems, *Ind. Eng. Chem. Fund.*, **5**, 553, 1966.

VAN HEUVAN, J.W. & BEEK, W.J.: *Proc. ISEC*, Amsterdam, 1971.

VENKATESAN, V.S.: Determination of Average Bubble Size and Its Distribution using a Video Technique, Technical Report, *Institut for Technische Chemie I*, Erlangen, Germany, 1991.

CHAPTER 8 LITERATURE REFERENCES

VERMEULEN, T., WILLIAMS, G.M. & LANGLOIS, G.E.: *Chem. Eng. Prog.*, **2**, 85F (1955).

VRIJ, A.: Possible Mechanism for the Spontaneous Rupture of Thin, Free Liquid Films, *Disc. Faraday Soc.*, **42**, 23 - 33, 1966.

VRIJ, A. & OVERBEEK, J.TH.G.: Rupture of Thin Liquid Films due to Spontaneous Fluctuations in Thickness, *J. Am. Chem. Soc.*, **90**, 3074 - 3078, 1968.

WARD, J.A. & KNUDSEN, J.G.: *A. I. Ch. E. J.*, **13**, 356, 1967.

WICHTERLE, K.: Drop Breakup by Impellers, *Chem. Eng. Sci.*, **Vol. 50**, No. 22, pp. 3581-3586, 1995.

WOODS, D.R. & DIAMADOPOULOS, E.: Importance of Surfactants and Surface Phenomena on Separating Dilute Oil-Water Emulsions and Dispersions, *Wasan et. al (eds.): Surfactant Science Series*, **28**, 369 - 540, Marcel Dekker, 1988.

WRIGHT, H. & RAMKRISHNA, D.: Factors Affecting Coalescence Frequency of Droplets in a Stirred Liquid-Liquid Dispersion, *A.I.Ch.E.J.*, **40**, No. 5, 767 - 776, 1994.

YANG, Y.M. & MAA, J.R.: Bubble Coalescence in Dilute Surfactant Solution, *J. Colloid Int. Sci.*, **98**, 120 - 125, 1984.

ZEITLIN, M.A. & TAVLARIDES, L.L.: Fluid-Fluid Interactions and Hydrodynamics in Agitated Dispersions: A Simulation Model, *Can. J. Chem. Eng.*, **50**, 207, 1972.

ZERFA. M. & BROOKS, B.W.: Prediction of Vinyl Chloride Drop Sizes in Stabilised Liquid-Liquid Agitated Dispersion, *Chem. Eng. Sci.*, **51**, pp. 3223 - 3233, 1996.

9 LIST OF SYMBOLS

Latin letters:

A	Droplet surface area	m^2
$A(v,t)$	Probability density of droplet size in a vessel	
$A_0(v,t)$	Probability density of droplet size in feed	
a	Interfacial area per unit volume	m^2/m3
	Characteristic diameter related to distribution function	m
a_1	Activity coefficient of species 1	$kmol/m^3$
a_B	Activity coefficient of bulk phase	$kmol/m^3$
B	Constant	
b	Constant	
C	Constant	
	Parameter (Lagrangian)	
C_2	Constant	
C_3	Constant	
C_4	Constant	
c_1	Concentration of species 1	$kmol/m^3$
c_D	Drag coefficient	
c	Force	N
D	Droplet diameter	m

CHAPTER 9 LIST OF SYMBOLS

	Pipe diameter	m
D_{max}	Maximum droplet diameter	m
$D_{\min}$	Minimum droplet diameter	m
D_0	Pipe diameter (empty pipe)	m
D_{32}	Sauter drop diameter	m
D_{32_0}	Sauter drop diameter upstream from the mixer	m
$\hat{D}$	Eddy wavelength	m
	Integral length scale in lateral direction	m
d	Pipe diameter	m
	Droplet diameter	m
	Particle diameter	m
d_h	Hydraulic diameter	m
d_0	Mean droplet diameter	m
d_1	Bubble diameter stable against breakup	m
d_{32}	Sauter mean diameter	m
d_{max}	Maximum stable droplet diameter	m
	Maximum observed droplet diameter	m
$d_{\min}$	Minimum observed droplet diameter	m
d_p	Equilibrium drop size	m
E	Energy dissipation per unit mass of fluid in mixer	W/kg
E_D	Direct energy dissipation rate	W/kg
$E(k)$	Energy spectrum function	m^3/s^2
e	Fractional liquid holdup	
F_γ	Surface force	N
F_H	Hydrodynamic force	N
F_S	Surface force at the drop tip	N
$F(v,t)$	Cumulative volume fraction	
f	Fanning friction factor	
f_D	Doppler frequency	Hz
f_0	Shift frequency (Doppler)	Hz
$f(\phi)$	Holdup function dispersed phase	
$f(v)$	Escape frequency of droplet size v	s^{-1}
G	Production of turbulence due to the main stream	

CHAPTER 9 LIST OF SYMBOLS

G_1	Parameter for electrolyte concentrations	
$G(v,v')$	Cumulative daughter drop distribution from the breakage of a parent drop of volume v'.	
$g(v)$	Breakage frequency of drops of volume v	s^{-1}
$h(v,v')$	Collision frequency between drops of size v and v'	s^{-1}
h_c	Critical film thickness for rupture	m
h_e	Equilibrium film thickness	m
h_f	Final thickness of the film	m
h_0	Quasi-equilibrium film thickness	m
I	Turbulence intensity	
K	Constant	
k	Constant	
k	Parameter	m^{-1}
k	Wave number	m^{-1}
k	Turbulent kinetic energy	J
L	Mixer length	m
L	Macroscale of turbulence Liquid phase (as a subscript)	m
L_E	Size of turbulent eddies	m
l	Prandtl mixing length Integral length scale for eddy	m m
N	Number of samples (LDA measurements)	
$N(t)$	Total number of drops in vessel at time t	
Ne	Newton number	
n	Number of samples	
n_j	Number of drops of size class j	
ΔP	Pressure drop	N/m^2
p	Surface pressure on droplet surface	N/m^2
Δp	Pressure drop	N/m^2
Q	Volumetric flowrate	m^3/s
R_1, R_2	Mean curvature radii of surface element dA	m
$R_{u'}$	Distance correlation coefficient	
$R(\tau)$	Lagrangian correlation function	
Re	Reynolds number $(\rho_c v d_h/\eta_c)$	
Re_λ	Eddy Reynolds number $\approx V_\lambda \lambda/\nu$	

CHAPTER 9 LIST OF SYMBOLS

r	Drop radius	m	
r	Radial direction, radial coordinate Lateral coordinate		
r_{sd}	Maximum stable drop size	m	
r_b	Bubble radius	m	
S_Φ	Source term (momentum conservation equation)		
T	Turbulence intensity (LDA measurements)		
T_L	Lagrangian time scale	s	
T_0	Time for passing a reference point 0	s	
	Entrance time	s	
t_D	Diffusion time	s	
t_b	Breaking time	s	
t_c	Coalescence time	s	
t_s	Stretching time	s	
t_0	Time period	s	
$\bar{t}$	Coalescence time	s	
U	Axial velocity	m/s	
$\overline{U}$	Mean velocity (LDA measurements)	m/s	
U_i	Velocity of sample i (LDA measurements)	m/s	
U_*	Friction velocity in a conduit	m/s	
u	Constant net velocity of stream in x direction	m/s	
$\bar{u}$	Superficial liquid velocity (mixer)	m/s	
u'	Root mean square turbulent fluctuating velocity in a dispersion of particles	m/s	
u_0'	Root mean square turbulent fluctuating velocity in a free particle fluid	m/s	
$\overline{u'}$	Deviating velocity in the x direction	m/s	
u_i	Instantaneous total velocity component in x direction		m/s
V	Variation coefficient, mixing homogenity		
V	Radial velocity	m/s	
	Rate of stretching of a drop	m/s	
V_d	Volume of dispersed phase	m^3	
V_M	Working volume of static mixer	m^3	
Vi	Viscosity group, $(\mu_d \overline{V}/\sigma)(\rho_c/\rho_d)^{1/2}$		
$\overline{V}$	Average fluid velocity	m/s	

CHAPTER 9 LIST OF SYMBOLS

V_λ	Eddy velocity	m/s
$\overset{*}{V}_1, \overset{*}{V}_2$	Volume flows	m^3/s
v	Mean fluid velocity across a drop	m/s
v_i	Instantaneous velocity component in y direction	m/s
v_{mean}	Local mean velocity	m/s
v_{rms}	Root mean square velocity	m/s
v_x	Particle velocity in the Doppler field	m/s
v	Particle velocity	m/s
v'	Deviating velocity in the y direction	m/s
	Standard root mean square velocity	m/s
W	Tangential velocity	m/s
We	Weber number $= \frac{\rho_c v^2 d_h}{\gamma}$ or $\frac{\rho_c V^2 D}{\sigma}$	
We_c	Critical droplet Weber number at which breakup occurs	
	$We_c = \frac{\bar{u}^2 D_{max} \rho}{\sigma}$	
w'	Deviating velocity in the z direction	m/s
w_i	Instantaneous velocity component in z direction	m/s
x	Axial direction	
x	Longitudinal coordinate	
	Value of locally measured variable	
$\bar{x}$	Mean value of locally measured variables	
x_i	Locally measured variable (e.g. concentration)	
Z	Scale of the smaller eddies	m
	Ion valency	

Greek letters:

α	Disruptive force coefficient	
	Volume fraction	
α_g	Volume fraction of gas	
α_l	Volume fraction of liquid	
Δ	Velocity difference across a bubble	m/s
δ_M	Thickness of the boundary layer	m

CHAPTER 9 LIST OF SYMBOLS

ε	Dispersed phase volume fraction	
ε	Rate of turbulent energy dissipation per unit mass	W/kg
$\bar{\varepsilon}$	Mean energy dissipation rate	W/kg
ξ	Lagrangian parameter	
γ	Interfacial tension	
	Surface tension	N/m
γ_M	Shear rate	s^{-1}
$\gamma(v)$	Coalescence frequency	
λ	Wavelength of Doppler beam	m
	Eddy length	m
λ_0	Dissipation length scale	m
$\lambda(v,v')$	Collision efficiency between drops of size v and v'	
κ	Proportionality constant (in Prandtl mixing length)	
η	Kolmogoroff microscale	m
$\bar{\eta}$	Kolmogoroff microscale	m
η_c	Dynamic viscosity of the continuous phase	kg/ms
μ_c	Dynamic viscosity of the continuous phase	kg/ms
μ_d	Dynamic viscosity of the dispersed phase	kg/ms
$\mu_{eff,k}$	Effective viscosity, defined as $\mu_{l,k} + \mu_{t,k}$	kg/ms
$\mu_{l,k}$	Molecular viscosity	kg/ms
$\mu_{t,k}$	Turbulent viscosity	kg/ms
ϕ	Volumetric fraction of the dispersed phase	
ρ	Density of the continuous phase	kg/m^3
ρ_c	Density of the continuous phase	kg/m^3
ρ_d	Density of the dispersed phase	kg/m^3
σ	Root mean square velocity (LDA measurements)	m/s
	Standard deviation (mixing homogeneity)	
	Interfacial tension	N/m
	Surface tension	
σ_0	Initial standard deviation (unmixed state)	
σ^2	Variance (LDA measurements)	
σ_Φ	Prandtl/Schmidt number	
τ	Newton shear stress	N/m^2
	Viscous force per unit surface area	N/m^2

CHAPTER 9 LIST OF SYMBOLS

τ	Residence time	s
τ_{app}	Reynold's shear stress, or apparent shear stress	N/m^2
τ_c	Turbulent disruptive force per unit area	N/m^2
Γ_i	Surface excess concentration of component i	mol/m^2
$\Gamma(v)$	The drop breakage rate for a drop of volume v	
$\Gamma_{\Phi,k}$	Transport coefficient $= \frac{\mu_{eff,k}}{\sigma_\Phi}$	
ν_c	Kinematic viscosity of continuous phase	m^2/s
Θ	Angle between shifted and unshifted Doppler beams	
Φ	Average rate of energy dissipation (static mixer)	W/kg
Ω	Frequency	m^{-1}